D.C. TRANSMISSION SYSTEM
HARMONIC ANALYSIS AND STABILITY
USING DESCRIBING FUNCTIONS

by

J. M. D. FERREIRA DE JESUS

DIPL. ENG.

Department of Electrical Engineering
Imperial College of Science and Technology
University of London

Thesis submitted for the degree of
Doctor of Philosophy
in the Faculty of Engineering

London, December 1982

Abstract

The instability due to feedback control of the direct current in a d.c. transmission system manifests itself through the presence of two types of self sustained oscillations

a. Oscillations synchronised with the a.c. system voltage - usually referred to as harmonic instability.

b. Oscillations at a frequency unrelated to that of the a.c. supply.

The theoretical tools that have been developed to study this problem are based on linearised models of a d.c. transmission system and are unsuited for predicting oscillations synchronised with the a.c. system voltage. The objective of this research is to develop a model capable of predicting such oscillations.

As the converter is a non-linear device, the describing function technique was used in order to evaluate the frequency response of the current control loop. To evaluate the describing functions, a harmonic analysis was performed of the d.c. side current and the a.c. side current associated with a converter.

An off-line digital computer program was developed to this purpose. The results from this program, together with the frequency response of the linear elements of the current control loop, were used to predict oscillations synchronised with the a.c. system voltage. Test results obtained on the Imperial College H.V.D.C. simulator were compared with theoretical predictions.

Operation under current control is conducive to abnormal harmonic generation. If the a.c. voltage is unbalanced and/or distorted, the direct current will contain abnormal harmonics.

In a closed loop situation these harmonics, even if filtered, may be sufficient to cause firing irregularities and thus precipitate harmonic magnification.

The experimental results were obtained on a d.c. transmission model whose converters were fired from a control system based on a commercially available microcomputer.

'To see a World in a Grain of Sand
And a heaven in a Wild Flower
Hold Infinity in the palm of your hand
and Eternity in an Hour'

'Auguries of Innocence' - William Blake

To Sara, Pedro and Joana

Acknowledgements

This work was carried out under the supervision of Dr L L Freris, M.Sc(Eng), Ph.D, DIC, MIEE, Reader in Electrical Engineering, whom I would like to thank for his constant guidance and encouragement.

I also wish to express my sincere gratitude to Prof Sucena-Paiva, Dipl Eng, DIC, Ph.D, MIEEE, for the advice, help and encouragement he provided throughout the project.

I would like to express my appreciation to my friends in the Power System Laboratory who made life so much more enjoyable.

I am grateful to Instituto Nacional de Investigacao Cientifica, Meisel Energy Systems Inc and to GEC Power Engineering Ltd for their financial support.

Finally I would like to extend my gratitude to Heather Stanley for typing the thesis and to Maria Luiza for her patience.

TABLE OF CONTENTS

List of symbols and abbreviations

Note: The following list does not include either symbols of limited usage (defined in their place of occurrence), or symbols of general usage in electrical engineering.

Latin letters

a	Transformation ratio
D.A.I.	Data acquisition interface
d.f.	Describing function
d.i.d.f.	Dual input describing function
d.t.f.a.	Digital transfer function analyser
e.p.u.	Error processing unit
G	Transfer function of linear part of control loop
I_a	a.c. current 'constant' term
I_{ah}	Amplitude of the h^{th} harmonic of a.c. current
I_d	d.c. current 'constant' term
$I_{d\ell}$	Amplitude of the ℓ^{th} harmonic of d.c. current
IFP	Interfiring period
IPC	Individual phase control
I_{ref}	Reference d.c. current
i_a	Converter side a.c. current
i_d	d.c. current
i_i	Commutation current in the incoming valve
i_o	Commutation current in the outgoing valve
K	Gain
L_{av}	Average value of converter internal inductance
L_i	Transfer inductance

m.s.	Modulating signal
N	Describing function of non-linearity
N.L.	Non-linearity
PFC	Pulse frequency control
PPC	Pulse phase control
R_{av}	Average value of converter internal resistance
R_i	Transformer resistance
s.c.r.	Short circuit ratio
T	Time constant
u	Commutation angle
V_c	Control voltage
V_d	d.c. voltage constant term
$V_{d\ell}$	Amplitude of the ℓ^{th} harmonic of d.c. voltage
V_i	Phase-to-neutral a.c. bus voltage
V_{ih}	Amplitude of the h^{th} harmonic of a.c. bus voltage
V'_{ik}	Valve side commutating voltage
V_m	Amplitude of modulating signal
v.z.c.	Voltage zero crossing
v_c^o	Nominal control voltage
v_d	d.c. voltage
X_s	Source reactance
Z_s	Source impedance
Z_f	a.c. filter impedance

Greek letters

α	Firing angle
α^o	Nominal firing angle
α_c	Correction due to the auxiliary α control loop

γ	Extinction angle
Δ	Increment
ε	Tolerance
ψ	Phase of modulating signal
ψ_{ah}	Phase of the h^{th} harmonic of a.c. current
$\psi_{d\ell}$	Phase of the ℓ^{th} harmonic of d.c. voltage
$\phi_{d\ell}$	Phase of the ℓ^{th} harmonic of d.c. current
ϕ_{ih}	Phase of the h^{th} harmonic of a.c. voltage
θ	Argument of transfer function G
ω	Modulating signal angular frequency
ω_o	'Mains' angular frequency

Chapter One

INTRODUCTION

1.1 General

A significant feature of an h.v.d.c. transmission link is that its power flow is set to a desired level by means of closed-loop control. For d.c. systems embedded in an a.c. power network, this feature may supersede strict economic consideration (e.g. the breakeven distance concept) when assessing the merits of d.c. transmission with respect to a.c. transmission.

The importance of h.v.d.c. link control requires that a great deal of attention has to be given to the enhancement of its transient response. A well designed controller should ensure fast and stable operation free from oscillatory modes, a low level of abnormal harmonic currents and, as a consequence, acceptable a.c. system voltage distortion levels.

The control of an h.v.d.c. link is implemented through direct action on the converter by advancing or delaying the firing instants of the individual valves. This process is much faster compared to the control actions necessary to regulate the active power flow in an a.c. network.

An overall dynamic study of a mixed a.c./d.c. power system requires the modelling of the a.c. system, the d.c. network and the d.c. terminal controls. Due to the difference in time scales of the dynamics of the a.c. and d.c. systems, a number of approximations are usually made in the representation of the d.c. controls. Often the dynamics of the d.c. controls may be altogether neglected and the response of the d.c. system may be taken to be instantaneous. In such a transient stability analysis it is assumed that the d.c. system control is stable and a relatively crude model is used for the converters.

The stability of the d.c. system controls is a major topic in itself and requires manipulation of electronic rather than power circuitry. The concept of stability in a d.c. system must not be confused with stability in an a.c. system. In the former, the stability of a number of closed loop control systems must be ensured. In the latter, it is necessary to ensure that all the machines in the system remain in synchronism in the presence of large or small disturbances.

The stability of d.c. system control requires a detailed model of the system, and in particular of the converters. These are highly non-linear devices controlled at discrete time instants only. The formulation of a sufficiently accurate model for this device presents considerable difficulty. If a small signal analysis is to be carried out with the converter

connected to an infinite a.c. bus, a linearised discrete model and the z-transform method of analysis can be used (1). However, with the converter connected to a weak a.c. bus, a much more complicated model becomes necessary, in which the unconventional modulation and demodulation processes inherent in converter operation are represented (1). If, however, a large signal analysis is required, the describing function method is probably the only technique which at present can be used to predict with reasonable accuracy the occurrence of self-sustained oscillations.

The instability due to feedback control of the direct current in a d.c. transmission system manifests itself through the presence of two types of self-sustained oscillations:

a. Oscillations synchronised with the a.c. system voltage, i.e. at a frequency which is a multiple or submultiple of the a.c. frequency - usually referred to as harmonic instability.

b. Oscillations at a frequency unrelated to that of the a.c. supply.

Harmonic instability may also be present without a direct current closed loop in cases where converter controllers are used in which the valve firing instants are dependent on the a.c. bus voltage waveshapes (2, 26) - the so-called individual phase control. However, this cause of instability has been eliminated through the use of phase-locked oscillator based firing systems (2).

The stability of the current control loop in an a.c./d.c. converter depends upon a number of system parameters, the most important of which are:

- Type of firing control system
- Unbalance and/or distortion of a.c. bus voltage
- A.C. network impedance
- A.C. and d.c. filter impedance
- D.C. system configuration
- Converter transformer saturation
- Unbalance in converter transformer impedance
- Error processing unit dynamics

The system designer has easily implementable control over a limited number of these parameters. For instance, the firing control system and the control amplifier can be readily modified. In contrast, the a.c. system impedance can only be changed through the addition of costly equipment - e.g. synchronous condensers. Similarly, the unbalance between converter transformer phase reactances may be reduced but at considerable expense. As a general rule, electronic rather than power circuitry should be manipulated in order to improve performance. In this respect the valve firing control system plays a major role and should be given appropriate attention.

1.2 Review of previous work

As early as 1951, Busemann (3, 4) explained albeit under certain restrictive assumptions the hunting of a rectifier supplying an inverter through a transmission line, under constant current control. He found that under certain conditions hunting occurred at half the firing frequency and derived a formula for the critical equivalent resistance of the rectifier under current control leading to instability.

Bjaresten (5) and Fallside (6, 7) modelled the rectifier as a pure sampler and were able to derive respectively a closed-form and an infinite series for the critical gain of the closed-loop system leading to instability at half the firing frequency. Fallside went further and using the describing function studied the instability for large disturbances at other subharmonics of the firing frequency. However, his analysis treated the converter as a fast amplifier and was restricted to low power devices (zero commutation angle and an infinite a.c. bus were assumed).

Hazell et al (8) modelled the converter as a sampler followed by a zero-order hold. This misrepresents the converter behaviour and leads to very conservative results when applied to the prediction of instability. Reider (9) used a similar model to study the stability of control of the Kashira-Moscow h.v.d.c. experimental line. Later Hazell (10) developed a general theory for converter systems which, as far as the author is aware, has yet to be applied to a real system and confirmed experimentally.

Parrish and McVey (11) used a simplified method of modelling the controlled converter by a constant gain followed by a pure delay of half the sampling period, permitting the use of continuous control systems theory in the analysis. This is however an over-simplification which leads to inaccurate results.

With the exception of Busemann, all other researchers viewed the controlled rectifier as a fast static amplifier, and not as the main piece of equipment for h.v.d.c. transmission.

They therefore neglect the existence of a finite commutation time due to the presence of reactance in the converter transformer. They also assume that the converter is connected to an infinite a.c. bus, thereby neglecting the a.c. network impedance.

The first of these restrictions was lifted by Sucena-Paiva and Freris (12-14), who developed a linearised discrete model, which represents accurately the intermittent control action of the converter with a finite commutation angle. It was shown that this angle plays a major role in the dynamic behaviour of the converter under closed-loop control. The z-transform method of analysis was used to calculate stability boundaries which were successfully confirmed on an h.v.d.c. simulator.

With the converter connected to an infinite a.c. bus this model predicts harmonic instability at half the firing frequency only if the converter is inserted in a control loop with a high cut-off frequency. For low cut-off frequencies (compared with the firing frequency) instability is predicted at oscillations of low frequency unrelated to the firing frequency. However, harmonic instability at other subharmonics of the mains frequency may develop under certain conditions and be sustained at values of the loop gain less than the critical value. This phenomenon is due to the non-linear properties of the converter and is not predicted by the linearised model.

The discrete converter model was also used to assess the stability of a d.c. link between two strong (infinite) a.c. systems (15), the rectifier operating under current control and the inverter under extinction angle control. Both harmonic

and non-harmonic instability modes were predicted, the harmonic instability being restricted to half the pulsing frequency. Simulator tests again showed that other modes of harmonic instability can develop, which are not predicted by this model.

With the converter connected to a weak a.c. system, the discrete model alone is not capable of representing the dynamic behaviour of the converter as the a.c. bus voltage is now a dependent variable. Further, as the filters are designed with high quality factors, parallel resonances occur at certain frequencies with the result that a high impedance is encountered by currents of those frequencies injected by the converter into the network. To model the interaction between the a.c. and d.c. system quantitites, the modulation and demodulation processes characteristic of converter operation have to be taken into account. The inherent modulation process of the converter is unique, exhibiting only vague resemblance to the modulation methods used in the communications field.

Persson (16) introduced the concept of 'conversion functions', which in fact are the carrier functions of the modulation and demodulation processes, to calculate the transfer function of a converter taking into account the effect of filter plus a.c. network impedance. Although this technique is similar to the describing function, he restricts his analysis to small disturbances. Sucena-Paiva and Freris (17) followed a similar path, but used sinusoidal carrier functions, an approximation that reduced considerably the computational requirements without significant loss of accuracy. In both works, only the onset of instability can be predicted, since

linearised models are used. Frequency domain techniques are employed.

Sakurai et al (18) use a describing function approach to analyse a particular mode of harmonic instability detected in the Shin-Shinano frequency converter, which is characterised by a fundamental frequency oscillation on the d.c. side and a 2nd-order harmonic on the a.c. side. This mode is likely to occur if the d.c. system resonates near the fundamental frequency and if the combined a.c. network plus filter impedance has an antiresonance between the 2nd and 3rd harmonic as is the case in many h.v.d.c. links.

Jotten et al (44) discuss the influence of resonances on the d.c. side and anti-resonances on the a.c. side on the behaviour of the current controller. They conclude that if the d.c. resonance and a.c. anti-resonance frequencies are related by the modulation process inherent to the converter, instability in the current control-loop might occur if the controller is given a high gain and bandwidth. The frequency of the resulting oscillation will be close to one of the lower harmonic frequencies.

Oliveira and Yacamini (19, 42) developed a program to calculate a.c. and d.c. harmonics in converter systems with both finite a.c. and d.c. impedances. Using an iterative method the final pattern of harmonics in the a.c. bus voltage, a.c. current, d.c. voltage and d.c. current with or without current control are evaluated. If the iterative process fails to converge the authors conclude that they are in the presence of harmonic instability. As no test results are presented, it is difficult to confirm whether we are in the presence of a

true or a numerical instability.

Yacamini and Smith (43) compute the negative sequence impedance of converters by applying an unbalanced voltage supply to the converter system and measuring the resultant a.c. line currents. They show that the negative sequence impedance depends on the type of firing system used and conclude that the v.c.o. based type of firing system is advantageous, as it leads to a higher negative sequence impedance.

The saturation of the converter transformer core due to spurious d.c. components can also contribute to harmonic instability as noted by Ainsworth (20). This particular type of instability is caused by a combination of a weak a.c. system and a resonance near the fundamental frequency on the d.c. side, and as shown in references (18, 19, 42) and suggested in reference (44) may be present even without transformer saturation. Core saturation does however aggravate this phenomenon.

1.3 Objectives of research

The linearised models developed (1, 15, 16) so far suffer from the following limitations:

i. They fail to predict limit cycle oscillations synchronised with the a.c. system voltage excepting the case of half the pulsing frequency.

ii. They cannot take into account an unbalance and/or harmonic distortion in the a.c. bus voltage.

iii. They cannot take into account imbalances in the commutating reactance.

The main objective of the research work undertaken is the development of a mathematical model for the converter, capable of predicting oscillations synchronised with the a.c. system voltage for a single converter and a complete d.c. link. The predictions from the analytical studies were supported with results from a d.c. system simulator.

The model in question is based on the describing function method. Referring to fig I.I a sinusoidal signal is injected at B and the component of the same frequency is calculated at C for a given voltage input A. The analysis is restricted to frequencies which are subharmonics of the pulsing frequency, i.e. only harmonic instability is investigated.

The distinctive trait of the frequency response of the converter at these particular frequencies is that the output becomes dependent on the phase of the input signal and instead of a single point on the complex plane, as is the case for frequencies unrelated to the pulsing frequency, a circle is traced. Moreover, due to the non-linearity of the system, the radius of the circle depends on the magnitude of the input signal. The linearised model does predict a circle only at half the pulsing frequency. a feature of all sampled-date systems.

Unbalance and/or distortion in the a.c. voltage has a definite effect on the magnitude of the circles, which can be significantly increased under certain circumstances, indicating that instability is more likely to occur. The same considerations apply to converter transformer core saturation, which has similar

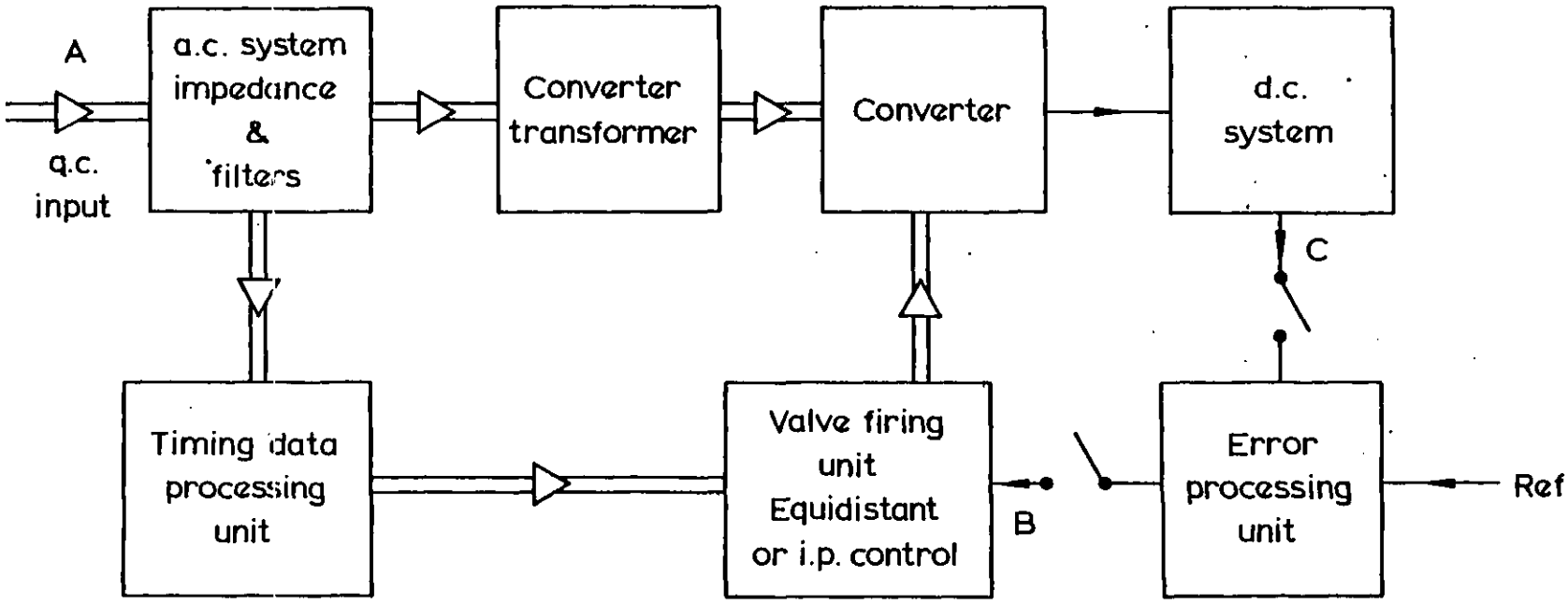

Fig. 1·1

Converter functional block diagram.

effects upon the frequency response of the converter system.

To evaluate the describing function a computer program was developed. First, analytical relationships were established to simulate the firing system and to evaluate the commutation angles. Then the program performs a Fourier analysis of both a.c. and d.c. quantities. In concept, the method used to evaluate the commutation angles and to calculate the a.c. and d.c. harmonics is similar to the one developed by Oliveira (19).

This new model, in conjunction with the existing linearised models which can predict the onset of instability, afford a fuller understanding of the mechanisms responsible for the development of large oscillations in h.v.d.c. systems.

1.4 Organisation of thesis

This thesis contains eight chapters. In Chapter Two the firing control systems for h.v.d.c. converters are reviewed. A new digital controller built around a commercially available microcomputer system was developed and is described and compared to previous systems.

Chapter Three deals with the non-linear converter model developed to compute the describing function. Imbalance and/or distortion in the a.c. voltage, imbalance in the converter transformer impedance and non-equidistant firing are taken into account. A general method for the determination of the commutation angle is developed. Mathematical models for the firing system, converter transformer, a.c. and d.c. systems are developed.

Chapter Four is concerned with the harmonic analysis of d.c. and a.c. voltages and currents. From the mathematical description of the d.c. voltage and a.c. current the Euler coefficients are calculated analytically under the most general conditions. A model for the inverter is proposed which takes into account the constant extinction angle mode of control. Flowcharts of the computer program developed for the steady-state analysis of an h.v.d.c. link both with infinite and finite terminal a.c. systems are presented.

The application of the describing function method to the direct current control loop of an h.v.d.c. system is the object of Chapter Five.

Input signals of 50, 100 and 150 Hz are considered and the influence of imbalance/distortion of the a.c. voltage waveform on the describing function locus are assessed. Several application examples are presented for both finite and infinite a.c. systems.

The use of the describing function for stability studies is also dealt with in this chapter. The Nichols chart is the technique used for the prediction of limit cycles.

Chapter Six deals with the experimental confirmation of the theoretical results. First the apparatus used to measure the describing function is outlined. Test describing functions for a 50, 100 and 150 Hz modulating signal and different short-circuit ratios are presented and compared with theoretical predictions. Also the experimental confirmation of predicted limit cycle oscillations is carried out for different bandwidths of the current control loop.

A new controller whose objective is to minimise the non-characteristic harmonics generated due to imperfections in the a.c. system is outlined in Chapter Seven. Two control policies are suggested. With the use of a spectrum analyser and a waveform generator the new controller was simulated and tested. Oscillograms of the behaviour of the new controller are shown, and its performance assessed.

Concluding remarks and scope for further work in this field are discussed in Chapter Eight.

Chapter Two

CONTROL SYSTEMS FOR H.V.D.C. CONVERTERS

2.1 Introduction

The basic control system of an h.v.d.c. converter normally controls either the direct current through the rectifier or the extinction angle of the inverter.

The basic control system performs two tasks:

a) It produces an error signal (normally current or extinction angle error) by comparing a reference quantity with a measured quantity;

b) Based on the error signal it produces a train of pulses which are applied sequentially to the converter valves. These pulses are generated according to a specified control law.

The basic control system can thus be divided into two separate units: the "error processing unit", which performs task a), and the firing control system, which performs task b).

As all the control functions are performed in the firing control system, this system is of paramount importance in the stability of converters under closed-loop control.

In the first h.v.d.c. system to be put into operation, the so-called individual phase control was used. In this type of firing system the pulses are generated individually for each

valve simply by detecting the voltage zero crossing of the respective commutating voltage and allowing a certain time to elapse before the pulse is generated. In terms of electronic circuitry this can easily be accomplished by starting a ramp generator at the voltage zero crossing, and producing a pulse when the output of this generator is equal to a control voltage. A linear relationship between firing angle and control voltage is therefore achieved. In order to achieve good accuracy, the slope of the ramp must be changed according to the a.c. system frequency.

The drawbacks of the individual phase control were pinpointed in 1967 by Ainsworth (26) and are well known. With unbalanced and/or distorted a.c. voltages, the voltage zero crossings are not equally spaced at 60 electrical degrees, with the result that the firing of the valves is not equidistant. The generation of uncharacteristic harmonics, due to the voltage unbalance and/or distortion is aggravated by the non-equidistant firing. This may result in a limit cycle characterised by great magnification of some of these harmonics. Note that this phenomenon named "harmonic or voltage loop instability" is prone to occur when the a.c. source impedance is relatively high and has nothing to do with current or extinction angle control. The converter may exhibit this type of instability under open-loop operating conditions.

The second generation of converter firing systems was based on a voltage-controlled oscillator (2, 21, 25), producing a train of pulses at the firing frequency - six times the a.c. frequency for a 3-phase bridge. The pulses are routed sequentially to the six converter valves via a ring counter. Since the firing

instants are not derived from the voltage zero crossings of the commutation voltages, the firing is truly equidistant in the steady-state. The conditions for magnification of a.c. bus voltage harmonics due to firing instant irregularities no longer exist. This, however, does not imply that there can be no uncharacteristic harmonic magnification which may be caused by other mechanisms. However, experience has shown that operation with much weaker a.c. systems is possible when v.c.o. based firing systems are used.

Operation under current control is detrimental with respect to abnormal harmonic generation. If the a.c. voltage is unbalanced and/or distorted, the direct current will contain abnormal harmonics. When this current is fed back into the controller, these harmonics, although filtered, may be sufficient to cause firing angle irregularity and precipitate harmonic magnification.

Both types of v.c.o. firing system can be built using either analogue or digital techniques.

Although in all h.v.d.c. schemes to date the firing control system has been implemented using analogue circuitry, proposals have been made for digital controllers using hard-wired logic (22, 23). Also minicomputers (24, 28) and microcomputers (29, 30, 31, 32, 33, 34) have been proposed to implement the firing control system.

This chapter describes the implementation of a firing control system using the T.M. 990/101M microcomputer, which is a TMS 9900 microprocessor based system.

Section 2.2 describes the principle of operation of the different types of v.c.o. based systems.

Section 2.3 briefly describes the basic design features of the firing control system, and section 2.4 discusses the behaviour of the firing control system implemented, comparing it with the behaviour of a previously implemented digital control system (33) and with its analogue equivalent (21).

2.2 Types of control systems

Since the individual phase control has long been abandoned, only the v.c.o. based systems will be considered.

In principle a voltage controlled oscillator is a voltage to frequency converter, i.e. it converts an input d.c. voltage into a train of pulses whose frequency is proportional to the input voltage.

In a converter system, the frequency of the firing pulses in steady-state must be an exact multiple of the a.c. bus frequency.

To control the converter d.c. voltage (and therefore the d.c. current) a change in the phase of the firing pulses rather than in the frequency must be implemented.

A change in phase can however be achieved by changing transiently the frequency of the oscillator with the proviso that this frequency returns to the steady-state value after the desired change in phase has been achieved.

Since the variation in phase with regard to some reference is the integral of the variation of frequency, a voltage to frequency converter exhibits from a control point of view an integral characteristic, i.e. the output is the integral of the input. This type of firing arrangement is sometimes named

Pulse Frequency Control System (PFC).

The operation of this firing control system is explained with the help of figure 2.1.

In figure 2.1(a) the sawtooth generator is basically a capacitor which is charged at a constant rate by a constant current source and discharged by the output pulses of the monostable, which are produced whenever the control voltage V_c equals the sawtooth voltage.

As long as the control voltage remains at a steady level, equidistant firing pulses will be generated. A step increase or decrease on the control voltage V_c will produce a continuous constant frequency change on the firing pulses with consequent cumulative changes on the firing angle. The period of the firing pulses is proportional to the control voltage.

$$T = \frac{K_1}{w_o} V_c \qquad (2.1)$$

where K_1 is the slope of the ramp in figure 2.1(b).

If the control voltage is changed by an amount ΔV_c the period will vary $K_1 \Delta V_c$ and the firing angle ϕ will change linearly with time:

$$\Delta\phi(nTs) = K_1 \Delta V_c n \qquad (2.2)$$

$$n = 1, 2, 3, \ldots.$$

An integral relationship therefore exists between the firing angle and the control voltage.

To ensure that the frequency of the oscillator returns to its steady state value, the control voltage is the output of the "error processing unit". This ensures the synchronisation of the firing pulses with the a.c. system voltage either through

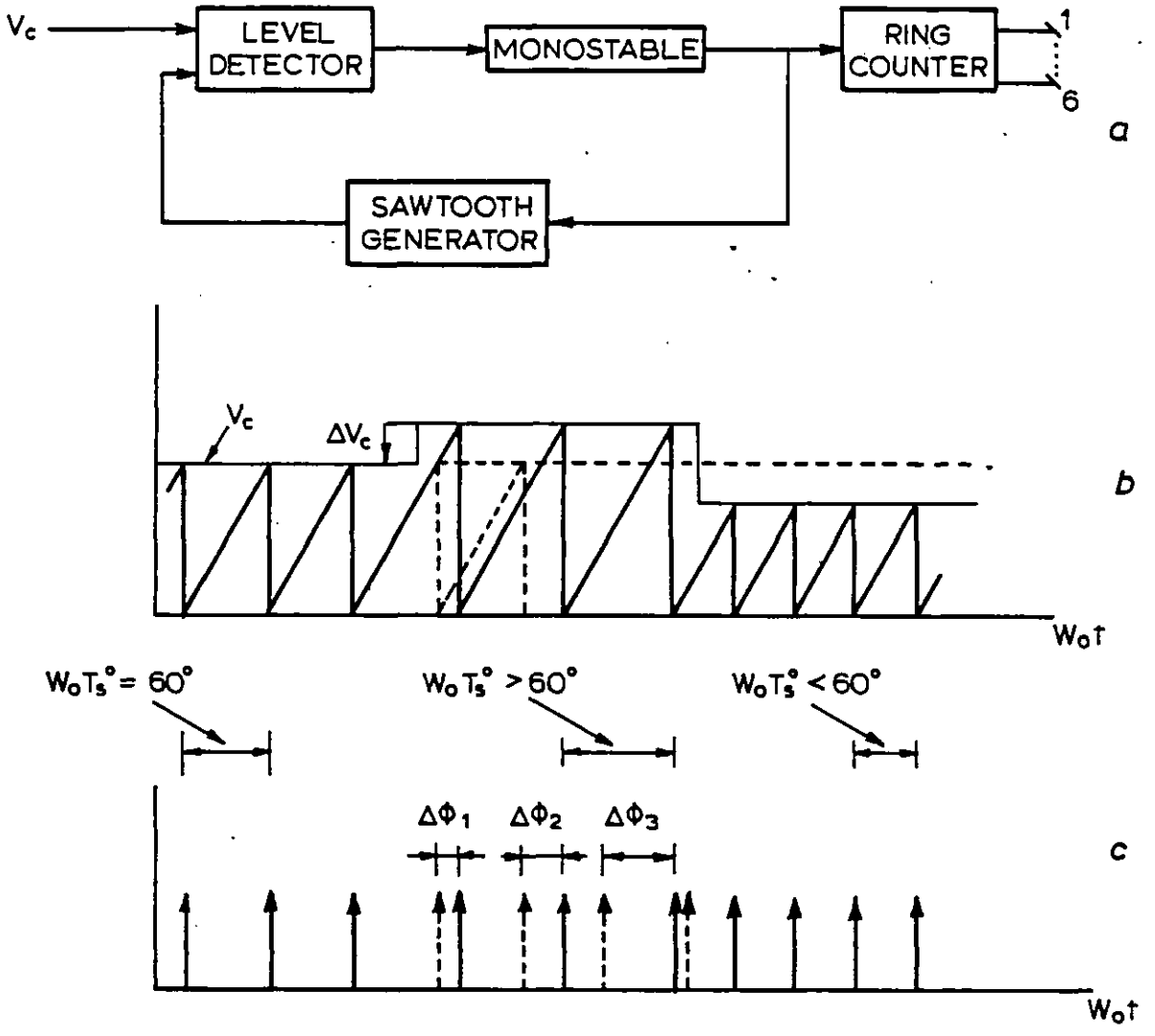

Fig 2.1: Analogue Pulse Frequency Control
(a) Functional block diagram
(b) Output of the Sawtooth Generator
(c) Firing pulse train

the d.c. current measurement or through the constant firing angle or constant extinction angle measurements, depending on the control mode of operation of the converter.

The voltage controlled oscillator can be modified in such a way that the phase of the pulses rather than the frequency is directly proportional to the input control voltage, resulting in the so-called Pulse Phase Control system (PPC).

One possible solution of achieving this modification is shown in figure 2.2. The v.c.o. capacitor is not discharged to zero voltage but only to voltage level V_{c_2}, charging beginning again immediately. V_{c_2} is given by the difference between V_c and V_{c_1}, assuming $V_{c_3} = 0$. As V_{c_1} is constant, any increase in V_c by a small amount ΔV_c will produce an identical increase in V_{c_2}, and the frequency of the firing pulses remains unchanged although their phase varies by an amount $\Delta\phi$ proportional to ΔV_c.

Synchronisation of the firing pulses with the network voltage is ensured through an auxiliary feedback loop yielding output voltage V_{c_3} which keeps the average value of α "tied" to a firing angle reference directly related to the control voltage and to any change in a.c. system frequency. The response of this loop is made very slow in order to prevent voltage-loop instability. Also the α-control amplifier is given a proportional-integral characteristic so that no steady-state error occurs in the actual value of α. This auxiliary α-control-loop also ensures a unique relationship between V_c and α.

Due to the auxiliary α control-loop the main feedback loop (either current or extinction angle) is not needed to ensure synchronisation with the a.c. system frequency and therefore the PPC can be used with the main feedback loop open.

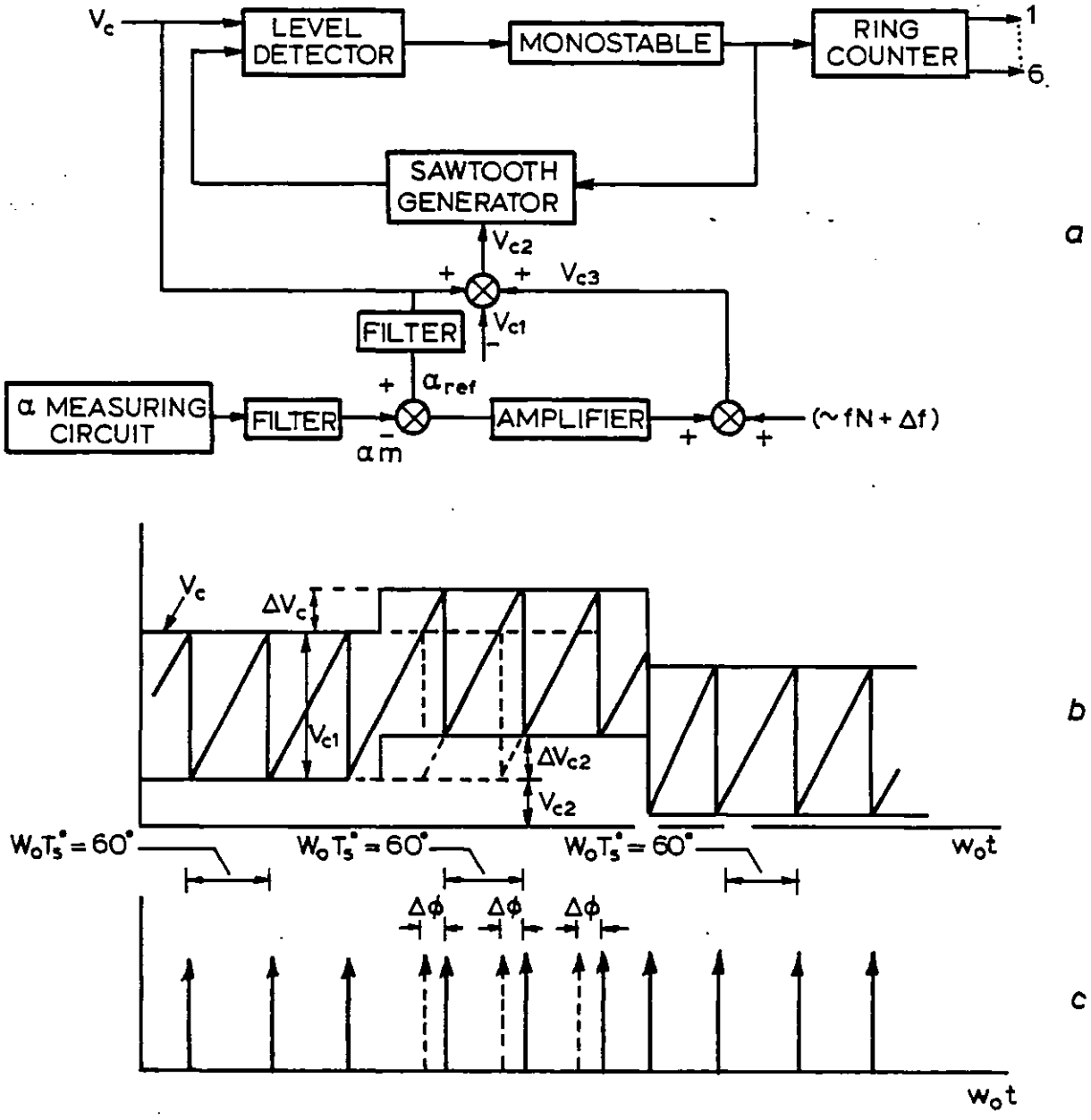

Fig 2.2: Analogue Pulse Phase Control
(a) Functional block diagram
(b) Output of the sawtooth generator
(c) Firing pulse train

The major difference between the PPC and PFC as far as hardware implementation is concerned resides in the fact that the sawtooth generator capacitor is discharged by a fixed amount rather than to zero volts.

Although the poor dynamic performance of PFC systems, due to the integral characteristic, can be overcome through compensation, the PPC possesses some advantages which make it more attractive for h.v.d.c. control, namely:

a) The proportional characteristic results in a larger stability margin;

b) Operation with constant firing angle is implemented simply by setting a constant control voltage;

c) The converter gain Vd/Vc can be made independent of the converter control angle α by introducing a $\cos^{-1}$ circuit between the "error processing unit" and the firing control system.

2.3 Microprocessor-based digital control system

2.3.1 Basic design features

The basic design features of the TM990/101M microcomputer based firing control system are similar to the ones described in (33).

The main differences result from the fact that the scheme implemented in (33) was based on a 24-bit purpose built bit-slice microprocessor, whereas the present scheme is based on a 16-bit general-purpose microprocessor, commercially available.

The TM990/101M (35) is a self-contained microcomputer on a single board. This microcomputer board includes a central processing unit (CPU) with hardware multiply and divide,

programmable serial and parallel input/output lines, external interrupts and a debug monitor to assist in programme development. It also includes

- 4K bytes of random-access memory
- 2K bytes of erasable programmable read-only memory (EPROM) preprogrammed with the debug monitor
- 2K bytes Eproms preprogrammed with a line-by-line assembler code
- 3 MHz crystal-controlled clock
- A 16 bit parallel input/output port as well as a local serial input/output port
- 17 prioritised interrupts - including Reset and Load functions.

The division of tasks performed by hardware and software was implemented with the aim of achieving as much as possible through software, thus minimising external hardware and increasing reliability (32, 33).

2.3.1.1 Hardware design features

The overall block diagram of the microcomputer based control system is shown in figure 2.3.

The data acquisition interface is a purpose-built interface unit whose main functions are:

- Firing angle evaluation
- Extinction angle evaluation
- Valve voltage states detection
- Voltage zero crossing interval evaluation
- Counting of the interfiring period - evaluation of real value of the interfiring period (IFP)

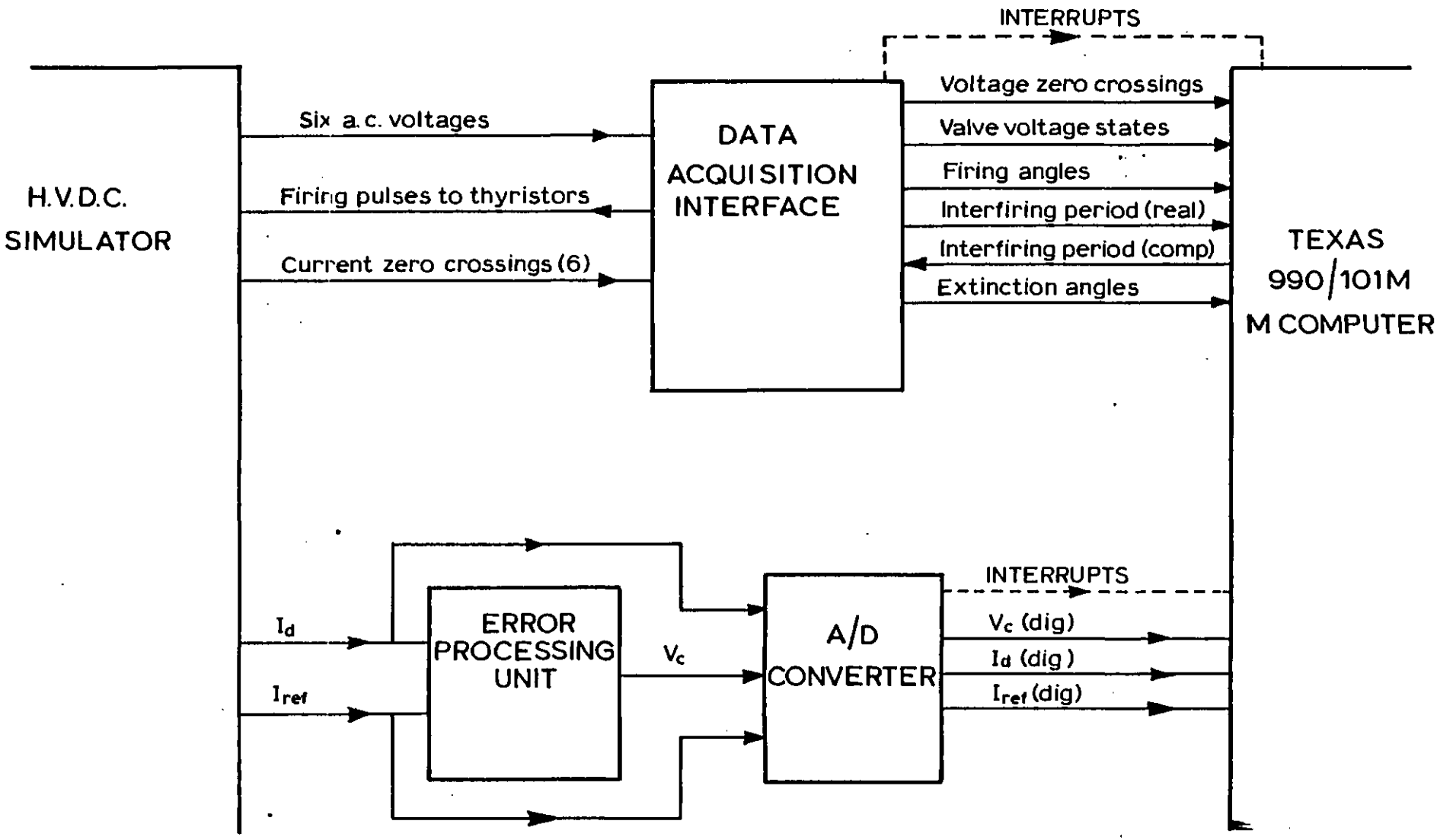

Fig 2.3: Block diagram of the microcomputer based control

- Generation of the firing pulses to the valves
- Organisation of data transfer between the microcomputer and the real system.

A clock generator locked with the a.c. bus voltage provides a synchronous time base for all counters of the DAI. The frequency of this clock generator sets the precision for all the measurements. As the clock oscillates at 180 KHz this corresponds to a definition of 0.1 electrical degrees at 50 Hz.

The "error processing unit" generates the control voltage V_c from the comparison of the reference direct current (Iref) with the measured d.c. current (Id).

An A/D converter digitises V_c, Id and Iref in order that these quantities may be used by the microcomputer. The A/D converter is an RTI 1241-R from Analog Devices (36). It possesses a 16 channel capacity in single-ended connection, an input range of $\pm$ 10v and a conversion time of 25 μs for successive conversions on one channel.

Both the DAI and the A/D converter are perceived by the host computer as a block of words in memory and communication between the microcomputer and the DAI or A/D converter is done in the same way as the microcomputer stores and retrieves memory data.

As most of the hardware design features are similar to the ones developed in (33), only the relevant differences are to be detailed. Appendix A details all the hardware for the microcomputer based control system.

The main difference between the scheme implemented and the one developed in (33) lies in the generation of the firing pulses to the thyristors.

The generation of firing pulses to the thyristors at the appropriate time is accomplished both through hardware and software.

Figure 2.4(a) shows the hardware arrangement for the generation of the firing pulses.

The value of IFP computed through software is stored in Register A. This value is compared with the value of a counter

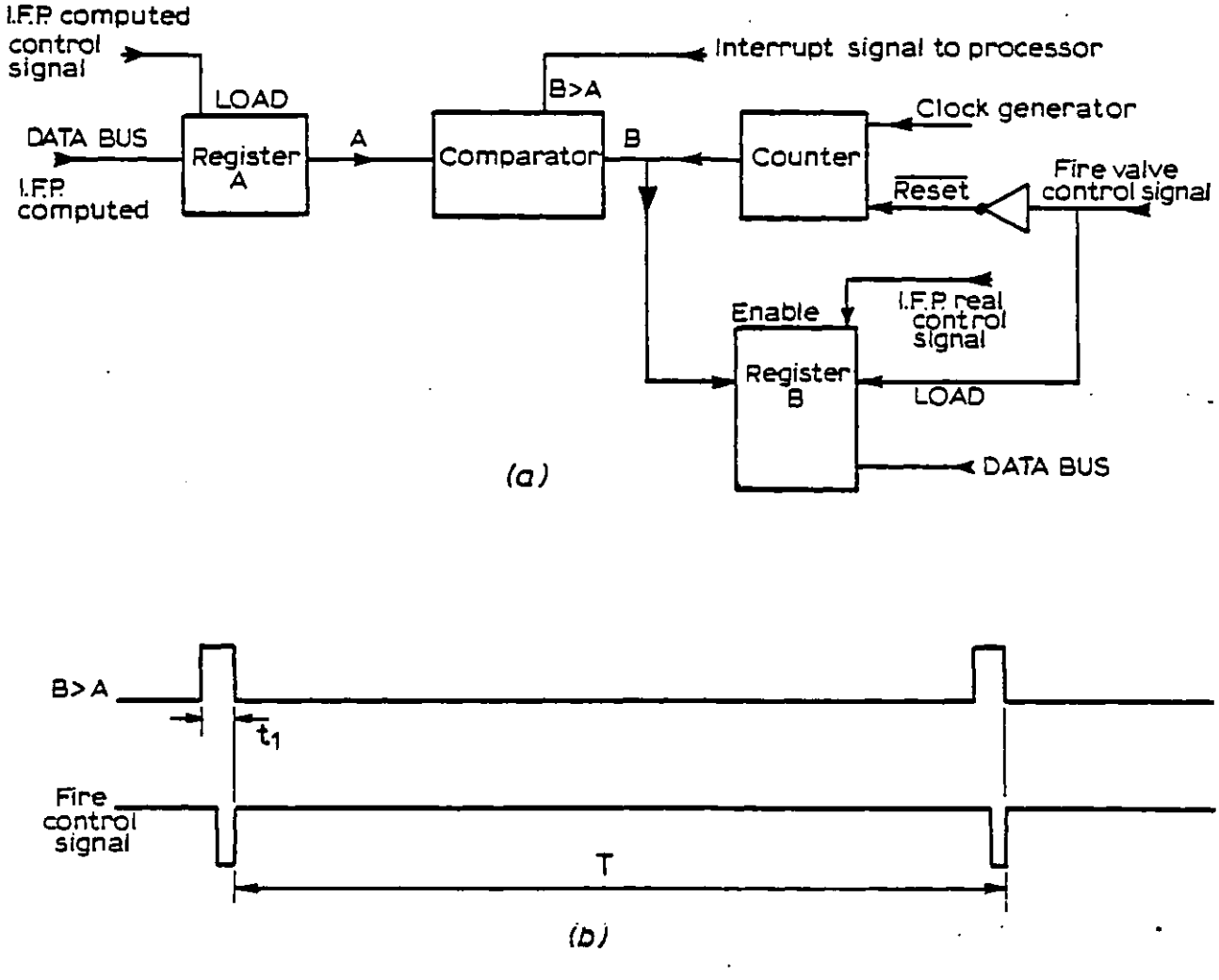

Fig 2.4: Generation of firing pulses
(a) Block diagram
(b) Timing diagram of relevant signals

which is reset every time a valve actually fires. Whenever the value of the counter, 'B', is larger than the value in Register A, an interrupt signal to the processor is generated.

This interrupt signal (which possesses the highest priority) routes the software program to a routine which generates the firing order if the voltage across the valve to fire is positive. If this voltage is not positive a waiting loop occurs. However, the value of the counter is stored in Register B and the counter reset, only when the firing of the valve actually occurs. This may be recognised in figure 2.4(b) by noticing that the signal B > A returns to the inactive state only when the fire control signal changes its state from the low level to the high level.

In (33) the generation of the interrupt signal is responsible for resetting the counter and loading the value of the counter in Register B, i.e. the transition of B > A from the low level to the high level is responsible for storing the value 'B' in Register B and resetting the counter.

2.3.1.2 Software design features

One of the main advantages of a digital controller stems from the fact that a change in control policy may be accomplished by simply changing the software, the hardware being the same. Thus with the present hardware set-up either the PFC or the PPC control algorithms may be implemented.

The type of control algorithm implemented was the PPC. This was chosen because the PPC controller may be operated under open-loop conditions, and thus the theoretical predictions for the describing function can be confirmed by tests.

Three versions of the PPC have been previously developed (32, 33). In the version implemented, multirate sampling of the control voltage is carried out between firings. In the present scheme, 17 samples of the control voltage are obtained between firings. The latest sample of the control voltage is the one used to determine the computed value of IFP.

As in the case of the analogue equivalent (section 2.2), an auxiliary α control loop is needed. A block diagram of the PPC controller implemented is shown in figure 2.5.

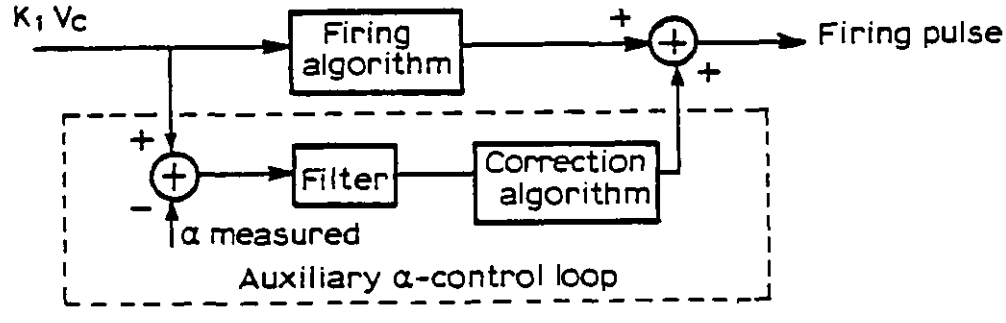

Fig 2.5: Pulse phase control. Functional block diagram.

The algorithm for the computation of IFP is given by:

$$(IFP)_n = (IFP)_{nom} + K_1 \left[(V_c)_n - (V_c)_{n-1}\right] + (\alpha_c)_{n-1} \qquad (2.3)$$

$$n = 1, 2, 3, \ldots$$

where $(IFP)_{nom}$ is a constant, defined when $(V_c)_n$ equals $(V_c)_n - 1$ and $(\alpha_c)_n - 1$ equals zero. This constant must be defined in such a way that the actual value of IFP under these conditions be 60°. $(V_c)_n$ stands for the last value of control

voltage V_c sampled immediately before the firing, $(V_c)_{n-1}$ stands for the control voltage at the previous firing instant, K_1 is a constant derived from the clock generator frequency and the A/D converter setting, and $(\alpha_c)_{n-1}$ is the correction due to the auxiliary α control-loop which is computed at the previous firing instant. The action of this α control-loop is made purposely slow in order that the direct influence of the system voltage waveshapes on the firing pulses be reduced to a minimum (21).

The filter implemented is a moving average filter, and its correction algorithm was given an integral characteristic in order that in steady state the mean value of α measured is identical to the mean value of $(K_1 V_c)$ denoted here by α reference.

Due to stability problems (32, 33) the gain of the filter has to be less than one.

As its dynamic performance is degraded for values of gain close to unity, the set value for the gain of the filter was chosen to be 0.25.

A simplified flowchart of the software algorithm implemented is shown in figure 2.6.

The value of $(V_c)_n$ is recomputed after the firing of each valve in order that the controller may withstand the occurrence of fast transients:

$$(V_c)_n = \frac{1}{K_1}\left[(IFP)_{real} - 60^{\circ} - \alpha_{c_{n-1}} + K_1(V_c)_{n-1}\right] \quad (2.4)$$

$$n = 1, 2, 3, \ldots$$

Three levels of interrupt exist, although only two can change the program flow. The highest priority level interrupt corresponds to the firing of a valve.

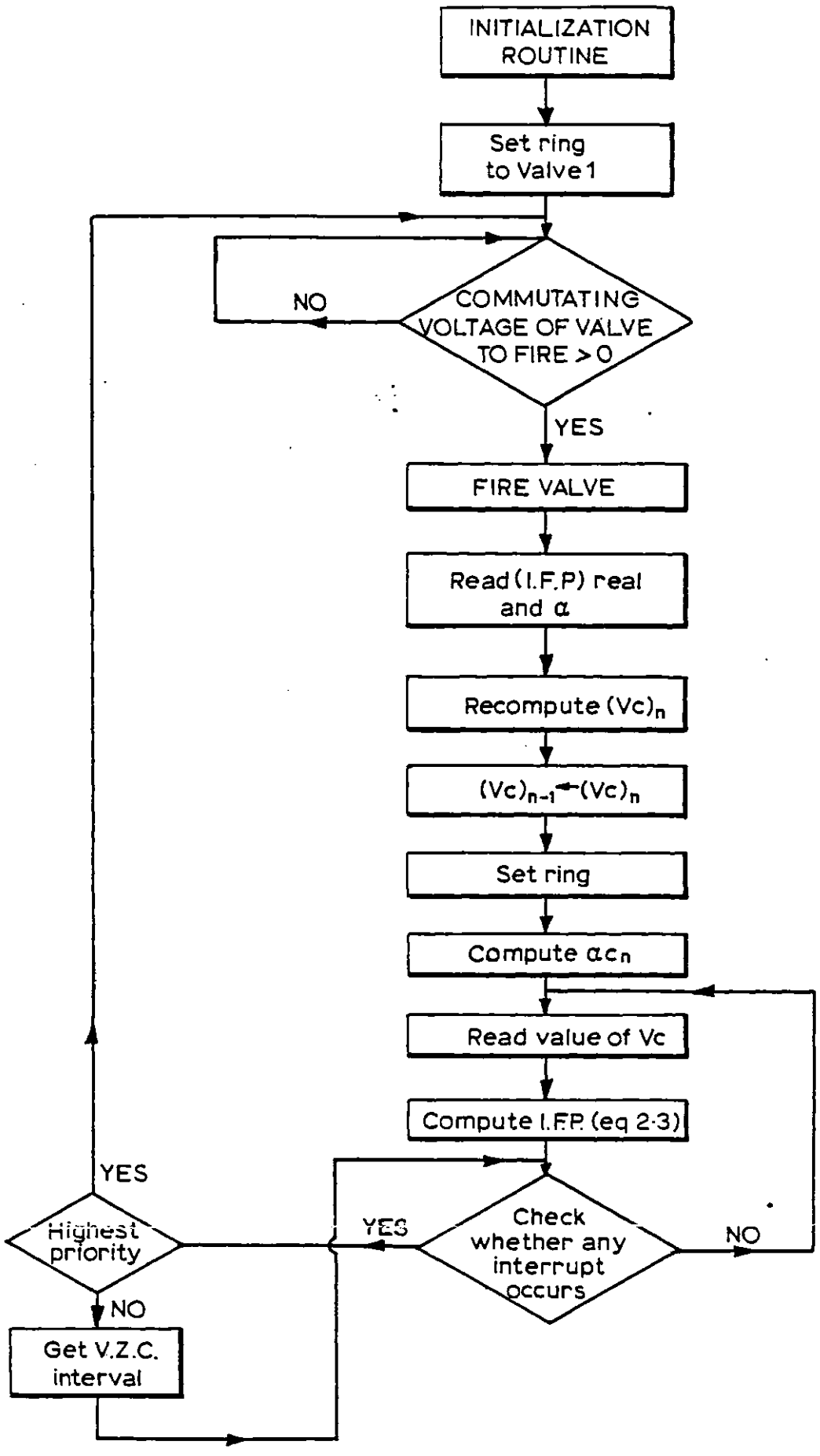

Fig 2.6: Simplified flowchart of control algorithm

The next priority interrupt corresponds to the Analog-to-digital end-of-conversion signal. The lowest priority interrupt occurs whenever a voltage zero crossing occurs. When this interrupt occurs, the program reads the value of the latest voltage zero crossing interval (v.z.c. interval).

Only the highest priority interrupt may occur at any stage of the software algorithm after the "Fire valve" stage in figure 2.6. The A/D end of conversion interrupt does not change the flow of the algorithm. The lowest priority interrupt may only occur after the block "Read value of V_c" in figure 2.6. The constant $(IFP)_{nom}$ is introduced in the algorithm in order that under constant control voltage V_c and with no correction due to the α control-loop the real value of IFP is in fact 60^o and therefore the firing pulses occur equidistantly.

To define $(IFP)_{nom}$ under these conditions, time t_1 of figure 2.4(b) must be known. This quantity corresponds to the time that elapses between the instant the interrupt signal to the processor is generated and the instant the valve actually fires. If the condition "commutating voltage of valve to fire > 0" in figure 2.6 holds, the value of t_1 is approximately 50 μs, i.e. 0.9 electrical degrees. If the condition "commutating voltage of valve to fire > 0" does not hold, time t_1 depends on the instant the commutating voltage becomes positive. This is an extreme case and only happens if the a.c. busbar voltage is very much distorted and/or a modulating signal of considerable amplitude is superimposed on the control voltage V_c. The value of 0.9^o was therefore considered as a basis for the computation of $(IFP)_{nom}$. Thus in principle the value of 59.1^o should be the value chosen for $(IFP)_{nom}$.

However, two other factors contribute for a change in this value:

a) The interrupt signal to the microcomputer is only generated when the value of the counter is greater than the value in Register A (see figure 2.4). As the definition due to the clock generator is 0.1^{o}, the interrupt signal is generated when the value of the counter is 0.1^{o} greater than the value of the register.

b) The reset of the counter in figure 2.4 is synchronous, in other words setting up a low level at the reset input disables the counter and causes the output 'B' to become zero after the next clock cycle. This means that a delay of one clock pulse (i.e. 0.1^{o}) is introduced before the counter begins counting again.

Due to these two factors, the value of $(IFP)_{nom}$ was finally fixed as 58.9^{o}.

In the present scheme the auxiliary α control-loop is needed in order to guarantee synchronism with the a.c. busbar frequency, despite the existence of a clock generator synchronised with the a.c. mains. This is due to the fact that the value of 50 μs evaluated for t_1 is approximated and thus a small slip exists between the actual frequency of firing and the a.c. mains frequency. The only way to cure this problem would be to use a better definition for the measured quantities, i.e. to use a clock generator with a higher frequency.

2.4 Performance of the microcomputer based control system

In all the tests carried out, the newly developed microcomputer based control system performed satisfactorily.

Although the number of samples of the control voltage V_c (17 in 60°) is smaller than the figure quoted in (33) (30 samples in 60°), no differences were detected when comparing the behaviour of both controllers under closed-loop conditions.

However, some differences exist between the behaviour of the two controllers under open-loop conditions:

a) The scheme in (33) does not need the auxiliary α control-loop to guarantee synchronism with the a.c. system frequency under constant control voltage. This is due to the fact that this scheme takes as real value of the interfiring period the instant the value in the counter is greater than the value stored in the register (see figure 2.4(a)) and not the value in the counter when the order to fire is actually given. As shown in figure 2.4(b), a time t_1 elapses between the instant the "B greater than A" signal goes high and the instant "the order to fire the valve" is actually given (the B >A signal becomes inactive).

b) As a consequence of (a) whenever an infringement of the hard α limit occurs in the scheme in (33) the relation between control voltage and firing angle is lost. This situation may be better understood by referring to figure 2.7. In figure 2.7(a) the firing pulse generation is shown, whereas in figure 2.7(b) the pattern of firing pulses is shown. Together with the pattern of firing pulses in figure 2.7(b), the voltage zero crossing instants are shown in hatched line. In this figure a hard α limit situation occurs initially for valve 3. The instant

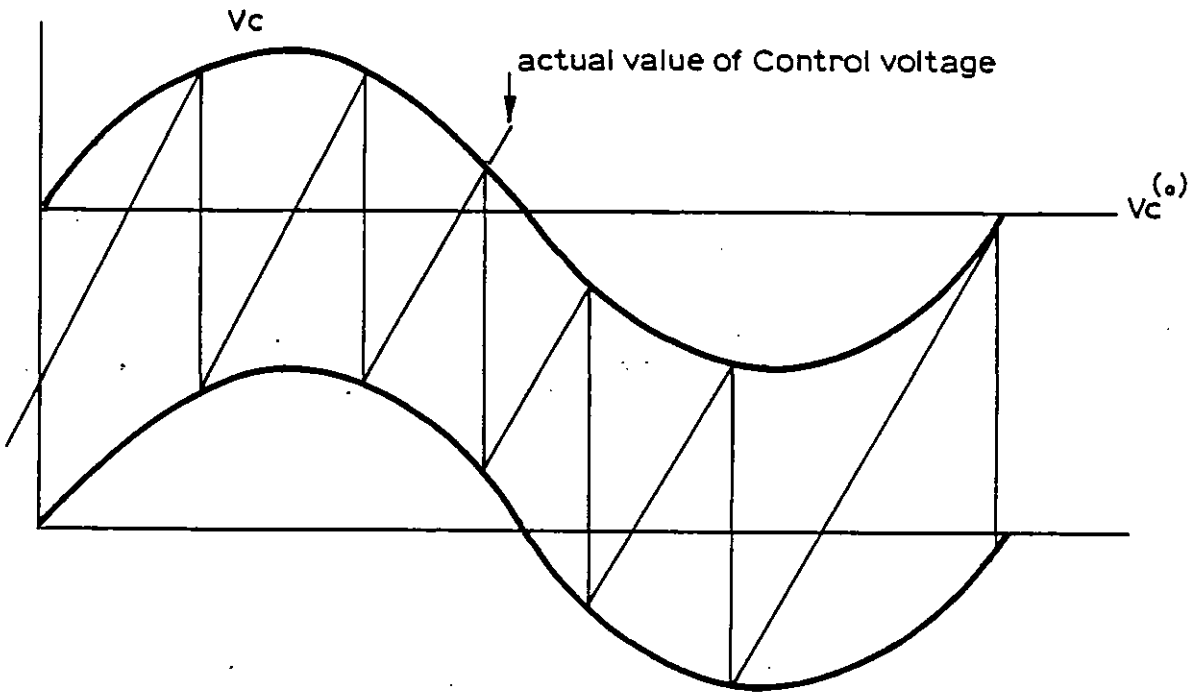

(a) Firing pulse generation

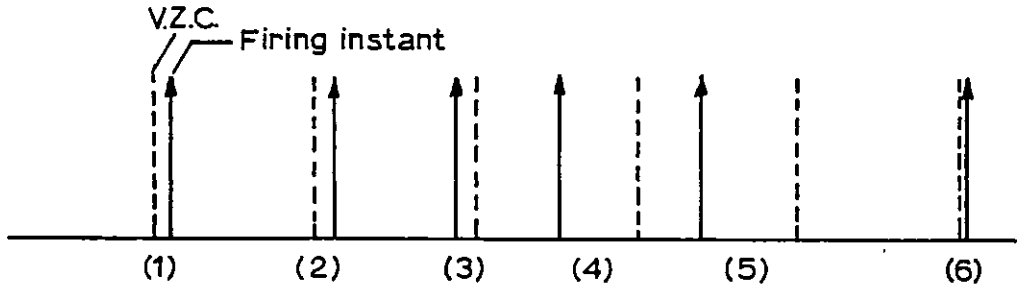

(b) Firing pulses + V.Z.C. instants

Fig 2.7: Hard α limit situation

the signal B > A in the counter of figure 2.4(a) becomes active, occurs before the voltage across the valve is positive. The software programme remains in a waiting loop up to the instant the voltage across the valve changes polarity. However, in the scheme implemented in (33) the instant the signal B > A becomes active is used to store the value of IFP and to reset the counter of figure 2.4(a). Thus the value of $(V_c)_{n-1}$ in equation (2.3) for the computation of the IFP for the next valve to fire (valve 4) does not take into account the actual value of control voltage shown in figure 2.7(a). Valves 4 and 5 tend likewise to hit the hard α limit, a situation that does not occur if the actual value of control voltage is considered.

This situation is only noticeable under open-loop conditions. If the α control loop is active, it tends to correct this situation and temporarily does so. This results in jumps in the firing pattern of the valves. If the α control-loop is not active, all the valves will eventually hit the hard α limit.

When comparing the behaviour of the digital controller with its analogue equivalent (21), some differences were noticed.

a) A digital controller always introduces a delay in the control action. This delay is due to the time necessary for the software to perform its computations. As already mentioned, in the scheme implemented the delay is approximately 3.5^{o} when no hard α limit situation occurs.

b) The digital controller can override a fast transient in the control voltage. This is due to the fact that a minimum limit was imposed on the interfiring period

value (33). In the present scheme this limit is 5 electrical degrees. This value was based on the minimum time necessary to compute the IFP after sampling the control voltage V_c, plus a "safety" factor. The analogue equivalent may miss a pulse whenever the fast transient occurs. The auxiliary α -control loop would then slowly correct this situation.

c) The main difference between the digital controller and its analogue equivalent lies, however, in the behaviour of the auxiliary α control-loop. This difference results from the quantisation error (which is inherent to all digital controlled systems), and the gain of the filter in the α control-loop.

As previously mentioned (see section 2.3.1.2) due to stability reasons the gain of the filter has to be less than unity. The correction algorithm (see figure 2.5) of the auxiliary α control-loop is given an integral characteristic. However, due to quantisation errors this means that the output of the filter is within

$$-0.1^{\circ} < \Delta\alpha < +0.1^{\circ} \qquad (2.5)$$

where $\Delta\alpha$ is the output of the filter. Within this band the correction factor (α_c) is zero.

The output of the filter $\Delta\alpha$ is the error between the mean value of α reference and the mean value of α measured. If the gain of this filter is unity equation (2.5) holds.

However, the gain of the filter has to be less than unity. Thus the correction algorithm acts on a value $K\,\Delta\alpha_{real}$, where $\Delta\alpha_{real}$ stands for the difference between the mean value of

α reference and the mean value of α measured when the gain of the filter is unity. Equation (2.5) results in:

$$-0.1^{\circ} < K\ \Delta\alpha_{real} < 0.1^{\circ}$$

or

$$\frac{-0.1^{\circ}}{K} < \Delta\alpha_{real} < \frac{0.1^{\circ}}{K} \qquad (2.6)$$

As the gain of the filter was fixed as $^{1}/4$:

$$-0.4^{\circ} < \Delta\alpha_{real} < 0.4^{\circ} \qquad (2.7)$$

i.e. in the digital controller for an absolute value of the difference between the mean value of α reference and a mean value of α measured smaller than 0.4° no action is taken by the correction algorithm. Therefore the value $\Delta\alpha_{real}$ is not within the accuracy required (0.1°).

This situation may be seen as an increase in the noise level due to quantisation, and it does not happen in the analogue equivalent.

2.5 Conclusions

This chapter has dealt with the different types of basic control systems used for h.v.d.c. converters, with a main emphasis on the v.c.o. based control systems. The actual implementation of a digital controller based on a Texas TM990/101M microcomputer was briefly mentioned. The relevant hardware and software design features were described, as well as the main differences in the behaviour of the controller implemented relatively to another digital controller and to its analogue equivalent.

The performance (both in steady-state and under transient conditions) of the digital controller was found to be identical to a previously implemented digital controller (33).

Chapter Three

NON LINEAR CONVERTER MODEL

3.1 Introduction

The models so far developed (1, 16) to assess the stability of control systems with controlled converters are only valid for small disturbances.

These models, although useful in predicting the onset of instability, are of limited usefulness for a number of reasons, namely:

1 They fail to predict limit cycle oscillations synchronised with the a.c. system voltage (harmonic instability).

2 They are incapable of taking into account unbalance and/or harmonic distortion in the a.c. bus voltage imposed by the a.c. system.

To determine the conditions of occurrence of harmonic instability the describing function technique is employed in this work. The evaluation of the describing function requires a steady-state non-linear model of the converter, valid for large perturbations. The control voltage is modulated by a signal and the component of the output direct current at a particular frequency is calculated. The complex ratio between

the two quantities yields the describing function.

To achieve this aim, a computer program was developed, since the problem is not amenable to an analytical approach. In this chapter the converter system model is presented, including firing system, converter transformer, a.c. and d.c. systems. Flowcharts of the computer routines are included where appropriate.

The calculation of the a.c. and d.c. harmonics, which is a major part of the computer program, will be dealt with in Chapter Four and the describing function evaluation in Chapter Five.

3.2 Firing System

The three firing control systems used in h.v.d.c. transmission may be simulated in the computer program; individual phase control (IPC), pulse frequency control (PFC) and pulse phase control (PPC). The simulation is based upon the analogue physical realisation of these firing systems.

Although the individual phase control system is no longer employed in new schemes, it was implemented in the initial stages of h.v.d.c. transmission and is still in operation. For this reason and also for comparative purposes it was decided to include the IPC in the computer program.

The purpose of the firing system simulation is the determination of the firing instants and the firing angles with arbitrarily distorted a.c. bus voltage and modulated control voltage. Prior to the determination of the firing angles the voltage zero crossings of the a.c. voltage must be calculated.

3.2.1 Voltage zero crossing evaluation

A three phase representation of the a.c. systems is assumed. The phase-to-neutral a.c. bus voltages are given by the general equation

$$V_i(\omega_o t) = \sum_{h=1}^{p} V_{ih} \sin (h\omega_o t + \phi_{ih}) \qquad (3.1)$$

where 'p' is the number of harmonics considered, ω_o is the fundamental frequency, V_{ih} and ϕ_{ih} are the amplitude and phase angle of harmonic 'h' in phase 'i' (i = R, Y or B).

The instant $\omega t = 0$ of the fundamental component of phase R voltage on the busbar side of the converter transformer is taken as the main reference.

The commutating voltage for a particular valve is given by (the prime denotes valve side quantities)

$$V'_{ik} = V'_i - V'_k \qquad (3.2)$$

where 'i' is the phase connected to the incoming valve and 'k' is the phase of the outgoing valve, which can be determined according to the following table.

Valve	Phases	
1	B, R	
2	Y, B	R - Red
3	Y, R	Y - Yellow
4	B, R	B - Blue
5	Y, B	
6	Y, R	

From equations (3.1) and (3.2) one obtains

$$V'_{ik}(\omega_o t) = \sum_{h=1}^{p} S_h \sin(h\omega_o t) + \sum_{h=1}^{p} C_h \cos(h\omega_o t) \qquad (3.3)$$

where

$$S_h = V'_{ih} \cos \phi'_{ih} - V'_{kh} \cos \phi'_{kh} \qquad (3.4)$$

$$C_h = V'_{ih} \sin \phi'_{ih} - V'_{kh} \sin \phi'_{kh} \qquad (3.5)$$

The voltage zero crossing of the commutating voltage for valve V (V = 1, ... , 6) can be obtained from

$$V'_{ik}(\omega_o t) = 0 \qquad (3.6)$$

This is a non-linear equation which can be solved by the Newton-Raphson method:

$$(\omega_o t)^{(n+1)} = (\omega_o t)^{(n)} + \Delta(\omega_o t)^{(n)} \qquad (3.7)$$

where

$$\Delta(\omega_o t)^{(n)} = - \left. \frac{V'_{ik}(\omega_o t)}{\frac{dV'_{ik}(\omega_o t)}{d(\omega_o t)}} \right|_{(\omega_o t)^{(n)}} \qquad (3.8)$$

$V'_{ik}(\omega_o t)$ is given by equation (3.3) and its first derivative by

$$\frac{dV'_{ik}(\omega_o t)}{d(\omega_o t)} = \sum_{h=1}^{p} h S_k \cos(h\omega_o t) - \sum_{h=1}^{p} h C_k \sin(h\omega_o t) \qquad (3.9)$$

The flowchart for the evaluation of the voltage zero crossings of the commutating voltage is presented in figure 3.1. As can be seen from the table, each commutating voltage corresponds to a pair of valves. The program therefore evaluates the two crossover points of the three commutating voltages (k=1 and k=2 respectively). Tolerance ε is taken equal to 1.0^{-4} kv. The initial estimates of $\omega_o t$ are close to the solutions for the case where there is no distortion and/or unbalance in the a.c. voltages, which are 30^o, 90^o, 150^o, 270^o and 330^o for valves 1 to 6 respectively.

3.2.2 Individual Phase Control (IPC)

Figure 3.2 explains how the firing pulses are produced in this type of firing system. A level detector senses the voltage zero crossing of the commutating voltage; at this point a ramp voltage is initiated and its value compared with a control voltage, a pulse being produced when both are equal. The pulse is amplified and routed to the valve gate.

Taking as time reference the voltage zero crossing of the corresponding commutating voltage, the ramp voltage is for all valves given by

$$R(t) = K_1 \omega_o t \qquad (3.10)$$

Let the control voltage be referred to the main reference

$$V_c(t) = v^o_c + V_m \sin(\omega t + \phi) \qquad (3.11)$$

where the first term v^o_c is set at a value that yields the steady-state firing angle α^o according to the relationship

$$v^o_c = \frac{\alpha^o}{K_1} \qquad (3.12)$$

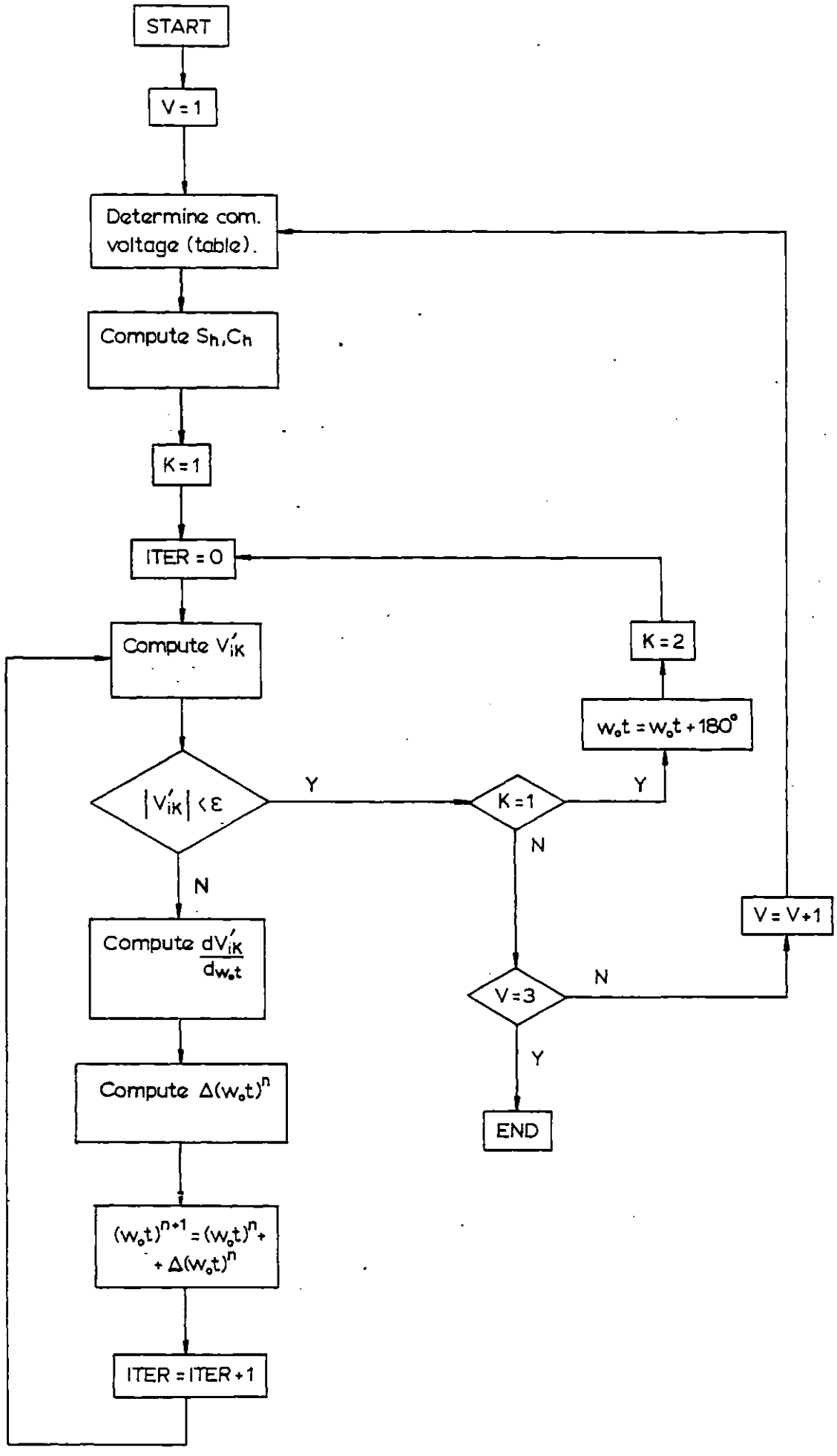

Fig. 3·1

Voltage zero crossings evaluation Flowchart

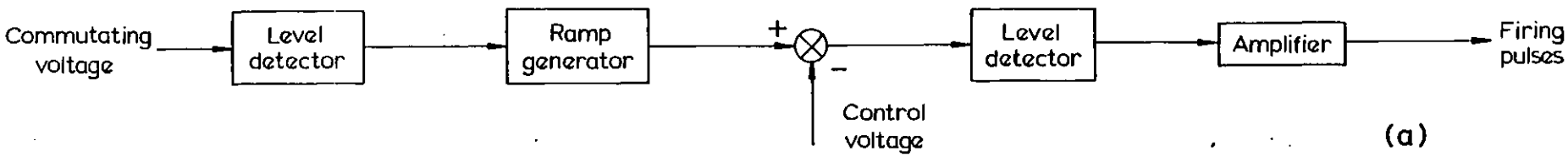

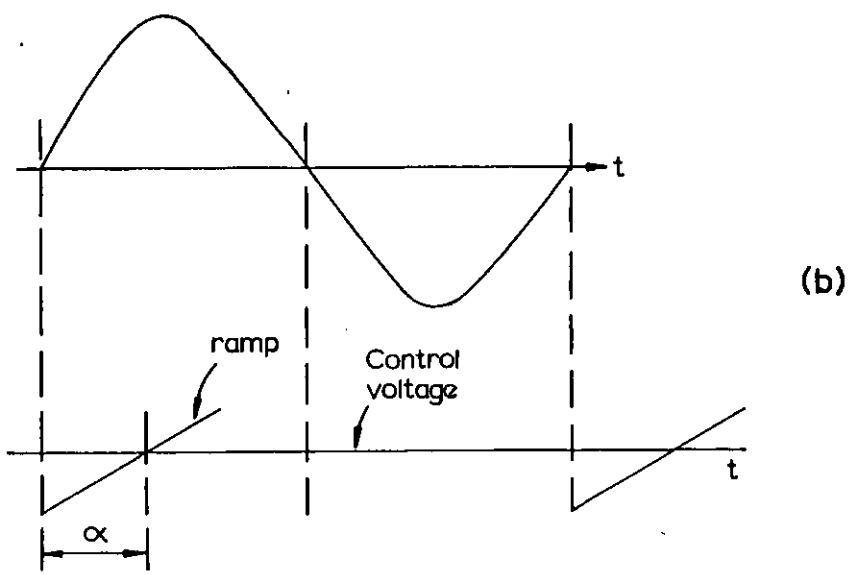

Fig. 3·2 Individual phase control (a) Functional block diagram (b) Firing pulse determination

If there is unbalance/distortion in the a.c. voltage, α^{o} should be interpreted as the average value of the firing angle for all six valves of the converter.

The second term of $V_c(t)$ is a modulating signal of amplitude V_m and frequency ω, which is needed to calculate the describing function. If only the steady-state calculation is derived, then $V_m = 0$.

The firing pulse is produced when

$$R(t) = v_c(t)$$

or

$$K_1 \omega_o t = v^o_c + V_m \sin(\omega t + \phi) \qquad (3.13)$$

Equation (3.13) is non-linear and can be solved by means of the Newton-Raphson method. Setting

$$F(t) = K_1 \omega_o t - v^o_c - V_m \sin(\omega t + \phi) \qquad (3.14)$$

then

$$F'(t) = k_1 \omega_o - V_m \omega \cos(\omega t + \phi) \qquad (3.15)$$

the Newton-Raphson algorithm yields

$$t^{n+1} = t^n + \Delta t^n \qquad (3.16)$$

where

$$\Delta t^n = - \frac{F(t^n)}{F'(t^n)} \qquad (3.17)$$

After convergence, the firing angle is obtained by

$$\alpha = \omega_o t \qquad (3.18)$$

The firing instant of a given valve V, referred to the main time reference can now be obtained

$$F.I.(V) = V.Z.C.(V) + \alpha(V) \qquad (3.19)$$

where V.Z.C.(V) is the voltage zero crossing for valve V, the calculation of which was discussed in section 3.2.1.

The flowchart for the subroutine that simulates the individual phase control is presented in fig 3.3.

3.2.3 Pulse Frequency Control (PFC)

The operation of a PFC system was described in section 2.2, the firing pulse determination being shown in fig 2.1. The system is based on a voltage-controlled oscillator, which in the steady-state operates at six times the a.c. frequency. The frequency of the firing pulses is proportional to the control voltage; the phase is therefore proportional to the integral of the control voltage. The interfiring period, rather than the firing angle, is directly controlled.

As was the case with the IPC system, a firing pulse is produced when the control voltage equals the ramp voltage, equation (3.13). The difference lies in that for the IPC, the ramp is initiated at the v.z.c. of the commutating voltage, whereas for the PFC, the ramp is initiated at the firing instant, since the ramp generator is reset by the firing pulse.

The starting instant of the ramp for the first valve to be fired (assumed to be valve 1) can be calculated from the steady state firing angle α^{o} through the expression

$$t_{in} = -\left[\frac{\pi}{3\,\omega_o} - \left(\frac{V.Z.C.(1)}{\omega_o} + \frac{\alpha^{o}}{\omega_o}\right)\right] \qquad (3.20)$$

This time is referred to the main reference and defines the new reference for the calculation of the firing angle for valve 1. The firing instant for valve 1 defines the reference for valve 2 and so forth. Equation (3.11) for $v_c(t)$ has to be changed accordingly for the calculation of the firing angle for each valve.

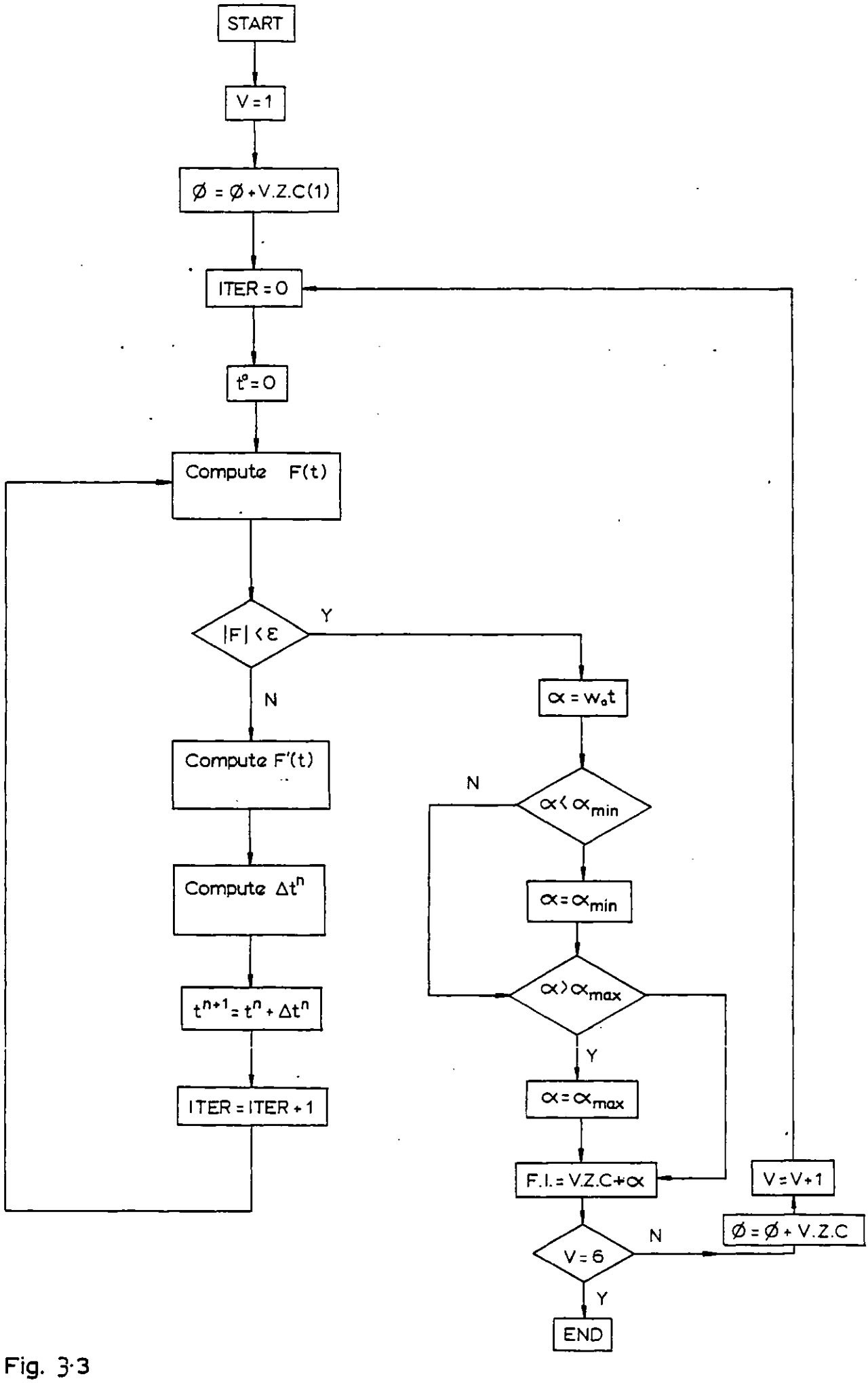

Fig. 3·3

Firing angle evaluation (IPC) Flowchart

The flowchart for the evaluation of the firing angle with the PFC system is presented in figure 3.4. As was the case for the IPC, the Newton-Raphson method is employed.

3.2.4 Pulse Phase Control (PPC)

The operation of the PPC system was described in section 2.2, the firing pulse determination being shown in fig 2.2. The system is also based on a voltage-controlled oscillator, which in the steady-state operates at six times the a.c. frequency. It differs from the PFC, in that the phase of the firing pulses, rather than the frequency, is proportional to the control voltage. This is achieved by letting the capacitor of the ramp generator discharge to voltage v_{c2} and not zero, as is the case for the PFC.

The ramp voltage is therefore

$$R(t) = K_1 \omega_o t + v_{c2} \tag{3.21}$$

where

$$v_{c2} = v_c - \frac{\pi}{3K_1} \tag{3.22}$$

Assuming $v_c(t)$ defined by equation (3.11), a pulse is generated when

$$R(t) = v_c(t) \tag{3.23}$$

or

$$K_1 \omega_o t + v_{c2} = v^o_c + V_m \sin(\omega t + \phi) \tag{3.24}$$

One can now define a function F(t)

$$F(t) = K_1 \omega_o t + v_{c2} - v^o_c - V_m \sin(\omega t + \phi) \tag{3.25}$$

which is formally equivalent to equation (3.14). The Newton-Raphson method can be employed again, the main difference in relation to the PFC being the calculation of v_{c2}.

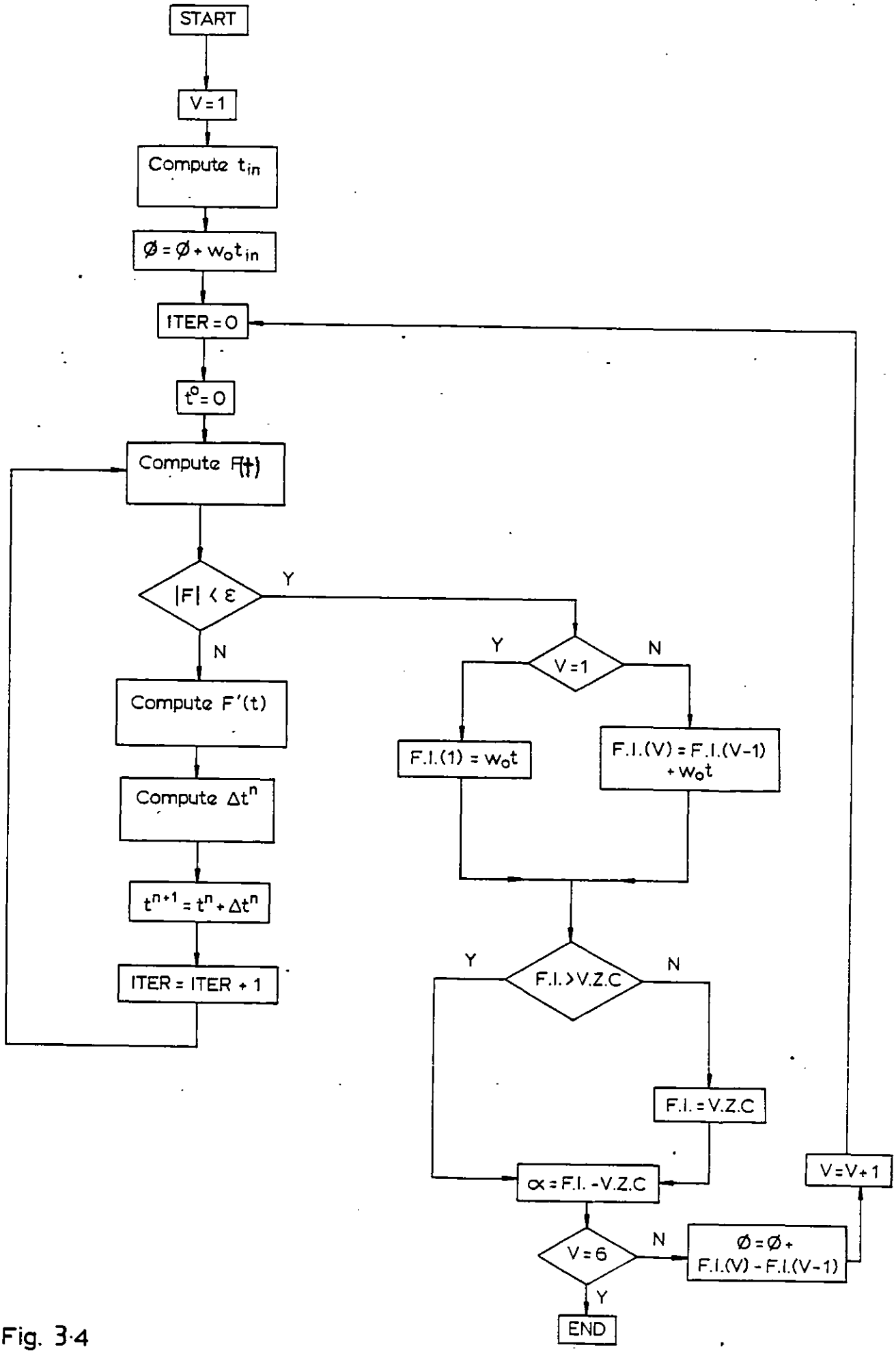

Fig. 3·4

Firing angle evaluation (PFC) Flowchart

Substituting equation (3.11) into equation (3.22), one obtains

$$v_{c2} = v^{o}_{c} + V_m \sin(\omega_o t + \phi) - \frac{\pi}{3K_I} \qquad (3.26)$$

This equation yields the value of v_{c2} at each firing instant.

The value of v^{o}_{c} is initially fixed to give a desired firing angle according to equation (3.12), which also applies to the PPC. A correction must however be added if the firing pulse is generated before the voltage zero crossing for the corresponding valve:

$$\Delta v^{o}_{c} = K_I \text{ (v.z.c. - F.I.)} \qquad (3.27)$$

The flowchart for the computer simulation of the PPC system is shown in fig 3.5.

3.3 Converter Model

A converter can be thought of as a device that transforms alternating voltage into direct voltage and direct current into alternating current. From the d.c. side point of view, given a set of a.c. voltages, the converter output is a d.c. voltage waveform depending upon the particular set of a.c. voltages imposed. From the a.c. side point of view the converter transforms a given d.c. current waveform into a set of three phase a.c. currents.

One can therefore say that from the d.c. viewpoint the converter behaves like a voltage transformer, while from the a.c. viewpoint its action is similar to that of a current transformer. These ideas lead to the "black box" representation of fig 3.6.

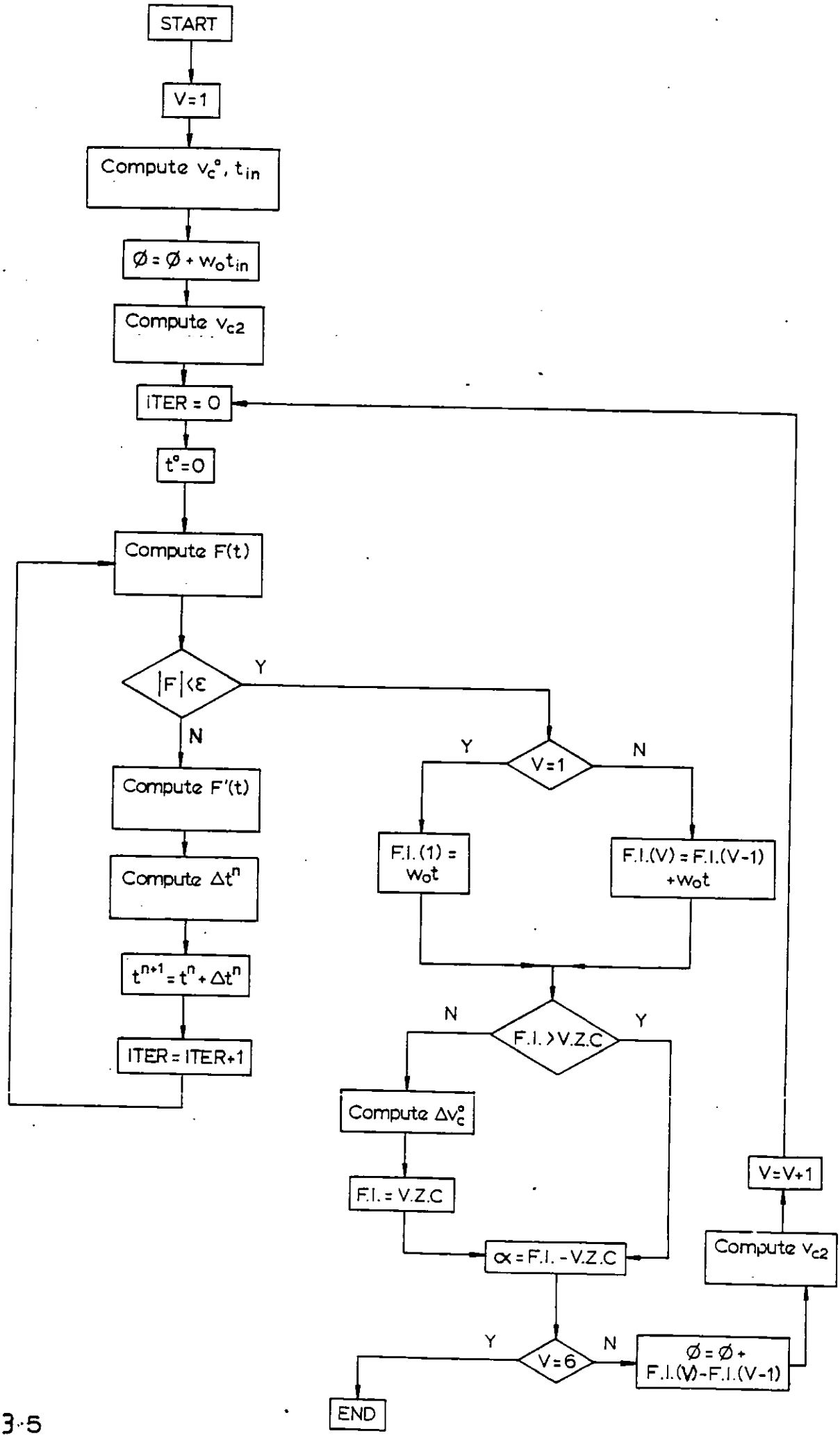

Fig. 3·5

Firing angle evaluation (PPC) Flowchart

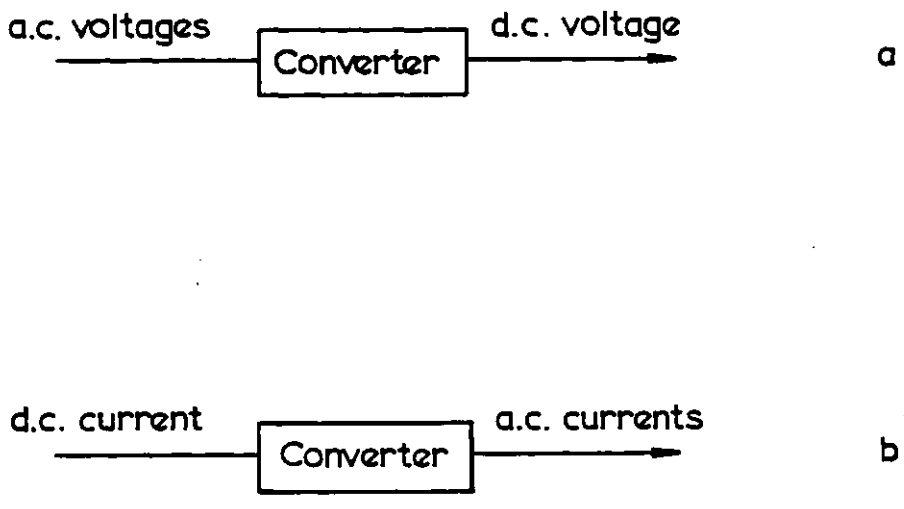

Fig. 3·6

Converter 'black box' representation
(a) From the d.c. side viewpoint
(b) From the a.c. side viewpoint

Both the d.c. voltage and the a.c. current waveforms depend upon the firing instants determined by the firing systems and upon the commutation angles. The existence of a non-negligible reactance in the converter transformer implies that the transfer of the direct current from one current path to another cannot take place instantly. A certain time elapses before commutation is completed, leading to a commutation angle, which has considerable influence on the dynamic behaviour of the converter.

3.3.1 Commutation Angle Evaluation

During a commutation period three valves are conducting as shown in fig 3.7. It is assumed that 'i' is the incoming valve, 'o' the outgoing valve and 'k' the third valve which is in a fully conducting state. The following equations can be easily established:

$$V_i = R_i i_i + L_i \frac{di_i}{dt} + V_{pn} \tag{3.28}$$

$$V_o = R_o i_o + L_o \frac{di_o}{dt} + V_{pn} \tag{3.29}$$

$$i_o + i_i = i_d \tag{3.30}$$

$$\frac{di_o}{dt} + \frac{di_i}{dt} = \frac{di_d}{dt} \tag{3.31}$$

Combining equations (3.28) and (3.29), and taking into account equations (3.30) and (3.31), one obtains

$$v_i - v_o = (R_i + R_o)i_i + (L_i + L_o)\frac{di_i}{dt} - (R_o i_d + L_o \frac{di_d}{dt}) \tag{3.32}$$

As V_i and V_o are phase-to-neutral voltages they can be represented by the general form of equation (3.1)

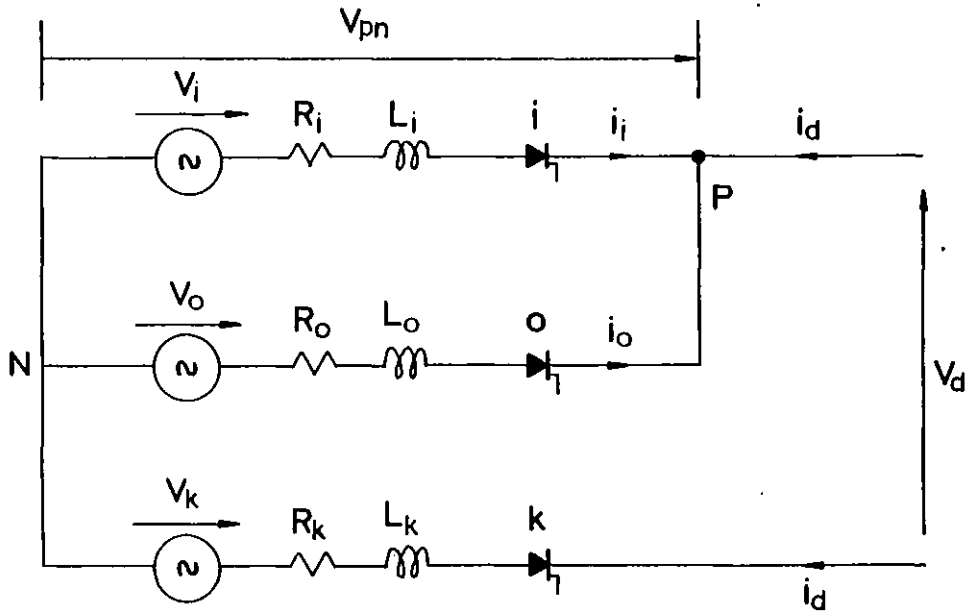

Fig. 3·7

3 - phase bridge during commutation

$$V_i = \sum_{h=1}^{p} V_{ih} \sin (h \omega_o t + \phi_{ih}) \qquad (3.33)$$

$$V_o = \sum_{h=1}^{p} V_{oh} \sin (h \omega_o t + \phi_{oh}) \qquad (3.34)$$

The commutation ceases when the current through the incoming valve equals the direct current,

$$i_i(t) = i_d(t) \qquad (3.35)$$

or, alternatively, when the current through the outgoing valve is zero

$$i_o(t) = 0 \qquad (3.36)$$

In order to solve equation (3.35) or (3.36), it is sensible to take the firing instant as reference. V_i and V_o, which in equations (3.33) and (3.34) are referred to the main reference (voltage zero crossing of phase R voltage) must be changed accordingly. Assuming that θ_i is the firing instant for valve 'i', one has

$$V_i = \sum_{h=1}^{p} V_{ih} \sin (h \omega_o t + \phi_{ih} + h \theta_i) \qquad (3.37)$$

$$V_o = \sum_{h=1}^{p} V_{oh} \sin (h \omega_o t + \phi_{oh} + h \theta_i) \qquad (3.38)$$

whence

$$V_i - V_o = V_{io} = \sum_{h=1}^{p} (S_h \sin h \omega_o t + C_h \cos h \omega_o t) \qquad (3.39)$$

where

$$S_h = V_{ih} \cos (\phi_{ih} + h \theta_i) - V_{oh} \cos (\phi_{oh} + h \theta_i) \qquad (3.40)$$

$$C_h = V_{ih} \sin (\phi_{ih} + h \theta_i) - V_{oh} \sin (\phi_{oh} + h \theta_i) \qquad (3.41)$$

The direct current $i_d(t)$ can be represented by its Fourier expansion as

$$i_d = I_d + \sum_{\ell=1}^{n_d} I_{d\ell} \sin(\ell\omega_o t + \phi_{d\ell}) \tag{3.42}$$

on a time reference defined by the firing instant of valve 1. The reason behind this assumption will become clear later.

A change of reference must now be implemented in $i_d(t)$ for the calculation of the commutation angle, since the chosen reference is the firing instant of the incoming valve θ_i:

$$i_d(t) = I_d + \sum_{\ell=1}^{n_d} I_{d\ell} \sin(\ell\omega_o t + \phi_{d\ell} + \ell(\theta_i - \theta_1)) \tag{3.43}$$

Defining

$$\beta_i = \theta_i - \theta_1 \tag{3.44}$$

equation (3.43) can be rewritten as

$$i_d(t) = I_d + \sum_{\ell=1}^{n_d} (F_\ell \sin \ell\omega_o t + G_\ell \cos \ell\omega_o t) \tag{3.45}$$

where

$$F_\ell = I_{d\ell} \cos(\phi_{d\ell} + \ell\beta_i) \tag{3.46}$$

$$G_\ell = I_{d\ell} \sin(\phi_{d\ell} + \ell\beta_i) \tag{3.47}$$

Note that for $i=1$, $\beta_i = 0$, i.e. there is no need for a change of reference in the calculation of the commutation angle for valve 1.

Inserting equation (3.45) and (3.39) into equation (3.32), one can obtain

$$L_{io}\frac{di_i}{dt} + R_{io}\,i_i = \sum_{h=1}^{p}(S_h \sin h\omega_o t + C_h \cos h\omega_o t) + R_o I_d + \sum_{\ell=1}^{n_d}(R_o F_\ell - \ell\omega_o L_o G_h)\sin \ell\omega_o t + \sum_{\ell=1}^{n_d}(R_o G_\ell + \ell\omega_o L_o F_h)\cos \ell\omega_o t \quad (3.48)$$

where

$$R_{io} = R_i + R_o \quad (3.49)$$

$$L_{io} = L_i + L_o \quad (3.50)$$

Defining the parameters

$$A_\ell = R_o F_\ell - \ell\omega_o L_o G_\ell \quad (3.51)$$

$$B_\ell = R_o G_\ell + \ell\omega_o L_o F_\ell \quad (3.52)$$

equation (3.48) simplifies into

$$L_{io}\frac{di_i}{dt} + R_{io}\,i_i = \sum_{h=1}^{p}(S_h \sin h\omega_o t + C_h \cos h\omega_o t) + R_o I_d + \sum_{\ell=1}^{n_d}(A_\ell \sin \ell\omega_o t + B_\ell \cos \ell\omega_o t) \quad (3.53)$$

This differential equation can be solved by the Laplace transform method, the initial condition being $i_i = 0$, as the incoming valve carries no current before the firing instant. The calculations are presented in Appendix B, the result being equation (B.16).

$$i_i(t) = \sum_{h=1}^{p} [X_{1h}\, e^{-t/T_{io}} + S_{1h} \sin (h\omega_o t + \phi_{1h})] + Y_1(1-e^{-t/T_{io}}) +$$

$$+ \sum_{\ell=1}^{n_d} [X_{2\ell}\, e^{-t/T_{io}} + S_{2\ell} \sin (\ell\omega_o t + \phi_{2\ell})] \qquad (3.54)$$

The various constants are defined in Appendix B.

In order to calculate the commutation angle, equation (3.35) must be solved. The Newton-Raphson method was employed, the function F(t) being in this case

$$F(t) = i_i(t) - i_d(t)$$

$$= \sum_{h=1}^{p} [X_{1h}\, e^{-t/T_{io}} + S_{1h} \sin (h\omega_o t + \phi_{1h})] + Y_1(1-e^{-t/T_{io}}) +$$

$$+ \sum_{\ell=1}^{n_d} [X_{2\ell}\, e^{-t/T_{io}} + S_{2\ell} \sin (\ell\omega_o t + \phi_{2\ell})] - I_d -$$

$$- \sum_{\ell=1}^{n_d} [F_\ell \sin \ell\omega_o t + G_\ell \cos \ell\omega_o t] \qquad (3.55)$$

The flowchart for the calculation of the commutation angle is presented in figure 3.8. An initial estimate of 5^o is assumed for the commutation angle. A three-phase representation is used for the a.c. system, since the phase voltages and the source impedances can be unbalanced. The unbalance in the impedance is mainly due to the converter transformer, since differences of 5 to 7.5% are not unusual for three-phase units. Phase-to-neutral voltages are used throughout the analysis.

The consideration of the d.c. current harmonics greatly increases the computation time, since it implies an iterative

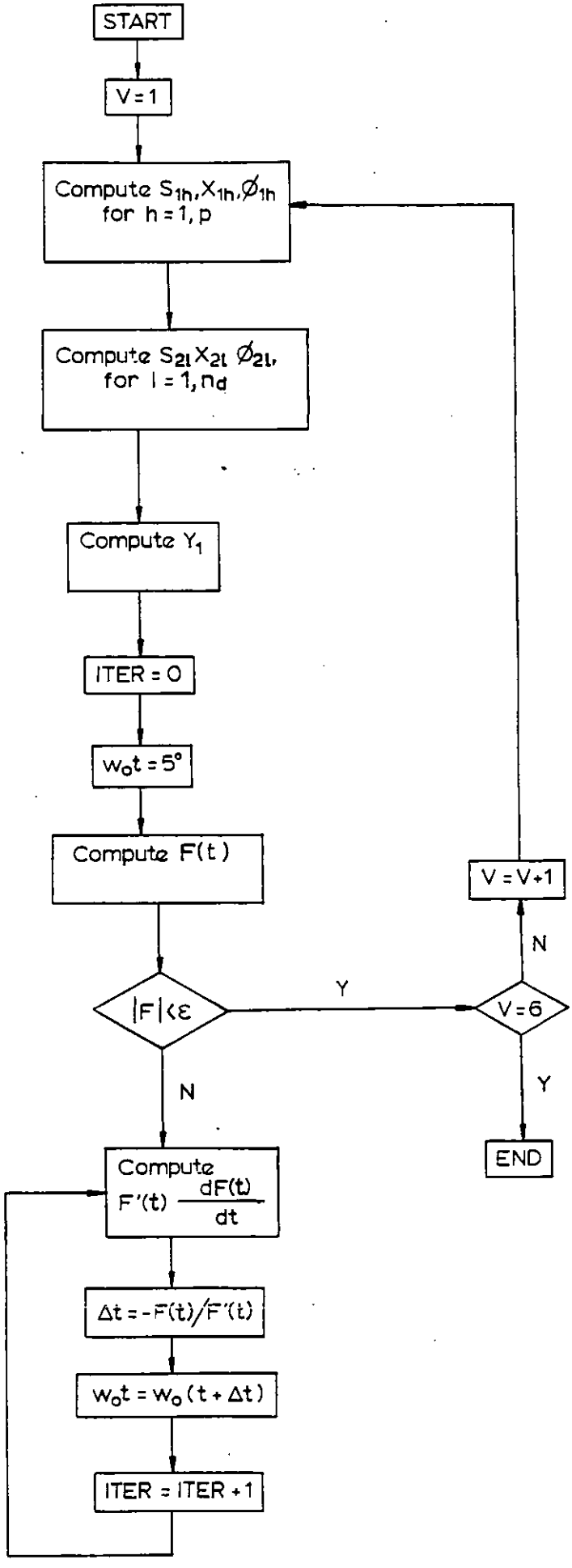

Fig. 3·8

Commutation angle evaluation Flowchart

process, distinct from that required by the Newton-Raphson solution of equation (3.35). The d.c. current harmonics are not known at the outset and must therefore be calculated. However, they are dependent upon the commutation angle which is the object of the calculation. A slowly convergent Gauss method was used to tackle the problem and assess the influence of the d.c. harmonics. This was found to be small, not justifying the expense of an increase by a factor of 50 to 80 in the computation time.

If the harmonics of the direct current are neglected, equation (3.55) simplifies to

$$F(t) = \sum_{h=1}^{p} \left[X_{1h}\, e^{-t/T_{io}} + S_{1h} \sin (h\omega_o t + \phi_{ih}) \right] + y_1 \left(1 - e^{-t/T_{io}}\right) - I_d \qquad (3.56)$$

Test system 1 shown in fig 3.9 was investigated with the following data:

transformer valve side line voltage:	94 kV
transformer reactance per phase:	7.76 Ω
transformer resistance per phase:	neglected
d.c. line resistance:	5 Ω
d.c. line phase smoothing inductance:	0.25 H
firing system:	PPC
nominal rectifier firing angle:	15^{o}
direct current:	0.5 kA
converter type:	six-pulse

Tables 3.1 and 3.2 show the results obtained with and without an input modulating signal at 50 Hz, respectively, for the approximate and correct models.

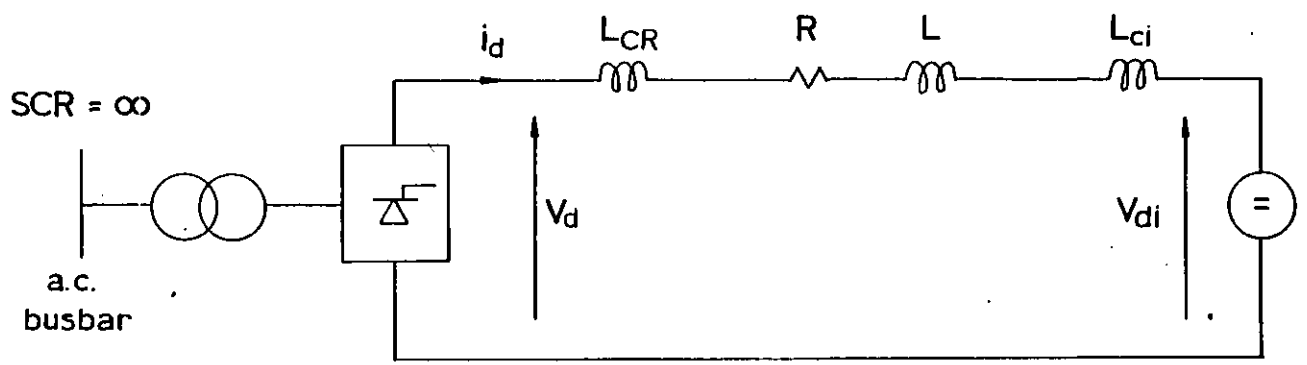

Fig. 3.9

Test system 1

Table 3.1

Commutation angles (no modulating signal)

Valve No.	Approximate Model	Correct Model
1	9.82	9.45
2	9.82	9.45
3	9.82	9.45
4	9.82	9.45
5	9.82	9.45
6	9.82	9.45

Table 3.2

Commutation angles (modulating signal at 50 Hz, $\Delta\alpha = 5^{o}$)

Valve No.	Approximate Model	Correct Model
1	8.54	8.35
2	8.27	7.63
3	9.38	8.54
4	11.25	10.64
5	12.06	11.94
6	10.39	10.49

As can be seen, if no modulating signal is present, the differences are only about 4%; with a modulating signal at 50 Hz, this can increase to nearly 10%.

3.3.2 D.C. voltage and A.C. current waveform description

The firing instant and commutation angle are known for each valve at the present state. The mathematical description of the outputs of the 'black boxes' of fig 3.6 is now possible.

In fig 3.10 the steady-state converter d.c. voltage waveform is shown. The d.c. voltage exhibits a fixed pattern of a commutation period followed by a full-conduction period.

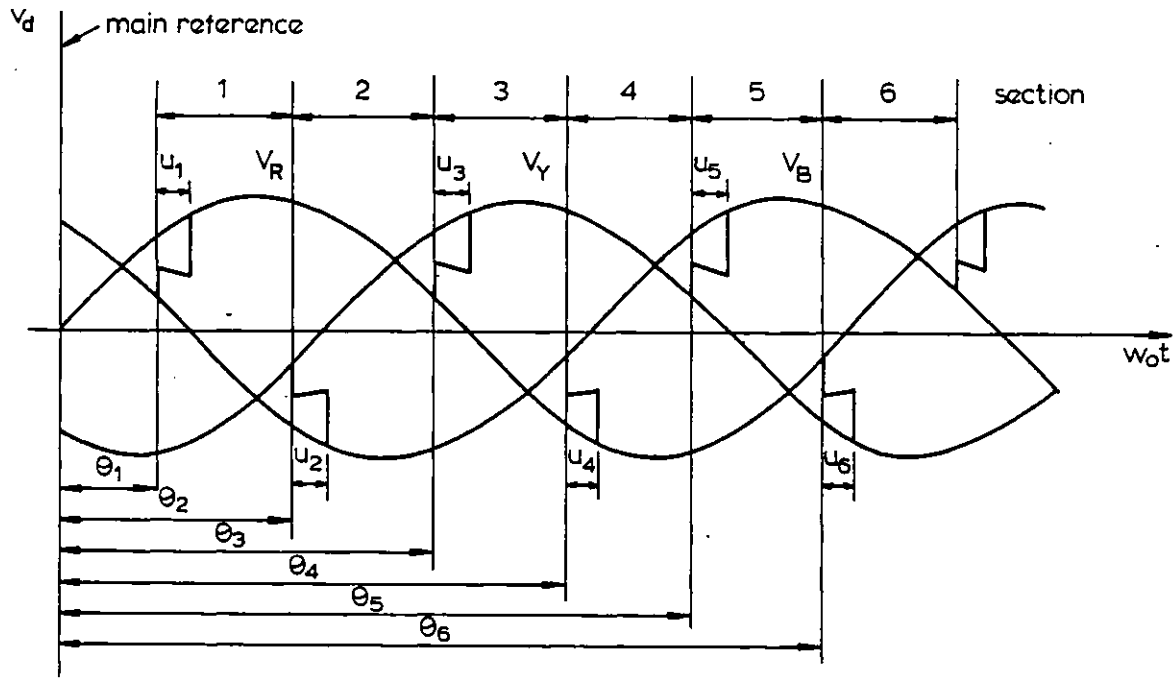

Fig. 3·10

Converter d.c. voltage waveform

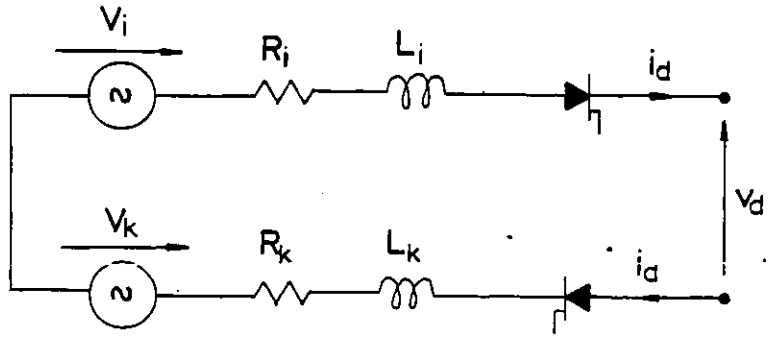

Fig. 3·11

3 - phase bridge during full conduction

In the first period, referring to fig 3.7, the d.c. voltage is given by

$$V_d = V_{pn} - V_k - R_k\, i_d - L_k \frac{di_d}{dt} \qquad (3.57)$$

From equation (3.28), V_{pn} can be written as

$$V_{pn} = V_i - R_i\, i_i - L_i \frac{di_i}{dt} \qquad (3.58)$$

Substitution of equation (3.58) into equation (3.57) yields

$$V_d = (V_i - V_k) - (R_i\, i_i + L_i \frac{di_i}{dt}) - (R_k\, i_d + L_k \frac{di_d}{dt}) \qquad (3.59)$$

From fig 3.11, which represents the converter bridge during full conduction, the d.c. voltage is given by

$$V_d = (V_i - V_k) - (R_i + R_k) i_d - (L_i + L_k) \frac{di_d}{dt} \qquad (3.60)$$

Equations (3.59) and (3.60) describe completely the d.c. voltage waveform. From fig 3.10 it is apparent that six full conduction sections alternate with six commutation sections during an a.c. voltage period. Equation (3.59) is valid for $\theta_i < \omega_o t < \theta_i + u_i$ and equation (3.60) for $\theta_i + u_i < \omega_o t < \theta_i + 1$. The Fourier analysis of the d.c. voltage will be carried out in Chapter Six.

In fig 3.12 the a.c. current waveform in an a.c. phase is shown. θ_i, θ_k, u_i and u_k stand for the firing instants and commutation angles of the valves that are connected to the particular phase represented; θ_l, θ_m, u_l and u_m stand for the firing instants and commutation angles of the valves that begin conduction after the valves connected to the particular phase have ceased to conduct.

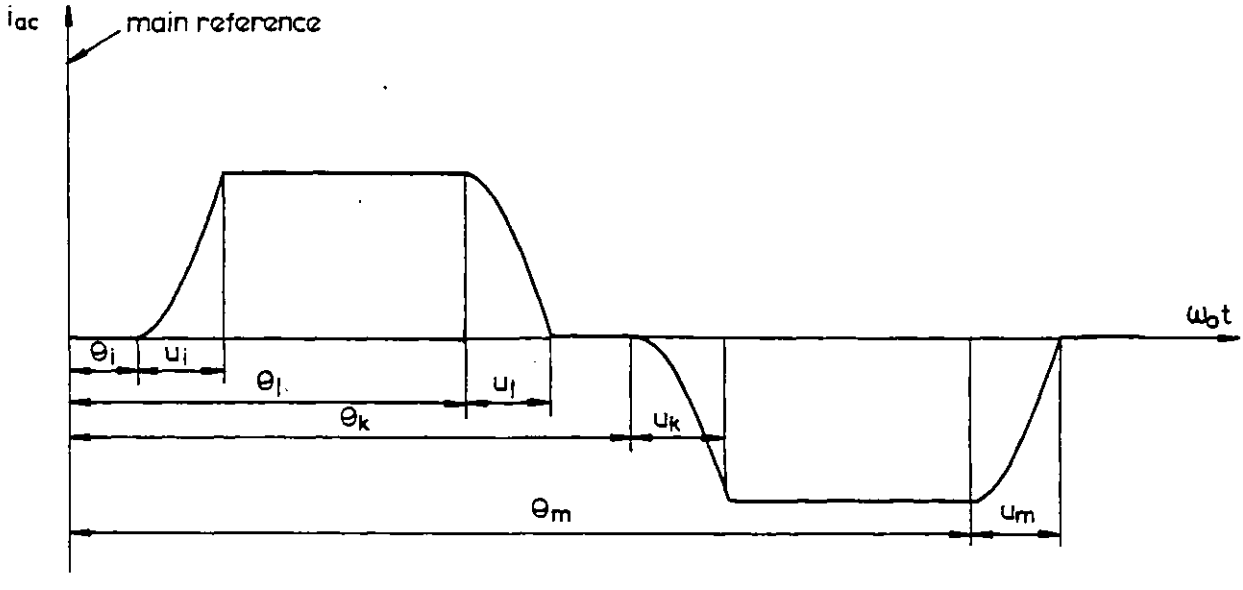

Fig. 3·12

A.C. current waveform

Although not shown in fig 3.12, the effect of the d.c. current harmonics is taken into account. The a.c. current waveform comprises three periods:

i) Full conduction period, in which

$$i_a(t) = i_d(t) \tag{3.61}$$

for

$$\theta_i + u_i < \omega_o t < \theta_l$$

and

$$i_a(t) = -i_d(t) \tag{3.62}$$

for

$$\theta_k + u_k < \omega_o t < \theta_m$$

ii) Commutation period, in which

$$i_a(t) = i_l(t) \tag{3.63}$$

for

$$\theta_i < \omega_o t < \theta_i + u_i \quad \text{or} \quad \theta_k < \omega_o t < \theta_k + u_k$$

and

$$i_a(t) = i_d(t) - i_l(t) \tag{3.64}$$

for

$$\theta_l < \omega_o t < \theta_l + u_l$$

and

$$i_a(t) = -i_d(t) - i_m(t) \tag{3.65}$$

for

$$\theta_m < \omega_o t < \theta_m + u_m$$

iii) Non-conduction period, in which

$$i_a(t) = 0 \tag{3.66}$$

for

$$0 < \omega_o t < \theta_i \quad \text{or} \quad \theta_l + u_l < \omega_o t < \theta_k \quad \text{or} \quad \theta_m + u_m < \omega_o t < 2\pi$$

The d.c. current $i_d(t)$ is described by equation (3.45) and the commutation currents $i_i(t)$, $i_l(t)$ and $i_m(t)$ by equation (3.54).

Equations (3.61) through to (3.66) describe the a.c. current waveform, i.e. the output of the 'black box' of fig 3.6b.

3.4 Converter Transformer

H.v.d.c. systems invariably operate at twelve-pulse, this mode being achieved by connecting two six-pulse converter bridges in series on the d.c. side and in parallel on the a.c. side. Twelve-pulse operation is benificial from the a.c. and d.c. harmonic generation viewpoint. This involves such a substantial reduction in the harmonic filters that in the most recent schemes, operation at six-pulse is not allowed.

The combination of two six-pulse bridges yields a twelve-pulse converter if one of the converter transformers introduces a 30° phase shift with regard to the other. In practice - one transformer is Yny connected, the other Ynd connected, the neutral being isolated from the earth in both cases. In the numerical simulation, each bridge is considered separately; the d.c. voltage and a.c. current of the twelve-pulse converter is the sum of the respective quantities of the individual six-pulse bridges.

The transformer transformation ratio is defined as

$$a = \frac{V_R}{V_r} e^{-j\phi} \qquad (3.67)$$

where V_R is the r.m.s. nominal voltage on the busbar side and

V_r the nominal voltage on the converter side, and ϕ the phase-shift due to the transformer connection (0 for Yny and 30^o for Ynd).

Since the transformer model must be able to handle unbalanced and/or distorted voltage conditions, symmetrical components were adopted in the simulation. For the nth harmonic of the voltage on the busbar side,

$$\begin{bmatrix} V_{Dn} \\ V_{In} \\ V_{on} \end{bmatrix} = [T]^{-1} \begin{bmatrix} V_{Rn} \\ V_{yn} \\ V_{Bn} \end{bmatrix} \tag{3.68}$$

Similarly for the nth harmonic of the current

$$\begin{bmatrix} I_{Dn} \\ I_{In} \\ I_{on} \end{bmatrix} = [T]^{-1} \begin{bmatrix} I_{Rn} \\ I_{Yn} \\ I_{Bn} \end{bmatrix} \tag{3.69}$$

where $[T]^{-1}$ is the inverse of the Fortescue matrix

$$[T] = \begin{bmatrix} 1 & 1 & 1 \\ \alpha^2 & \alpha & 1 \\ \alpha & \alpha^2 & 1 \end{bmatrix} \quad [T]^{-1} = \frac{1}{3} \begin{bmatrix} 1 & \alpha & \alpha^2 \\ 1 & \alpha^2 & \alpha \\ 1 & 1 & 1 \end{bmatrix} \tag{3.70}$$

The positive sequence voltages and currents on the converter side may be obtained through

$$V_{dn} = \frac{V_{Dn}}{a} \tag{3.71}$$

$$I_{dn} = a^* I_{Dn} \tag{3.72}$$

where * is the conjugate of the transformation ratio 'a'.

For the negative sequence, the phase angle of the transformation ratio has to be negated, yielding:

$$V_{in} = \frac{V_{ln}}{a^*}$$

$$I_{in} = a\, I_{ln}$$

This fact is of no importance for the Yny transformer, in which case $\phi = 0$; it should however be fully taken into account for the Ynd transformer.

In fig 3.13 the model of the converter transformer is presented both for the positive and negative sequences. The transformer impedance is the same for both sequences and is taken into account in the calculation of the commutation angle; it should therefore not be included in the transformer model.

The models of fig 3.13 do not apply to the zero sequence. In fig 3.14 the zero-sequence equivalent circuits of the Yny and Ynd transformers are shown. It is clear that since the neutral is isolated on the converter, there can be no zero-sequence currents on this side. Note that the converter under no circumstances generates zero-sequence currents.

$$V_o = 0$$

$$I_o = 0$$

As far as the busbar side is concerned, there can be no zero-sequence currents for the Yny transformer.

$$V_o = 0$$

$$I_o = 0$$

For the Ynd transformer, however, zero-sequence currents can circulate on the busbar side

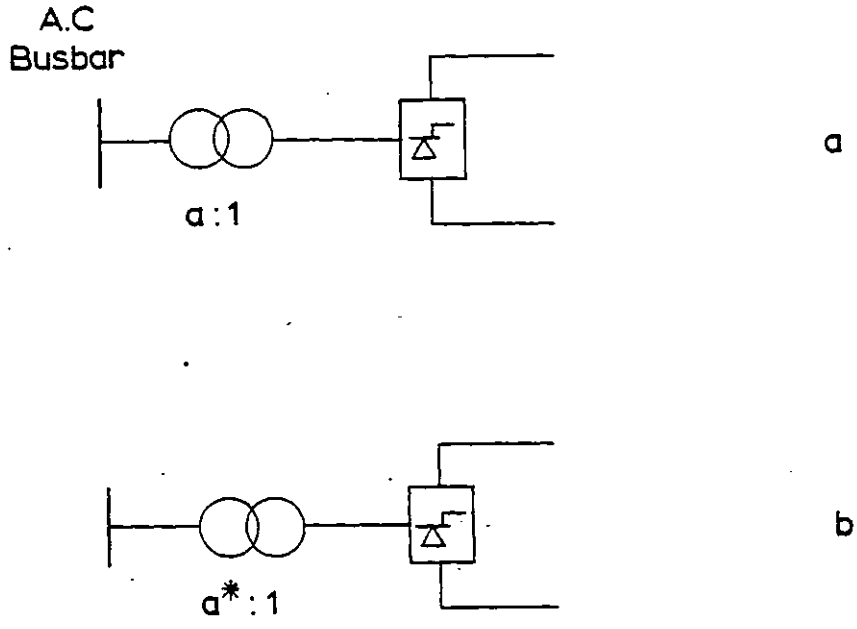

Fig. 3·13

Converter transformer model
(a) Direct sequence
(b) Inverse sequence

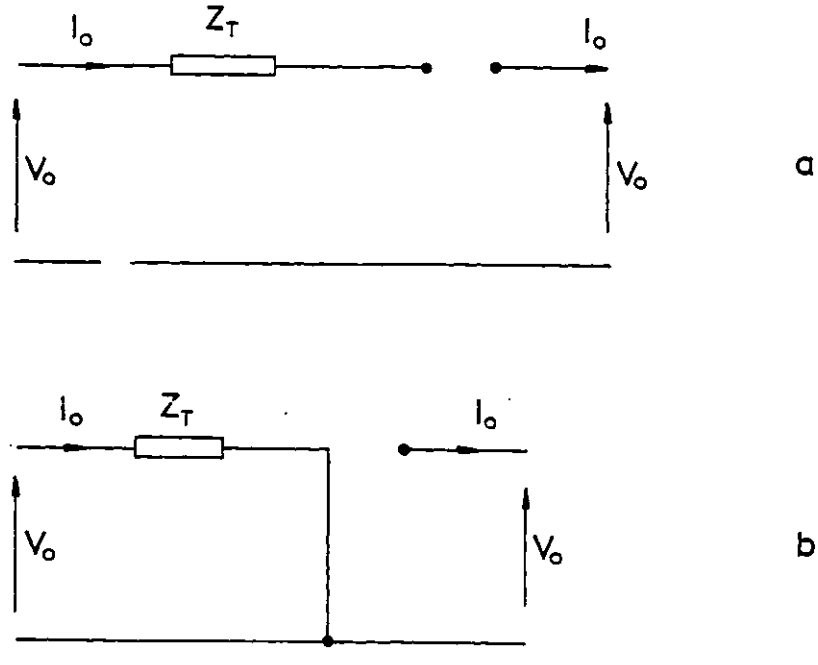

Fig. 3·14

Transformer zero - sequence equivalent circuit
(a) Yn Y connection
(b) Yn Δ connection

$$I_o = \frac{V_o}{Z_r}$$

where Z_r is the short-circuit impedance of the transformer. The zero-sequence current is not generated by the converter, but is the result of a zero-sequence voltage imposed by the a.c. network.

From the computed values of the symmetrical components of the voltages and currents on the converter side of the transformer, the phase voltages and currents may be obtained through

$$\begin{bmatrix} I_{rn} \\ I_{yn} \\ I_{bn} \end{bmatrix} = [T] \begin{bmatrix} I_{dn} \\ I_{in} \\ 0 \end{bmatrix} \qquad (3.73)$$

$$\begin{bmatrix} V_{rn} \\ V_{yn} \\ V_{bn} \end{bmatrix} = [T] \begin{bmatrix} V_{dn} \\ V_{in} \\ 0 \end{bmatrix} \qquad (3.74)$$

3.5 D.C. system representation

The converter can be thought of as an ideal source of harmonic voltages which cause harmonic currents to circulate on the d.c. system. The analysis will be restricted here to two-terminal d.c. links.

Figure 3.15 shows the general configuration considered for the d.c. system. The d.c. line is represented by an equivalent T-section. Smoothing reactors are assumed on

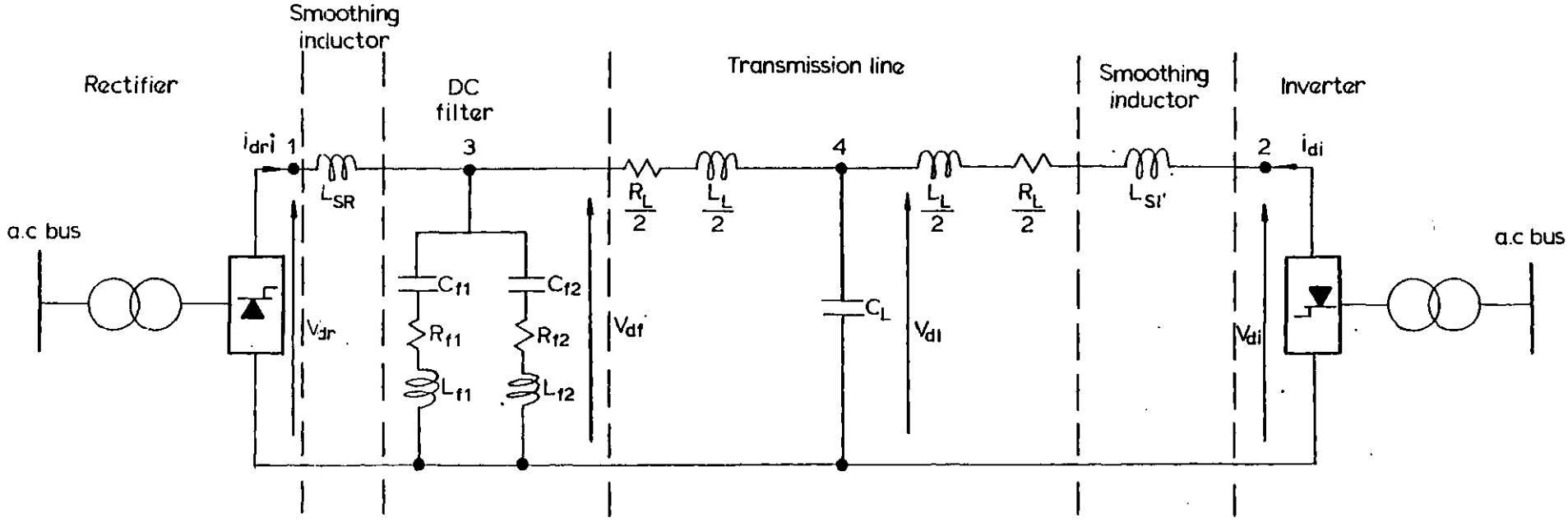

Fig. 3·15

Equivalent circuit for the d.c. system

both the rectifier and inverter ends. A two-branch d.c. filter is assumed on the rectifier side; it is omitted on the inverter side since the smoothing reactor inductances will in practice dominate the associated branch impedance.

From the d.c. voltage waveform description it is possible to find the harmonic content of the d.c. voltage, both at the rectifier and at the inverter end (see Chapter Four). The d.c. voltage is therefore of the form

$$V_d(t) = V_d + \sum_{\ell=1}^{n_d} V_{d\ell} \sin(\ell\omega_o t + \psi_{d\ell}) \qquad (3.75)$$

where V_d is the constant term of the Fourier expansion and $V_{d\ell}$ and $\psi_{d\ell}$ are the magnitude and phase of the harmonic 'ℓ'.

In order to calculate the d.c. currents at both ends of the line, the nodal equations will be employed

$$[I] = [Y][V] \qquad (3.76)$$

where $[I]$ is the vector of the nodal injected currents, $[V]$ the vector of the voltages and $[Y]$ the admittance matrix.

Since the admittances of the various d.c. system branches depend upon the frequency, a matrix $[Y]$ has to be computed for each harmonic. For the general harmonic 'n', equation (3.76) can be expanded as

$$\begin{bmatrix} I_{dr\ell} \\ I_{di\ell} \\ 0 \\ 0 \end{bmatrix} = \begin{bmatrix} Y_{11\ell} & Y_{12\ell} & Y_{13\ell} & Y_{14\ell} \\ Y_{21\ell} & Y_{22\ell} & Y_{23\ell} & Y_{24\ell} \\ Y_{31\ell} & Y_{32\ell} & Y_{33\ell} & Y_{34\ell} \\ Y_{41\ell} & Y_{42\ell} & Y_{43\ell} & Y_{44\ell} \end{bmatrix} \begin{bmatrix} V_{dr\ell} \\ V_{di\ell} \\ V_{df\ell} \\ V_{di\ell} \end{bmatrix} \qquad (3.77)$$

The indices 'r', 'i', 'f', and 'ℓ' stand for rectifier , inverter, filter and line respectively.

Defining the following vectors

$$\left[I_{\ell} \right] = \begin{bmatrix} I_{dr\ell} \\ I_{di\ell} \end{bmatrix} \tag{3.78}$$

$$\left[V_{1\ell} \right] = \begin{bmatrix} V_{dr\ell} \\ V_{di\ell} \end{bmatrix} \tag{3.79}$$

$$\left[V_{2\ell} \right] = \begin{bmatrix} V_{df\ell} \\ V_{dl\ell} \end{bmatrix} \tag{3.80}$$

It is possible to rewrite equation (3.77) in the form:

$$\begin{bmatrix} I_{\ell} \\ 0 \end{bmatrix} = \begin{bmatrix} Y_{11\ell} & Y_{12\ell} \\ Y_{21\ell} & Y_{22\ell} \end{bmatrix} \begin{bmatrix} V_{1\ell} \\ V_{2\ell} \end{bmatrix} \tag{3.81}$$

where

$$Y_{11\ell} = \begin{bmatrix} y_{11\ell} & y_{12\ell} \\ y_{21\ell} & y_{22\ell} \end{bmatrix} \tag{3.82}$$

$$Y_{12\ell} = \begin{bmatrix} y_{13\ell} & y_{14\ell} \\ y_{23\ell} & y_{24\ell} \end{bmatrix} \tag{3.83}$$

$$Y_{21\ell} = \begin{bmatrix} Y_{31\ell} & Y_{32\ell} \\ Y_{41\ell} & Y_{42\ell} \end{bmatrix} \tag{3.84}$$

$$Y_{22\ell} = \begin{bmatrix} Y_{33\ell} & Y_{34\ell} \\ Y_{43\ell} & Y_{44\ell} \end{bmatrix} \tag{3.85}$$

Using Kron's reduction, equation (3.81) becomes

$$\left[I_{\ell}\right] = \left(Y_{11\ell} - Y_{12\ell}\ Y_{22\ell}^{-1}\ Y_{21\ell} \right) \left[V_{1\ell}\right] \tag{3.86}$$

Vector $\left[V_{1\ell}\right]$ is calculated from a.c. systems quantities. Equation (3.86) therefore enables the evaluation of $\left[I_{\ell}\right]$, the vector of injected currents by the rectifier and the inverter, for harmonic 'ℓ'. Vector $\left[V_{2\ell}\right]$ can now be obtained from

$$\left[V_{2\ell}\right] = -\left(Y_{22\ell}^{-1}\ Y_{21\ell} \right) \left[V_{1\ell}\right] \tag{3.87}$$

The constant ferm of the d.c. current at the rectifier and inverter ends is simply calculated by

$$I_{dr} = -I_{di} = \frac{V_{dr} - V_{di}}{R_L} \tag{3.88}$$

In fig 3.16 a flowchart for the d.c. current evaluation is presented for two-terminal d.c. systems only. The nodal formulation together with the Kron's reduction was introduced with a view to the multiterminal d.c. system case which is a simple extension of the technique developed here.

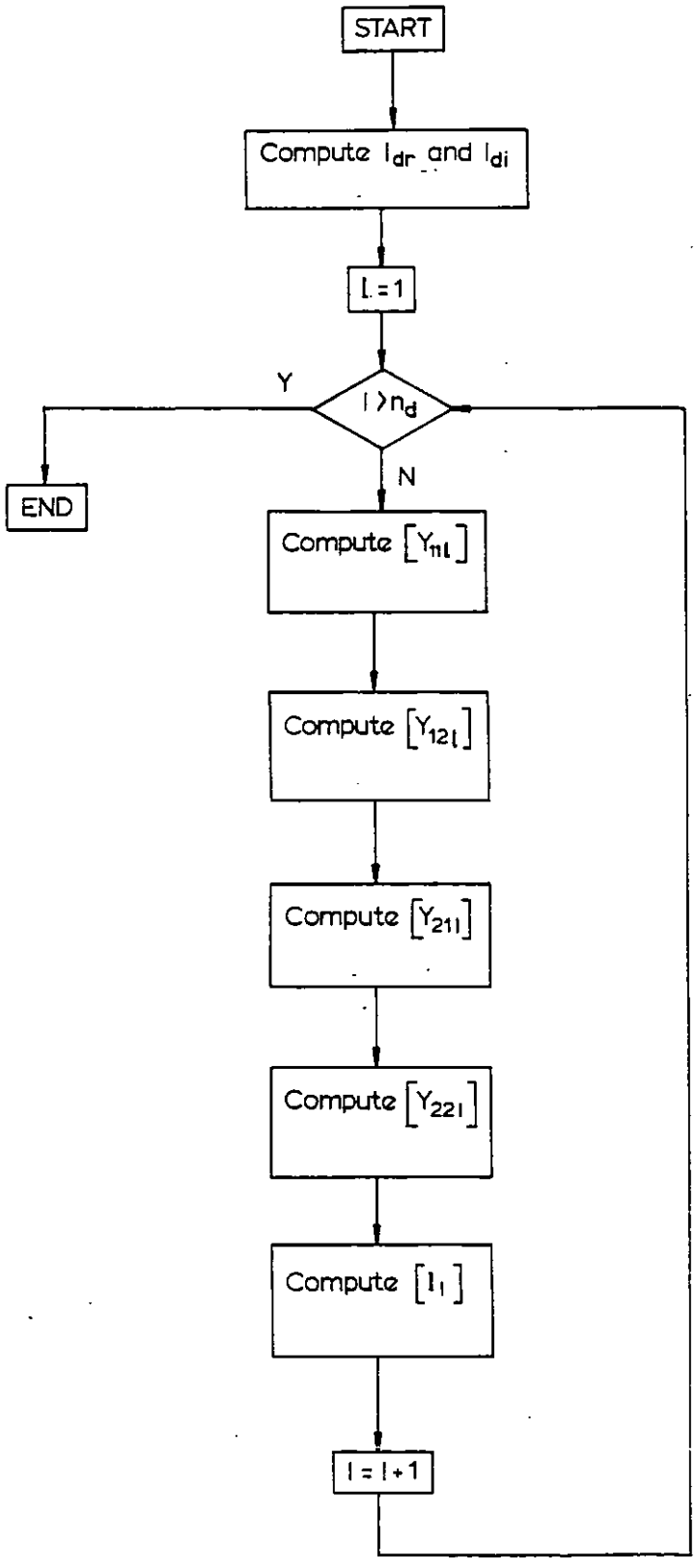

Fig. 3·16

D.C. current evaluation (2-terminal d.c. system) Flowchart

3.6 A.C. System representation

The a.c. system source impedance seen from the converter busbar is a complex function of frequency which in all but exceptional cases is not accurately known. From the converter point of view this impedance is in parallel with the harmonic filters and reactive support sources, the total impedance being highly dependent upon the frequency with a number of resonance and anti-resonance points.

For h.v.d.c. schemes in which six-pulse operation is allowed, the a.c. filter bank normally comprises tuned arms for the 5th, 7th, 11th and 13th harmonics, plus a damped arm for the higher harmonics. The recent trend is to use exclusively twelve-pulse converters, and dispense with the 5th and 7th harmonic filters. In some installations, only damped filters have been installed.

The a.c. network source impedance can be modelled by very complex circuits if its dependence upon the frequency is to be accurately taken into account. However, this is normally not justified in stability studies, since resonances are only likely to occur at low frequencies. Therefore the a.c. system was simply represented by an e.m.f. in series with an impedance $Z_s = R_s + jX_s$.

Since $R_s << X_s$, the value of X_s at the fundamental frequency ω_o is given by

$$Z_s = \sqrt{(R_s^2 + X_s^2)} \simeq X_s = \frac{U_n^2}{S_{sc}} \qquad (3.89)$$

where S_{sc} is the short-circuit power (MVA) and U_n the rated voltage (kV) of the converter busbar.

Damping is provided by the resistance R_s. A usual measure of the damping is given by the impedance angle ψ which for the fundamental frequency ranges from 80^o to 85^o.

$$\tan\psi = \frac{X_s}{R_s} \qquad (3.90)$$

The value of R_s is set to yield the specified impedance angle at the rated frequency:

$$R_s = \frac{X_s}{\tan\psi} \qquad (3.91)$$

For a rectifier station fed solely by a generating plant with little local load, an angle of 85^o is normally adequate. For an inverter station with a substantial load in its vicinity, an angle of 75^o gives, in general, enough accuracy.

Unlike the a.c. network, the impedance-frequency characteristic of the filters can be accurately calculated. For a tuned filter (LCR series arm) the relevant parameters are:

i) The characteristic frequency

$$f_o = \frac{1}{2\pi\sqrt{LC}} \qquad (3.92)$$

ii) The characteristic impedance

$$x_o = \sqrt{\frac{L}{C}} \qquad (3.93)$$

ii) The quality factor Q

$$Q = \frac{x_o}{R} \qquad (3.94)$$

The same parameters define the impedance of a damped filter, however in this case the quality factor is

$$Q = \frac{R}{X_o} \tag{3.95}$$

From the knowledge of the impedance characteristic of the a.c. network and filters, it is possible to derive an equivalent circuit for each harmonic, as shown in fig 3.17. For the harmonic 'n' the relationship between the current injected by the converter and the current which flows in the a.c. system is

$$I_{sn} = \frac{Z_n}{Z_{sn} + Z_{fn}} I_n \tag{3.96}$$

The voltage drop per phase is therefore

$$\Delta V_n = Z_{sn} I_{sn} = \frac{Z_{sn} Z_{fn}}{Z_{sn} + Z_{fn}} I_n \tag{3.97}$$

$$= Z_{acn} I_n$$

where Z_{acn} is the combined a.c. network plus filters impedance.

The busbar voltage is accordingly

$$V_n = E_n \frac{Z_{fn}}{Z_{sn} + Z_{fn}} - Z_{acn} I_n \tag{3.98}$$

where E_n is the harmonic e.m.f. of order 'n' imposed by the a.c. system. If the a.c. source e.m.f. does not contain harmonic 'n', equation (3.98) reduces to .

$$V_n = -Z_{acn} I_n \tag{3.99}$$

Equation (3.98) or (3.99) enables the calculation of the nth component of the converter busbar voltage, once the nth harmonic of the converter a.c. current is known.

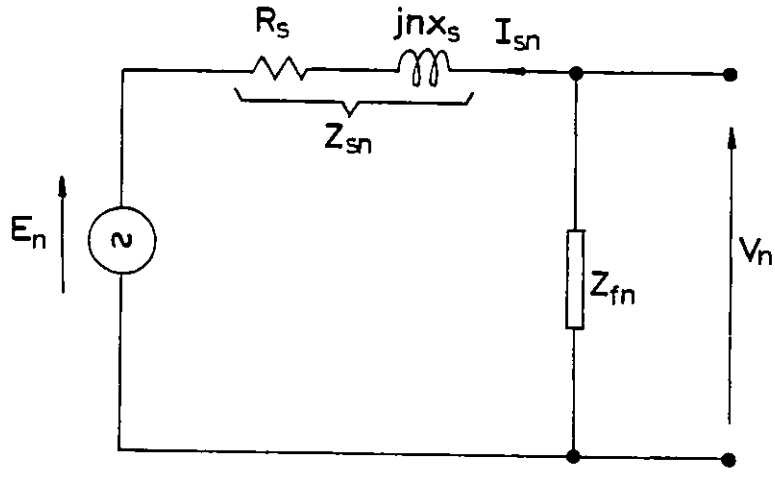

Fig. 3·17

A.C. system plus filter equivalent for harmonic n

3.7 Conclusions

In this chapter a mathematical model for a converter system was presented, with a view to the calculation of the describing function. For this reason, the input control voltage consists of a static component plus a modulating signal of arbitrary magnitude and phase, and a frequency which is either a harmonic or sub-harmonic of the a.c. system frequency.

Computer subroutines to calculate the firing instants were developed for individual phase (IPC), pulse frequency (PFC) or pulse phase (PPC) control systems. This calculation requires the previous knowledge of the busbar voltage zero crossings with arbitrary unbalance or distortion.

The commutation angle is calculated under the most general conditions, namely a.c. voltage unbalanced and/or distorted and taking into account the influence of the direct current harmonics. The latter was however found to be small, not justifying the expense of an increase in computation time by a factor of up to 80.

Once the firing instants and commutation angles are known for each valve of the converter, the d.c. output voltage and the a.c. current can be mathematically described. The waveforms are made up of several sections, the transition from one to the other occurring at the firing instant and at the end of commutation. Being periodic, these waveforms can be expanded in Fourier series, the harmonic analysis being the object of Chapter Four.

H.v.d.c. converters normally operate on a twelve-pulse mode, which is accomplished by connecting two converters in series on the d.c. side and feeding Y_{ny} and Y_{nd} transformers

respectively. Care has to be taken in modelling the converter transformers, in particular the Y_{nd} connected type, since it introduces a phase shift which is dependent upon the sequence of phases of the a.c. voltage.

The d.c. system was modelled by the nodal equations, the d.c. current harmonics injected by the converter being calculated by Kron's reduction. This technique will allow easy expansion into the multiterminal case.

A simple equivalent was assumed for the a.c. system source impedance, since the main emphasis is on the comparison of theoretical predictions with simulator results. In the computer program, however, more complex representation of the a.c. system can be easily introduced if the relevant data are available for the particular a.c. network. Since this is not generally the case it was decided not to enhance the a.c. system representation beyond the simple T-section, which is generally accurate enough for the range of frequencies of interest in converter stability studies.

Chapter Four

HARMONIC EVALUATION

4.1 Introduction

As was pointed out in section 3.3, the converter transforms a set of three phase voltages into direct voltage, which comprises a constant term plus a number of harmonics of the a.c. frequency. On the other hand, from the current point of view, the converter transforms a d.c. current, defined by the d.c. voltage and the d.c. system impedance, into a set of three phase currents which are injected into the a.c. network. These currents contain a term at the fundamental frequency and a number of harmonics.

If the three phase a.c. voltages are balanced and undistorted and the firing pulses are equidistant, the order of the harmonics is determined by the pulse number 'p' of the converter. These so-called characteristic harmonics are of order

$$l = kp$$

on the d.c. side, and

$$h = kp \pm 1$$

on the a.c. side, where k is an integer ranging from 1 to infinity.

The amplitude and phase of the characteristic harmonics in relation to the fundamental depend on the firing angle and the commutation angle.

In practice the a.c. busbar voltage exhibits always a measure of unbalance and/or distortion. Also an unbalance of the converter transformer reactances is to be expected. The firing of the valves cannot be exactly equidistant, since even with modern control equipment, the tolerance for the firing instants is 0.1 to 0.2 degrees.

These three factors result in the generation of uncharacteristic harmonics. Since the harmonic filters are tuned for the characteristic harmonics and it is not economical to install filters for all the uncharacteristic harmonics, these are injected into the a.c. system. While their amplitude is small, there is no reason for concern; however, under certain circumstances they could be magnified giving rise to unacceptable operating conditions. This phenomenon named harmonic instability is likely to occur when the converter is under closed-loop control and will be dealt with in Chapter Five.

In the present chapter, a method is presented which enables the calculation of both d.c. and a.c. harmonics with arbitrarily distorted a.c. voltages, non-equidistant firing instants and unequal transformer reactances. The input control voltage can either be constant or modulated by a sinusoidal signal with a frequency $k\omega_o$. The Fourier expansion

coefficients are calculated analytically from the waveform description of the d.c. voltage and a.c. current established in section 3.3.2.

4.2 D.C. voltage

4.2.1 Mathematical description

To calculate the harmonic content of the d.c. voltage it is necessary to define a function which can describe the d.c. voltage waveform. As was pointed out in section 3.3.2 this waveform comprises, for each valve, two sections, named commutation section and full conduction section, which are described by equations (3.59) and (3.60) respectively. The function $v_{di}(t)$ can therefore be written as follows:

$$v_{di}(t) = \begin{cases} (V_i - V_k) - (R_i i_i + L_i \dfrac{di_i}{dt}) - (R_k i_d + L_k \dfrac{di_d}{dt}) \\ \qquad\qquad \theta_i < \omega_o t < \theta_i + u_i \\ (V_i - V_k) - (R_i + R_k) i_d - (L_i + L_k) \dfrac{di_d}{dt} \\ \qquad\qquad \theta_i + u_i < \omega_o t < \theta_k \end{cases} \quad (4.1)$$

θ_i is the firing angle of a particular valve, in the main reference domain; u_i is the commutation angle for that valve; θ_k is the firing instant of the next valve to conduct.

As in a six pulse converter there are six valves; six functions of the type of equation (4.1) can be defined, each function representing the contribution of a particular valve for the d.c. voltage. If the a.c. voltage is unbalanced or

distorted or the firing instants are not equidistant, the contribution of each valve is different. On the contrary, for balanced a.c. voltages and equidistant firing, the contributions are equal, resulting in a periodic waveform, with a period of 1/6 the a.c. voltage period. In the general case, the period is the same as that of the a.c. voltage, i.e. the lowest harmonic is at frequency ω_o.

An exception to this rule does however occur if the firing angle for a particular valve is not the same after $2\pi/\omega_o$. This can occur if the frequency of the control voltage modulating signal ω_m is not a multiple of the a.c. voltage frequency ω_o. In this situation the fundamental frequency for the Fourier series expansion has to be the maximum common divisor of ω_m and ω_o, since these must be terms in the expansion containing ω_m and ω_o. Assuming that

$$\omega_m = \frac{p}{q}\omega_o \tag{4.2}$$

the fundamental frequency for the Fourier expansion is

$$\omega_{fund} = \frac{\omega_m}{p} = \frac{\omega_o}{q} \tag{4.3}$$

The reference for the calculation of the harmonics is taken as the firing instant of valve 1, which was also used in the evaluation of the commutation angle (section 3.3.1). Although this choice involves in some cases changes from the main reference, the overall balance is positive due to considerable simplifications in other instances.

Equation (4.1) can be rewritten in the new reference as

$$V_{ik} - (R_k i_d + L_k \frac{di_d}{dt}) + V_{ic} \qquad (\theta_i - \theta_l) < \omega_o t < (\theta_i - \theta_l) + u_i$$

$$v_{di}(t) = \begin{cases} & \\ & \end{cases} \tag{4.4}$$

$$V_{ik} - (R_{ik} i_d + L_{ik} \frac{di_d}{dt}) \qquad (\theta_i - \theta_l) + u_i < \omega_o t < (\theta_k - \theta_l)$$

where θ_l is the firing instant of valve l and

$$R_{ik} = R_i + R_k \tag{4.5}$$

$$L_{ik} = L_i + L_k \tag{4.6}$$

$$V_{ik} = V_i - V_k \tag{4.7}$$

$$V_{ic} = -(R_i i_i + L_i \frac{di_i}{dt}) \tag{4.8}$$

V_i and V_k are defined by equation (3.1) and are referred to the main reference; i_d is given by equation (3.42) and is referred to the valve l firing instant reference; i_i is given by equation (3.54), referred to the firing instant of valve i.

In the valve l firing instant reference, equation (3.1) becomes

$$V_i = \sum_{h=1}^{p} V_{ih} \sin(h\omega_o t + \phi_{ih} + h\theta_l) \tag{4.9}$$

wherefrom

$$V_{ik} = V_i - V_k = \sum_{h=1}^{p} S_h \sin(h\omega_o t) + \sum_{h=1}^{p} C_h \cos(h\omega_o t) \tag{4.10}$$

where

$$S_h = V_{ih} \cos (\phi_{ih} + h \theta_l) - V_{kh} \cos (\phi_{kh} + h \theta_l) \quad (4.11)$$

$$C_h = V_{ih} \sin (\phi_{ih} + h \theta_l) - V_{kh} \sin (\phi_{kh} + h \theta_l) \quad (4.12)$$

The commutation current i_i must also be the object of a change of reference. Both i_i and V_p are only defined in the interval

$$\theta_i < \omega_o t < \theta_i + u_i \quad (4.13)$$

θ_i and $\theta_i + u_i$ are defined in the main reference. In the new reference, equation (4.13) becomes

$$\theta_x < \omega_o t < \theta_x + u_i \quad (4.14)$$

where

$$\theta_x = \theta_i - \theta_l \quad (4.15)$$

When expressed by equation (3.54), i_i is only defined in the interval

$$0 < \omega_o t' < u_i \quad (4.16)$$

From equations (4.14) and (4.16) the relation between t and t' can be established

$$\omega_o t' = \omega_o t - \theta_x \quad (4.17)$$

or

$$t' = t - t_x \quad (4.18)$$

where

$$t_x = \frac{\theta_x}{\omega_o} \quad (4.19)$$

By substituting in equation (3.54) t by $t-tx$ and $\omega_o t$ by $\omega_o t - \theta_x$, the commutation current i_i is obtained in the new reference as

$$i_i(t) = \sum_{h=1}^{p} [X_{1h} e^{-(t-t_x)/T_{io}} + S_{1h} \sin(h\omega_o t + \phi_{1h} - h\theta_x)] + Y_1(1-e^{-(t-t_x)/T_{io}}$$

$$+ \sum_{\ell=1}^{n_d} [X_{2\ell} e^{-(t-t_x)/T_{io}} + S_{2\ell} \sin(\ell\omega_o t + \phi_{2\ell} - \ell\theta_x)] \qquad (4.20)$$

Substituting equation (4.20) into equation (4.8) the expression for V_{ic}, the voltage drop in the transformer impedance due to the commutation current, can be obtained as

$$V_{ic}(t) = W e^{-(t-t_x)/T_{io}} + \sum_{h=1}^{p} [M_{1h} \cos(h\omega_o t) + N_{1h} \sin(h\omega_o t)] +$$

$$+ \sum_{\ell=1}^{n_d} [M_{2\ell} \cos(\ell\omega_o t) + N_2 \sin(\ell\omega_o t)] + k_i \qquad (4.21)$$

where

$$R_i' = \frac{L_i}{T_{io}} - R_i \qquad (4.22)$$

$$W = R_i\left(\sum_{h=1}^{p} X_{1h} - \sum_{\ell=1}^{n_d} X_{2\ell}\right) \qquad (4.23)$$

$$K_i = -R_i Y_1 \qquad (4.24)$$

$$\delta_{ih} = \phi_{1h} - h\theta_x \qquad (4.25)$$

$$\delta_{2\ell} = \phi_{2\ell} - \ell\theta_x \qquad (4.26)$$

$$M_{1h} = -(h\omega_o L_i S_{1h} \cos\delta_{1h} + R_i S_{1h} \sin\delta_{1h}) \qquad (4.27)$$

$$M_{2\ell} = -(\ell\omega_o L_i S_{2\ell} \cos\delta_{2\ell} + R_i S_{2\ell} \sin\delta_{2\ell}) \qquad (4.28)$$

$$N_{1h} = (h\omega_o L_i S_{1h} \sin\delta_{1h} - R_i S_{1h} \cos\delta_{1h}) \qquad (4.29)$$

$$N_{2\ell} = (\ell\omega_o L_i S_{2\ell} \sin\delta_{2\ell} - R_i S_{2\ell} \cos\delta_{2\ell}) \qquad (4.30)$$

and now defines

$$V_{kd} = R_k\, i_d + L_k \frac{di_d}{dt} \tag{4.31}$$

$$V_{ikd} = R_{ik}\, i_d + L_{ik} \frac{di_d}{dt} \tag{4.32}$$

By substituting the expression for i_d, referred to the firing instant of valve 1, given by equation (3.42), one obtains

$$V_{kd} = R_k I_d + \sum_{\ell=1}^{n_d} \left(R_k F_\ell - \ell\omega_o L_k G_\ell \right) \sin\left(\ell\omega_o t\right) + \sum_{\ell=1}^{n_d} \left(R_k G_\ell + \ell\omega_o L_k F_\ell \right) \cos(\ell\omega_o t) \tag{4.33}$$

and

$$V_{ikd} = R_{ik} I_d + \sum_{\ell=1}^{n_d} \left(R_{ik} F_\ell - \ell\omega_o L_{ik} G_\ell\right) \sin(\ell\omega_o t) + \sum_{\ell=1}^{n_d} \left(R_{ik} G_\ell + \ell\omega_o L_{ik} F_\ell \right) \cos\left(\ell\omega_o t\right) \tag{4.34}$$

where

$$F_\ell = I_{d\ell} \cos \phi_{d\ell} \tag{4.35}$$

$$G_\ell = I_{d\ell} \sin \phi_{d\ell} \tag{4.36}$$

Equations (4.10), (4.21), (4.33) and (4.34) fully describe the contribution of valve i to the d.c. voltage waveform. Equation (4.4) can now be written in the form

$$v_{di}(t) = \begin{cases} V_{ik} - V_{kd} + V_{ic} & (\theta_i - \theta_1) < \omega_o t < (\theta_i - \theta_1) + u_i \quad (4.37) \\ V_{ik} - V_{ikd} & (\theta_i - \theta_1) + u_i < \omega_o t < (\theta_k - \theta_1) \quad (4.38) \end{cases}$$

Equations (4.37) and (4.38) are valid for the odd numbered valves only, i.e. the valves connected to the positive pole of the converter. For the even numbered valves, V_{ik} and V_{ic} must have their sign changed, as the following reasoning will show.

Fig 4.1 shows a 3-phase bridge during commutation of two even numbered valves (compare with fig 3.7). The following equations apply in this case:

$$v_d = -V_{pn} + V_k - R_k i_d - L_k \frac{di_d}{dt} \tag{4.39}$$

$$V_{pn} = V_i - (R_i i_i + L_i \frac{di_d}{dt}) = V_i + V_{ic} \tag{4.40}$$

Substitution of equation (4.40) into (4.39), yields

$$v_d = V_k - V_i - R_k i_d - L_k \frac{di_d}{dt} - V_{ic} \tag{4.41}$$

Taking into account equation (4.31),

$$v_d = -V_{ik} - V_{kd} - V_{ic} \tag{4.42}$$

for similar reasons, during a full conduction period,

$$v_d = -V_{ik} - V_{ikd} \tag{4.43}$$

Assuming at this stage a modulating signal with a frequency multiple of the a.c. system frequency, the fundamental frequency of the d.c. voltage is ω_o. Therefore one period of $V_d(t)$ can be partitioned into six sections, each in turn comprising two sub-sections, as shown in Table 4.1. If the fundamental frequency was ω_o/q, the number of sections would be

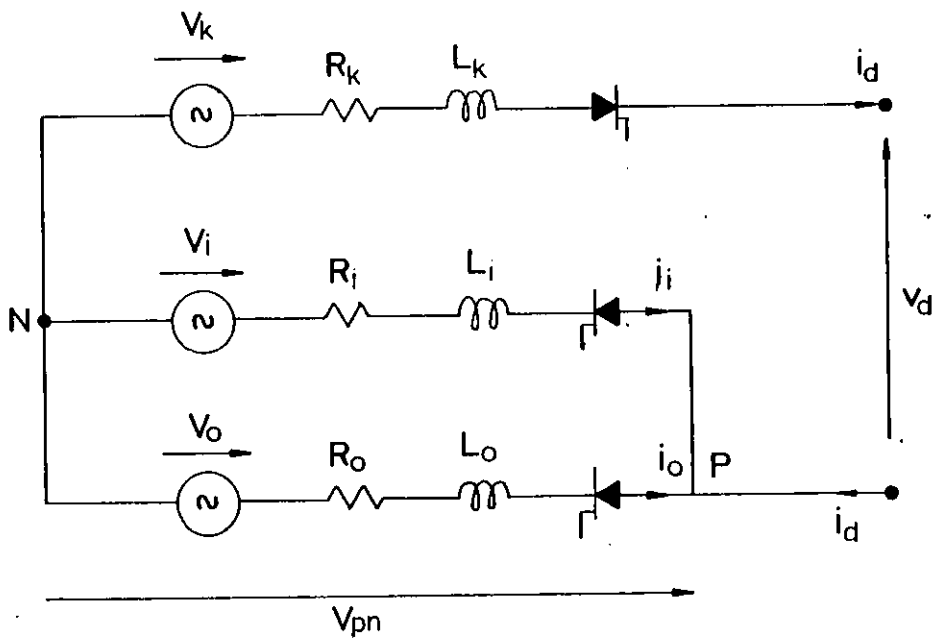

Fig. 4.1

3 - phase bridge during commutation of even - numbered valves

6q. In this case the reference for the harmonic evaluation would be the first firing instant of valve 1 within the repetition period.

Table 4.1: D.C. Voltage Decomposition

Section	Time Limits	Equation	
1	$0 < \omega_o t < u_1$	$\theta_x = 0$	(4.37)
	$u_1 < \omega_o t < \theta_2 - \theta_1$		(4.38)
2	$\theta_2 - \theta_1 < \omega_o t < \theta_2 - \theta_1 + u_2$	$\theta_x = \theta_2 - \theta_1$	(4.42)
	$\theta_2 - \theta_1 + u_2 < \omega_o t < \theta_3 - \theta_1$		(4.43)
3	$\theta_3 - \theta_1 < \omega_o t < \theta_3 - \theta_1 + u_3$	$\theta_x = \theta_3 - \theta_1$	(4.37)
	$\theta_3 - \theta_1 + u_3 < \omega_o t < \theta_4 - \theta_1$		(4.38)
4	$\theta_4 - \theta_1 < \omega_o t < \theta_4 - \theta_1 + u_4$	$\theta_x = \theta_4 - \theta_1$	(4.42)
	$\theta_4 - \theta_1 + u_4 < \omega_o t < \theta_5 - \theta_1$		(4.43)
5	$\theta_5 - \theta_1 < \omega_o t < \theta_5 - \theta_1 + u_5$	$\theta_x = \theta_5 - \theta_1$	(4.37)
	$\theta_5 - \theta_1 + u_5 < \omega_o t < \theta_6 - \theta_1$		(4.38)
6	$\theta_6 - \theta_1 < \omega_o t < \theta_6 - \theta_1 + u_6$	$\theta_x = \theta_6 - \theta_1$	(4.42)
	$\theta_6 - \theta_1 + u_6 < \omega_o t < 2\pi$		(4.43)

4.2.2 Fourier Series Expansion

The d.c. voltage can be expanded in Fourier series:

$$v_d(t) = \frac{A_o}{2} + \sum_{n=1}^{\infty} A_n \cos n\omega_o t + \sum_{n=1}^{\infty} B_n \sin n\omega_o t \quad (4.44)$$

where A_n and B_n, the Euler-Fourier coefficients, are given by ($\omega_o T = \pi$).

$$A_n = \frac{\omega_o}{T} \int_0^{2T} V_d(t) \cos n\omega_o t \, dt \quad (4.45)$$

$$B_n = \frac{\omega_o}{T} \int_0^{2T} V_d(t) \sin n\omega_o t \, dt \quad (4.46)$$

Alternatively

$$v_d(t) = V_d + \sum_{\ell=1}^{\infty} V_{d\ell} \sin (n\omega_o t + \Psi_{d\ell}) \quad (4.47)$$

where

$$V_d = \frac{A_o}{2} \quad (4.48)$$

$$V_{d\ell} = \sqrt{A_n^2 + B_n^2} \quad (4.49)$$

$$\Psi_{d\ell} = \tan^{-1} \frac{A_n}{B_n} \quad (4.50)$$

Since $V_d(t)$ is piecewise defined, equations (4.45) and (4.46) develop into

$$A_n = \frac{\omega_o}{T} \left[\int_0^{t_1} V_{d1}(t) \cos n\omega_o t \, dt + \int_{t_1}^{t_2} V_{d2}(t) \cos n\omega_o t \, dt + \ldots \right.$$

$$\left. + \int_{t_{n-1}}^{2T} V_{dn}(t) \cos n\omega_o t \, dt \right] \quad (4.51)$$

$$B_n = \frac{\omega_o}{T}\left[\int_0^{t_1} V_{d1}(t) \sin n\,\omega_o t\, dt + \int_{t_1}^{t_2} V_{d2}(t) \sin n\,\omega_o t\, dt + \ldots\right.$$

$$\left. + \int_{t_{n-1}}^{2T} V_{dn}(t) \sin n\,\omega_o t\, dt\right] \qquad (4.52)$$

where the integration limits t_{i-1}, t_i define the interval during which valve i is conducting. For this valve, the corresponding term in equation (4.51) is

$$A_{ni} = \int_{t_{i-1}}^{t_i} V_{di}(t) \cos n\,\omega_o t\, dt = \int_{t_{i-1}}^{t_i'} (V_{ik} - V_{kd} + V_{ic}) \cos n\,\omega_o t\, dt$$

$$+ \int_{t_i'}^{t_i} (V_{ik} - V_{ikd}) \cos n\,\omega_o t\, dt \qquad (4.53)$$

and in equation (4.52)

$$B_{ni} = \int_{t_{i-1}}^{t_i} V_{di}(t) \sin n\,\omega_o t\, dt = \int_{t_{i-1}}^{t_i'} (V_{ik} - V_{kd} + V_{ic}) \sin n\,\omega_o t\, dt$$

$$+ \int_{t_i'}^{t_i} (V_{ik} - V_{ikd}) \sin n\,\omega_o t\, dt \qquad (4.54)$$

The evaluation of the Euler coefficients therefore requires the following integrals:

$$\int_{t_a}^{t_b} V_{ik} \cos n\,\omega_o t\, dt \qquad (4.55)$$

$$\int_{t_a}^{t_b} V_{ik} \sin n\,\omega_o t\, dt \qquad (4.56)$$

$$\int_{t_a}^{t_b} V_{ic} \cos n\omega_o t \, dt \qquad (4.57)$$

$$\int_{t_a}^{t_b} V_{ic} \sin n\omega_o t \, dt \qquad (4.58)$$

$$\int_{t_a}^{t_b} V_{kd} \cos n\omega_o t \, dt \qquad (4.59)$$

$$\int_{t_a}^{t_b} V_{kd} \sin n\omega_o t \, dt \qquad (4.60)$$

where t_a and t_b are general limits of integration. There is no need to define the integrals containing V_{ikd}, since V_{ikd} and V_{kd} are of the same form (see equations (4.33) and (4.34)), with only different parameters.

The integrals (4.55) through (4.60) can be calculated by inserting equations (4.10), (4.21) and (4.33) in the appropriate cases. Each integral has to be evaluated for n ranging from zero to the maximum number of harmonics considered in the calculation. The latter was assumed to be 30 in this work, both on the a.c. and d.c. side. Evaluation of the integrals (4.55) to (4.60) are shown in Appendix D.

Equations (D.1) through (D.31) together with the integration limits defined in Table 4.1 allow the calculation of the

coefficients A_n and B_n of the Fourier expansion, from which parameters V_d, V_{dn} and ψ_{dn} (equation (4.47)) can be obtained.

In fig 4.2 a flowchart for the computation of the d.c. voltage harmonics is presented. Variable KI is a key which indicates whether the contribution to the Euler coefficients is being calculated during a commutation period (KI=0) or during a full conduction period (KI=1). It should be noted that the contribution of integrals (4.55) to (4.58) for the coefficients A_n and B_n is positive for the odd-numbered valves and negative for the even-numbered valves, as shown in section 4.2.1.

4.3 A.C. Current

4.3.1 Mathematical description

As for the direct voltage, the harmonic evaluation of the converter alternating current requires a mathematical description of its waveform. As was shown in section 3.3.2, three periods can be identified in the a.c. current waveform, namely: i) Full conduction period described by equations (3.61) and (3.62); ii) Commutation period, described by equations (3.63), (3.64) and (3.65); and iii) Non-conduction period, described by equation (3.66).

In fig 4.3 the three phase a.c. line currents are represented. Each current can be divided into six sections, the beginning of commutation defining the borderline between the sections. Section 1 is initiated at the commutation from phase B to R, section 2 at the commutation from phase Y to B, and so forth.

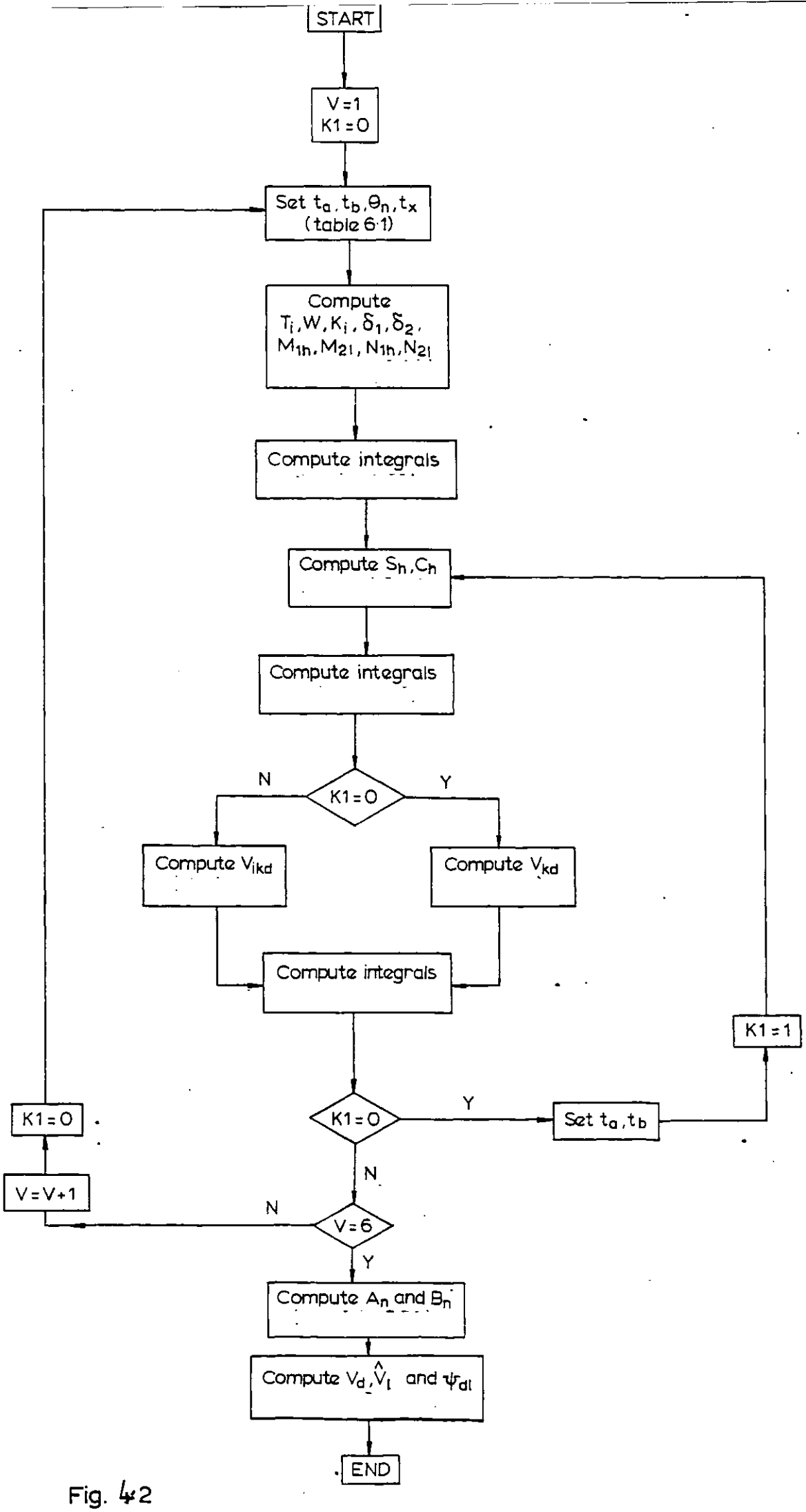

Fig. 42

D.C. voltage harmonic calculation Flowchart

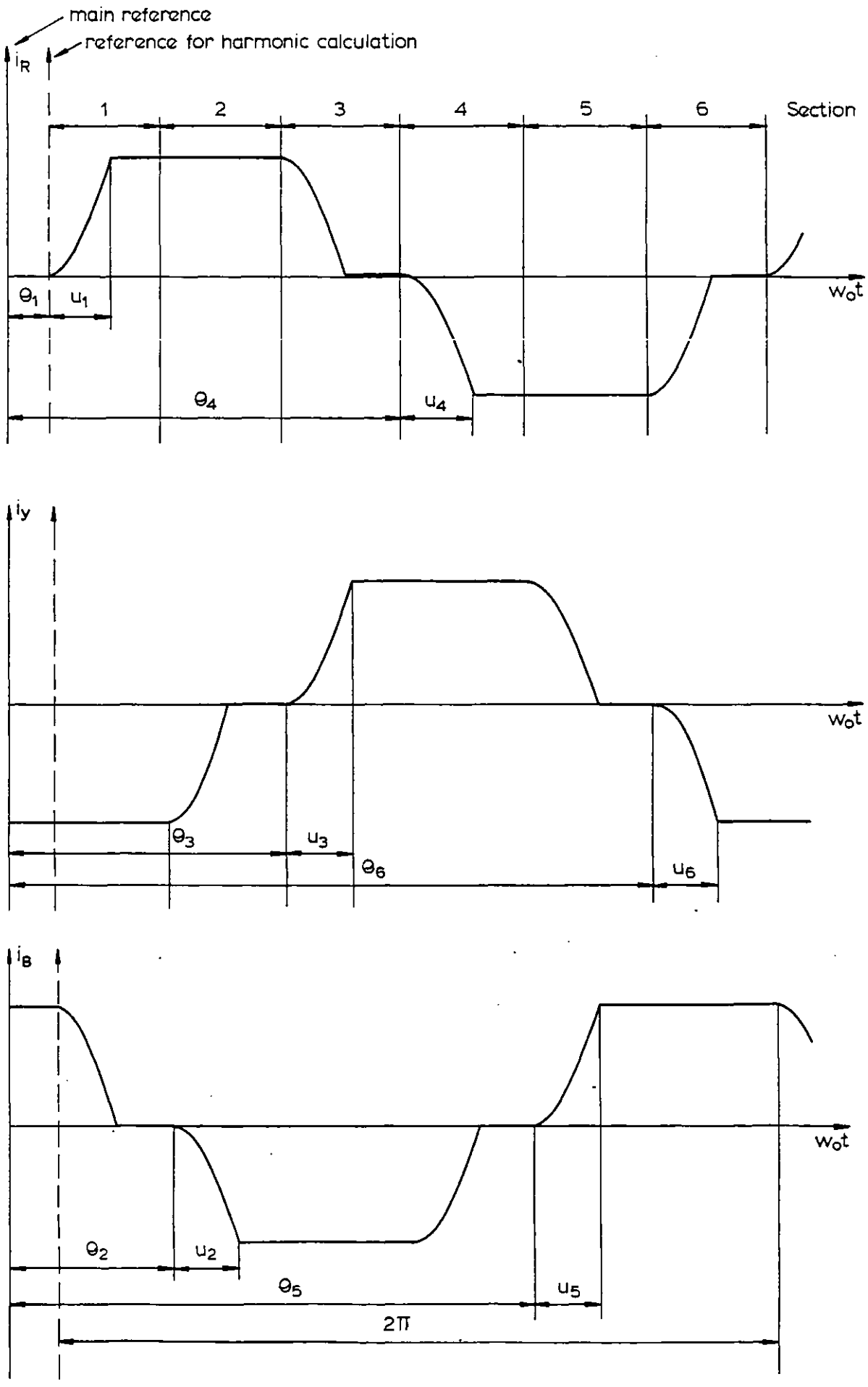

Fig. 4·3

3 - phase bridge a.c. line currents

Each of these sections can be decomposed into two subsections. In the first, two of the valves are in a commutation period and a third valve is in a full conduction period, i.e. three valves are conducting. In the second, two valves are in full conduction and the others are in a non-conduction period. Table 4.2 gives a full description of the a.c. current waveform decomposition.

The firing instant of valve 1 is taken as reference as previously in the calculation of the d.c. voltage harmonics. In Table 4.2, $i_i(t)$ stands for the current in the incoming valve, $i_o(t)$ for the current in the outgoing valve, and $i_d(t)$ for the direct current. For the odd-numbered valves (see Fig 3.7),

$$i_i + i_o = i_d \tag{4.61}$$

whereas for the even numbered valves (fig 4.2),

$$i_i + i_o = -i_d \tag{4.62}$$

As can be seen from Table 4.2, the current in the outgoing valve $i_o(t)$ is invariably calculated from equations (4.61) or (4.62) as a function of $i_i(t)$ and $i_d(t)$, an explicit expression not being necessary. $i_i(t)$ and $i_d(t)$ are given by equations (4.20) and (3.42) respectively.

Equation (3.42) can be rewritten as

$$i_d(t) = I_d + \sum_{\ell=1}^{n_d} (L_\ell \sin \ell\omega_o t + M_\ell \cos \ell\omega_o t) \tag{4.63}$$

where

$$L_\ell = I_{d\ell} \cos \phi_{d\ell} \tag{4.64}$$

$$M_\ell = I_{d\ell} \sin \phi_{d\ell} \tag{4.65}$$

The six sections and respective sub-sections in Table 4.2 are as defined in Table 4.1, with respect to the calculation of the d.c. voltage harmonics.

Table 4.2: A.C. Current Decomposition

Section	Time Limits	i_R	i_Y	i_B
1	$0 < \omega_o t < u_1$	i_i	$-i_d$	$i_d - i_i$
	$u_1 < \omega_o t < \theta_2 - \theta_1$	i_d	$-i_d$	0
2	$\theta_2 - \theta_1 < \omega_o t < \theta_2 - \theta_1 + u_2$	i_d	$-i_d - i_i$	i_i
	$\theta_2 - \theta_1 + u_2 < \omega_o t < \theta_3 - \theta_1$	i_d	0	$-i_d$
3	$\theta_3 - \theta_1 < \omega_o t < \theta_3 - \theta_1 + u_3$	$i_d - i_i$	i_i	$-i_d$
	$\theta_3 - \theta_1 + u_3 < \omega_o t < \theta_4 - \theta_1$	0	i_d	$-i_d$
4	$\theta_4 - \theta_1 < \omega_o t < \theta_4 - \theta_1 + u_4$	i_i	i_d	$-i_d - i_i$
	$\theta_4 - \theta_1 + u_4 < \omega_o t < \theta_5 - \theta_1$	$-i_d$	i_d	0
5	$\theta_5 - \theta_1 < \omega_o t < \theta_5 - \theta_1 + u_5$	$-i_d$	$i_d - i_i$	i_i
	$\theta_5 - \theta_1 + u_5 < \omega_o t < \theta_6 - \theta_1$	$-i_d$	0	i_d
6	$\theta_6 - \theta_1 < \omega_o t < \theta_6 - \theta_1 - u_6$	$-i_d - i_i$	i_i	i_d
	$\theta_6 - \theta_1 + u_6 < \omega_o t < 2\pi$	0	$-i_d$	i_d

4.3.2 Fourier series expansion

The a.c. current can be expanded in Fourier series as

$$i_a(t) = \frac{A_o}{2} + \sum_{n=1}^{\infty} A_n \cos n\omega_o t + \sum_{n=1}^{\infty} B_n \sin n\omega_o t \quad (4.66)$$

where

$$A_n = \frac{\omega_o}{T}\int_0^{2T} i_a(t) \cos n\omega_o t \, dt \quad (4.67)$$

$$B_n = \frac{\omega_o}{T}\int_0^{2T} i_a(t) \sin n\omega_o t \, dt \quad (4.68)$$

Alternatively

$$i_a(t) = I_a + \sum_{h=1}^{\infty} I_{ah} \sin (h\omega_o t + \psi_{ah}) \quad (4.69)$$

where

$$I_a = \frac{A_o}{2} \quad (4.70)$$

$$I_{ah} = \sqrt{A_n^2 + B_n^2} \quad (4.71)$$

$$\psi_{ah} = \tan^{-1}\left(\frac{A_n}{B_n}\right) \quad (4.72)$$

According to Table 4.2, $I_a(t)$ (a=R, Y, B) can be expressed as a function of $i_l(t)$ and $i_d(t)$. The calculation of the Euler coefficients A_n and B_n therefore requires the evaluation of the integrals

$$\int_{t_a}^{t_b} i_l \cos n\omega_o t \, dt \quad (4.73)$$

$$\int_{t_a}^{t_b} i_l \sin n\omega_o t \, dt \quad (4.74)$$

$$\int_{t_a}^{t_b} i_d \cos n \omega_o t \, dt \qquad (4.75)$$

$$\int_{t_a}^{t_b} i_d \sin n \omega_o t \, dt \qquad (4.76)$$

which are developed in Appendix E.

Equations (E.1) and (E.22) together with the time limits defined in Table 4.2 are sufficient to calculate the coefficients A_n and B_n of the Fourier series, from which the parameter I_a, I_{an} and ψ_{an} can be obtained.

In fig 4.4 a flowchart for the computation of the magnitude and phase of the a.c. current harmonics is presented, assuming a fundamental frequency equal to the a.c. system nominal frequency.

In the flowchart, variable KI has the same meaning as in fig 4.2 (0 for commutation period, 1 for full conduction period). The contributions of i_i and i_d to the Euler coefficients (integrals (4.73) to (4.76) are assigned to phases R, Y and B current according to Table 4.2.

The computer routine based upon this flowchart evaluates the harmonics on the valve side of the converter transformer. Therefore a constant term may occur under some circumstances, which will cause the saturation of the transformer core. The harmonics on the busbar side can be calculated using the symmetrical component approach, as pointed out in section 3.4. On this side, the constant term of the current cannot exist since the transformer is a filter for zero frequency.

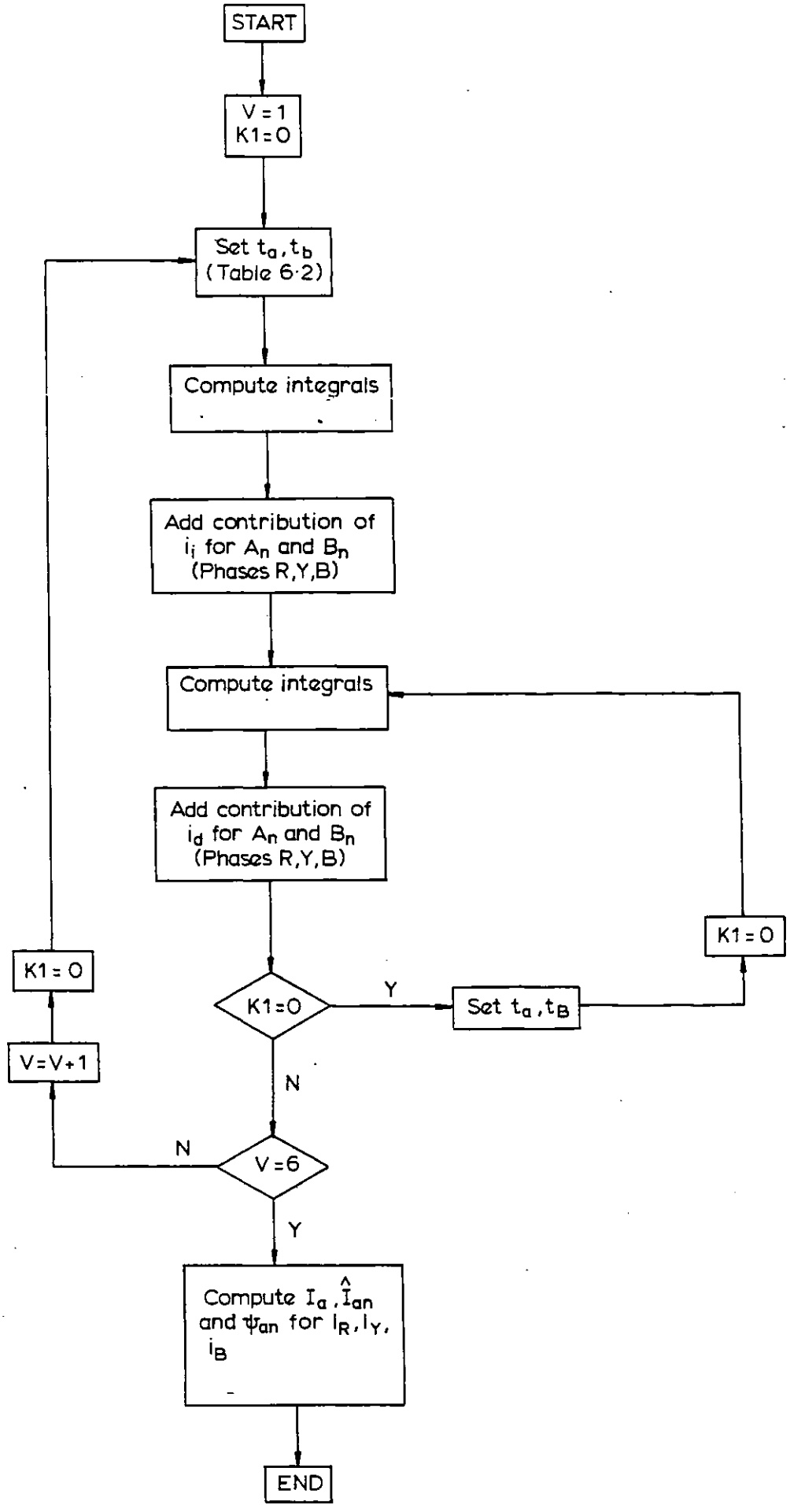

Fig. 4

A.C. current harmonic calculation Flowchart

A number of simplifications can be implemented on the calculation of both d.c. and a.c. harmonics which afford reduction of computer times without appreciable loss of accuracy. This matter will be discussed in the next sections.

4.4 Steady-state analysis of an h.v.d.c. link

The non-linear converter model developed in Chapter Three and the harmonic calculation presented in this chapter enable the calculation of all quantities of interest for a biterminal h.v.d.c. link in the steady-state. The d.c. system is assumed to be operating in open-loop, i.e. without current control, the input control voltage being constant. Its value is set to a level which yields the desired firing angle in the steady-state. If there is imbalance and/or distortion in the a.c. voltage, the firing angle is not the same for all valves (although the interfiring period may be constant with PPC or PFC firing systems, but not with IPC), the average value is made equal to the desired value.

The degree of imbalance and/or distortion of the a.c. bus voltage can be set at will, on both rectifier and inverter ends. If the a.c. system is assumed to be infinite, the imbalance/distortion imposed will not be changed throughout the calculation. On the other hand, for a finite a.c. system, the final pattern of distortion in the a.c. bus is different from the initial assumption, due to the voltage drop caused by the a.c. current harmonics in the source network impedance. In this case an iterative process is necessary, since the voltage drop is not known a priori.

The computer program accepts as data

- Three phase-to-neutral a.c. bus voltages, fundamental component (magnitude and phase); both on the rectifier and inverter ends.
- Up to 30 harmonic components of the a.c. voltage generated by the a.c. supply systems.
- Nominal firing angle of the rectifier.
- Nominal extinction angle of the inverter.
- Converter transformer impedance.
- Converter transformer voltage ratio.
- Transmission line parameters.
- D.C. filter parameters.
- A.C. filter parameters.
- D.C. current.

and yields results

- Voltage zero crossings of the commutating voltages.
- Firing angle for each valve and average of six valves.
- Firing instant for each valve.
- Commutation angle.
- D.C. current harmonic content.
- A.C. current fundamental component and harmonic content on both sides of the converter transformer.
- A.C. voltage fundamental component and harmonic content on the converter busbar (if a.c. system is finite).

4.4.1 Infinite a.c. systems

The case where both rectifier and inverter a.c. system are infinite will be dealt with in this section. Due to this feature the a.c. bus voltages are constant (fundamental and harmonic), irrespective of the operating conditions.

The calculation is particularly simple under these conditions because no iterative process is required to adjust the a.c. bus voltage. However, since the commutation angle and the d.c. voltage harmonics are dependent upon this d.c. current harmonic content (see figs 3.8 and 4.2), which is not known a priori, an iterative process is, in principle, necessary to calculate these quantities.

A flowchart is presented in fig 4.5 for the steady-state calculation of the d.c. link with infinite a.c. systems. The inverter is simulated by a fixed e.m.f., its equivalent negative resistance due to commutation being included in the d.c. line resistance. Since the d.c. current is imposed and the rectifier voltage constant term is not known a priori (it depends on the commutation angle), the inverter e.m.f. is allowed to vary from iteration to iteration until convergence is achieved.

As was pointed out in section 3.3.1, the iterative process is slowly convergent and greatly increases the computation time. Fortunately, the influence of the d.c. current harmonics on the commutation angle is small and can be disregarded without appreciable error. Its influence on the d.c. voltage is, however, sizable, due to the voltage drop on the transformer impedance. Taking again Test System 1, represented in fig 3.9, the results obtained for the d.c. current harmonics with and without a modulating signal at 50 Hz are shown in Tables 4.3 and 4.4 respectively.

To reduce the excessive computing time resulting from the iterative method, an approximate non-iterative method was

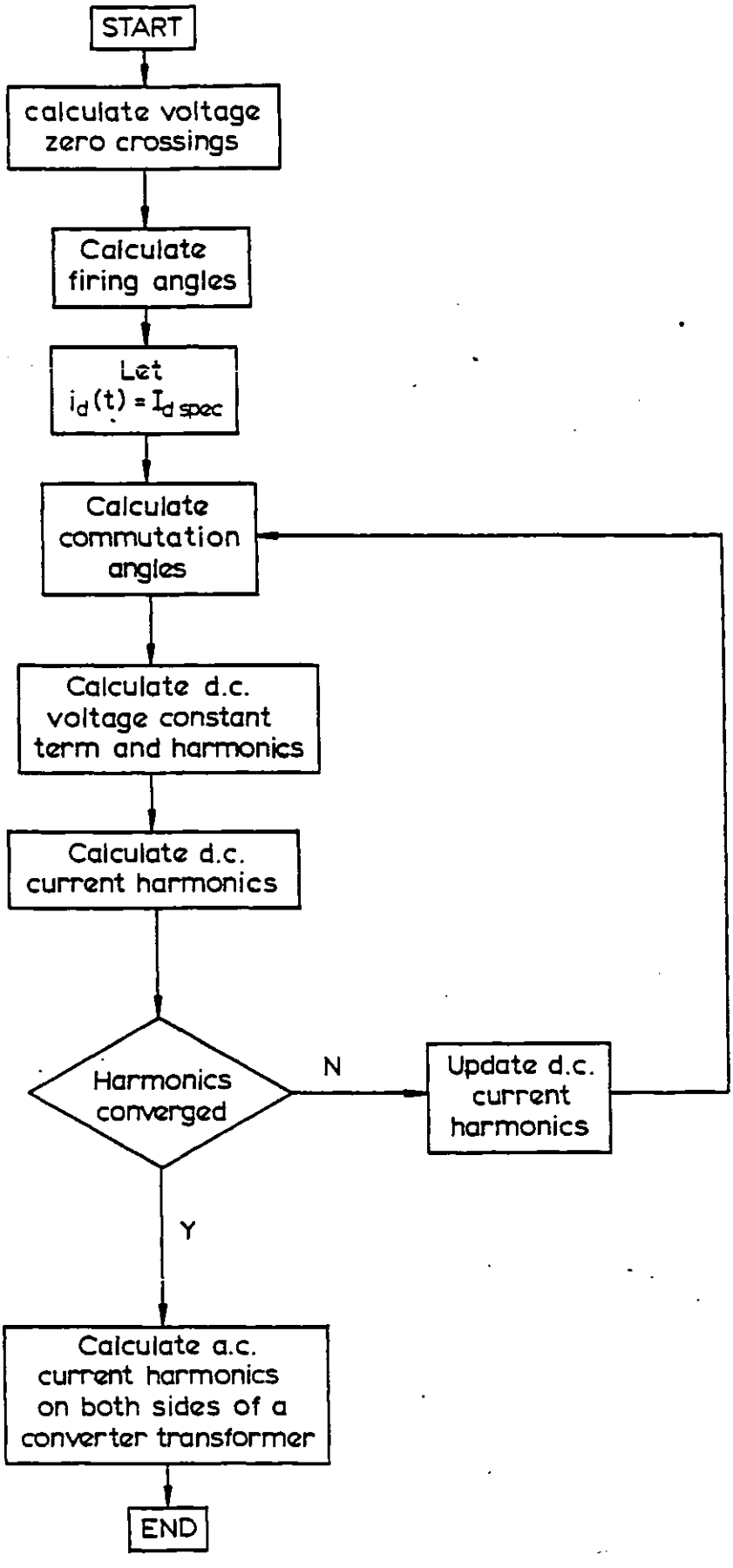

Fig. 4.5

Steady - state calculation of d.c. link.
Infinite a.c. systems.

Table 4.3: D.C. Current Harmonics (no modulating signal)

	First iteration		Converged values	
Harmonic Order	Magnitude (KA)	Phase (deg)	Magnitude (KA)	Phase (deg)
6	0.03198	-149.00	0.02680	-145.50
12	0.00472	150.00	0.00397	-177.00
18	0.00083	99.74	0.00075	107.19
24	0.00093	-9.04	0.00074	2.24
30	0.00103	-53.67	0.00080	-44.28

Table 4.4: D.C. Current Harmonics (modulating signal at 50 Hz)

	First iteration		Converged values	
Harmonic Order	Magnitude (KA)	Phase (deg)	Magnitude (KA)	Phase (deg)
1	0.03633	137.50	0.03073	143.10
2	0.00151	96.70	0.00130	101.56
3	0.00021	-173.50	0.00020	-177.20
4	0.00650	-147.50	0.00102	-152.08
6	0.03154	-129.30	0.02638	-128.21
7	0.00423	-124.80	0.00385	134.00
8	0.00050	40.67	0.00047	44.50
9	0.00012	-167.10	0.00010	-164.40
10	0.00056	-163.20	0.00045	-165.80

devised which yields results very close to the former. The internal resistance and inductance of the converter can be averaged and located externally to the converter in series with the d.c. current. Denoting by R_t and L_t the transformer resistance and inductance per phase, the internal resistance and inductance of the converter change from $\frac{3}{2} R_t$ and $\frac{3}{2} L_t$ when three valves are conducting ($0 < \omega_o t < u^o$) to $2R_t$ and $2L_t$ when two valves are conducting ($u^o < \omega_o t < \frac{\pi}{3}$). The average values are consequently:

$$R_{av} = \frac{u^o \frac{3}{2} R_t + (\frac{\pi}{3} - u^o) 2R_t}{\frac{\pi}{3}}$$

$$= 2R_t (1 - \frac{3u^o}{4\pi}) \qquad (4.77)$$

and similarly

$$L_{av} = 2L_t (1 - \frac{3u^o}{4\pi}) \qquad (4.78)$$

R_t and L_t should be interpreted as mean values if they are different for the three phases; the same applies to u^o, if different for the six valves.

For the same conditions as in Table 4.4 the results of the calculation using the approximate method are compared in Table 4.5 with the converged values of the exact method. The difference in the amplitude is only about 0.5%; the computing time is reduced by a factor of 80. The benefits of the approximate method are so obvious that it will be systematically used throughout this work.

Table 4.5: D.C. Current Harmonics (modulating signal at 50 Hz)

	Exact method		Approximate method	
Harmonic Order	Magnitude (KA)	Phase (deg)	Magnitude (KA)	Phase (deg)
1	0.03073	143.10	0.03056	136.95
2	0.00130	101.56	0.00127	95.78
3	0.00020	-177.20	0.00017	-173.73
4	0.00102	-152.08	0.00101	-147.65
5	0.00528	-146.83	0.00546	-142.63
6	0.02638	-128.21	0.02652	-129.44
7	0.00385	134.00	0.00356	134.73
8	0.00047	44.50	0.00042	40.62
9	0.00010	-164.40	0.00010	-167.20
10	0.00045	-165.80	0.00042	-165.20

In Table 4.6 to 4.10 the results of selected calculations are shown for Test System 2 represented in fig 4.6, with the following parameters:

D.C. voltage per bridge at rated current	250 kV
Rated d.c. current	2 kA
Converter transformer	
Rating	591 MVA
Copper loss	2500 kW
Voltage ratio	400±15%/209 kV
Nominal firing angle (rectifier)	15^{o}
Nominal extinction angle (inverter)	18^{o}
Smoothing inductor (per station)	
Resistance	0.325Ω
Inductance	0.5 H
Transmission line	
Length	800 km
Resistance	10 Ω
Inductance	0.48 H
Capacitance	23-28μ F

The d.c. line has a resonance at 50 Hz if the capacitance is 27.38 μF. For the range considered the resonance varies between 54.5 and 49.5 Hz.

Table 4.6 refers to the base case with balanced and undistorted a.c. voltages, yielding the characteristic harmonics both on the d.c. and on the a.c. side. Only one six-pulse converter is assumed to be in operation.

In Table 4.7, 1% second harmonic distortion with positive sequence was assumed on the a.c. busbar. A component at the

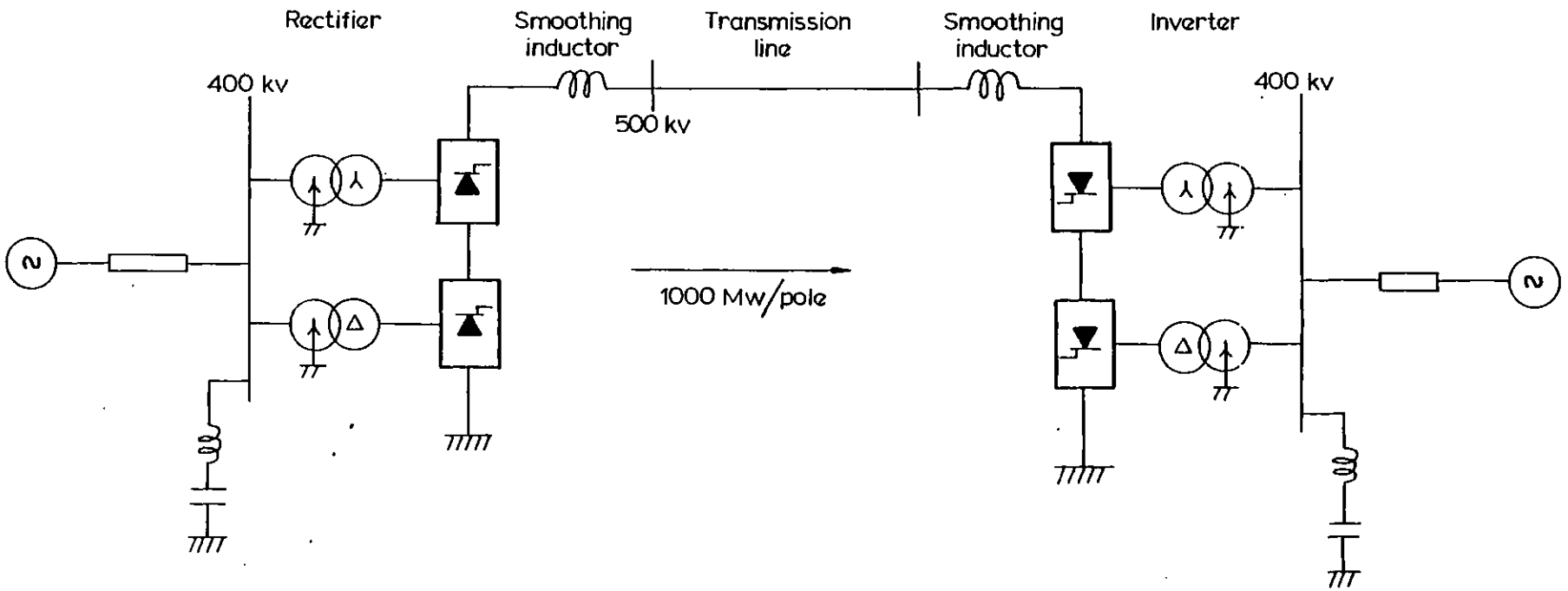

Fig. 4·6

Test system 2

Data a.c. busbar voltages

	PHASE R		PHASE Y		PHASE B	
Order	KV	DG	KV	DG	KV	DG
1	230.94	0	230.84	-120.00	230.94	120.00

D.c. voltage constant term (KV) 250.32
D.c. current constant term (KA) 2
D.c. current harmonics

Order	KA	DG
6	.0193	164.82
12	.0036	-8.14
18	.0029	-100.57
24	.0009	166.22
30	.0006	-9.23

A.c. currents - busbar side

	PHASE R		PHASE Y		PHASE B	
Order	KA	DG	KA	DG	KA	DG
1	1.1469	-26.40	1.1469	213.60	1.1469	93.60
5	.2076	46.94	.2076	166.94	.2076	-73.06
7	.1234	-3.99	.1234	236.01	.1234	116.01
11	.0520	65.11	.0520	185.11	.0520	-54.89
13	.0330	9.48	.0330	249.48	.0330	129.48
17	.0091	42.65	.0091	162.65	.0091	-77.35

Table 4.6

Base case s.c.r. =∞

Data a.c. busbar voltage

	Phase R		Phase Y		Phase B	
Order	KV	DG	KV	DG	KV	DG
1	230.34	0	230.34	-120°	230.34	$+120^{\circ}$
2	2.3	0	2.3	-120°	2.3	$+120^{\circ}$

D.c. voltage constant term (KV): 250.32
D.c. current constant term (KA): 2

D.c. current harmonics

Order	KA	DG
1	.1182	85.71
5	.0005	-99.71
6	.0194	164.83
7	.0005	-159.67
11	.0002	137.51
12	.0037	-8.19
13	.0001	77.66

A.c. currents - busbar side

	Phase R		Phase Y		Phase B	
Order	KA	DG	KA	DG	KA	DG
1	1.147	-26.39	1.147	213.60	1.147	93.61
2	.0349	-80.99	.0349	159.01	.0349	39.00
4	.0051	64.85	.0051	184.88	.0051	-55.13
5	.2077	46.99	.2077	166.96	.2078	-73.04
6	.0097	-21.45	.0049	115.42	.0070	186.83
7	.1237	-3.98	.1235	236.01	.1236	116.08
8	.0045	257.32	.0045	147.28	.0045	27.27
10	.0016	14.05	.0016	134.21	.0016	254.18
11	.0523	65.17	.0321	185.13	.0522	-54.99
12	.0037	-55.70	.0023	106.61	.0016	150.36
13	.0332	9.26	.0331	249.41	.0332	129.51

Table 4.7

Second harmonic distortion, positive sequence

s.c.r. = ∞

fundamental frequency is obtained for the d.c. voltage, yielding a corresponding large d.c. current due to the line resonance. On the a.c. side, besides the characteristic harmonics, all the even harmonics are obtained.

If the second harmonic on the a.c. busbar has negative rather than positive sequence, as shown in Table 4.8, the harmonic pattern is profoundly affected. On the d.c. side, all triplen harmonics are generated, but not a component of the fundamental frequency. On the a.c. side all harmonics but triplens are present. The difference between this case and that of Table 4.7 is of great importance on the system stability, as will be shown later.

In Table 4.9 imbalance both in amplitude (1%) and phase (2%) was assumed for the fundamental component of the a.c. voltage. This means that there is both a negative and a zero sequence. The latter is, however, of no importance, since it is filtered out by the converter transformers. The harmonic pattern is in this case as follows: on the d.c. side all even harmonics are produced; on the a.c. side the characteristic harmonics together with the multiples of three are generated. Of particular interest are the 3rd and 9th harmonics, the other uncharacteristic harmonics being of rather small amplitude.

The addition of a ±10% imbalance in the converter transformer impedances does not change the harmonic pattern, although it does contribute to the magnification of the uncharacteristic harmonics. This is shown in Table 4.10, which shows the results of the steady-state calculation with

Data a.c. busbar voltage

	Phase R		Phase Y		Phase B	
Order	KV	DG	KV	DG	KV	DG
1	230.94	0	230.94	-120	230.94	120
2	2.3	0	2.3	120	2.3	-120

D.c. voltage constant term: 250.32
D.c. current constant term: 2

D.c. current harmonics

Order	.KA	DG
3	.0046	-74.08
6	.0194	164.83
9	.0003	-167.48
12	.0037	-8.19
13	.0001	37.24

A.c. currents - busbar side

	Phase R		Phase Y		Phase B	
Order	KA	DG	KA	DG	KA	DG
1	1.147	-26.41	1.147	213.59	1.147	93.59
2	.0048	-63.55	.0048	56.45	.0048	176.45
4	.0025	267.23	.0025	147.23	.0023	27.23
5	.2076	46.93	.2076	166.93	.2076	-73.07
7	.1234	4.00	.1234	236.	.1234	116.
8	.0027	-2.15	.0027	77.85	.0027	197.85
10	.0024	259.05	.0024	139.05	.0024	19.05
11	.0520	65.11	.0520	185.11	.0520	-54.89
13	.0330	9.49	.0330	249.49	.0330	129.49

Table 4.8

Second harmonic distortion, negative sequence

s.c.r. =∞

Data a.c. busbar voltages

	Phase R		Phase Y		Phase B	
Order	KV	DG	KV	DG	KV	DG
1	230.94	0	228.64	-118	230.94	120

D.c. voltage constant term (KV) 249.4
D.c. current constant term (KA) 2

D.c. current harmonics

Order	KA	DG
2	.0082	120.77
4	.0010	37.20
6	.0193	164.56
8	.0004	57.33
10	.0002	-67.16
12	.0037	-8.83

A.c. currents - busbar side

	Phase R		Phase Y		Phase B	
Order	KA	DG	KA	DG	KA	DG
1	1.143	-25.91	1.146	214.44	1.151	94.14
3	.0002	141.25	.0054	121.74	.0056	-67.45
5	.2082	49.32	.2094	170.65	.2046	-69.72
7	.1221	-.67	.1219	241.42	.1258	120.45
9	.0014	113.23	.0031	110.76	.0045	-66.46
11	.0518	69.83	.0535	193	.0521	-46.81
13	.0316	15.29	.0323	260.58	.0345	136.93

Table 4.9

A.c. unbalance in amplitude and phase

s.c.r. =∞

Data a.c. busbar voltages

	Phase R		Phase Y		Phase B	
Order	KV	DG	KV	DG	KV	DG
1	230.94	0	228.64	-118	230.94	120

D.c. voltage constant term (KV) 249.4
D.c. current constant term (KA) 2.

D.c. current harmonics

Order	KA	DG
2	.0126	96.56
4	.0007	-140.92
6	.0193	164.64
8	.0014	-8.43
10	.0002	-84.39
12	.0037	-8.89

A.c. currents - busbar side

	Phase R		Phase Y		Phase B	
Order	KA	DG	KA	DG	KA	DG
1	1.137	-25.82	1.151	214.67	1.153	93.83
3	.010	105.51	.0027	158.55	.0118	-64.07
5	.2129	49.08	.2049	171.96	.2012	-70.73
7	.1174	.14	.1254	242.85	.1265	118.37
9	.0092	106.24	.0005	234.90	.0089	-71.15
11	.0545	68.37	.0535	196.90	.0469	-48.46
13	.0290	19.04	.0350	263.05	.0342	132.19

Table 4.10

A.c. voltage plus transformer unbalance

s.c.r. =∞

simultaneous imbalance in a.c. voltage and transformer impedance.

4.4.2 Finite a.c. system on rectifier side

If the a.c. system connected to the rectifier is finite, the bus voltage has to be adjusted iteratively due to the voltage drop in the a.c. source impedance. The iterative process used is the accelerated Gauss method with some simplifications to reduce the computation time.

In fig 4.7 a flowchart for the calculation of the steady-state conditions of a two-terminal d.c. link with a finite a.c. system on the rectifier side is shown. The a.c. system on the inverter side is assumed to be infinite, the inverter being simply modelled as a back e.m.f. with a value which yields the specified d.c. current (constant term).

A Gauss-type iterative process is used to adjust the a.c. bus voltage which depends upon the a.c. current harmonics, which are not known a priori. Initial values of the imbalance and/or distortion of a.c. voltage can be specified, as well as imbalance in the converter transformer reactance.

The iterative process is fairly slow, therefore an acceleration factor was introduced to speed it up. The logic for the acceleration factor, which is only effective after the second iteration, is as follows:

a. The a.c. voltage amplitude in iteration 'n' is compared with that in iteration 'n-1'. If the convergence is monotonic, an acceleration factor is used; if the convergence is oscillatory, a deceleration factor is employed instead.

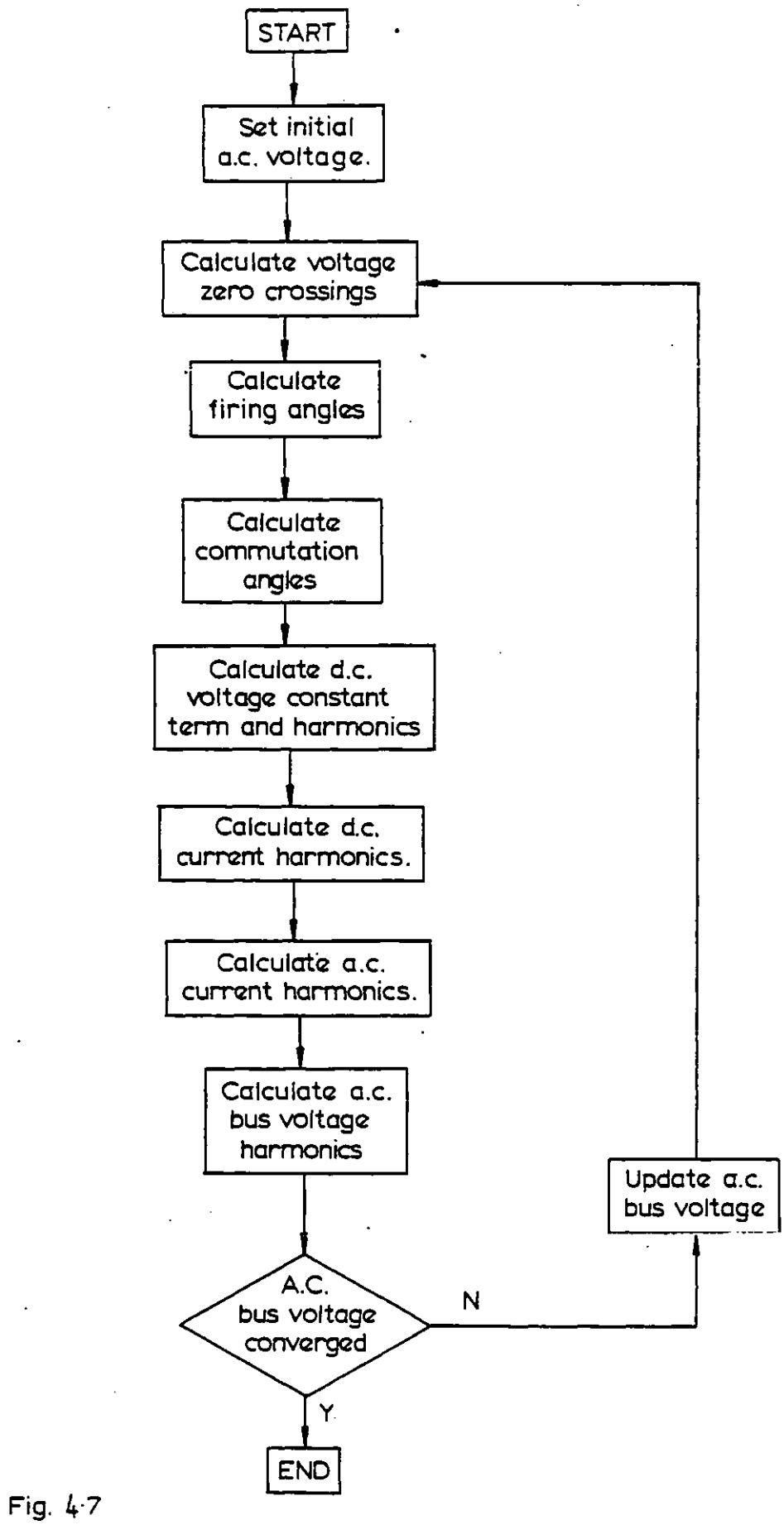

Fig. 4·7

Steady-state calculation of d.c. link.
Finite a.c. system on rectifier side.

b. The acceleration and deceleration factors are applied separately for each harmonic and each phase. Its value can be chosen by the user, being typically 1.4 for acceleration and 0.6 for deceleration.

c. A protection against divergence is implemented. If the mismatch for a particular harmonic is greater than the overall mismatch in iteration 'n-1', the acceleration (deceleration) factor is set to unity in iteration 'n'.

In Tables 4.11 to 4.17 the results of calculations are shown for Test System 2 with variable values of the short-circuit ratio on the rectifier a.c. system.

Tables 4.11 and 4.12 refer to the base case with a short-circuit ratio of 15 and 2 respectively. Convergence was achieved in three iterations for s.c.r. = 15 and four iterations for s.c.r. = 2. The difference between the results for both cases is fairly small, the reason being that the combined a.c. network plus filter impedance for the characteristic harmonics is approximately the same in both instances. Since no imbalance/distortion was assumed, no uncharacteristic harmonics are generated.

In Tables 4.13 and 4.14, 1% second harmonic distortion with positive sequence is assumed to be imposed on the a.c. converter busbar by the a.c. system. Table 4.13 refers to s.c.r. = 15 and Table 4.14 to s.c.r. = 3, convergence was achieved in 14 and 17 iterations, respectively. In this case, as was seen in section 4.4.1, a d.c. voltage component at

D.c. voltage constant term (KV) 250.60
D.c. current constant term (KA) 2

D.c. current harmonics

Order	KA	DEG
6	.0193	164.26
12	.0037	-9.79
18	.0031	-106.92
24	.0008	162.77
30	.0006	-15.34

A.c. voltage harmonics - busbar side

	Phase R		Phase Y		Phase B	
Order	KV	DG	KV	DG	KV	DG
1	230.9400	0	230.9400	-120.00	230.9400	120.00
5	.2770	217.24	.2770	-22.76	.2770	97.24
7	.3131	220.45	.3131	100.45	.3131	-19.55
11	.0483	236.28	.0483	-3.72	.0483	116.28
13	.0583	141.76	.0583	21.76	.0583	216.76
17	.6946	-74.33	.6946	45.67	.6946	165.67
19	.8279	133.27	.8279	13.27	.8279	253.27

Table 4.11

Base case s.c.r. = 15

D.c. voltage constant term (KV) 250.62

D.c. current constant term (KA) 2

D.c. current harmonics

Order	KA	DG
6	.0193	164
12	.0037	-9
18	.0030	-109
24	.0008	162
30	.0006	-15

A.c. voltage harmonics - busbar side

	Phase R		Phase Y		Phase B	
Order	KV	DG	KV	DG	KV	DG
1	230.9400	0	230.9400	-120.00	230.9400	120.00
5	.2763	214.44	.2763	-23.56	.2763	96.44
7	.3176	219.68	.3176	99.68	.3176	-20.32
11	.0482	236.14	.0482	-3.86	.0482	116.14
13	.0578	141.64	.0578	21.64	.0578	261.64
17	.8886	-83.10	.8886	36.90	.8886	156.90
19	.7778	113.73	.7778	-6.27	.7778	233.73

Table 4.12

Base case s.c.r. = 2

D.c. voltage constant term (KV) 250.60
D.c. current constant term (KA) 2

D.c. current harmonics

Order	KA	DG
1	.0727	78.40
5	.0004	-98.65
6	.0193	164.28
7	.0000	170.04
11	.0001	122.86
12	.0037	-9.84
13	.0001	113.08

A.c. voltage harmonics - busbar side

	Phase R		Phase Y		Phase B	
Order	KV	DG	KV	DG	KV	DG
1	230.9400	0	230.9400	-120.00	230.9400	120.00
2	1.2777	1.01	1.2776	242.01	1.2776	121.02
4	.1508	183.74	.1508	-56.24	.1507	63.76
5	.2771	217.27	.2771	-22.75	.2772	97.25
6	.5014	92.68	.2499	208.04	.4544	-57.52
7	.3134	220.46	.3132	100.45	.3133	-19.51
8	.8351	44.97	.8354	-75.07	.8347	164.93

Table 4.13

Second harmonic distortion, positive sequence

s.c.r. = 15

D.c. voltage constant term (KV) 250.61
D.c. current constant term (KA) 2

D.c. current harmonics

Order	KA	DG
1	.0832	35.53
5	.0014	-86.17
6	.0194	164.32
7	.0014	-177.81
11	.0005	148.86
12	.0037	-10.19
13	.0003	71.66

A.c. voltage harmonics - busbar side

	Phase R		Phase Y		Phase B	
Order	KV	DG	KV	DG	KV	DG
1	230.94	0	230.94	-120^{o}	230.94	-120^{o}
2	6.324	-13.31	6.325	226.70	6.325	106.69
4	.2166	267.57	.2167	27.59	.2166	147.61
5	.2765	216.46	.2766	-23.55	.2765	96.48
6	.2009	152.43	.3048	162.06	.5040	-21.76
7	.3174	219.66	.3175	99.70	.3177	-20.33
8	.3619	60.86	.3623	-59.15	.3620	180.8

Table 4.14

Second harmonic distortion, positive sequence

s.c.r. = 3

the fundamental frequency is generated. Since the d.c. line resonates at close to 50 Hz, a strong d.c. current component at this frequency is generated, which in turn gives rise to a second harmonic current on the a.c. side.

For s.c.r. = 3, the a.c. system plus filter impedance exhibits a resonance at close to 100 Hz, which results in a large magnification of the second harmonic on the a.c. busbar, as can be appreciated from Table 4.14. The d.c. line resonance is at 54.5 Hz; if the line capacitance is adjusted to yield a resonance of precisely 50 Hz, the programme fails to converge. It is therefore not possible to evaluate the degree of harmonic magnification in the real system.

For s.c.r. = 15, the a.c. system plus filter impedance possesses a resonance at close to the 8th and the 19th harmonics, which results in an appreciable magnification of these two harmonics of the a.c. busbar voltage.

As a general rule, the presence of resonances either on the d.c. or the a.c. side occurring at the same frequency as any uncharacteristic harmonic, results in a considerable increase in the number of iterations and sometimes even to divergence of the computer simulation program.

Tables 4.15, 4.16 and 4.17 refer to the same conditions as Tables 4.8, 4.9 and 4.10, but with s.c.r. = 3. Since in none of these cases a d.c. component at fundamental frequency is generated, convergence is relatively fast: five, four and four iterations respectively. The a.c. resonance at close to 100 Hz gives rise to a relatively strong second harmonic in Table 4.15; it does not affect the study cases of Tables

D.c. voltage constant term (KV) 250.61
D.c. current constant term (KA) 2

D.c. current harmonics

Order	KA	DG
3	.0060	-66.36
6	.0194	164.25
9	.0003	-139.77
12	.0038	-9.83
15	.0002	43.39

A.c. voltage harmonics - busbar side

	Phase R		Phase Y		Phase B	
Order	KV	DG	KV	DG	KV	DG
1	230.54	0	230.94	-120	230.94	120
2	3.296	11.08	3.296	131.06	3.296	251.06
4	.0936	-1.69	.0936	238.31	.0937	118.31
5	.2764	216.46	.2764	-23.54	.2764	96.46
7	.3172	219.69	.3172	99.69	.3172	-20.31
8	.3525	61.38	.3525	181.38	.3525	-58.62
10	.0388	-1.85	.0388	238.15	.0388	118.15

Table 4.15

Second harmonic distortion, negative sequence

s.c.r. = 3

D.c. voltage constant term (KV) 249.67
D.c. current constant term (KA) 2

D.c. current harmonics

Order	KA	DG
2	.0084	115.91
4	.0011	48.96
6	.0193	163.97
8	.0003	53.17
10	.0002	-55.60
12	.0038	-10.48
14	.0001	-76.66

A.c. voltage harmonics - busbar side

	Phase R		Phase Y		Phase B	
Order	KV	DG	KV	DG	KV	DG
1	230.94	0	228.64	-118	230.94	120
3	.0004	123.75	.0058	120.59	.0061	-59.23
5	.2082	50.33	.2088	171.63	.2044	-68.88
7	.1216	.61	.1215	242.82	.1256	121.76
9	.0017	118.97	.0030	112.98	.0047	-64.88
11	.0515	71.79	.0530	195.15	.0496	-44.96
13	.0312	17.47	.0319	262.98	.0342	139.18

Table 4.16

A.c. voltage imbalance in amplitude and phase

s.c.r. = 3

D.c. voltage constant term (KV) 249.67
D.c. current constant term (KA) 2

D.c. current harmonics

Order	KA	DG
2	.0125	90.77
4	.0110	-173.52
6	.0193	164.96
8	.0014	-11.76
10	.0001	-46.66
12	.0037	-10.53
14	.0006	-118.15

A.c. voltage harmonics - busbar side

	Phase R		Phase Y		Phase B	
Order	KV	DG	KV	DG	KV	DG
1	230.94	0	228.64	-118	230.94	120
3	.6878	198.59	.1298	255.57	.7663	26.75
5	.2839	218.65	.2763	-18.44	.2678	98.68
7	.3007	223.85	.3230	106.67	.3256	-18.10
9	.2779	202.20	.0219	5.88	.2570	23.57
11	.0508	239.47	.0494	6.12	.0434	122.15
13	.0500	151.20	.0616	35.44	.0602	263.93

Table 4.17

A.c. voltage plus transformer unbalance

s.c.r. = 3

4.16 and 4.17, since no second harmonic is produced on the a.c. side.

4.4.3 Finite a.c. systems on rectifier and inverter sides

If the a.c. system connected to the inverter terminal is finite, the a.c. busbar voltage at this terminal has to be adjusted iteratively as for the rectifier. Furthermore, a harmonic evaluation has also to be carried out on the inverter side to determine the final pattern of a.c. and d.c. harmonic voltages.

As the inverter operates on extinction angle control mode, the evaluation of the firing instants is somewhat different from the evaluation of the firing instants on the rectifier side.

To control the extinction angle, feedback control (2) is assumed and a PFC type of firing system considered (see section 3.2.3).

Extinction angle control keeps the smallest of six extinction angles at the prescribed value. As the value of the firing angle is not known a priori from the specified value of the extinction angle, an estimate of the firing angle is needed.

At the beginning of the process (first iteration), an estimate of the firing angle is obtained from the classic equation:

$$\cos \alpha_{est} + \cos \gamma_{sp} = \frac{\omega_o (L_i + L_o)}{|V_{io}|} \qquad (4.79)$$

where $|V_{io}|$ is obtained from equation (3.39) for h=1.

$$V_{io} = S_1 \sin \omega_o t + C_1 \cos \omega_o t \qquad (4.80)$$

thus:

$$|V_{io}| = (S_1^2 + C_1^2)^{\frac{1}{2}} \qquad (4.81)$$

In the remaining iterations the value of firing angle obtained in the previous iteration is taken as an estimate of the firing angle for the current iteration.

From the estimate of α the starting instant of the ramp for the first valve to be fired can be computed (see section 3.2.3):

$$t_{in} = -\left[\frac{\pi}{3\omega_o} - \left(\frac{\text{v.z.c.(1)}}{\omega_o} + \frac{\alpha_{est}}{\omega_o}\right)\right] \qquad (4.82)$$

The firing angles and commutation angles for the six valves can now be evaluated using the subroutines developed for the rectifier.

From the values of the firing angles, commutation angles and voltage zero crossing between valves connected to the same a.c. phase, the extinction angles for the six valves can be computed:

$$\gamma = (\text{v.z.c.})_{int} - (\alpha + u) \qquad (4.83)$$

where $(\text{v.z.c.})_{int}$ stands for voltage zero crossing interval.

The minimum extinction angle is compared with the set value, the difference giving rise to an adjustment of α^o and repetition of the computations until convergence is achieved.

During this iterative procedure a situation may occur in which no solution for the commutation angle evaluation exists. This is due to a "bad" estimate of the firing angle and occurs only during the first iterations when the a.c. voltage waveform

is badly distorted.

If such a situation occurs, a new estimate of α_{est} is taken by decreasing its value by γ_{sp}.

Figure 4.8 shows the flowchart of the subroutine that evaluates the firing, commutation and extinction angles.

All computations are similar for rectifier and inverter with the exception of the firing instants.

Once the d.c. voltage constant term and harmonics are obtained for both stations the d.c. current can be evaluated. In order to maintain the rated d.c. current, the d.c. voltage constant term on the inverter side has to be adjusted. This is achieved by acting on the inverter tap changer.

The contribution of each valve to the d.c. voltage waveform is given by equation (4.4)

$$v_{di}(t) = \begin{cases} V_{ik} - (R_k i_d + L_k \frac{di_d}{dt}) + V_{ic} & (\theta_i - \theta_l) < \omega_o t < (\theta_i - \theta_l) + \mu_i \\ V_{ik} - (R_i k_d + L_{ik} \frac{di_d}{dt}) & (\theta_i - \theta_l) + \mu_i < \omega_o t < (\theta_k - \theta_l) \end{cases} \tag{4.4}$$

All the a.c. voltages in equation (4.4) are referred to the converter side of the transformer. It is thus possible to rewrite this equation as a function of the a.c. voltages on the busbar side, and the transformer's ratio 'a'. Furthermore, if the influence of d.c. current harmonics in equation (4.4) is neglected, the constant term of d.c. voltage V_d depends only on the a.c. voltages on the busbar side, on the transformer's ratio 'a' and on the voltage drop in the transformer resistance due to the constant term of d.c. current. V_d can then be

Fig 4.8: Calculation of firing, commutation and extinction angles for the inverter

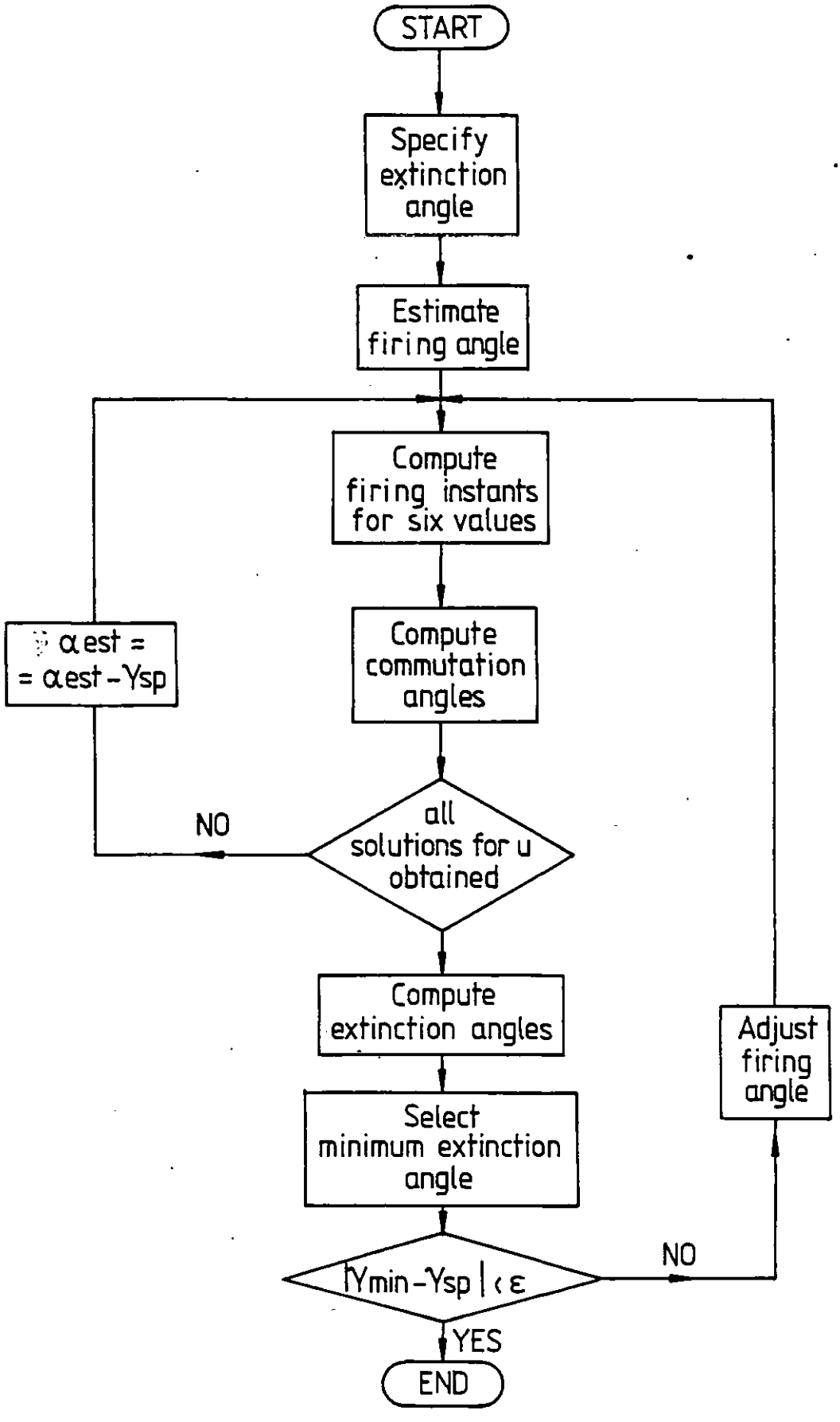

expressed as:

$$V_d = V'_d - \Delta V \qquad (4.84)$$

where V'_d represents the component of V_d that depends on the a.c. voltages (busbar side) and on the transformation ratio 'a' and ΔV represents the voltage drop in the transformer resistance.

Denoting by $V_{d\ comp}$ the constant term of d.c. voltage computed when performing the Fourier analysis of the d.c. voltage waveform, and by $V_{d\ imp}$ the constant term of d.c. voltage obtained in order to maintain the constant term of direct current at the specified value, $V_{d\ comp}$ and $V_{d\ imp}$ may be decomposed as in (4.84).

$$V_{d\ comp} = V'_{d\ comp} - \Delta V_{comp}$$

$$V_{d\ imp} = V'_{d\ imp} - \Delta V_{imp}$$

Thus:

$$V'_{d\ comp} = V_{d\ comp} + \Delta V_{comp} \qquad (4.85(a))$$

$$V'_{d\ imp} = V_{d\ imp} + \Delta V_{imp} \qquad (4.85(b))$$

An approximation to the value of ΔV is obtained by considering

$$\Delta V \simeq R_{av}\ I_d \qquad (4.86)$$

where R_{av} is given by equation (4.77).

The value of 'a' is finally obtained from

$$a = \frac{V'_{d\ comp}}{V'_{d\ imp}} \qquad (4.87)$$

Figure 4.9 shows the flowchart of the computer program when a finite a.c. system is considered on both the rectifier

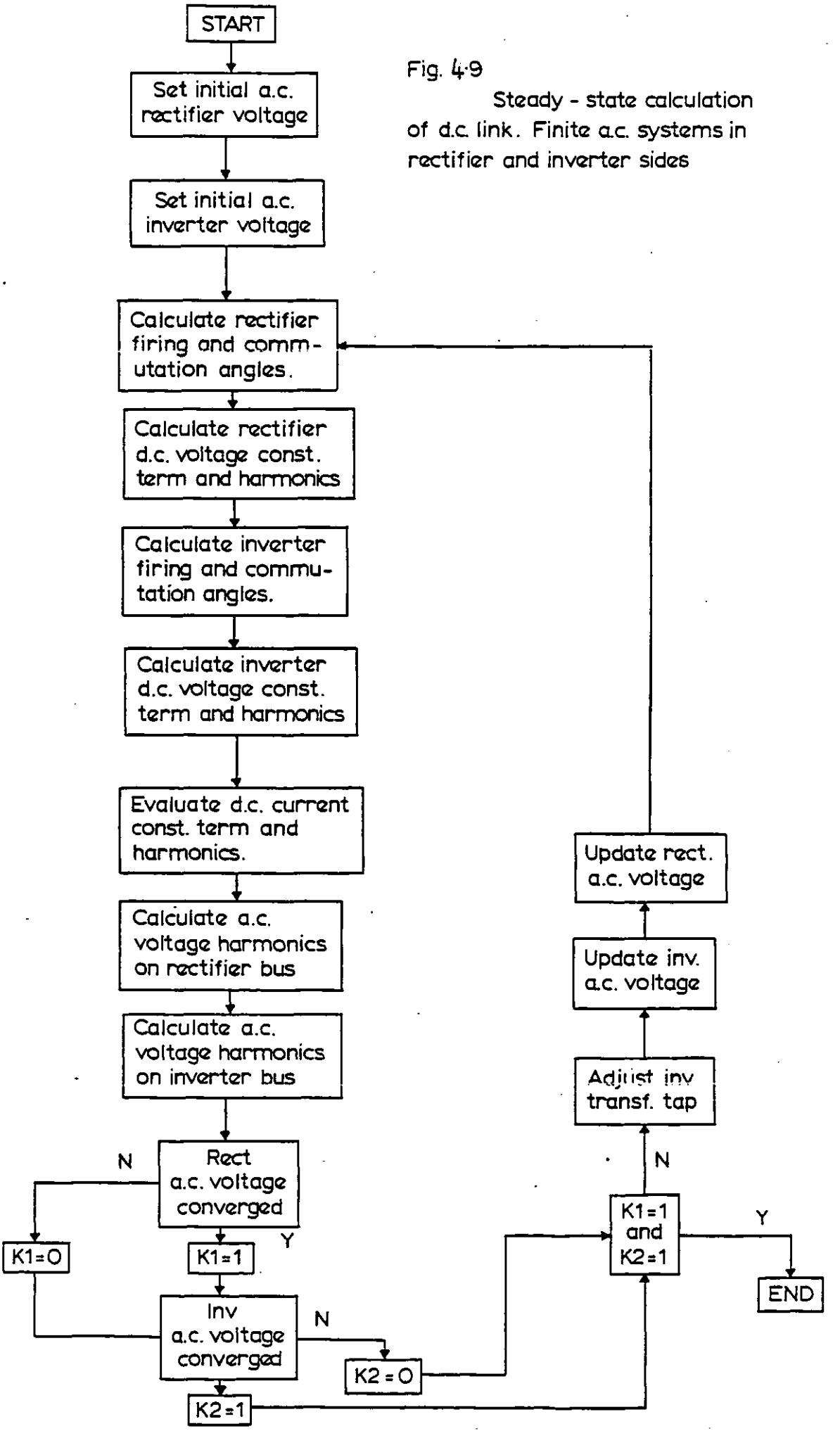

Fig. 4·9

Steady - state calculation of d.c. link. Finite a.c. systems in rectifier and inverter sides

and inverter sides.

The acceleration and deceleration procedures are identical to the ones detailed in section 4.4.2.

Tables (F.1) to (F.8) in Appendix F compile some of the studies carried out.

Comparison of these tables with the ones shown in section 4.4.2 allow the following conclusions:

a) For the base case with both high and low s.c.r. the d.c. voltage and current harmonics show no significant difference from the results obtained in section 4.4.2.

b) The 100 Hz d.c. harmonic generated by an imbalance in the fundamental voltage either on the rectifier or on the inverter has negligible influence on the a.c. voltage distortion in the terminal in which no voltage distortion was assumed. This means that the d.c. line acts as a filter for the 100 Hz. Also the consideration of an imbalance in the fundamental voltage both on the rectifier and inverter does not affect considerably the 100 Hz harmonic on the rectifier side. Modelling the inverter as a constant e.m.f. seems sufficient.

c) A second harmonic distortion with negative sequence in one of the terminals (yielding a 150 Hz d.c. harmonic) has no effect on the other terminal.

d) The only case which gives results significantly different from the ones obtained in section 4.4.2 is the one that generates a 50 Hz harmonic on the d.c. side.

Due to the s.c.r. considered both terminals possess a source impedance with a high value, capacitive characteristic and poor damping (damping angle equals 85^{o}). As the d.c. line

resonates at a frequency near 50 Hz, convergence was not achieved for the values of d.c. line capacitance given for fig 4.6 (23 μF). The value of capacitance was changed to 20 μF.

- Analysis of this case shows that when a 50 Hz harmonic appears on the d.c. current the final solution for both terminals is affected.

Thus for a 50 Hz d.c. current harmonic it is not valid to model the inverter as a constant e.m.f.

4.5 Conclusions

The calculation of d.c. voltage and a.c. current harmonics generated by a three phase bridge converter was dealt with in this chapter. Both characteristic and uncharacteristic harmonics are considered. The latter arising when the a.c. bus voltage is imbalanced and/or distorted, the firing is non equidistant or the converter transformer impedances are unequal for the three phases.

The Euler coefficients of the Fourier series expansion are calculated analytically, giving rise to rather involved mathematical expressions. However, this procedure is computationally much faster than the alternative method of a computer harmonic analysis of the waveforms obtained by numerical integration of the differential equations.

Both the d.c. voltage and a.c. current are periodic waveforms which can be decomposed in six sections, each in turn having two sub-sections, if their period is the same as the a.c. voltage fundamental period. This assumption implies

a modulating signal with a frequency multiple of the a.c. system fundamental frequency, which is of practical interest. If on the contrary, the frequency of the modulating signal were a submultiple of the a.c. fundamental frequency, a larger number of sections would have to be considered. Due to this feature of the waveforms, the Euler coefficients turn out to be a summation of a finite number of terms. In this study, the maximum number of harmonics considered is thirty, both on the a.c. and the d.c. sides.

The technique developed for the harmonic analysis of the converter voltage and current enables the steady-state calculation of and h.v.d.c. link under the most general conditions. A computer program was developed to perform this task both with infinite and finite a.c. terminal systems.

In the first case a non-iterative method can be used, since the a.c. bus voltage is fixed. To be precise, iterations are still necessary to take into account the influence of the d.c. current harmonics on the commutation angle and d.c. voltage. However, the first effect can be neglected altogether without significant error and the second can be approximated very closely by averaging the converter transformer resistance and reactance and placing them externally in series with the d.c. circuit.

With finite a.c. systems, a Gauss iterative method has to be used to adjust the a.c. bus voltage, which is dependent through the a.c. source plus filter impedance on the converter a.c. current which is not known a priori. The method is slowly convergent and acceleration and deceleration factors had

to be implemented to reduce the computation time. The numerical method may in some instances be divergent, when a d.c. system resonance occurs at $k\ \omega_o$, the frequency of the input signal and simultaneously an a.c. system anti-resonance occurs at $(k \pm 1)\ \omega_o$.

The computer program, with some modifications, can also be used for the calculation of describing functions, if a modulating signal of suitable frequency is superimposed to the constant input control voltage used in the steady-state analysis.

Chapter Five

DESCRIBING FUNCTION EVALUATION

5.1 Introduction

The steady-state simulation program described in Chapters Three and Four can be used with minor adaptations to calculate the describing function for h.v.d.c. systems. This method appears at the present time to be the most suitable for the analysis of harmonic stability of converter systems and was chosen for its simplicity and reliability. This method was also chosen because it is a natural extension of the frequency response methods previously used in the study of small-signal stability.

The describing function is defined as the ratio of the fundamental component of the output of a nonlinear system to the amplitude of the input signal. In general, the describing function depends on the input signal amplitude and frequency and is complex because a phase shift may occur between the input and the fundamental component of the output. For converter systems (and sampled-data systems in general) the describing function also depends upon the phase of the input signal measured in relation to the firing instants.

If the input to a non-linear device is a sinusoidal signal the describing function method assumes that the output is a periodic signal having the same fundamental frequency as the input. Therefore the analysis is concerned only with the fundamental component of the output waveform, all harmonics, subharmonics, and any d.c. component being neglected.

The assumption of a sinusoidal signal applied to the input of the non-linearity is based on the fact that the amplitude of all harmonics and subharmonics of the input frequency are generally much smaller than the amplitude of the fundamental. Furthermore the low-pass characteristic of the linear element further attenuates the amplitudes of all the harmonics of the input frequency. The describing function assumes the existence of only one non-linear element in the feedback loop control system which (element) is not time varying. If a system contains more than one non-linearity they must be lumped together to allow the evaluation of an overall describing function.

In this chapter the evaluation of the describing function for a two terminal h.v.d.c. system is dealt with. It is shown that the steady-state simulation program described in Chapter Four can be used to evaluate the describing function (d.f.) by considering a modulating signal superimposed on the input control voltage and determining the output harmonic of the relevant frequency.

5.2 Review of the describing function method

In order to derive a mathematical expression for the describing function consider the non-linear feedback system

of fig 5.1. If the input to the non-linear element N is given by

$$x(\omega t) = X \sin \omega t \tag{5.1}$$

the steady-state output y can be expressed by the series

$$y(\omega t) = Y_1 \sin (\omega t + \phi_1) + Y_2 \sin (2\omega t + \phi_2) + \ldots \tag{5.2}$$

The describing function is by definition the ratio of the phasor representation of the output component of frequency ω and the phasor representation of the input:

$$N(X,\omega) = \frac{Y_1(X,\omega)}{X} e^{j\phi_1(X,\omega)} \tag{5.3}$$

The describing function depends upon the amplitude and frequency of the input signal. The nonlinear element is thus considered to possess a gain and phase shift varying with the amplitude and frequency of the input signal.

The conditions for existence of a limit cycle in a non-linear feedback system can be predicted through the describing function, assuming that the linear element has a low-pass characteristic which effectively filters the harmonics of frequency higher than ω. It can be shown (24) that a sustained oscillation of amplitude X and frequency ω can exist if the following equation is satisfied:

$$1 + N(X, \omega)\, G(j\omega) = 0 \tag{5.4}$$

This condition can be written as

$$G(j\omega) = -\frac{1}{N(X, \omega)} \tag{5.5}$$

or, alternatively,

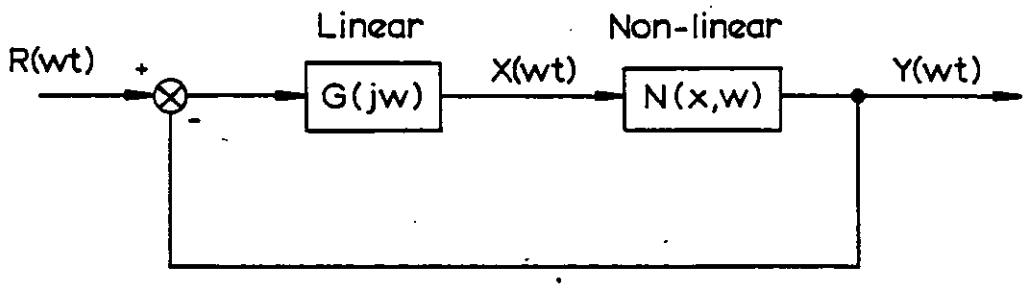

Fig. 5.1 General non-linear feedback system

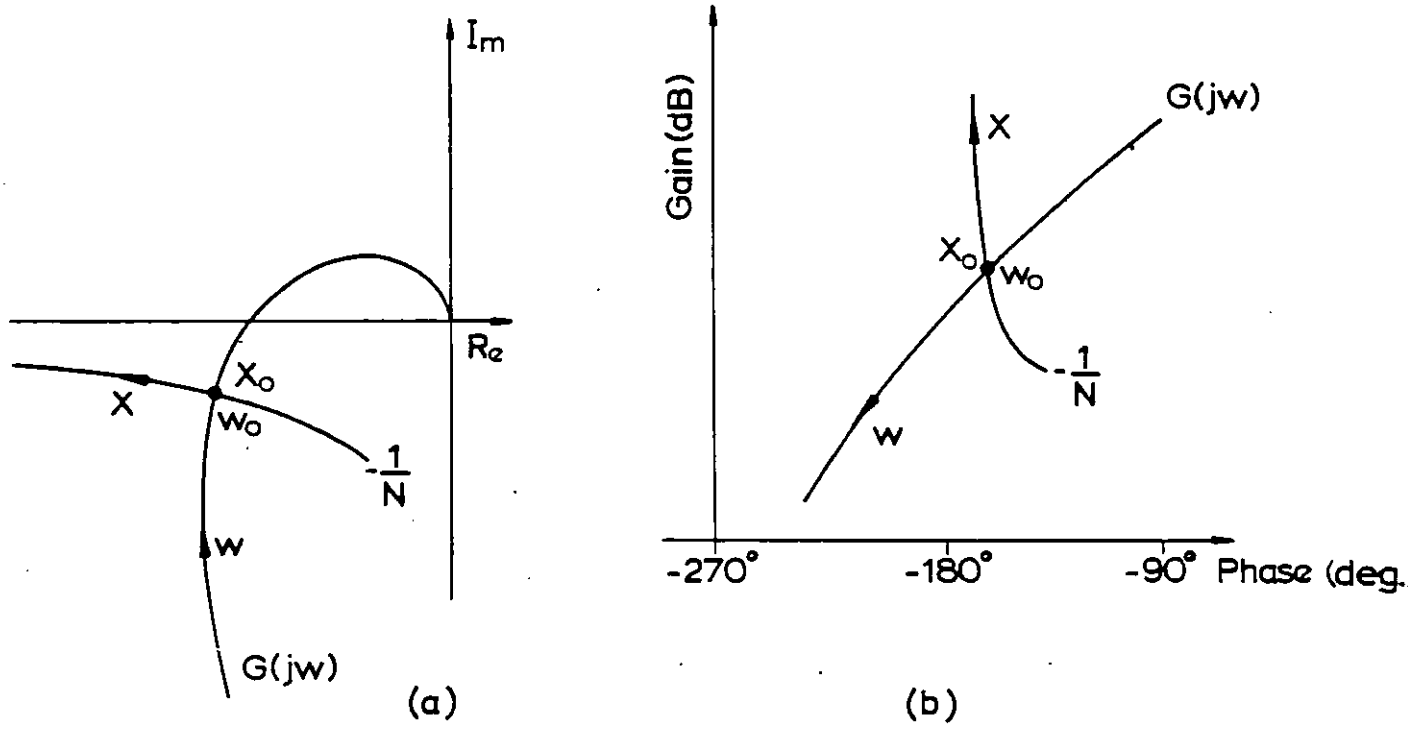

Fig. 5.2 Limit cycle with frequency w_o and amplitude X_o
(a) Polar plot (Nyquist)
(b) Gain-phase plot (Nichols)

$$N(X, \omega) = -\frac{1}{G(j\omega)} \qquad (5.6)$$

The Nyquist diagram or the Nichols chart (gain-phase plot) are the most widely used techniques for stability analysis utilising the describing function method. Two separate sets of loci, corresponding to $G(j\omega)$ and $-1/N(X, \omega)$ (or, alternatively $-1/G(j\omega)$ and $N(X, \omega)$) are plotted on the same graph for either of the two methods. In general, the sketch of $-1/N(X, \omega)$ will be a family of curves for different amplitudes X and frequencies ω.

Intersections of the two loci indicate possible solutions of equation (5.4) and yield information as to the magnitude and frequency of the sustained oscillation. If no intersection occurs, an oscillation is unlikely. This is illustrated in fig 5.2, which indicates the possibility of a limit cycle of frequency ω_o and amplitude X_o.

It remains to be discussed whether the limit cycle is itself stable or unstable. This can be determined by means of a perturbation analysis around the limit cycle. A generalised rule can be established for the gain-phase plot as shown in fig 5.3a. If the two loci are assigned a positive sense so that the linear locus $G(j\omega)$ is pointing towards increasing frequency and the non-linear locus $-1/N$ is pointing in the direction of increasing amplitude, then a stable limit cycle occurs when the non-linear locus appears to an observer, stationed on the linear locus and facing the direction of increasing frequency, to cross from left to right in the direction of increasing amplitude.

If a polar plot is used instead, then the limit cycle is stable when the non-linear locus crosses the linear locus from

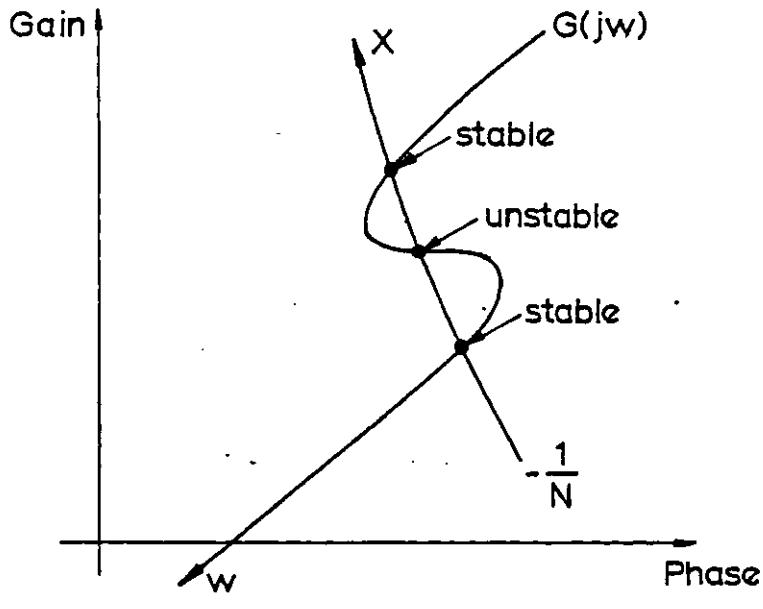

a

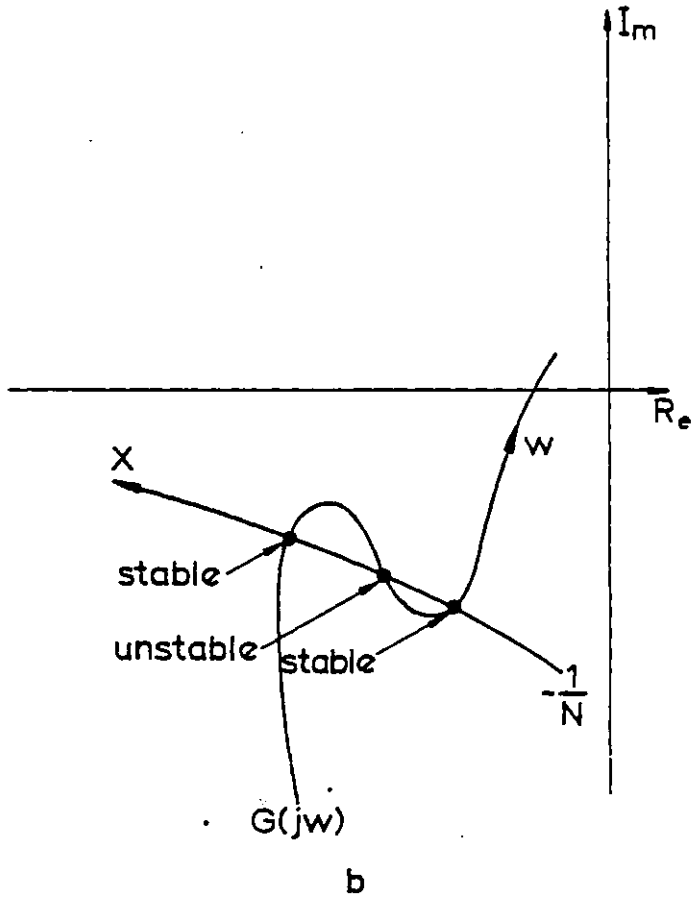

b

Fig. 5.3

Stability and instability of limit cycles
(a) Gain-phase plot
(b) Polar plot

right to left in the direction of increasing amplitude, as illustrated in fig 5.3b.

5.3 Describing function for sampled-data systems

A non-linear sampled-data system is represented in fig 5.4. For such a system it should be borne in mind that frequencies other than the fundamental are generated by both the non-linearity and the sampler.

The output of an ideal sampler, the input to which is a sinusoidal signal of frequency ω, is

$$Y^*(j\omega) = \frac{1}{T_s} \sum_{k=-\infty}^{+\infty} Y(j(\omega + k\omega_s)) \qquad (5.7)$$

where ω_s is the sampling frequency and T_s the sampling period ($\omega_s = 2\pi/T_s$).

Referring to fig 5.4 the frequency components of $x(t)$, $y(t)$ and $y^*(t)$ are:

Signal	Frequency components
$x(t)$	$\pm \omega$
$y(t)$	$\pm \ell\omega$
$y^*(t)$	$\pm \ell\omega \pm k\omega_s$

If ω/ω_s is irrational, i.e., if the frequency of $x(t)$ is not locked to the sampling frequency, $y^*(t)$ is aperiodic. If on the contrary, $\omega/\omega_s = m/n$, $y^*(t)$ is periodic with a period multiple of $2\pi m/\omega$. A particular case of this occurs when $\omega/\omega_s = 1/n$, i.e., the input frequency is a subharmonic of the sampling frequency: $y^*(t)$ is periodic with a period of $2\pi/\omega$.

N - Non-linearity
D - Digital controller
H - Hold device
L - Linear system

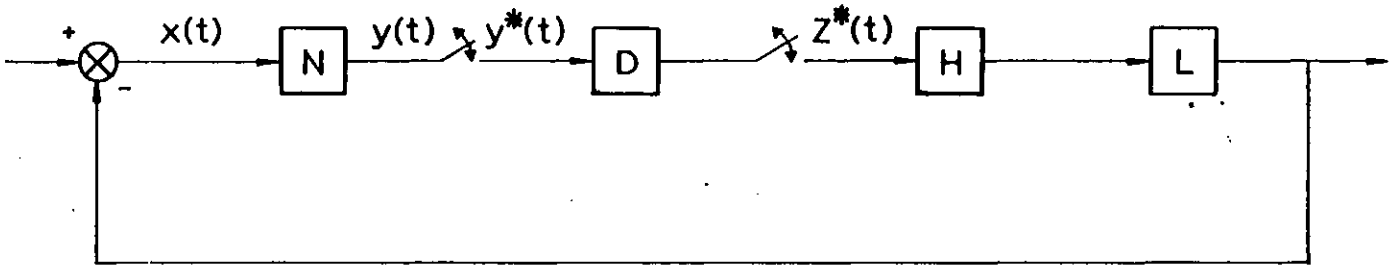

Fig. 5·4
Non-linear sampled-data feedback system

If ω/ω_s is irrational or $\omega/\omega_s = m/n$ then $y^*(t)$ may contain frequencies less than ω. These are produced by modulation of higher frequency harmonics of y, since the frequency spectrum of y^* is $\ell\omega_s \pm k\omega_s$. If $\omega/\omega_s = 1/n$, y^* contains no frequencies (other than d.c.) lower than ω. One can therefore conclude that the filtering hypothesis upon which the describing function method is based is only valid when the input signal is a subharmonic of the sampling frequency. This is also the case of greatest practical importance.

Furthermore, the phase relationship between the sampling instants and the input signal affects both the magnitude and phase of the describing function. For a given amplitude of the input, and letting the phase vary from zero to 2π radians, a closed curve is obtained. The describing function is therefore defined as

$$N(X, \omega, \phi) = \frac{Y_1(X, \omega, \psi)}{X} e^{j[\phi_1(X, \omega, \phi) - \psi]}$$

for an input signal

$$x(\omega t) = X \sin(\omega t + \psi) \qquad (5.9)$$

The condition for existence of a limit cycle can therefore be rewritten as

$$1 + N(X, \omega, \psi)\, G(j\omega) = 0 \qquad (5.10)$$

A feedback system with controlled converters is in many ways similar to a sampled-data system (1), in particular, when the converter is connected to an infinite busbar. If the

a.c. bus is finite, the similarity is not so close, however, many features of the d.f. for sampling systems also apply to power converters.

5.4 The dual input describing function

A relaxation of the conditions imposed on the signal fed back to the non-linearity can be obtained by introducing a generalisation to the d.f. definition.

In the so-called refined d.f. method (24) the exact output waveform is fed back and is therefore assumed as a new input to the non-linearity, the new fundamental output component being evaluated. Since the input signal to the non-linearity possesses a number of harmonics in addition to the fundamental, the fundamental term of the output will not normally be in phase with the fundamental term of the input even for a single valued non linearity.

The refined d.f. is however defined in the same way as the single input d.f., the difference being that in the refined d.f. the influence of the input harmonics affect the fundamental of the output.

The dual input describing function is a particular case of the refined d.f. method. In the dual input describing function the input signal to the non-linear element is assumed to possess two frequencies only, i.e.:

$$x(t) = X_1 \sin \omega_1 t + X_2 \sin (\omega_2 t + \psi_2) \qquad (5.11)$$

where ψ_2 is the phase of the signal at frequency ω_2 relatively to some reference.

The steady-state output $y(t)$ can be expressed as:

$$y(t) = \sum_{k=0}^{\infty} Y_k \sin (\omega_k t + \phi_k) \qquad (5.12)$$

The dual input describing function for frequency ω_1 is therefore:

$$N_{\omega 1} (X_1, X_2, \omega_1, \omega_2) = \frac{y_1 e^{j \phi_1}}{X_1} \qquad (5.13(a))$$

and for frequency ω_2

$$N_{\omega 2} (X_1, X_2, \omega_1, \omega_2) = \frac{y_2}{x_2} e^{j(\phi_2 - \psi_2)} \qquad (5.13(b))$$

It can be shown (38) that the influence of the signal with frequency $\omega_2 (\omega_1)$ in $N_{\omega 1}$ ($N_{\omega 2}$) depends on whether the two frequencies ω_1 and ω_2 are related or not. If the ratio ω_1 / ω_2 is not a ratio of integers (these frequencies are known as incommensurate) $N_{\omega 1} (N_{\omega 2})$ depends only on the amplitude of both input frequencies and not on the phase ψ_2.

If the ratio ω_1 / ω_2 is a ratio of integers (these frequencies are known as commensurate), $N_{\omega 1}$ ($N_{\omega 2}$) depends both on the amplitude and phase of the input signals.

In the case of control loops with controlled converters the frequencies of the input signal are commensurate and thus only this case will be dealt with here.

For commensurate frequencies the dual input describing function is a closed curve even for a continuous system (see fig 5.5).

For each amplitude of the fundamental frequency signal ω_1,

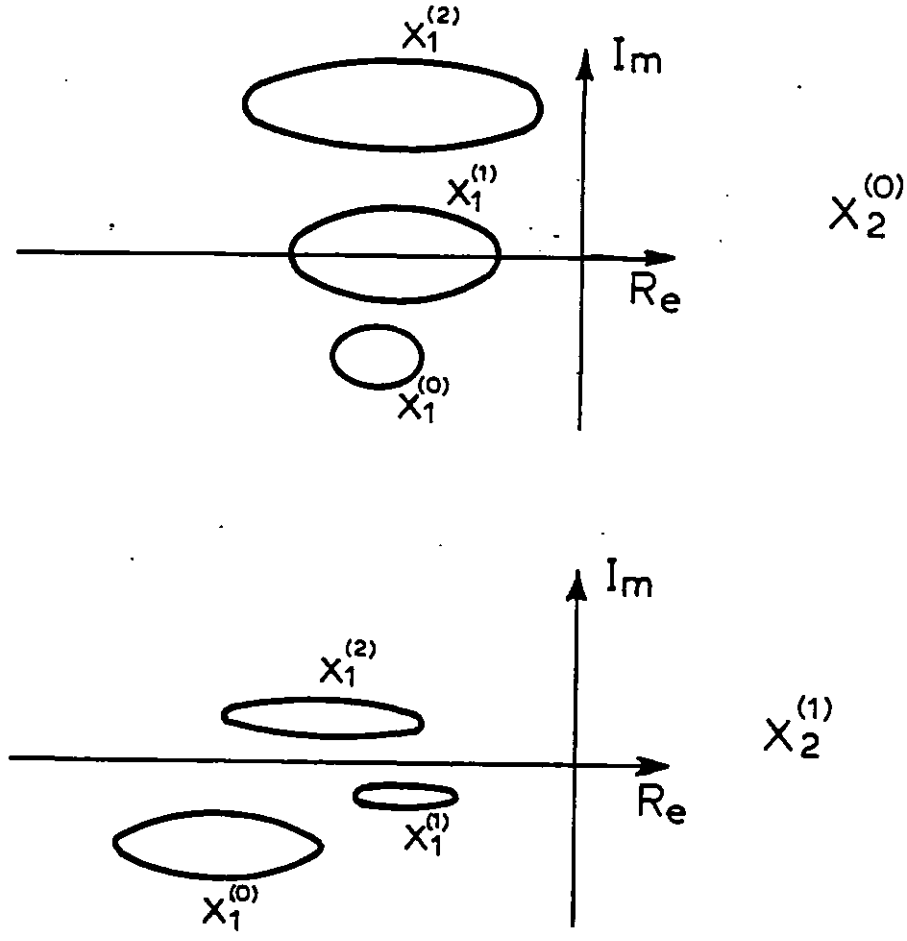

Fig 5.5: Dual input describing function N_{ω} for amplitudes of bias signal equal to $X_2^{(o)}$ and $X_2^{(1)}$

and for each amplitude of the bias signal ω_2 the phase difference must vary between 0 and 360°. The d.i.d.f. must be plotted for a large number of the amplitudes of the fundamental and bias signals.

The prediction of a limit cycle is a natural extension of the evaluation of limit cycles for single input d.f.s:

$$G(j\,\omega_1) = -\frac{1}{N_{\omega_1}(X_1, X_2, \omega_1, \omega_2, \psi_2)} \qquad (5.14)$$

In case equation (5.14) holds a sustained oscillation with frequencies ω_1 and ω_2, amplitudes X_1 and X_2 at a phase ψ_2 of the signal at frequency ω_2 is predicted.

The stability of limit cycles is determined using the rules described in section 5.2.

For sampled-data systems the d.i.d.f. for input frequency ω_1 can be defined as:

$$N_{\omega_1}(X_1, X_2, \omega_1, \omega_2, \psi_1, \psi_2) =$$

$$= \frac{Y_1(X_1, X_2, \omega_1, \omega_2, \phi_1)}{X_1}\, e^{j(\phi_1(X_1, X_2, \omega_1, \omega_2, \psi_1, \psi_2) - \psi_1)} \qquad (5.15)$$

for an input signal

$$x(t) = X_1 \sin(\omega_1 t + \psi_1) + X_2 \sin(\omega_2 t + \psi_2)$$

The condition for existence of a limit cycle can therefore be rewritten as:

$$1 + N_{\omega_1}(X_1, X_2, \omega_1, \omega_2, \psi_1, \psi_2)\, G(j\,\omega_1) = 0 \qquad (5.16)$$

5.5 Describing function for h.v.d.c. systems

H.v.d.c. systems invariably operate under constant current control. This is achieved by a feedback control loop, represented in fig 5.6.

The describing function refers to the hatched box, which contains the converter (non-linear element), the firing system and the d.c. system. To evaluate the d.f., a signal of amplitude V_m, frequency ω , and phase ψ is superimposed on to the steady-state control voltage v_c^o. The d.c. current i_d will contain a term at frequency ω with amplitude I_d and phase $\phi_{d\omega}$. The d.f. is defined as

$$N(V_m, \omega, \psi) = \frac{I_{d\omega}}{V_m} e^{j(\phi_{d\omega} - \psi)} \qquad (5.17)$$

For a given frequency and amplitude of the input signal, the d.f. depends upon its phase. Letting the phase vary from 0^o to 360^o a closed curve is obtained.

To evaluate the dual input describing function a signal of the form

$$V_m(t) = V_{m_1} \sin(\omega_1 t + \psi_1) + V_{m_2} \sin(\omega_2 t + \psi_2) \qquad (5.18)$$

is superimposed on to the steady-state control voltage V_c^o. The d.c. current i_d will contain terms at frequency ω_1 and ω_2. The d.i.d.f. for input signal at frequency ω_1 is defined as

$$N(V_{m_1}, V_{m_2}, \psi_1, \psi_2, \omega_1, \omega_2) = \frac{I_{d\omega 1}}{V_{m_1}} e^{j(\phi_{d\omega 1} - \psi_1)} \qquad (5.19)$$

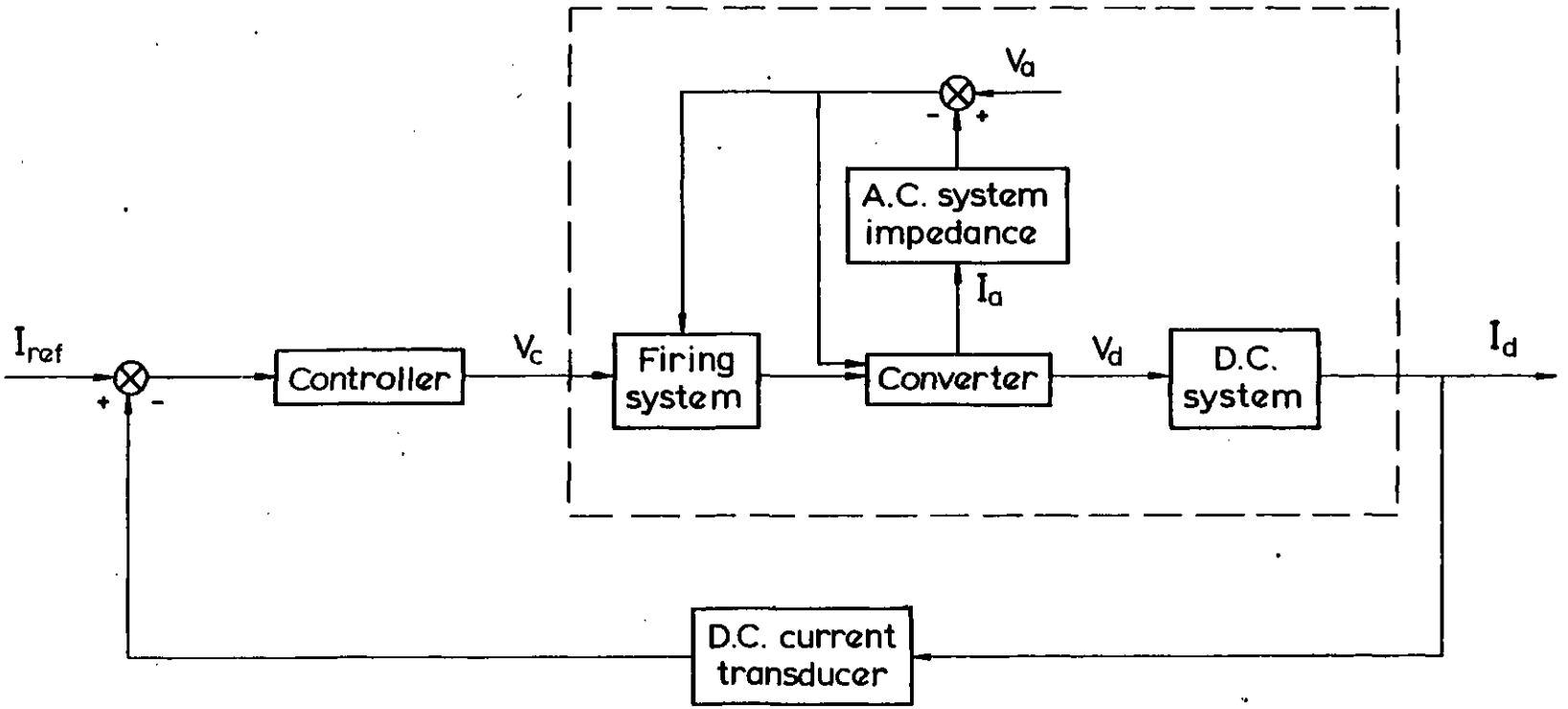

Fig. 5·6

Current control for h.v.d.c. system

The d.i.d.f. for input signal at frequency ω_2 is defined similarly. Thus for a given frequency (ω_1) and amplitude (V_{m_1}) of the input signal the d.i.d.f. depends on the phase ψ_1, the amplitude and frequency of the bias signal (V_{m_2}, ω_2) and on the phase of the bias signal ψ_2. For each phase ψ_1 of the input signal at frequency ω_1 the phase of the bias signal is varied from 0 to 360°. An example of the plot of a d.i.d.f. for h.v.d.c. systems is shown in fig 5.7. The hatched line corresponds to the d.f. locus for a signal with frequency ω_1 and amplitude V_{m_1}. When a bias signal of frequency ω_2 and amplitude V_{m_2} is introduced, each point of the d.f. locus develops into a closed curve.

Both the evaluation of the d.f. and d.i.d.f. can be achieved through the computer program described in Chapter Four. The phase of the input signal is increased from 0° to 350° in steps of 10°. If the d.i.d.f. is to be computed for each phase of the input signal at frequency ω_1 the phase of the bias signal is varied from 0 to 350° in steps of 10°. Thus for the d.f. 36 steady-state solutions of the h.v.d.c. system are carried out whereas for the d.i.d.f. 1296 solutions have to be obtained.

However, the computation of the d.i.d.f. is only needed in some cases. It was found that for the prediction of limit cycles it is sufficient to plot the d.i.d.f. for points of the d.f. where the gain and/or phase margins are quite small. Moreover the influence of this bias signal is generally small, i.e. in most cases it is sufficient to evaluate the single input describing function. The use of the dual input describing

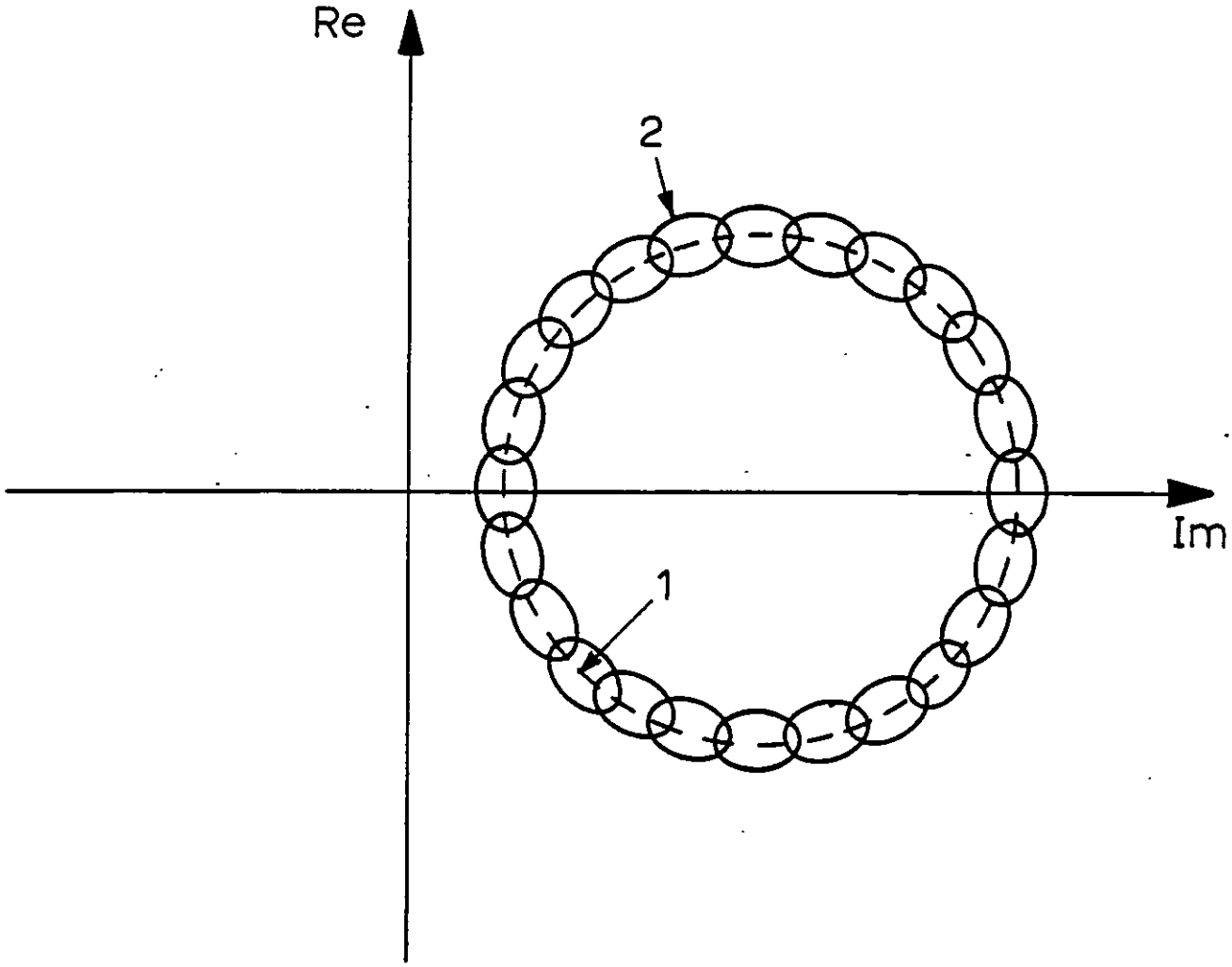

Fig 5.7: Example of a d.i.d.f. plot

1 Single input d.f. frequency ω_1, amplitude Vm_1

2 d.i.d.f. at frequency ω_1, amplitude Vm_1 for a bias signal of amplitude Vm_2, frequency ω_2

function has been restricted to the comparison between theoretical and test results (see Chapter Six).

As mentioned earlier, the steady-state solution requires a Gauss iterative process to take the a.c. system impedance into account. The iterative process is slowly convergent, requiring in some cases as many as 20 iterations, even with acceleration factor. This corresponds to 9 min CPU time on a CDC 6600. These extreme cases occur when resonances exist both on the a.c. and the d.c. sides, close to the frequency of any uncharacteristic harmonic generated by the converter.

The solution time depends to a great extent upon the number of harmonics considered in the calculation. When a modulating signal is superimposed to the control voltage, all harmonics are generated both on the a.c. and the d.c. sides, which considerably increase the computation time. In principle the program handles all the harmonics up to the 30th. However, to bring the computer time to a reasonable value, some simplifications had to be introduced.

The main justification for a drastic reduction in the number of harmonics handled lies in the fact that a particular harmonic of frequency $k\ \omega_o$ on the d.c. side affects mainly the value of the a.c. side harmonics of frequency $(k+1)\ \omega_o$ and $(k-1)\ \omega_o$. The effect on the other a.c. side harmonics is rather small.

The first approach tried was to neglect all d.c. side harmonics except that of the frequency of the modulating signal. Test system 2 with no capacitance on the d.c. side was used, together with unbalanced a.c. busbar voltages

(u_R = 230.94 $\angle 0^\circ$, u_Y = 228.64 $\angle -118^\circ$, u_B = 230.94 $\angle 120^\circ$). The short-circuit ratio was assumed to be 15 and a modulating signal at 50 Hz and an amplitude corresponding to 5° variation in the firing angle was injected.

The results are shown in Table 5.1 with respect to case A (all harmonics considered), the error in the d.f. being 0.3% in amplitude and 2° in phase (case B). Since the d.c. line capacitance was not considered, there is no resonance on the d.c. side, and all uncharacteristic harmonics except that of the frequency of the modulating signal are negligible. The characteristic harmonics are of no importance since they give rise on the a.c. side to 5th, 7th, 11th, 13th, etc, which are eliminated by the filters.

Next, the number of harmonics considered was progressively reduced. The results obtained are in Table 5.1, cases C through G, revealing the importance of the consideration of the resonances on the a.c. side. For s.c.r. = 15, the combined a.c. network plus filter impedance exhibits two anti-resonance points close to the third and eighth harmonics. From Table 5.1 it is apparent that the error in the d.f. is only acceptable when the 3rd and 8th harmonics are considered.

As far as the number of iterations is concerned, the 3rd harmonic is responsible for the jump in the number of iterations from case C to D. This happens precisely because of the high inductive value of the a.c. impedance at the frequency of 150 Hz, which causes a large variation of the 3rd harmonic component of the a.c. bus voltage.

The conclusion can therefore be drawn that the a.c. harmonics which are magnified by existing resonances of the a.c. impedance cannot be ignored in the calculation of the d.f., because they contribute to the d.c. current harmonic at the frequency of the modulating signal (50 Hz).

Table 5.1: Influence of d.c. and a.c. harmonics on d.f.

Case	d.c. harmonics	a.c. harmonics	d.f.	No. iterations
A	All	All	0.04921 /80.6	22
B	Fundamental only	All	0.04938 /80.4	14
C	Fundamental only	2nd	0.06355 /77.2	4
D	Fundamental only	2nd & 3rd	0.06353 /78.	15
E	Fundamental only	2nd & 3rd &4th & 5th	0.05680 /74.8	14
F	Fundamental only	2nd & 3rd & 4th & 6th & 8th	0.05115 /81.7	14
G	Fundamental only	2nd & 3rd & 8th	0.05782 /84.4	10

In case G of Table 5.1 only the 2nd harmonic and the harmonics for which there are resonances (3rd and 8th) were considered. The error in the d.f. amplitude with regard to case A is 15%, which shows that the 4th and 6th harmonics are also non-negligible.

It is consequently not possible to state a priori that a particular a.c. harmonic is not important for the calculation of the d.f., with the exception of the characteristic harmonics, which are filtered out. There is some kind of

interaction between the a.c. voltage harmonics, since each one contributes to each one of the d.c. current harmonics and each of these in turn contributes to each a.c. voltage harmonic, albeit in different proportions.

As a result of the above considerations the following approach was devised to adapt the steady-state simulation program to the calculation of the d.f.

a. On the d.c. side only the harmonic at the input signal frequency is taken into account.

b. On the a.c. side only the harmonics which in the first iteration have an amplitude greater than the maximum harmonic amplitude divided by a factor (typical value 9-10) are retained for the following iterations.

This approach implies that in the first iteration all a.c. harmonics have to be calculated. To reduce further the computation time, a modification was introduced in the a.c. harmonic calculation, as follows:

a. At the beginning of the program, the a.c. harmonic impedance is computed. All the harmonics for which the impedance is greater than a specified value are calculated, as well as the harmonics between $(k+3)\,\omega_o$ and $(k-3)\,\omega_o$.

b. From the second iteration, a further reduction in the number of harmonics is implemented: only those that possess an amplitude larger than the maximum harmonic amplitude divided by a factor are retained. An exception is made for the $(k+1)\,\omega_o$, and $(k-1)\,\omega_o$,

which are always calculated.

This modification allowed the reduction in the number of harmonics handled in the first iteration by a factor of 2.5. From the second iteration, another reduction by a factor of 1.5 is effective. A further reduction in the number of harmonics necessarily leads to a larger error in the d.f. and was not thought to be practicable.

5.6 Examples of d.f. evaluation

In this section some application examples are presented referring to test systems 1 and 2. Two cases are dealt with in this section. In the first case the rectifier possesses infinite s.c.r. and the inverter is simulated by a constant e.m.f. Test system 1 was used to obtain the d.f.s for this case. In the second case the rectifier possesses a finite s.c.r. and the inverter is simulated by a constant e.m.f. Test system 2 was used to obtain the d.f.s for those two cases.

5.6.1 Input signal at 50 Hz

Fig 5.8 is the d.f. for test system 1 for an input signal frequency of 50 Hz and amplitude corresponding to a variation of 5^{o} in the firing angle. If no unbalance or distortion is imposed on the a.c. voltage, the d.f. reduces to a point (a). The presence of imbalance in amplitude (1%)

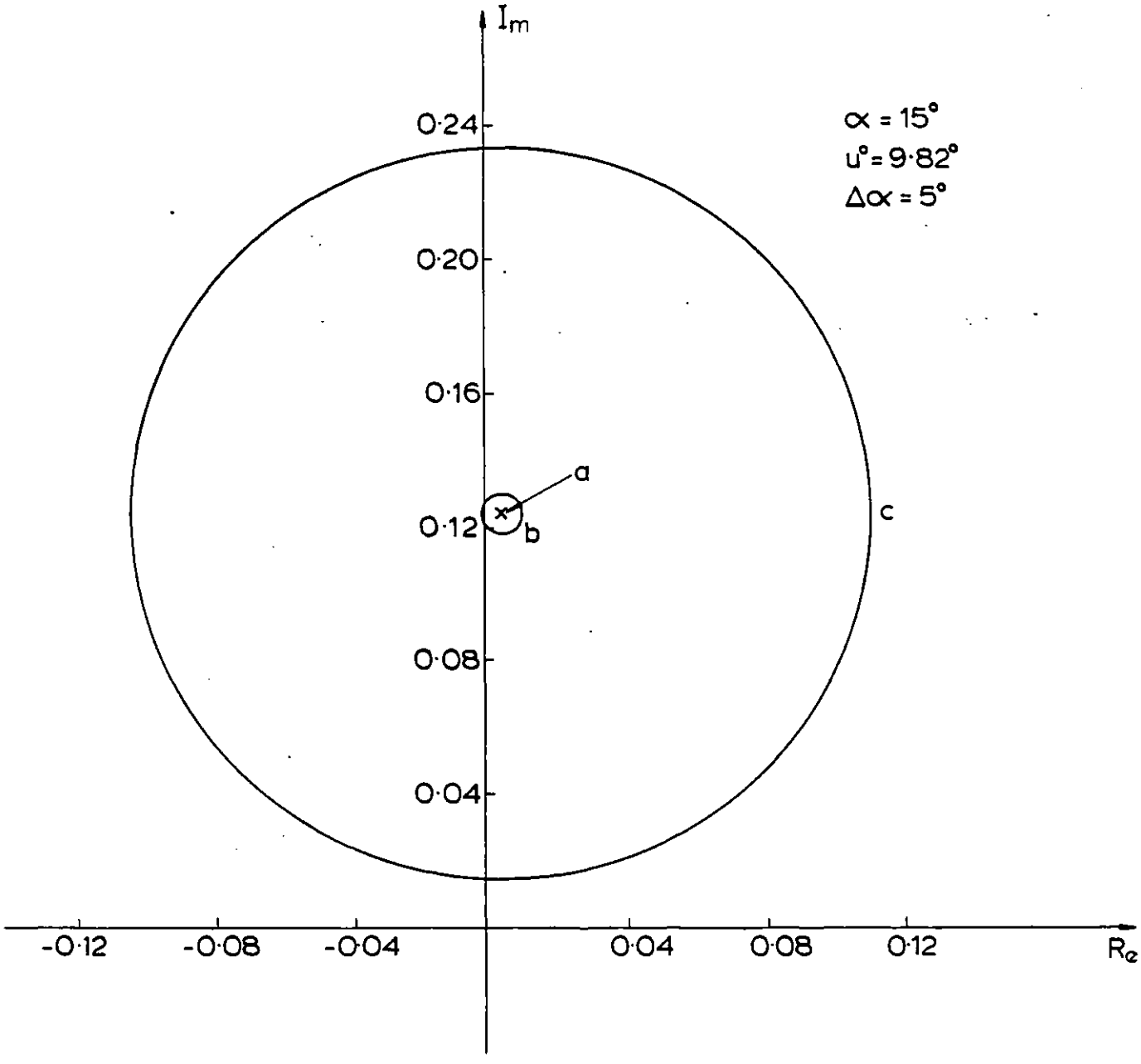

Fig. 58

Describing function for 50 Hz S.C.R. = ∞

(a) No unbalance or distortion in a.c. voltage

(b) Unbalance in amplitude (-1%) and phase angle (-2%) of phase Y

(c) 2nd harmonic distortion in a.c. voltage (2%) direct phase sequence

and phase (-2^{o}) in one of the a.c. voltages yields a small circle (curve b). The d.f. expands into a large circle if a 2% second harmonic distortion with positive sequence is assumed. Note that this type of distortion leads to an uncharacteristic harmonic of 50 Hz on the d.c. side, even without the injection of a modulating signal (m.s.)

If the s.c.r. is finite, the a.c. busbar voltage will be distorted, due to the presence of the m.s., even if no distortion is assumed a priori. It was found that the 2nd harmonic on the busbar voltage increases approximately in a linear fashion with the amplitude of the m.s. (at 50 Hz). For small amplitudes, the 2nd harmonic is balanced; however as the amplitude increases, an unbalance develops due to violation of the α limits. This unbalance is characterised by a negative sequence component (but no zero sequence).

Fig 5.9 shows the d.f.s for test system 2 with two different s.c.r.s and increasing amplitude of the m.s. No imbalance/distortion was imposed by the a.c. system. For several amplitudes the d.f. again reduces to a point; as the amplitude increases, the area enclosed by the d.f. locus increases.

When the d.f. is a point, the amplitude of the output harmonic current at the frequency of the input is independent of the phase of the input signal, its phase varying in synchronism with the phase of the latter. If this phase varies by $\Delta\phi$, the phase of the output also changes by $\Delta\phi$. This synchronism is up to a certain extent lost when the amplitude of the input increases, yielding an expansion of the area enclosed by the d.f.

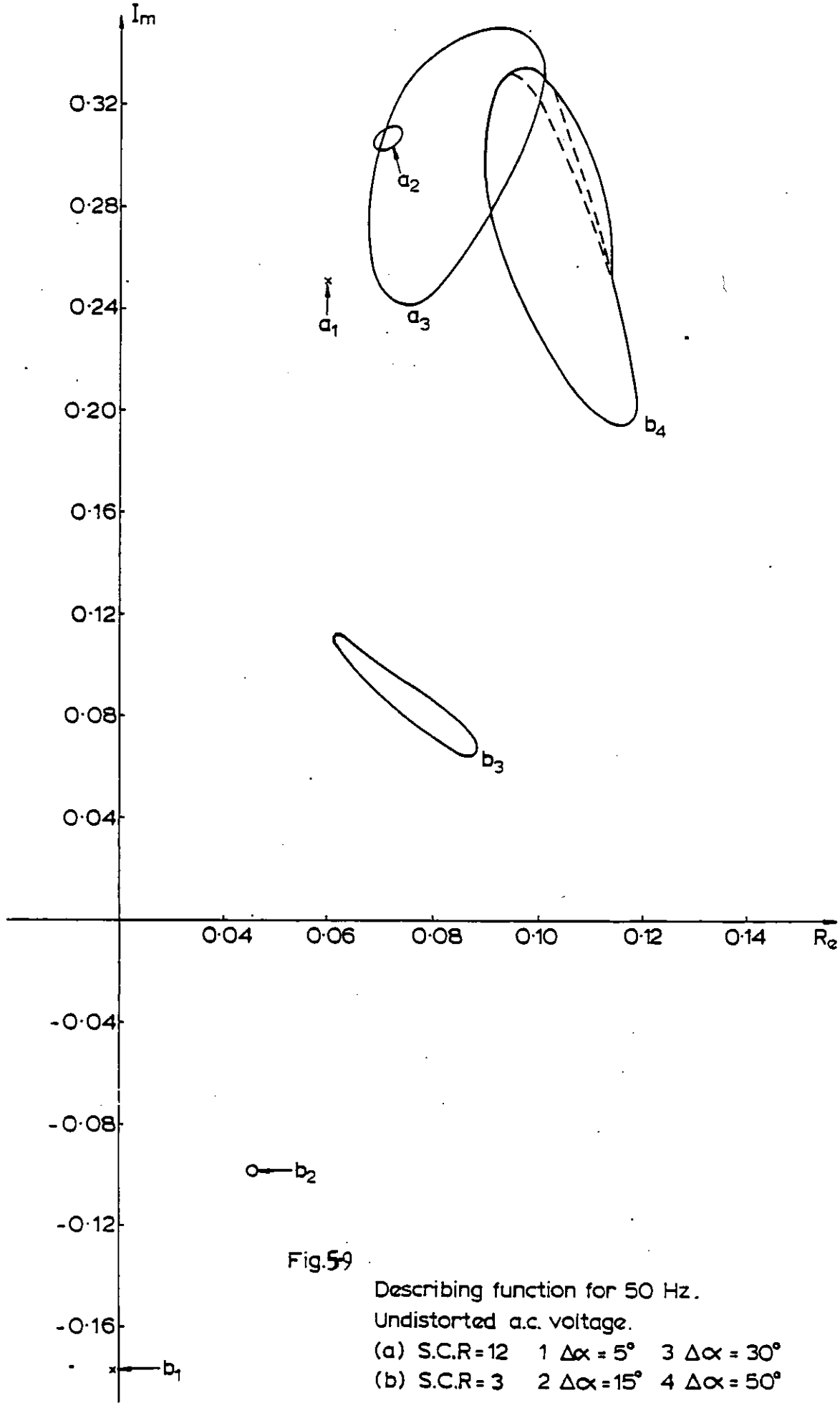

Fig.5-9

Describing function for 50 Hz.
Undistorted a.c. voltage.
(a) S.C.R = 12 1 $\Delta\alpha = 5°$ 3 $\Delta\alpha = 30°$
(b) S.C.R = 3 2 $\Delta\alpha = 15°$ 4 $\Delta\alpha = 50°$

From fig 5.9 it is also apparent that, for low s.c.r., the d.f. is considerably displaced as the amplitude of the input is increased, whereas for high s.c.r. the loci are situated in the same region, although an enlargement does take place. Also the area encircled by the d.f. is larger for high s.c.r. than for low s.c.r.. This is because, for the particular system studied, a higher a.c. impedance results in a larger distortion of the a.c. voltage.

Fig 5.10 shows the polar plot of the d.f. for test system 2 with an amplitude of the m.s. corresponding to 5^{o}, for the base case, unbalanced a.c. voltage, unbalanced transformer impedance, and 2nd harmonic distortion with positive sequence. The loci are similar to those of fig 5.8 for infinite s.c.r. The imbalance in a.c. voltage or in transformer reactance does not cause a considerable expansion of the d.f. In contrast, for the 2nd harmonic distortion the magnification of the d.f. and hence the possibility of instabilities is considerable. The reason for this phenomenon lies in the fact that the distortion imposed by the a.c. network has a fixed phase angle which is not linked to the phase of the input signal. The converter itself originates 2nd harmonic distortion which is however related phasewise to the modulating signal.

The magnification of the area encircled by the d.f. is only important when the imposed a.c. distortion contributes to the d.c. harmonic of interest. An unbalance in the fundamental a.c. voltage gives in the steady-state d.c. harmonics which are multiples of 2. Since no component at the frequency of the input signal is produced, the magnification of the d.f.

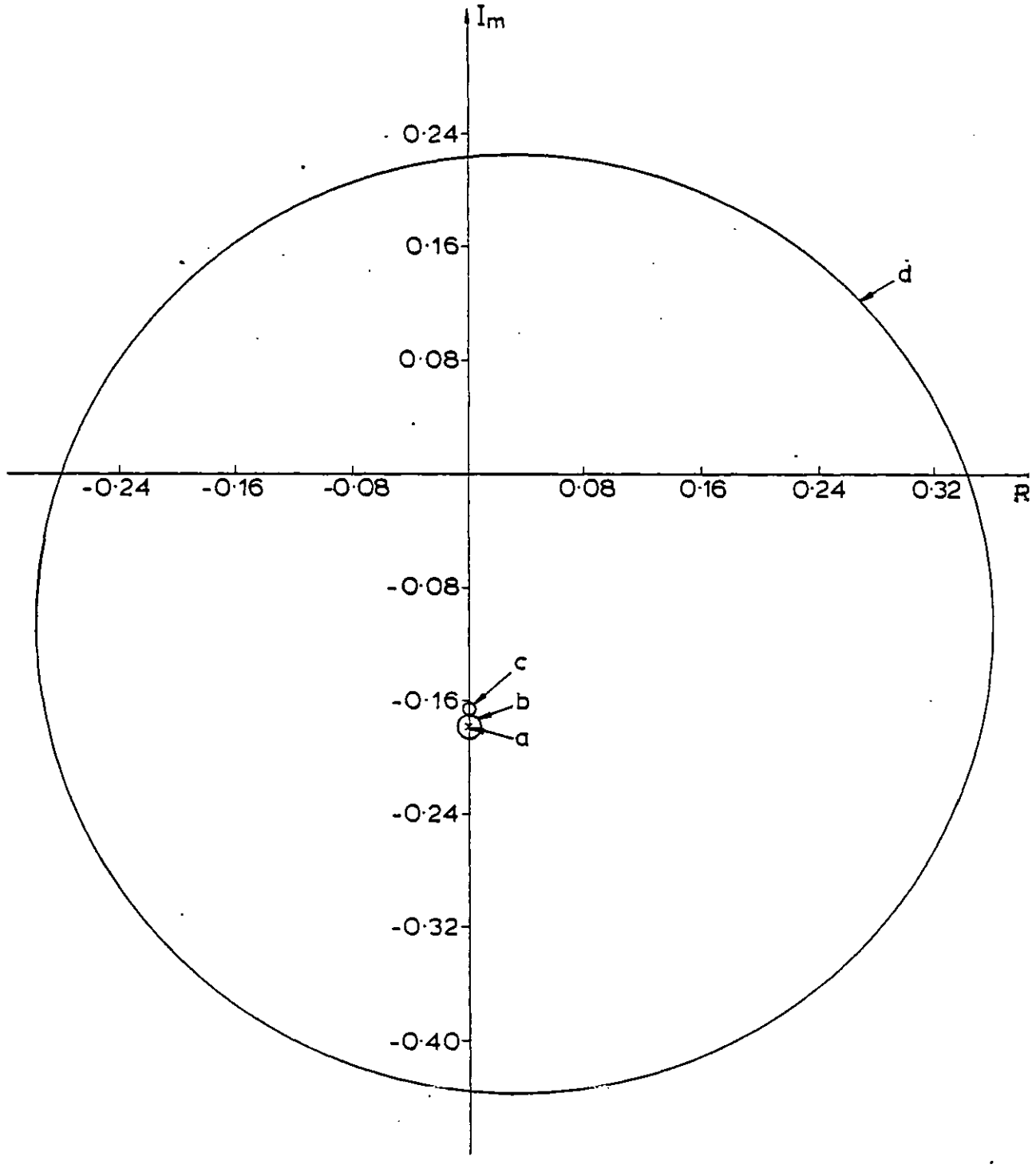

Fig. 5·10 Describing function for 50 Hz, S.C.R.=3
(a) Base case
(b) Unbalanced a.c. voltage (1%)
(c) Unbalanced transformer impedance (7%)
(d) 2nd harmonic distortion, positive sequence (1%)

is rather small and probably only takes place at all due to the modulation of the commutation angle.

The fact that a 2nd harmonic distortion with positive sequence gives rise in the steady-state to a d.c. harmonic at fundamental frequency is coherent with the fact that an input signal at fundamental frequency yields a d.c. harmonic at the same frequency, which in turn produces a 2nd harmonic with positive sequence on the a.c. side. It also produces a d.c. component which is filtered out by the converter transformer.

The amplitude and phase of the a.c. current harmonics for a m.s. at 50 Hz corresponding to a variation of 5° in the firing angle is shown in Table 5.2 for the base case. Note the relatively high value of the 2nd harmonic. Also note that the 3rd and 6th harmonics are highly unbalanced, in contrast with the other harmonics which are balanced. The fundamental component is practically not affected by the modulating signal, since a d.c. component at 50 Hz does not contribute to the a.c. component at the same frequency.

Table 5.2: A.c. current harmonics (base case) input signal at 50 Hz

Harmonic order	I_R(KA)	I_Y(KA)	I_B(KA)
1	1.147 /-26.2	1.146 /213.6	1.145 /93.7
2	0.0435 /169.0	0.0438 /48.9	0.0436 /-71.4
3	0.0029 /54.0	0.0023 /193.2	0.0019 /-74.4
4	0.0241 /39.9	0.0244 /159.8	0.0243 /-79.7
5	0.0337 /-70.3	0.0189 /-34.8	0.0504 /122.4
6	0.0256 /201.8	0.0256 /81.1	0.0254 /-33.5

Fig 5.11 shows the polar plot of the d.f. for 50 Hz with a second harmonic distortion (positive sequence) imposed on the a.c. busbar and a s.c.r. equal to 3. Increasing the amplitude of the m.s. results in a deflation of the d.f.

5.6.2 Input signal at 100 Hz

Figure 5.12 shows the d.f. for test system I for an input signal frequency of 100 Hz and amplitude of the m.s. equal to 1^{o}, 5^{o} and 15^{o}. From this figure it is apparent that even for small amplitudes of the m.s. the d.f. is a closed curve. The area enclosed by the d.f. curve enlarges when the amplitude of the modulating signal increases.

For the 100 Hz modulating signal case it was found that the consideration of an unbalance in the fundamental of the a.c. voltage and the existence of a third harmonic (possessing either a positive or negative sequence) led to considerable magnification of the d.f. locus. Figure 5.13 shows the influence of a negative sequence in the fundamental of the a.c. voltage upon the 100 Hz d.f.

As 100 Hz on the d.c. side contribute directly to the fundamental of the a.c. voltage, and any imbalance in the fundamental on the a.c. side affects the 100 Hz describing function, it is not valid to assume that the fundamental of the a.c. voltage in the busbar is constant. For the 50 Hz and 150 Hz m.s. cases the harmonic pattern on the d.c. side does not affect significantly the fundamental on the a.c. side and therefore the amplitude of the a.c. voltage may be considered constant on the busbar side of the converter transformer. Table 5.3 summarises these results.

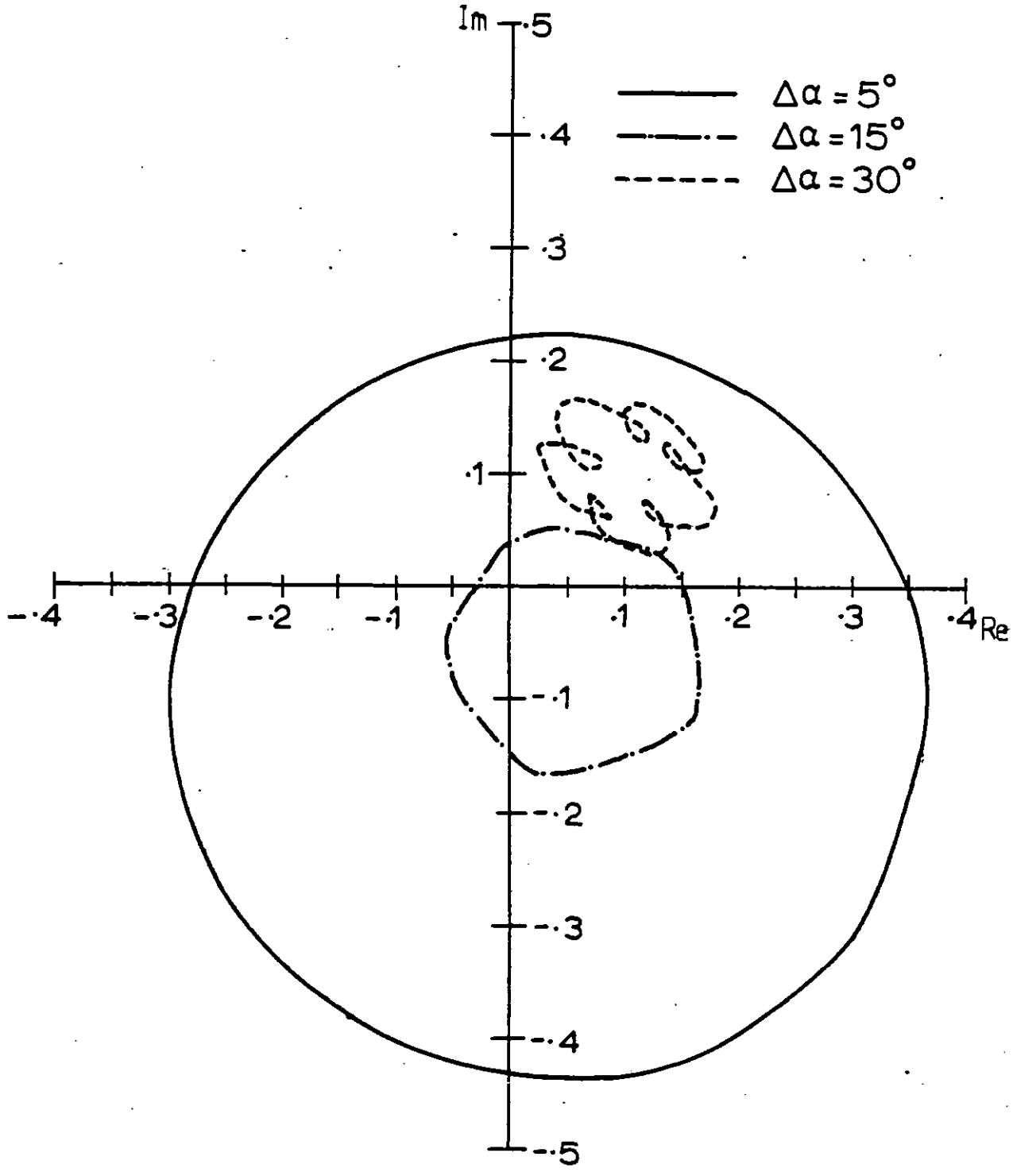

Fig 5.11: Describing function for 50 Hz. s.c.r. = 3, $\alpha^{\circ} = 15^{\circ}$
2nd harmonic distortion (positive sequence - 1%)

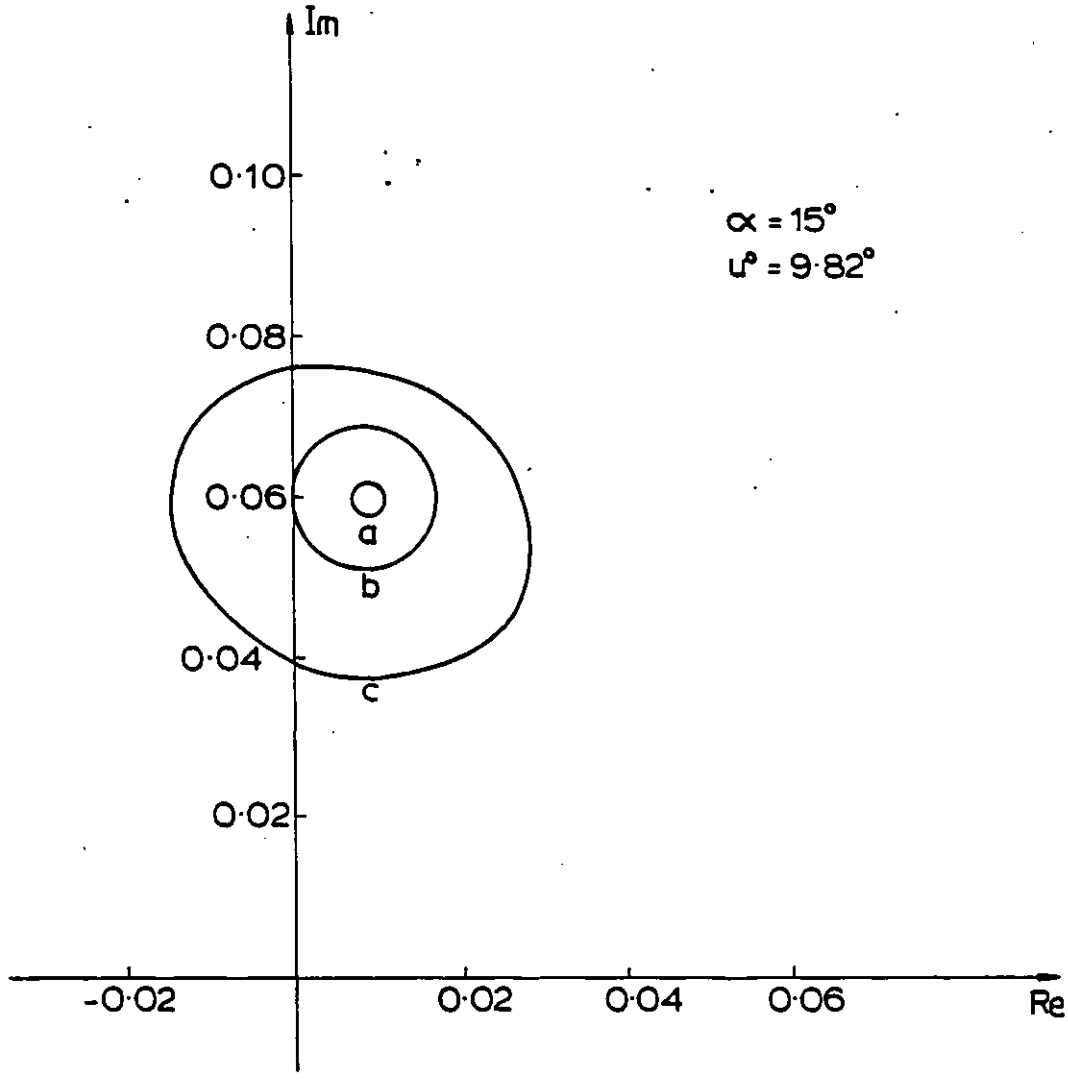

Fig. 5-12

Describing function for 100 Hz. No unbalance or distortion in a.c. voltage S.C.R. = ∞

(a) $\Delta\alpha = 1°$

(b) $\Delta\alpha = 5°$

(c) $\Delta\alpha = 15°$

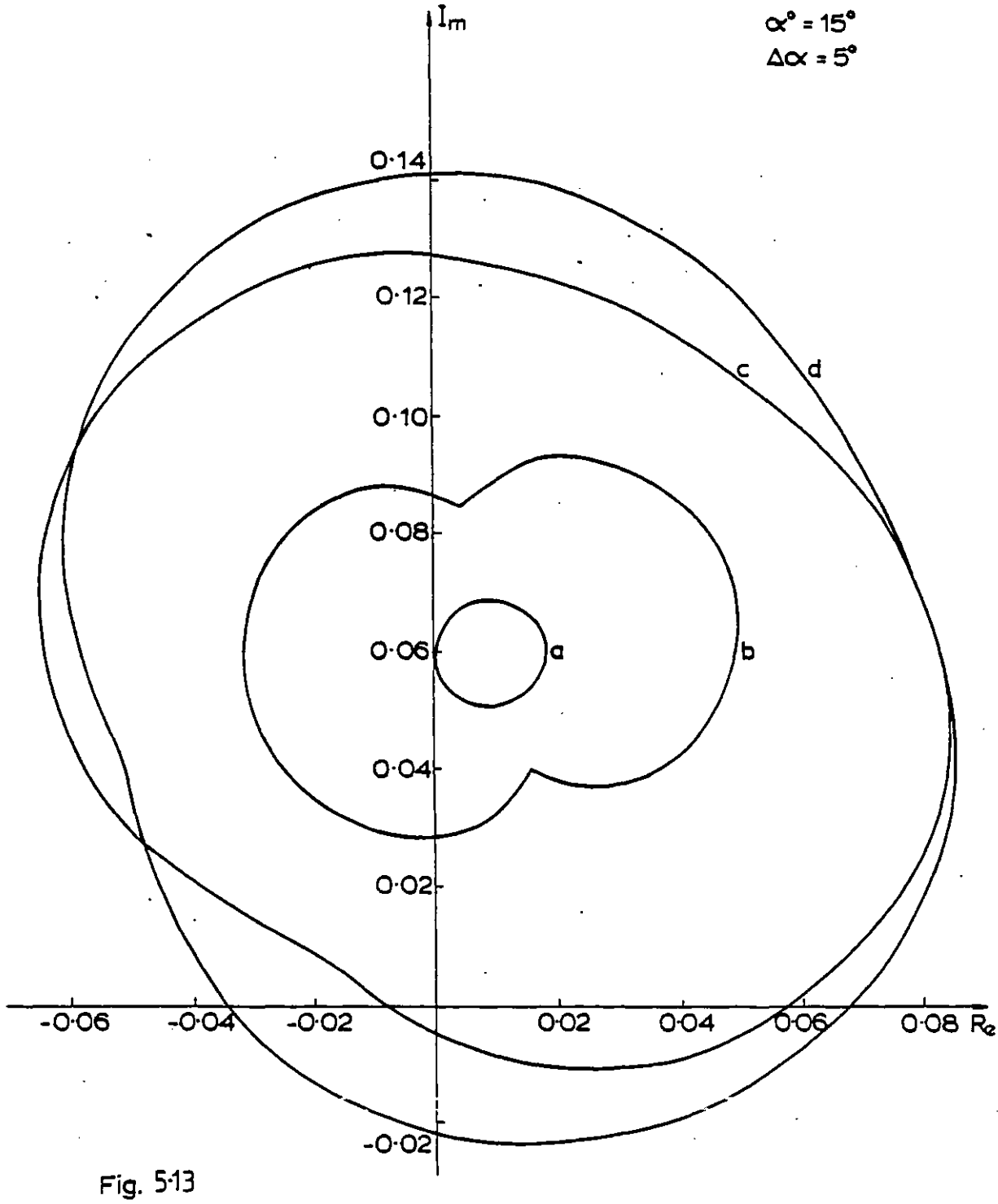

Fig. 5·13

Describing function for 100 Hz. S.C.R. = ∞
(a) No unbalance or distortion in a.c. voltage
(b) Unbalance in phase angle of phase Y (-2°)
(c) Unbalance in amplitude of phase Y (-7%)
(d) Combination of (b) and (c)

Modulating signal	0 Hz and 150 Hz	50 Hz	100 Hz
	I_r 1.146 ∠-25.9	1.147 ∠-26.4	1.115 ∠-27.2
Fundamental a.c.	I_y 1.146 ∠214.1	1.146 ∠213.6	1.149 ∠215.3
Current (KA)	I_B 1.146 ∠94.1	1.145 ∠93.7	1.174 ∠92.6

Table 5.3: Influence of modulating signal in a.c. current fundamental at the busbar side of the converter transformer.

Figures 5.14 and 5.15 show the d.f. for test system 2, m.s. amplitudes of 5°, 15° and 30°, and for s.c.r.s of 12 and 3 respectively.

The locus of the d.f. with increasing amplitude of the modulating signal is approximately the same. As in the infinite s.c.r. case the d.f. tends to expand with increasing amplitude of the m.s. For an amplitude of the m.s. equal to 30° the d.f. is not a closed curve. This result seems to be independent of the s.c.r.

Figure 5.16 shows the effect on the d.f. of an unbalance of the converter transformer reactances. The d.f. is enlarged around the base case solution.

Figs 5.17, 5.18 and 5.19 show the d.f. plots for unbalanced a.c. voltages, a range of amplitudes of the m.s. (5°, 15° and 30°) and a range of s.c.r.s.

As in the base case, for an amplitude of the m.s. equal to 30°, the d.f. is not a closed curve. Also the enlargement of the d.f. seems to be greater for a.c. voltage imbalances than for imbalances in the converter transformer reactances.

In figs 5.17, 5.18 and 5.19 it is noticeable that increments in the amplitude of the modulating signal are not

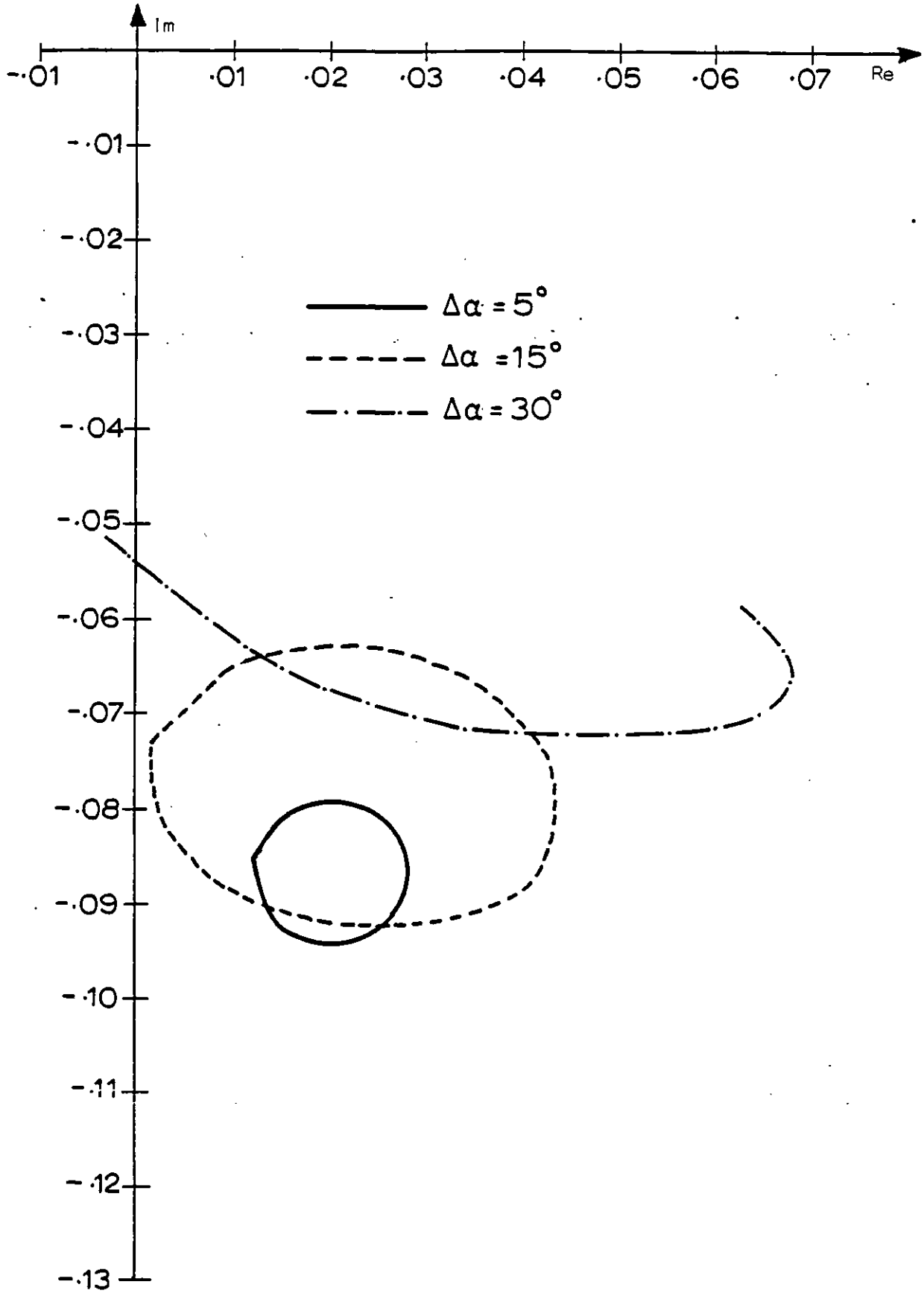

Fig 5.14: Describing function for 100 Hz. Base Case. s.c.r. = 12

α° = 15°

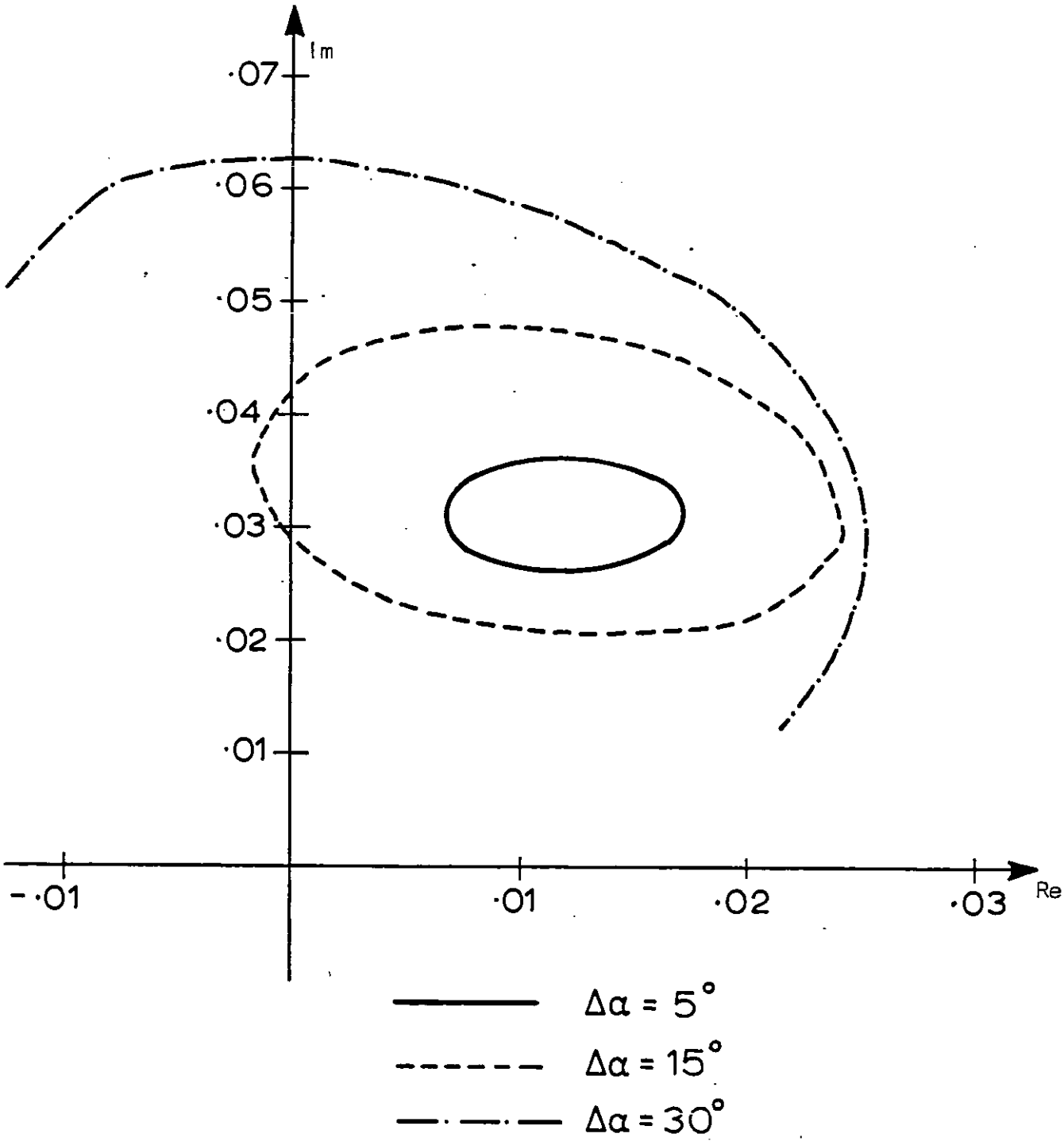

Fig 5.15: Describing function for 100 Hz. Base Case. s.c.r. = 3
$\alpha^{\circ} = 15^{\circ}$

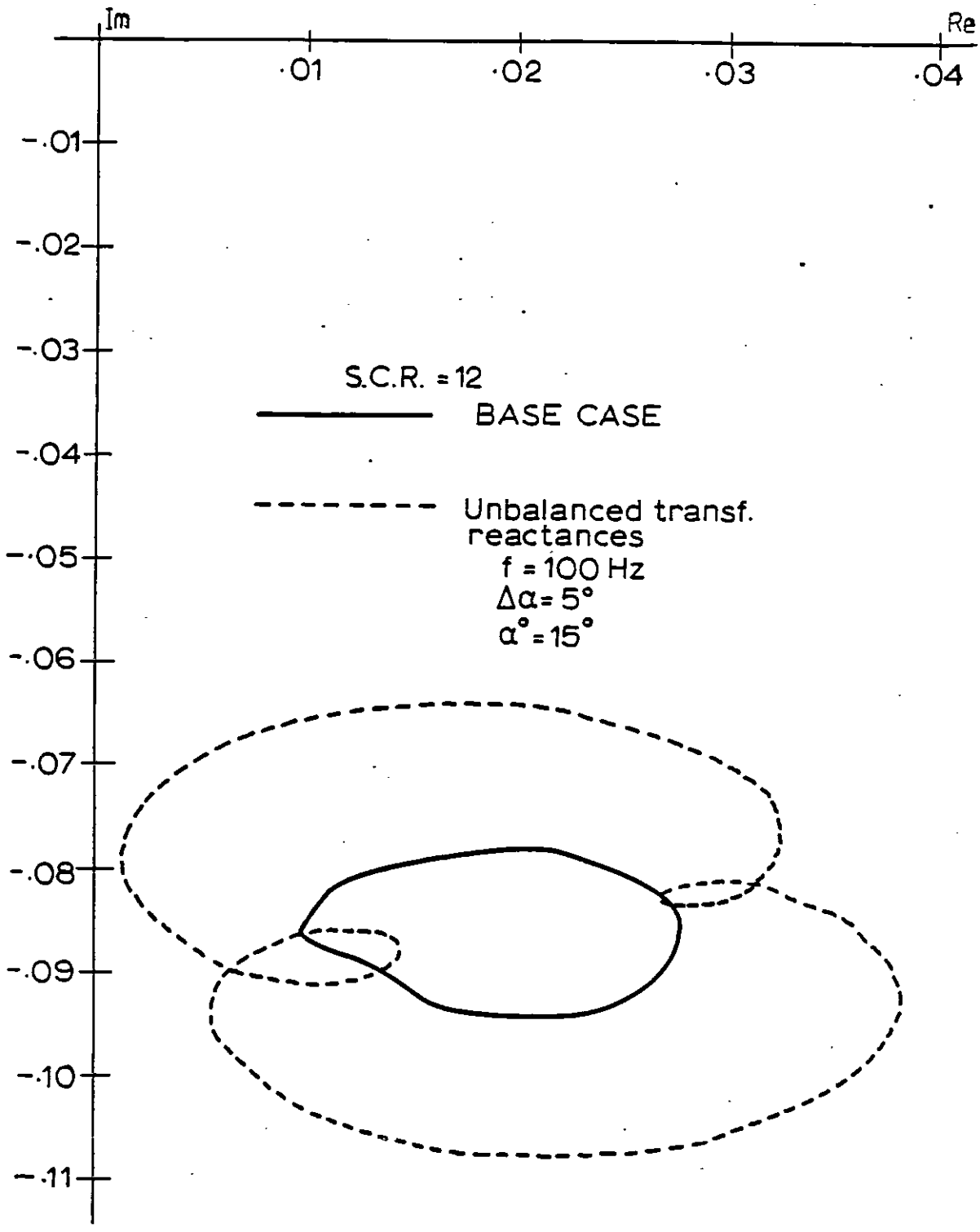

Fig 5.16: Describing function for 100 Hz. s.c.r. = 12

Fig 5.17: Describing function for 100 Hz. s.c.r. = 12. $\alpha^{\circ} = 15^{\circ}$
Unbalanced a.c. voltages (1%)

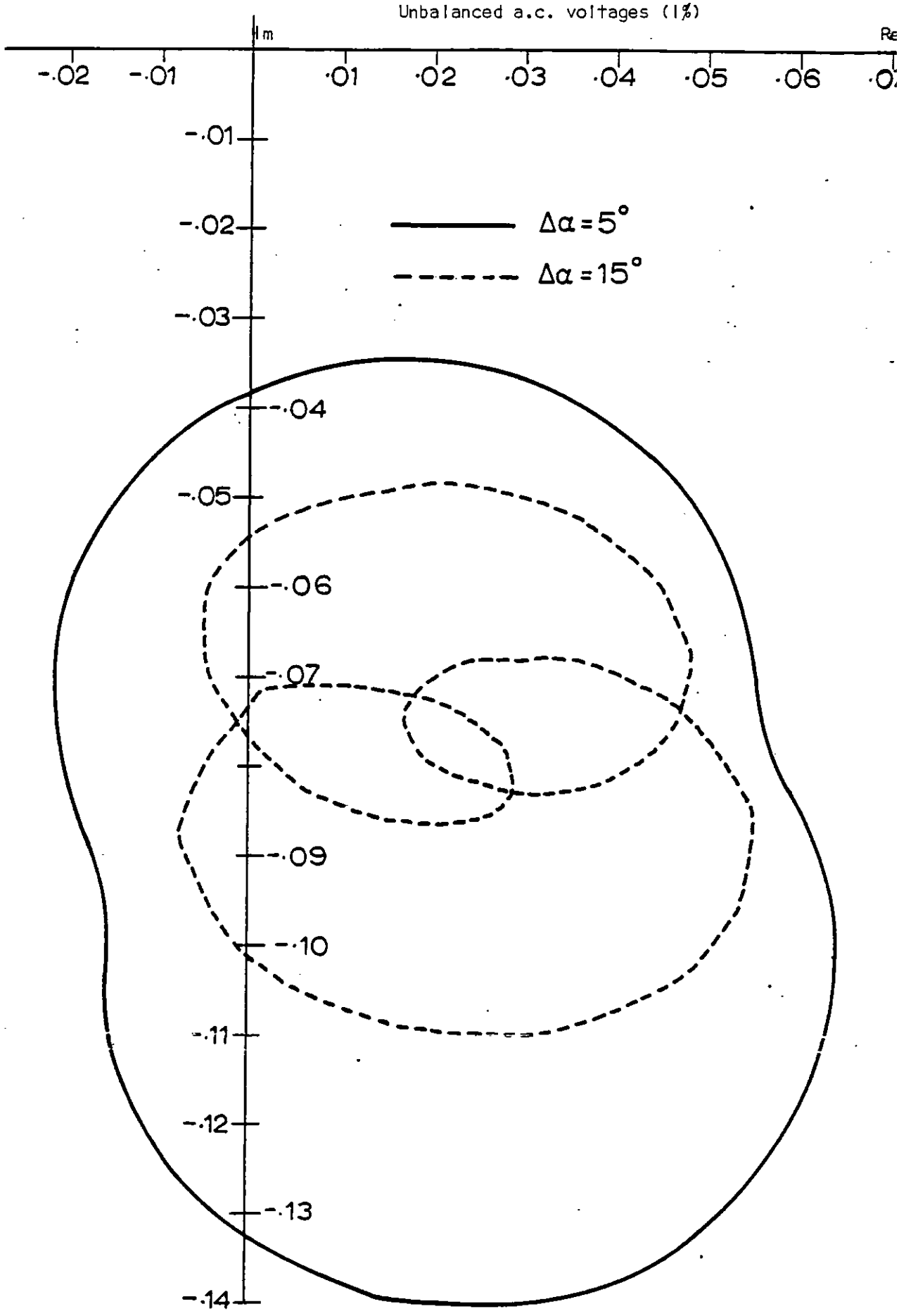

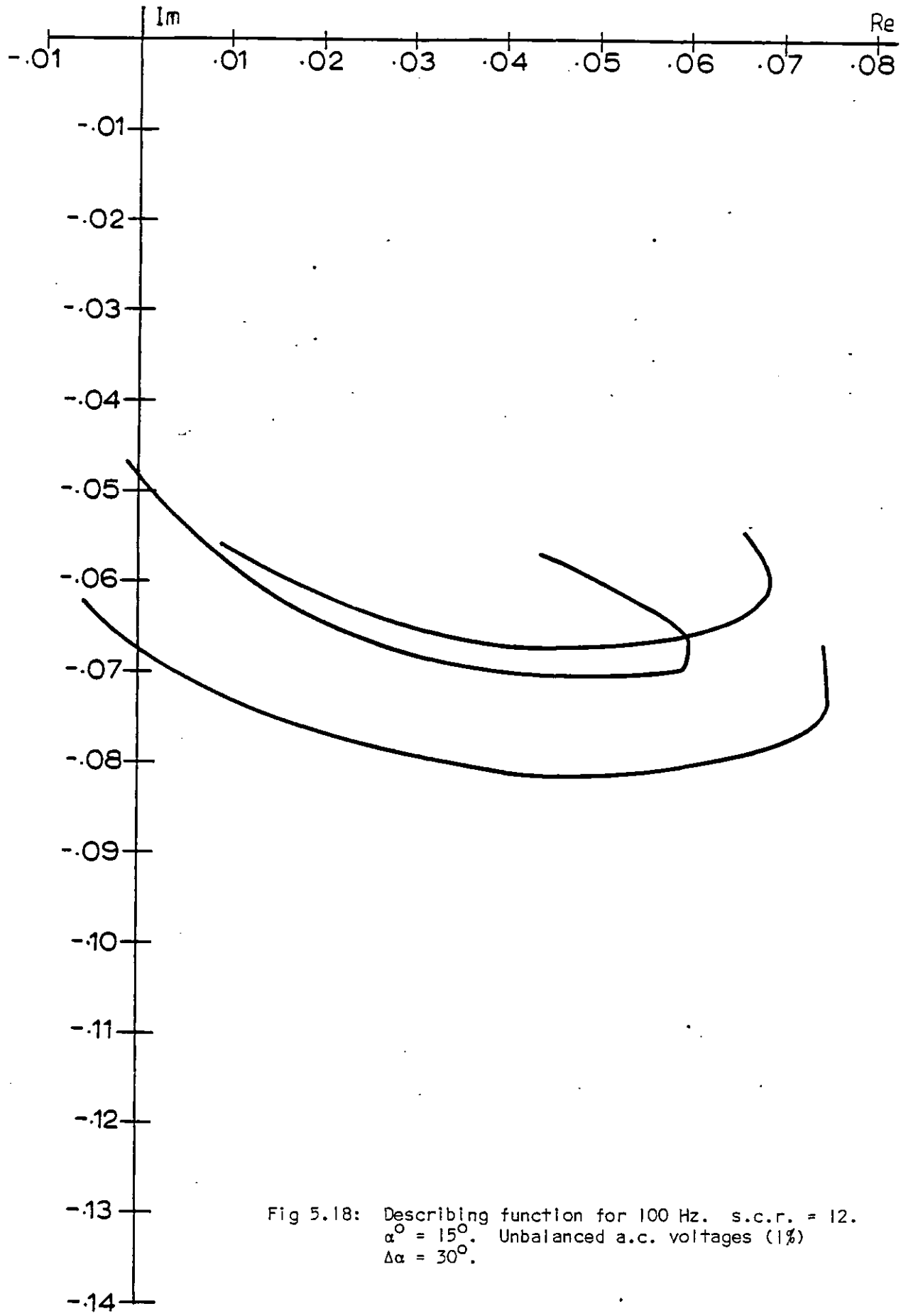

Fig 5.18: Describing function for 100 Hz. s.c.r. = 12.
$\alpha^{o} = 15^{o}$. Unbalanced a.c. voltages (1%)
$\Delta\alpha = 30^{o}$.

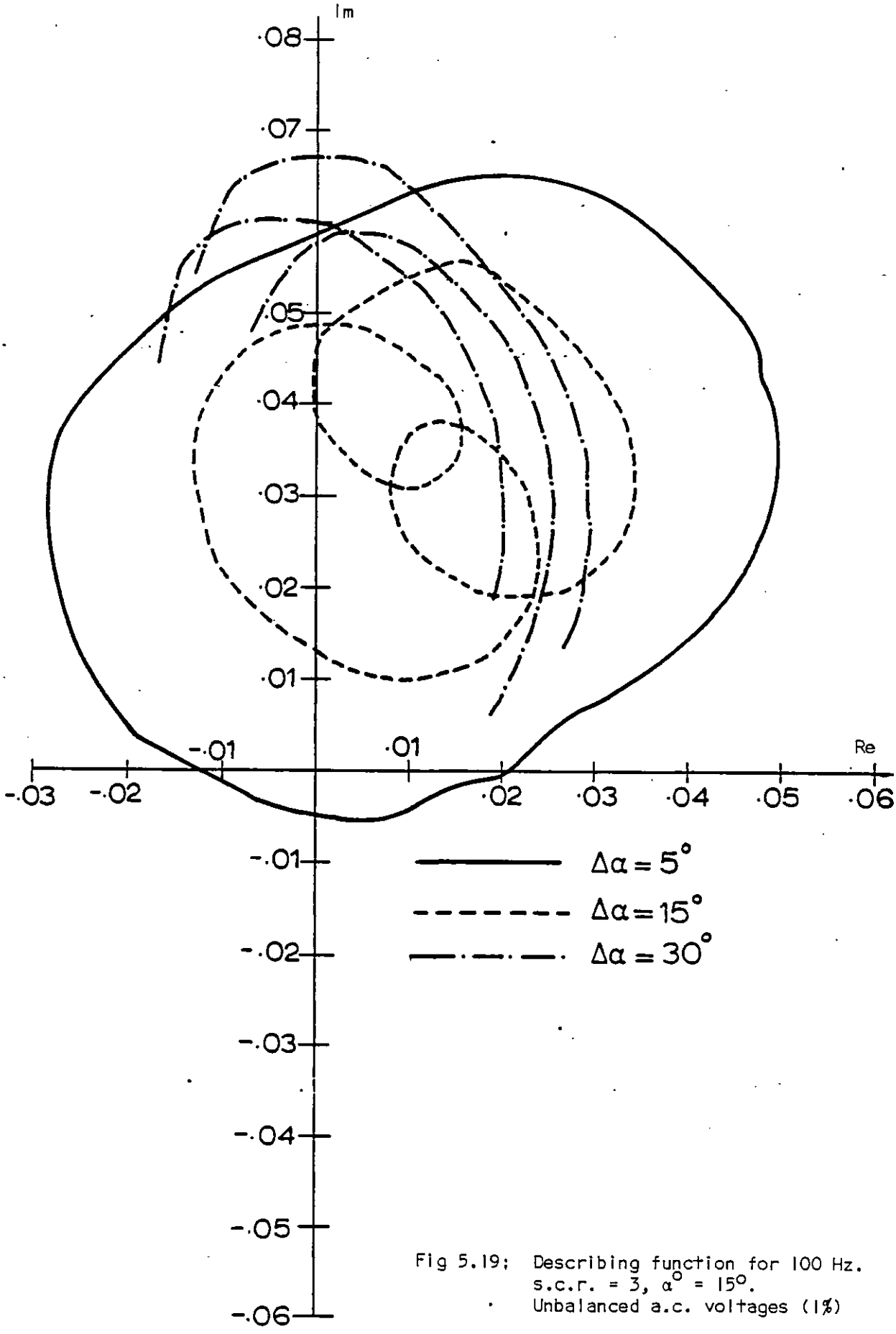

Fig 5.19: Describing function for 100 Hz. s.c.r. = 3, α^{o} = 15°. Unbalanced a.c. voltages (1%)

followed by enlargements of the d.f. locus; instead a deflation of the d.f. locus occurs.

This result was also found in the 50 Hz m.s. case.

These results confirm the fact that even for small amplitudes of the modulating signal, the d.f. is a closed curve.

Table 5.4 shows the d.c. voltage and d.c. current harmonic at the frequency of the input signal. The values refer to test system 2, with a resonance on the d.c. side at 54.5 Hz, and correspond to two values of the phase of the input signal, 0° and 10°, and an amplitude yielding a 5° variation in the firing angle. No distortion and/or imbalance was imposed by the a.c. system (base case).

The results of Table 5.4 indicate that the 'synchronism' between the phase of the input and of the output d.c. current harmonic at the same frequency, evident for the 50 Hz, no longer exists for the 100 and 150 Hz, particularly for the latter. This means that the d.f. for 50 Hz reduces to a point, becoming a circle for 100 Hz and 150 Hz. The cirle is larger for 150 Hz.

Table 5.4: Voltage harmonic of input signal frequency (base case)

Input signal frequency	50 Hz	100 Hz	150 Hz
D.C. voltage $\psi = 0^{\circ}$	3.967 $\angle$58.9	3.948 $\angle$251.9	14.92 $\angle$255.8
Harmonic (kv) $\psi = 10$	3.964 $\angle$68.9	3.707 $\angle$259.1	12.41 $\angle$253.9
D.C. Current $\psi = 0^{\circ}$	44.1 $\angle$-41.2	9.3 $\angle$162.6	21.04 $\angle$166.2
Harmonic (A) $\psi = 10^{\circ}$	44.1 $\angle$-31.2	8.7 $\angle$169.8	17.5 $\angle$164.3

5.6.3 Input signal at 150 Hz

Figure 5.20 shows the d.f. for test system I for an input signal frequency of 150 Hz and amplitudes of the m.s. equal to 1^{o} - 5^{o} and 15^{o} respectively. In contrast to the 50 and 100 Hz cases an enlargement of the d.f. locus does not occur.

In order to predict the harmonic likely to contribute to an enlargement of the d.f., Table 5.5 was assembled.

In this table the resulting a.c. voltage harmonics are displayed for the same conditions as in Table 5.4. It can be observed that for 50 and 150 Hz, the voltage harmonics, with the exception of the 3rd and the 6th, are balanced. For 50 Hz, the 2nd and 8th have a positive sequence, whereas the 4th has a negative sequence; for 150 Hz the sequence is reversed.

A 2nd harmonic distortion with negative phase sequence imposed by the a.c. system is consequently bound to cause an appreciable expansion of the d.f. locus for 150 Hz. This assumption is fully confirmed by the loci of fig 5.21. Also a 2nd harmonic distortion with positive phase sequence yields a considerable magnification of the d.f. locus for 50 Hz, as was noted in section 5.6.1.

A 4th harmonic with negative sequence should cause the magnification of the d.f. for 50 Hz; if the sequence were negative, the 150 Hz d.f. would in turn be enlarged. Similar conclusions could be drawn for other types of harmonic distortion.

Only the 100 Hz modulating signal produces a third harmonic on the a.c. busbar. This harmonic is highly

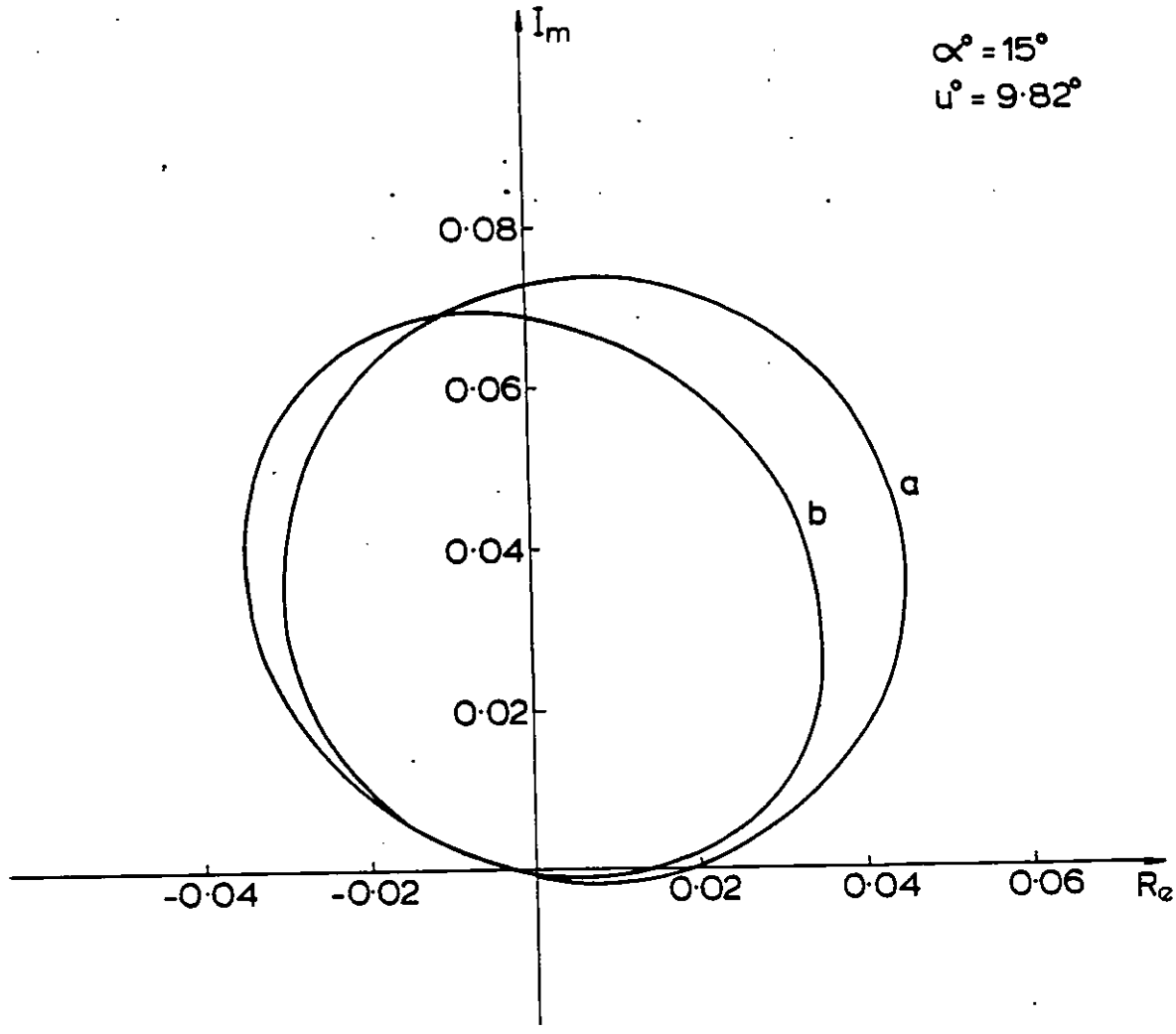

Fig. 5·20

Describing function for 150 Hz. No unbalance or distortion in a.c. voltage

(a) $\Delta\alpha = 1 - 5^\circ$

(b) $\Delta\alpha = 15^\circ$

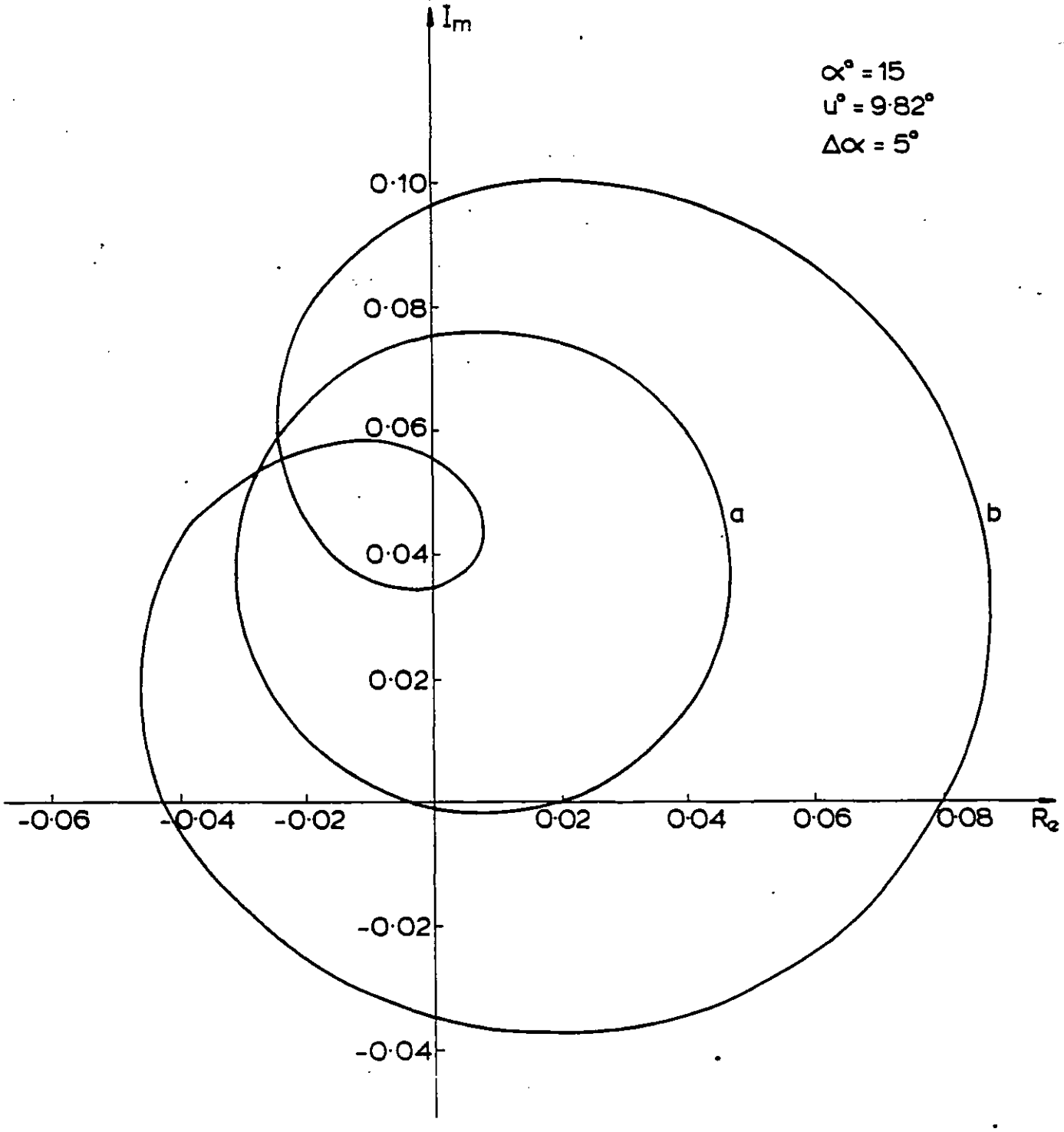

Fig. 5·21

Describing function for 150 Hz S.C.R. = ∞

(a) No unbalance or distortion in a.c voltage

(b) 2nd harmonic distortion in a.c. voltage (2%), inverse phase sequence.

Table 5.5: A.c. voltage harmonics (base case)

Input signal frequency		50 Hz	100 Hz	150 Hz
Input signal phase	Harmonic order	u_R u_Y u_B (kv/deg)	u_R u_Y u_B (kv/deg)	u_R u_Y u_B (kv/deg)
0°	2	7.82/254.4 7.97/134.3 7.89/13.4	-	9.18/227.0 9.18/-13.0 9.18/107.0
	3	-	3.331/192.0 0.328/-13.2 3.038/14.7	-
	4	0.737/140.8 0.758/260.5 0.751/22.1	-	1.097/172.9 1.097/52.9 1.097/-67.1
	6	1.368/19.4 1.366/51.1 2.647/50.5	-	-
	8	2.75/-68.7 2.72/170.3 2.67/50.5	-	3.19/264.6 3.19/24.6 3.19/144.6
10°	2	7.86/264.2 7.92/144.0 7.88/23.8	-	7.65/227.3 7.65/-12.7 7.65/107.3
	3	-	2.902/190.9 0.357/231.1 3.183/15.1	-
	4	0.744/130.8 0.752/250.7 0.750/11.3	-	0.916/173.4 0.916/53.4 0.916/-66.6
	6	1.747/24.1 0.978/59.6 2.61/216.7	-	-
	8	2.711/-59.0 2.712/180.3 2.683/60.6	-	2.67/265.7 2.67/25.7 2.67/145.7

unbalanced, possessing positive and negative sequence components of comparable magnitude. Therefore the presence of 3rd harmonic distortion in the a.c. busbar should result in enlarged d.f.s at 100 Hz, as mentioned in section 5.6.2.

Figs 5.22 and 5.23 show the d.f. for increasing amplitudes of the m.s. and for s.c.r.s equal to 12 and 3 respectively, using test system 2. The behaviour of the d.f. for s.c.r. equal to 3 is similar to the one observed in fig 5.20. However the behaviour of the d.f. for a s.c.r. equal to 12 seems to follow the pattern found for 50 and 100 Hz, i.e. an enlargement of the d.f. locus occurs with increasing amplitude of the modulating signal. Fig 5.24 shows the comparison between the d.f. plot for s.c.r. equal to 3 and for s.c.r. equal to 12. The amplitude of the modulating signal is 5^{o}. The reason for the enlargement of the d.f. locus with decreasing s.c.r. lies in the fact that for s.c.r. equal to 3 an antiresonant point for the second harmonic exists on the a.c. side.

Fig 5.25 shows the effect on the d.f. of imposing a 1% second harmonic distortion with negative sequence. Again, as for the other input signal frequencies the expansion of the d.f. occurs around the base case solution. This result seems to be a common feature for all frequencies of the modulating signal studied.

The effect of increasing the amplitude of the modulating signal when a second harmonic distortion with negative sequence is imposed on the a.c. side can be seen in figs 5.26 and 5.27. Again the deflating effect on the d.f. is produced. This

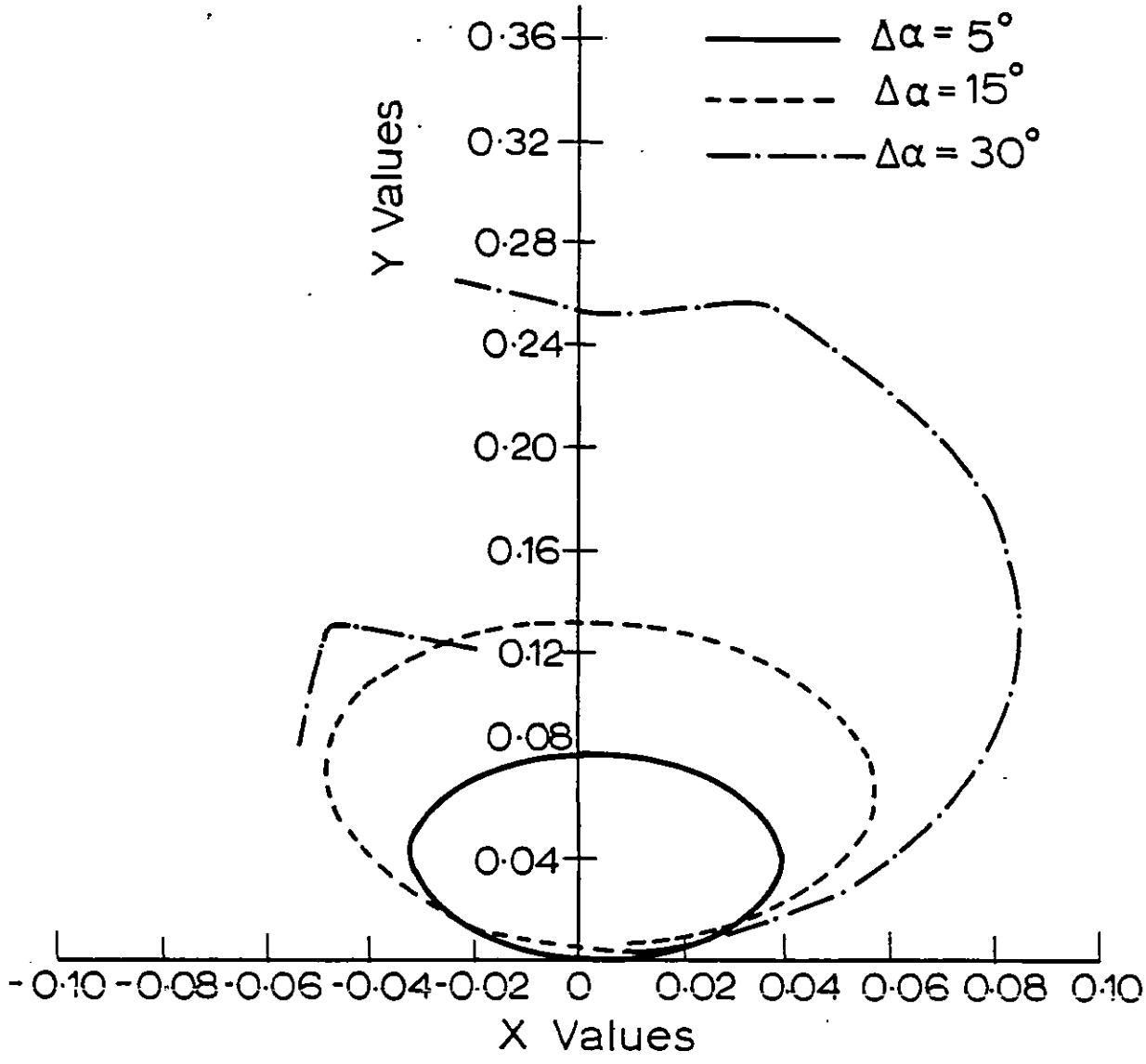

Fig 5.22: Describing function for 150 Hz. Base case. s.c.r. = 12. α^{o} = 15°

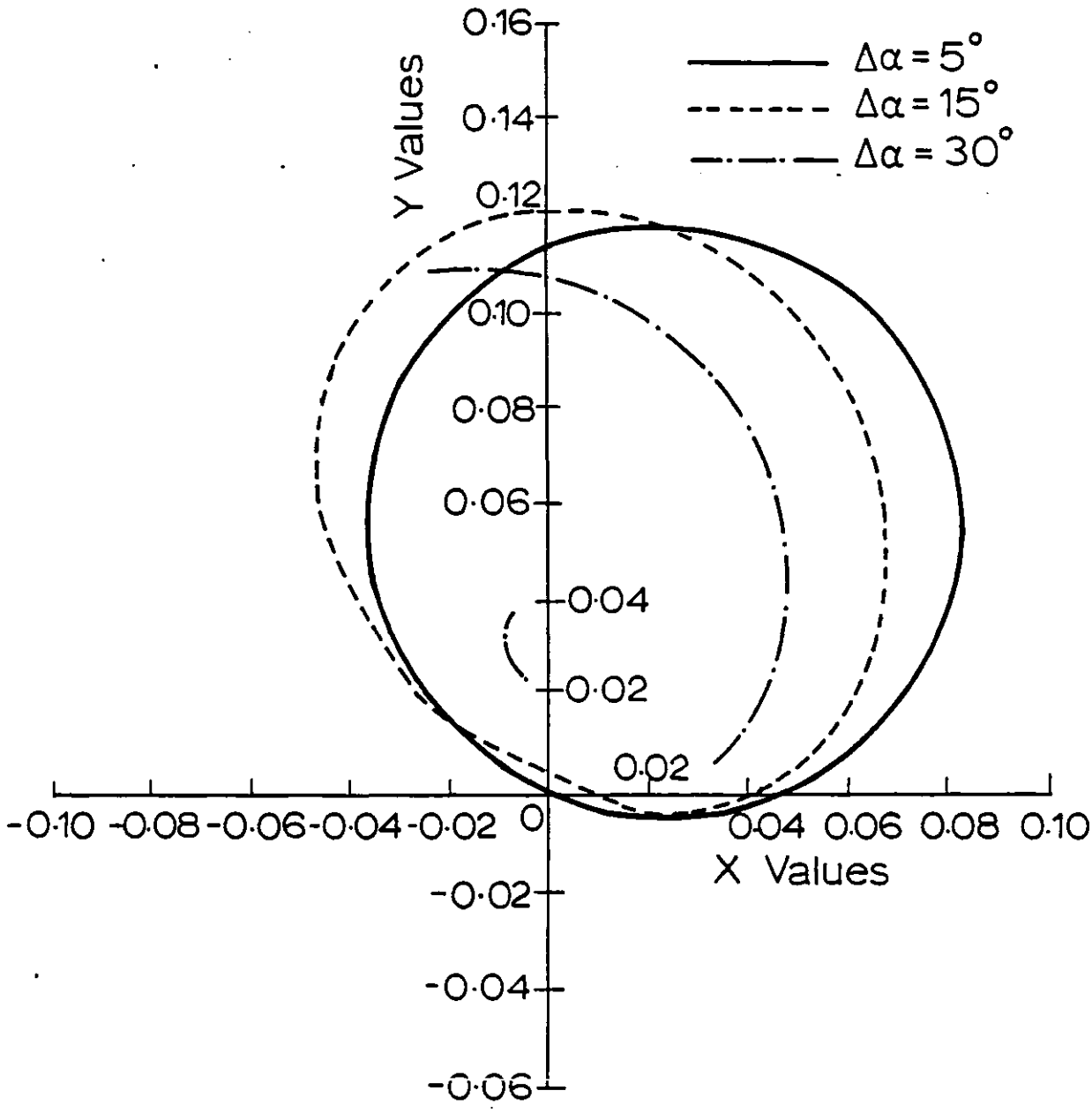

Fig 5.23: Describing function for 150 Hz. Base case. s.c.r. = 3. α^{o} = 15°

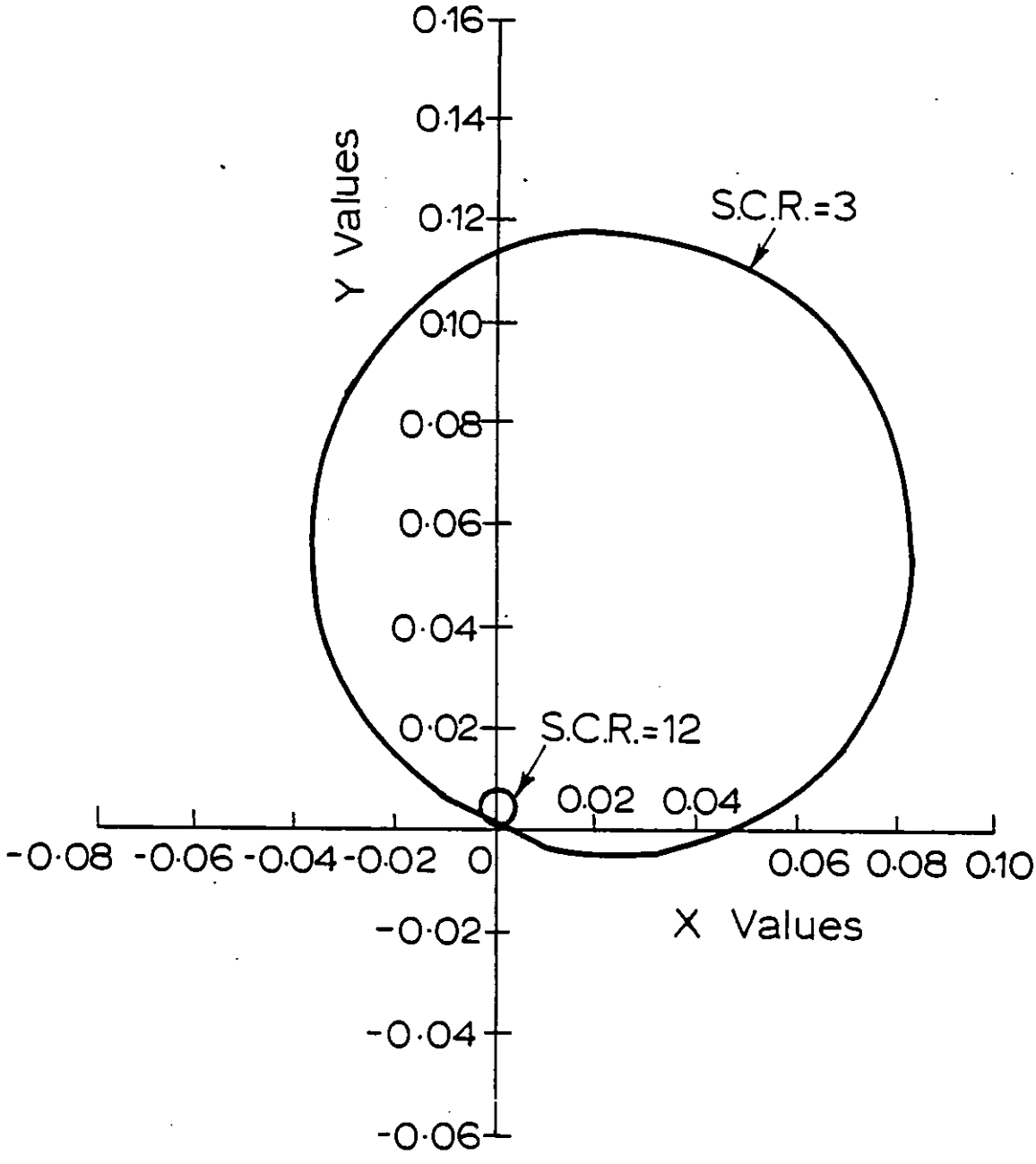

Fig 5.24: Describing function for 150 Hz. Comparison between the d.f. for s.c.r. = 3 and for s.c.r. = 12. Base case; $\Delta\alpha = 5^{o}$, $\alpha^{o} = 15^{o}$

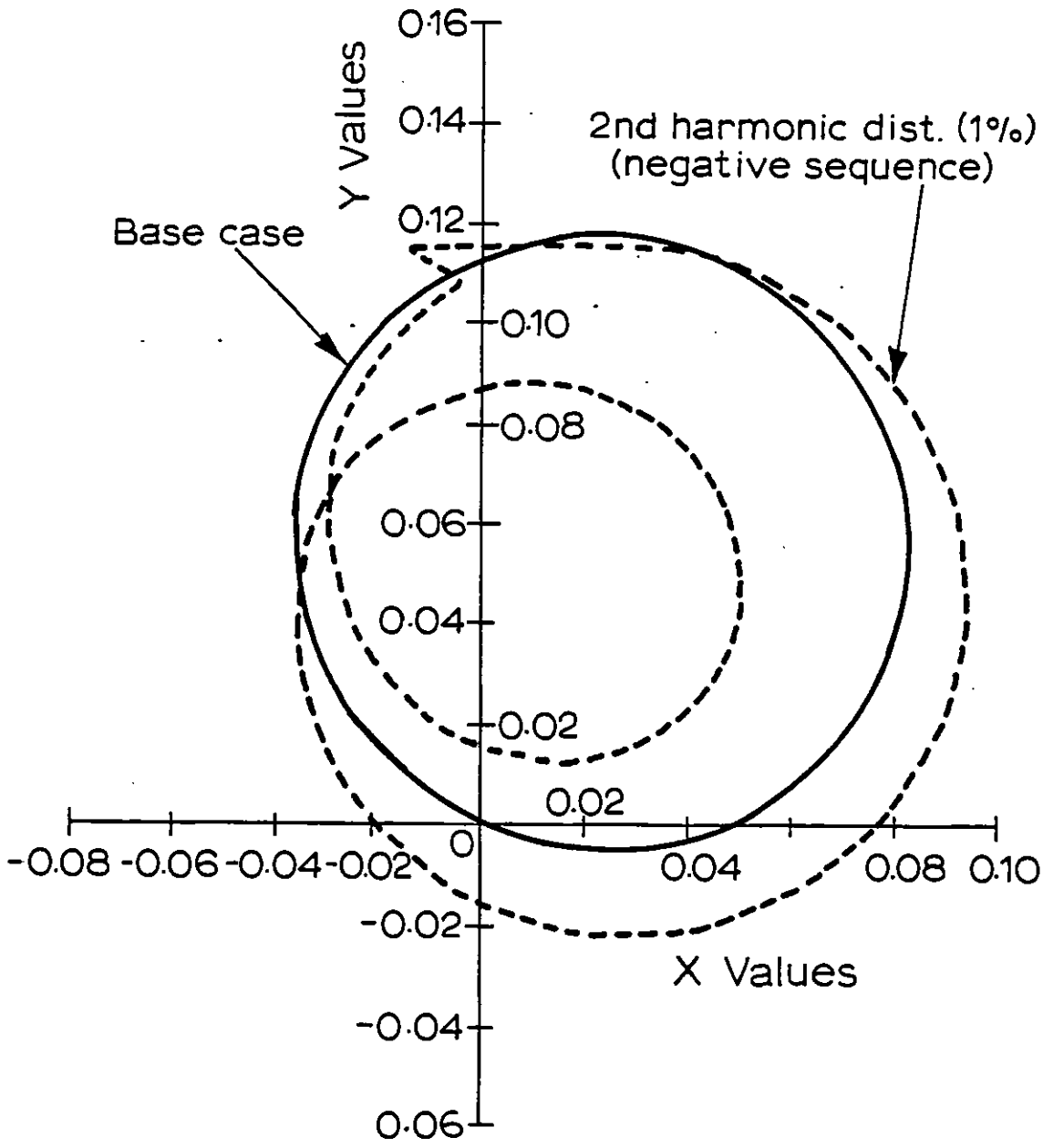

Fig 5.25: Describing function for 150 Hz. Effect of a second harmonic distortion on the d.f. locus. s.c.r. = 3; $\alpha^{o} = 15^{o}$; $\Delta\alpha = 5^{o}$

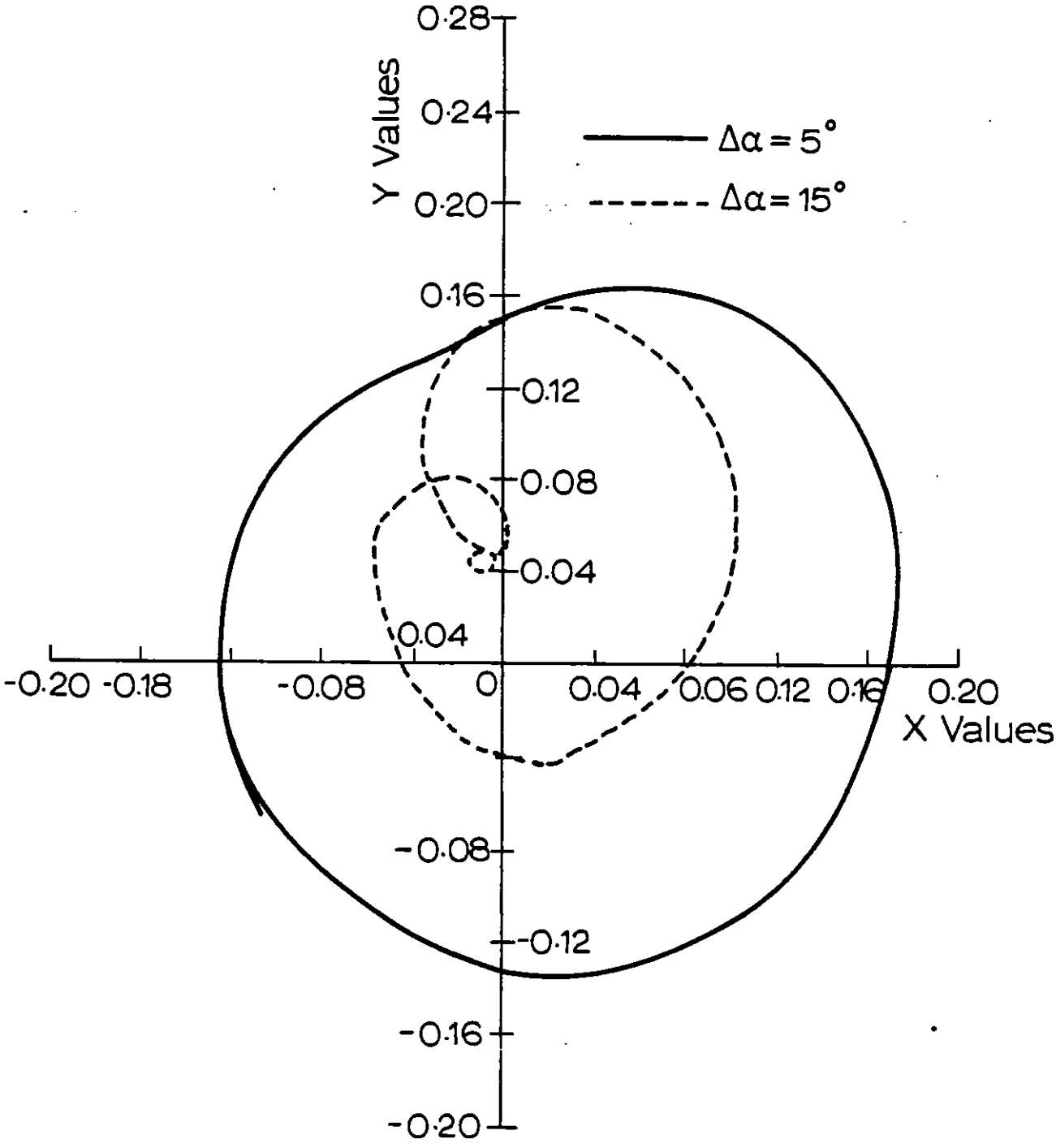

Fig 5.26: Describing function for 150 Hz. 2nd harmonic distortion negative sequence (1%). α^{o} = 15°, s.c.r. = 12

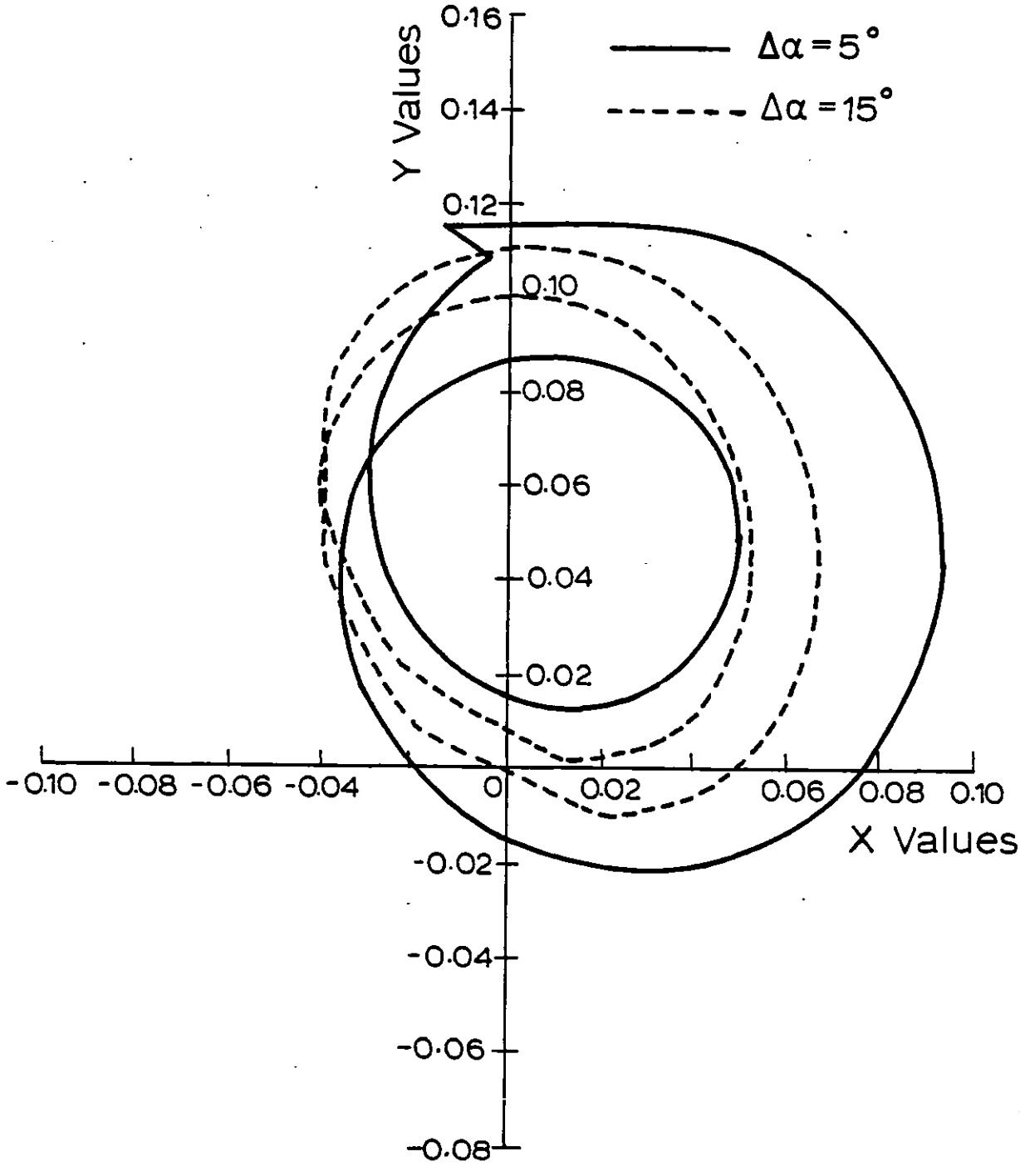

Fig 5.27: Describing function for 150 Hz. 2nd harmonic distortion negative sequence (1%). α^{o} = 15°, s.c.r. = 3

feature is common to all frequencies of the modulating signal studied.

5.7 Prediction of limit cycles using the Nichols chart

As pointed out in section 5.2, the Nyquist diagram or the Nichols chart are commonly used for stability analysis when the describing function method is employed.

Equation 5.5 gives the conditions for the existence of limit cycles. A plot of $G(j\omega)$ and $-1/N(x, \omega)$ is required to determine these conditions.

$G(j\omega)$ represents the transfer function of the linear part of the control loop. In all studies carried out the error processing unit possesses a transfer function of the type:

$$G(j\omega) = \frac{+K}{1 + j\omega T} \qquad (5.20)$$

where K is the gain and T the time constant.

Any transfer function of the type of equation (5.20) may be expressed in the form

$$20 \log_{10} G(j\omega) = 20 \log_{10}(K) - 10 \log_{10}\left((\omega T)^2 + 1\right) - j \tan^{-1}(\omega T) \qquad (5.21)$$

With a gain K of unity equation (5.21) reduces to

$$20 \log_{10} G(j\omega) = 10 \log_{10}\left((\omega T)^2 + 1\right) - j \tan^{-1}(\omega T) \qquad (5.22)$$

From equations (5.21) and (5.22) it is apparent that a variation in K causes a vertical displacement of $G(j\omega)$ in the Nichols chart. This result is shown in fig 5.28.

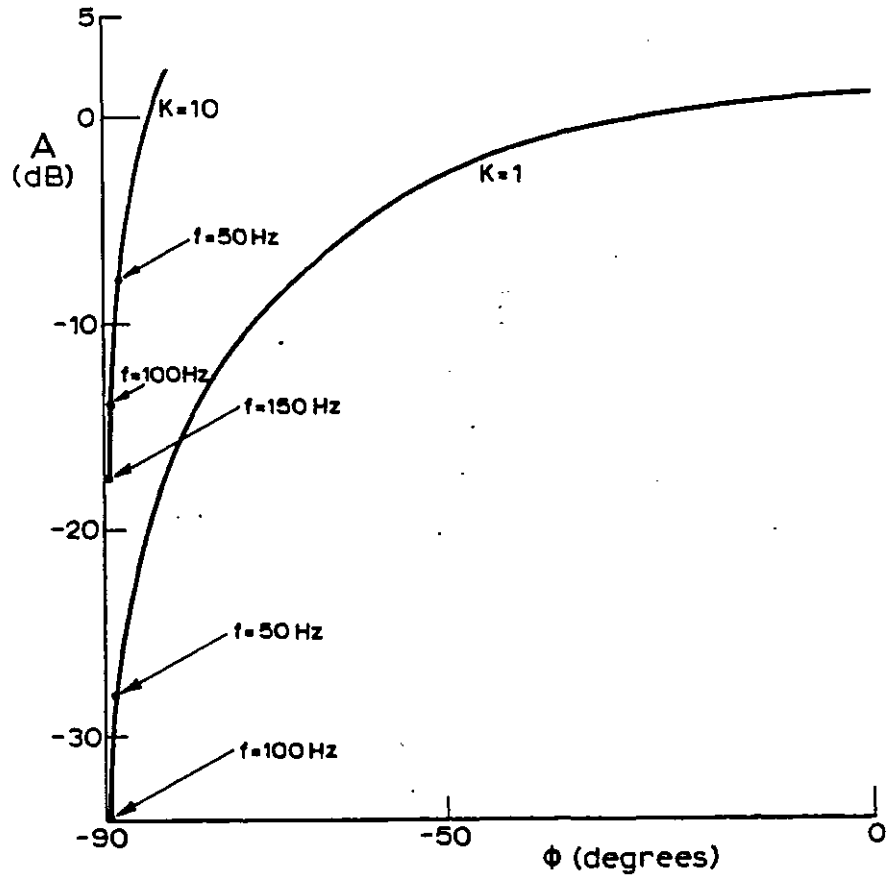

Fig 5.28 Nichols chart of G(jω)

The plot of $-1/N(x, \omega)$ together with that of $G(j\omega)$ on the Nichols plane provide a simple method of finding the solution of equation (5.5). Fig 5.28 also indicates that only the part of the locus of $-1/N(x, \omega)$ included between -90° and 0° is of interest as far as $G(j\omega)$ is concerned.

Taking as example the 50 Hz studies, fig 5.29 shows the Nichols plot for an a.c. system s.c.r. of 12 and for a modulating signal amplitude resulting in a perturbation of α of 5°. Three cases are shown and a comparison of figs 5.28 and 5.29 reveals that no intersection of $G(j\omega)$ with

$-1/N(x, \omega)$ is predicted.

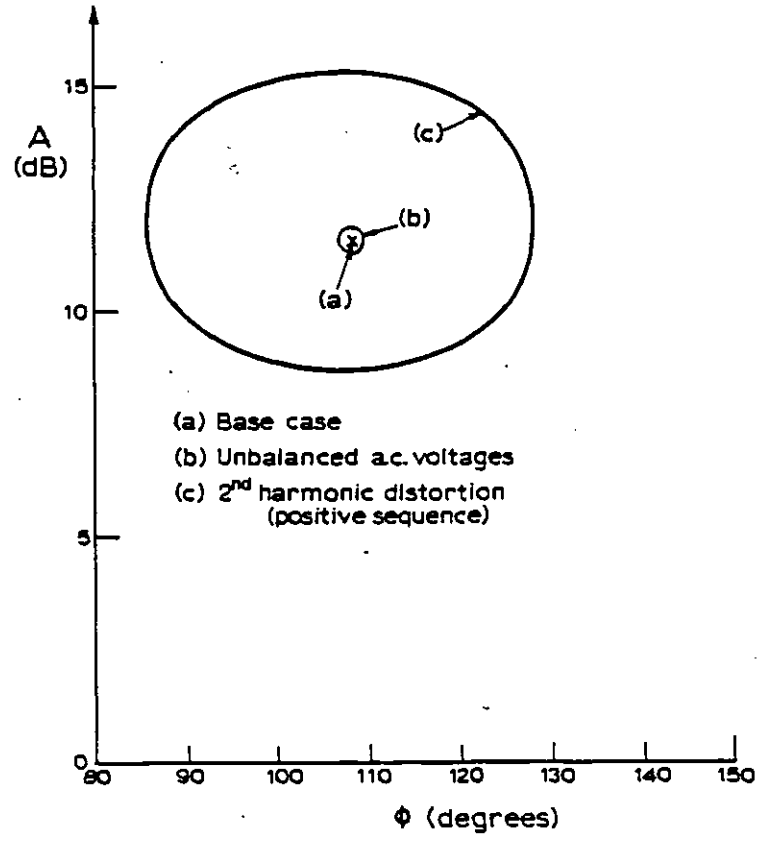

Fig. 5.29 Nichols chart
$f = 50$ Hz, S.C.R. = 12, $\Delta\alpha = 5°$

Table 5.6: Limit cycle predictions, f = 50 Hz, s.c.r. = 3, $\Delta\alpha = 5^{\circ}$

	Prediction of limit cycle	Stability margin	Gain K
Base case	No	18°	141.2
Negative sequence in fundamental a.c. voltage	Yes	-	136.5
Unbalance in transformer reactances	No	1°	140
2nd harmonic distortion (positive sequence)	Yes	-	58.2

In fig 5.30 the plots of fig 5.29 are repeated but for a s.c.r. of 3. A comparison of figs 5.30 and 5.28 shows that limit cycle oscillation are now predicted. The result of this comparison is shown in fig 5.31. Table 5.6 summarises the study of limit cycle prediction for a frequency of the modulating signal of 50 Hz, an amplitude of the modulating signal of 5^{o} and a s.c.r. equal to 3.

Considering that for the case of Table 5.6 limit cycle oscillations are predicted, further studies were performed with this s.c.r. but for an amplitude of the modulating signal equal to 15^{o}. It was found that only a second harmonic distortion with positive sequence would give rise to limit cycle oscillations.

The Nichols chart for this case is shown in fig 5.32. The inverse of d.f. $(-1/N(x,\omega))$ is plotted for amplitudes of the modulating signal equal to 5^{o}, 15^{o} and 30^{o}.

Also plotted is the locus of $G(j2\pi 50)$ for different values of the gain K. The values of K for which a limit cycle is predicted may be obtained by reading the value of A for which an intersection of $-1/N(x,\omega)$ and $G(j2\pi 50)$ occurs, and using

$$A = 20 \log_{10} K - 10 \log_{10}\left((2\pi 50T)^2 + 1\right) \qquad (5.22)$$

where T = 80 ms.

5.8 Conclusions

From the studies carried out, the following conclusions can be drawn:

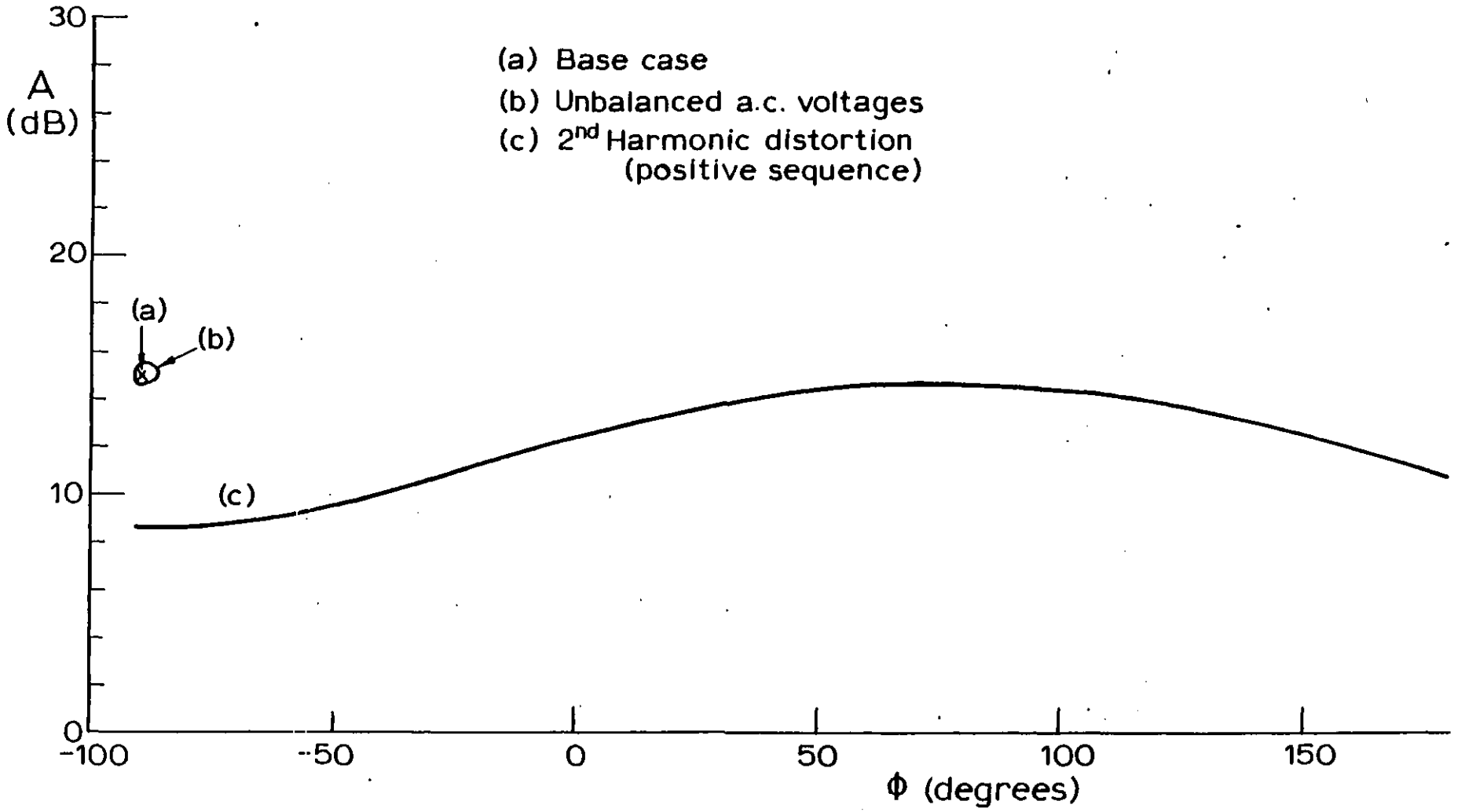

Fig. 5-30 Nichols chart $f = 50$ Hz, S.C.R. = 3, $\Delta\alpha = 5^\circ$

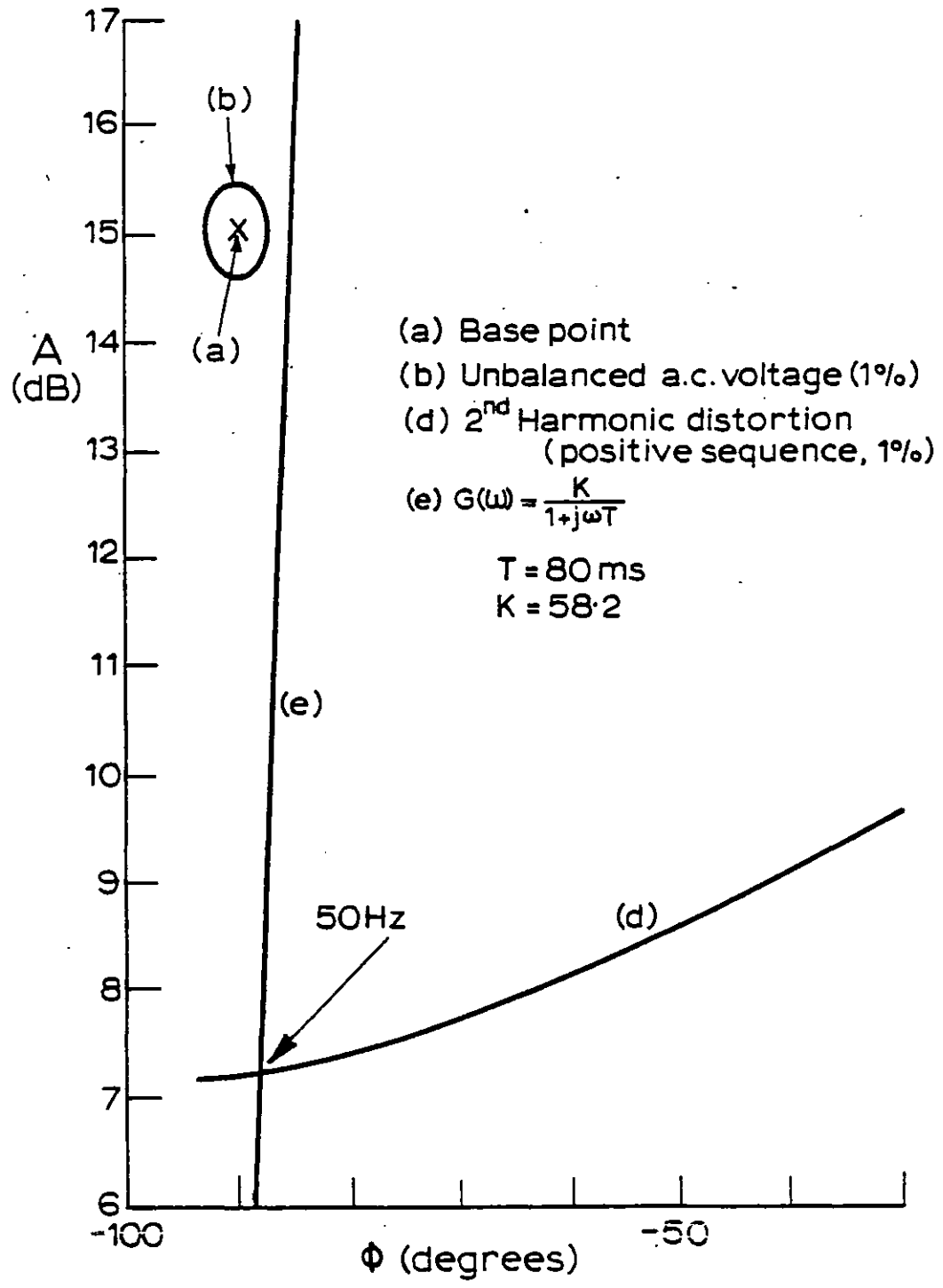

Fig.5·31 Nichols chart f=50 Hz, S.C.R.=3, $\Delta\alpha = 5°$

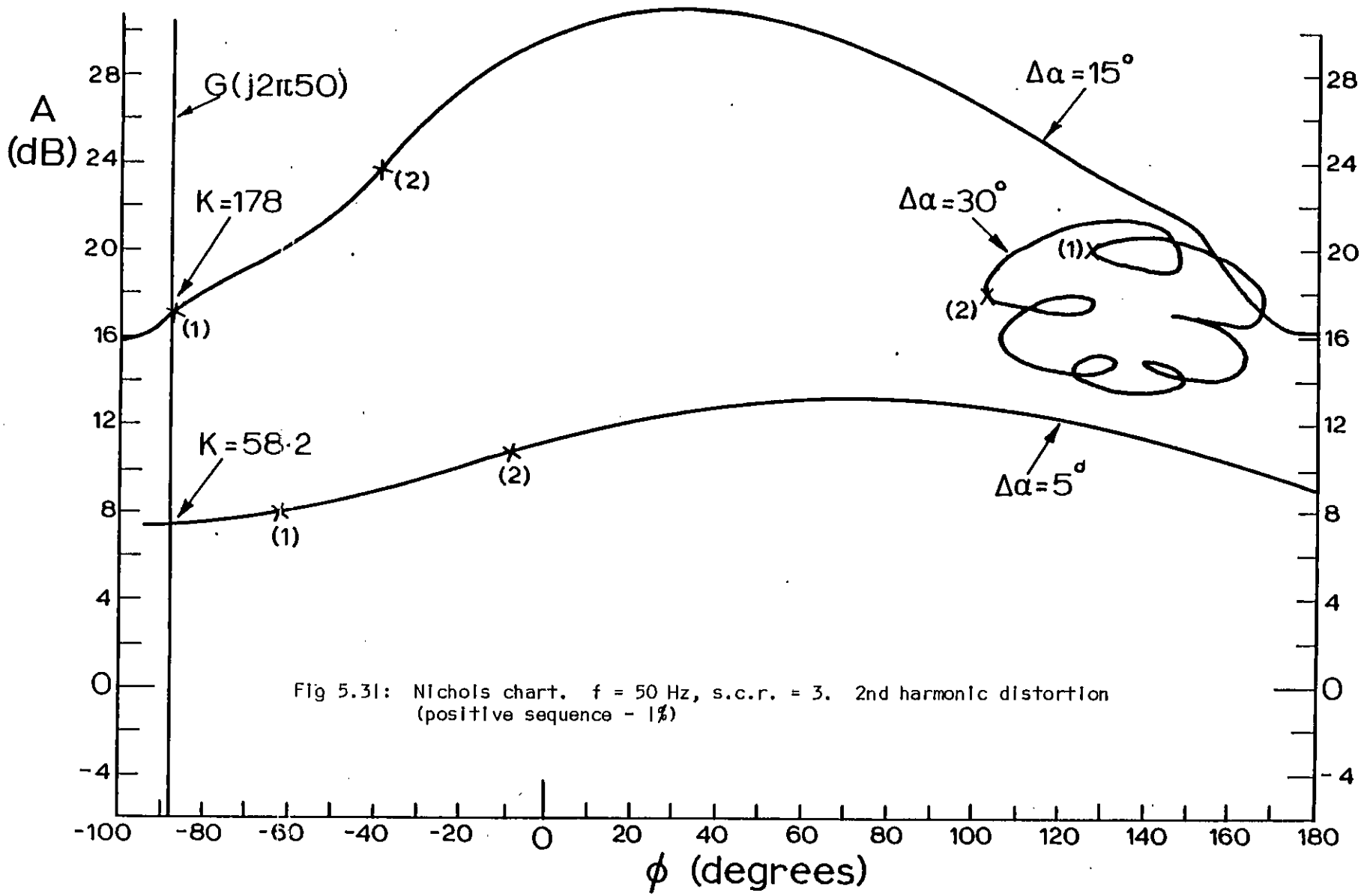

Fig 5.31: Nichols chart. f = 50 Hz, s.c.r. = 3. 2nd harmonic distortion (positive sequence - 1%)

1 The describing function for a small amplitude m.s. at the a.c. fundamental frequency is a point, for any value of the s.c.r., if there is no unbalance and/or distortion in the a.c. busbar voltage.

As the amplitude of the modulating signal becomes larger, the d.f. develops into a closed curve, due to the intervention of the firing angle limits. This behaviour applies to both high and low short-circuit ratio. However, when the s.c.r. is low the d.f. locus is considerably displaced in the polar plane as the amplitude increases, whereas for high s.c.r. the locus stays in the same region.

2 For an input signal at 100 Hz, the d.f. also reduces to a point for very small amplitudes. However, the point develops into a closed curve for values of the amplitude of the modulating signal which are considerably smaller than those necessary to produce the same effect at 50 Hz. This is thought to be due to the contribution to the fundamental on the a.c. side of a second harmonic on the d.c. side.

3 The d.f. for 150 Hz, which is the only one predicted by the linearised model (1) exists for infinitesimal input signals. Incrementing the signal amplitude produces quite different effects on the d.f. For test system 2 and a s.c.r. of 3, the results show no enlargement of the d.f. with increasing amplitude of the m.s. The same behaviour was observed for test system 1 and infinite s.c.r. conditions. For test system 2 and a s.c.r. of 12 an enlargement of the d.f. with increasing amplitude of the modulating signal occurs.

4 In all the cases studied, for a particular value of the introduction of an imbalance and/or distortion on the a.c. busbar led to an expansion of the d.f. centred on the base case solution. This enlargement is, however, only significant in those cases where the a.c. currents generated by the converter with a modulated input signal contain the same harmonics which are being imposed on the a.c. busbar.

5 As a corollary of the previous point, the following conclusions can be drawn:

a. The d.f. for 50 Hz is expanded by a second harmonic distortion with positive sequence (+2).

b. The d.f. for 100 Hz is expanded by voltage imbalance and/or by any imbalance in the converter transformer reactances, i.e. by a harmonic of order -1.

c. The d.f. for 150 Hz is expanded by a second harmonic distortion with negative sequence (order -2).

6 When the a.c. currents generated by the converter with a modulated input signal contain the same harmonics as those imposed on the a.c. busbar, the enlargement experienced by the d.f. depends on the amplitude of the m.s. This enlargement is more pronounced for small amplitudes of the m.s.

Chapter Six

EXPERIMENTAL DETERMINATION OF THE DESCRIBING FUNCTION AND LIMIT CYCLE OSCILLATIONS

6.1 Introduction

The previous chapters describe a non-linear converter model which allows the prediction of limit cycle oscillations synchronised with the a.c. system voltage, using the describing function technique.

In order to assess the validity of the proposed model, a number of test results were obtained using the Imperial College h.v.d.c. simulator.

The controller used was the one described in Chapter Two.

The experimental set-up included a Digital Transfer Function Analyser (39) and a Spectrum Analyser (40) which allowed the evaluation of the relevant d.c. current harmonic, and the determination of all the relevant harmonics both on the a.c. system voltage and in the control voltage.

The main purpose of the set of tests carried out was to confirm experimentally the theoretically evaluated describing

functions and the predicted limit cycles.

To obtain the plots, the digital transfer function analyser was used. A function generator with a frequency range from 10^{-5} Hz to 159.9 Hz provides the modulating signal to be superimposed on the control voltage. A correlator with a frequency range identical to the function generator performs the measurement of the relevant harmonic of d.c. current. The current control loop of the converter is thus open.

To verify a limit cycle oscillation, tests were performed with the converter under the constant-current mode of operation. A spectrum analyser was used to measure a.c. voltage harmonic distortion and control voltage harmonics. These measurements provide data for the off-line computer program developed. The spectrum of the control voltage enables the determination of the amplitude of the modulating signal to be superimposed on the steady-state control voltage in the computer off-line studies, whereas the spectrum of a.c. voltage harmonics enables the evaluation of the a.c. harmonic distortion present when limit cycle oscillation occurred.

Section 2 of this chapter describes the experimental set-up. The parameters of the h.v.d.c. simulator used for the theoretical studies are determined and the measuring apparatus described.

In section 3 a comparison between theoretical and test describing functions both with infinite s.c.r. and finite s.c.r. is performed.

Section 4 describes the theoretical prediction of limit cycles and comparison with test results. The Nichols chart is the technique used to perform this comparison.

6.2 Experimental set-up

6.2.1 Parameters of the h.v.d.c. simulator

A single line diagram of the system under test is shown in figure 6.1.

Eac stands for the a.c. voltage at the mains supply. Vac_1, Vac_2 and Vac_3 denote the a.c. voltage at the busbar side, converter side and tertiary of the converter transformer respectively.

E_{DI} is the constant e.m.f. that simulates inverter behaviour. In the test circuit it is 48V and is provided by series connected accumulators.

The filter bank, denoted in figure 6.1 by F, consists of 5th, 7th, 11th and 13th tuned arms plus a high pass arm and is connected to the tertiary of the converter transformer.

Measurements were performed on both the commutating reactances and smoothing inductors in order to evaluate R_{com}, L_{com}, R_{ch}, and L_{ch}. The source impedance was also measured.

The values of R, L and C for the filter bank are design values. R_T is also a design value.

The resistances were measured using d.c. voltage, whereas all the inductances were measured at 50 Hz. No d.c. bias was considered when measuring L_{ch} as for the range of d.c. current used in the tests (1A - 5A), the influence of the d.c.

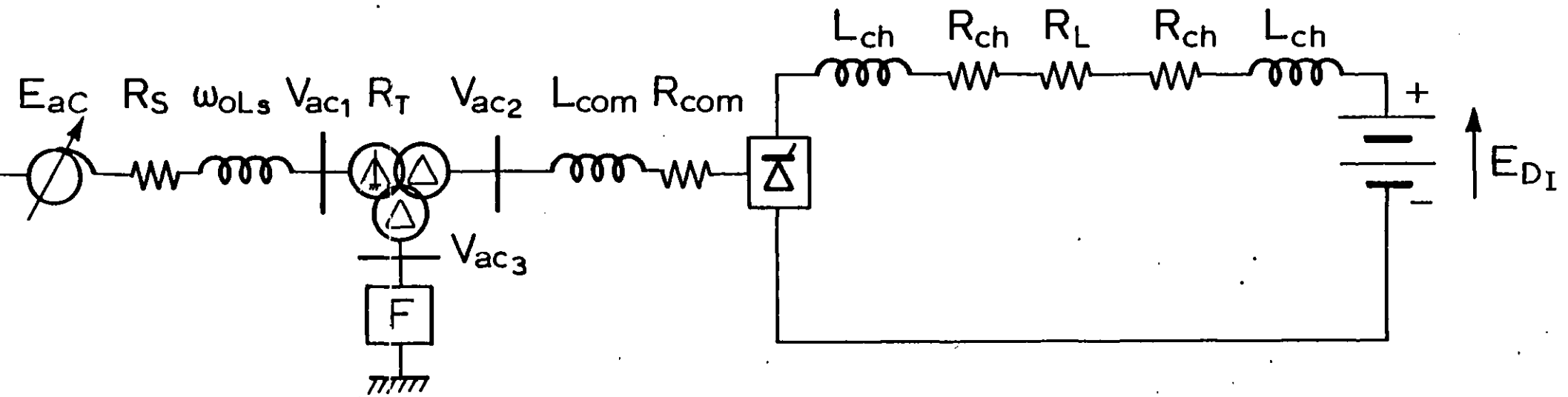

R_T - Series resistance of the converter transformer
R_{ch} - Smoothing inductor resistance
R_s - Source resistance
R_{com} - Commutating reactances resistance
L_{com} - Commutating reactances inductance
L_{ch} - Smoothing inductor inductance
ω_{oLs} - Source impedance reactance

Fig 6.1: On-line diagram of system under test

bias is negligible (41). The value of R_T considered is the one mentioned in (41). The parameters for the filter bank are the ones listed in (1).

The source impedance is a simple air-cored inductor with 10 taps.

Table 6.1 summarises all the relevant data concerning the a.c. source impedance, converter transformer, commutating reactances and d.c. side parameters. Table 6.2 lists the filter bank data.

Table 6.1: Parameters of h.v.d.c. system

Vac_1 (nom) [V]	220
Vac_2 (nom) [V]	80
Vac_3 (nom) [V]	110
R_T [Ω]	0.17
R_{com} [Ω]	0.6
L_{com_R} [H]	5.09×10^{-3}
L_{com_Y} [H]	5.12×10^{-3}
L_{com_B} [H]	5.18×10^{-3}
L_{ch} [H]	0.4
R_{ch} [Ω]	1.6
R_L [Ω]	1
R_{Smax} [Ω]	2.5
$\omega_o L_{smax}$ [Ω]	64.21

Table 6.2: Parameters of filter bank (1)

Filter	R [Ω]	L [mH]	C[μF]
5th	4.6	78	5.25
7th	3.88	54.4	3.75
11th	3.24	30	2.75
13th	4.12	24.8	2.5
H.P.	100	20	1.75

In Table 6.1, the transformer resistance and the commutating inductance and resistance are referred to the converter side of the converter transformer.

In Table 6.2 the parameters of the filter bank are all referred to the a.c. busbar side of the converter transformer.

6.2.2 Measurement set-up

To obtain a describing function from tests it is necessary to modulate the steady state control voltage with a signal of known amplitude, frequency and phase, and to measure the d.c. current harmonic of the same frequency.

The d.f. is given by equation (5.17)

$$N(V_m, \omega, \psi) = \frac{Id\, e^{j\phi}\, d\omega}{V_m e^{j\psi}} \qquad (5.17)$$

A Solartron JM 1600 (39) digital transfer function analyser was used to generate the modulating control voltage Vc and to measure the harmonic of d.c. current of interest.

The JM 1600 comprises a function generator as a source of excitation to the system under test and a digital correlator.

The digital correlator picks out the sine wave component that possesses the same frequency as the one set in the function generator and rejects harmonics and noise. The 'in phase' and 'quadrature' components of the waveform to be analysed are measured relatively to sine and cosine reference signals derived directly from the function generator.

A block diagram of the digital transfer function analyser is shown in fig 6.2.

In order to lock the output of the function generator to the a.c. system voltage a special purpose circuit had to be designed. This circuit is shown in fig 6.3.

The +6V is obtained from the digital transfer function analyser (d.t.f.a.), and V_{RN} is the line-to-neutral voltage of phase R. The instant this voltage goes through zero with a positive slope is taken as time reference for both the theoretical and test studies.

Tests showed that no phase shift existed between the output of the function generator and voltage V_{RN}.

The describing function of a controlled converter is generally obtained for a particular value of steady state control voltage, which corresponds to a nominal firing angle α^{o}. Thus a d.c. voltage level must define the value of α^{o}.

The d.f. for converters (see section 5.3) also depends on the amplitude, frequency and phase of the input signal.

As the function generator of the d.t.f.a. generates a signal whose mean value is zero, a d.c. level must be set independently. Also the d.t.f.a. does not allow variations in phase of the output of the function generator. The hardware

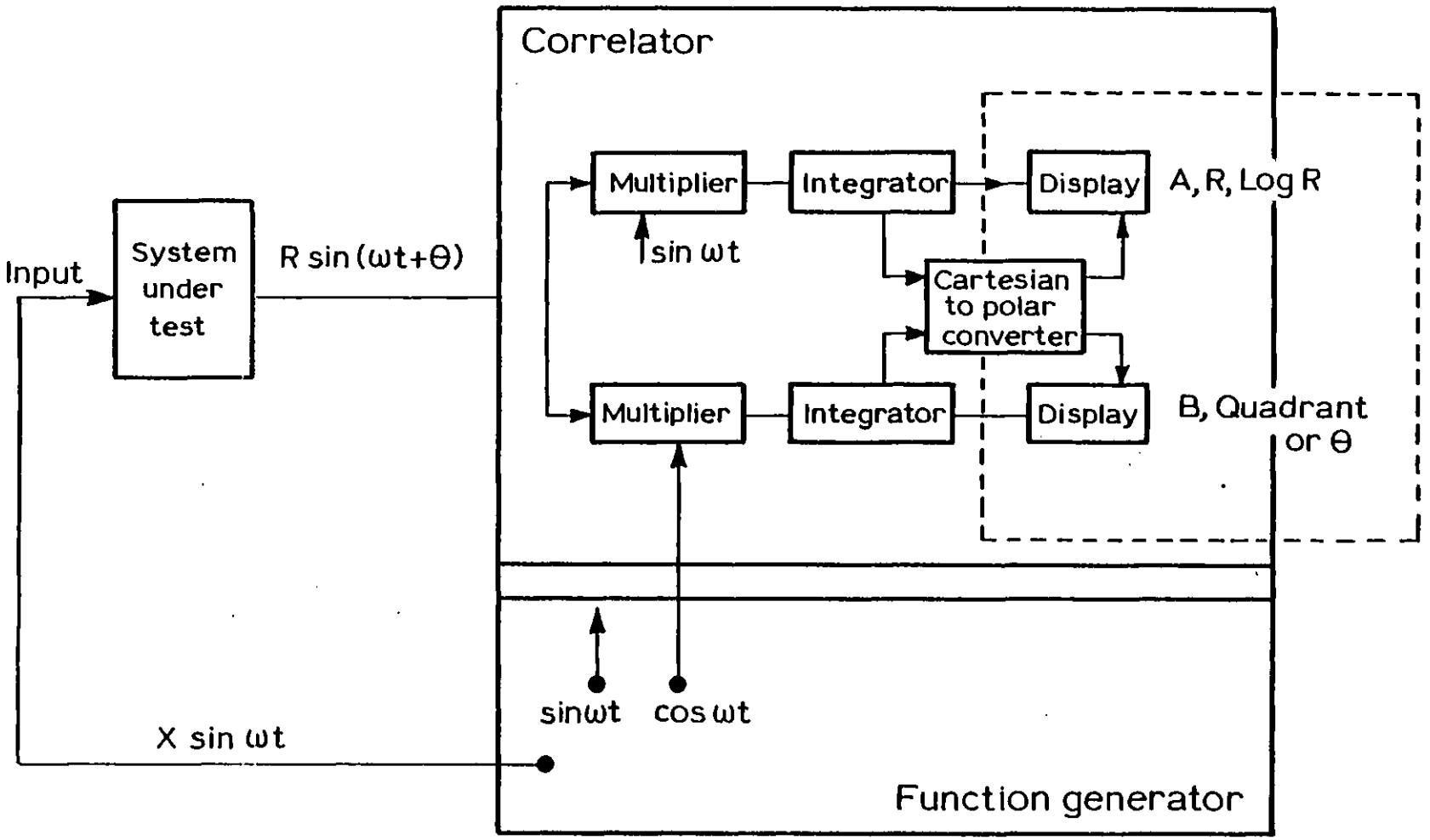

Fig 6.2: D.T.F.A. block diagram (39)

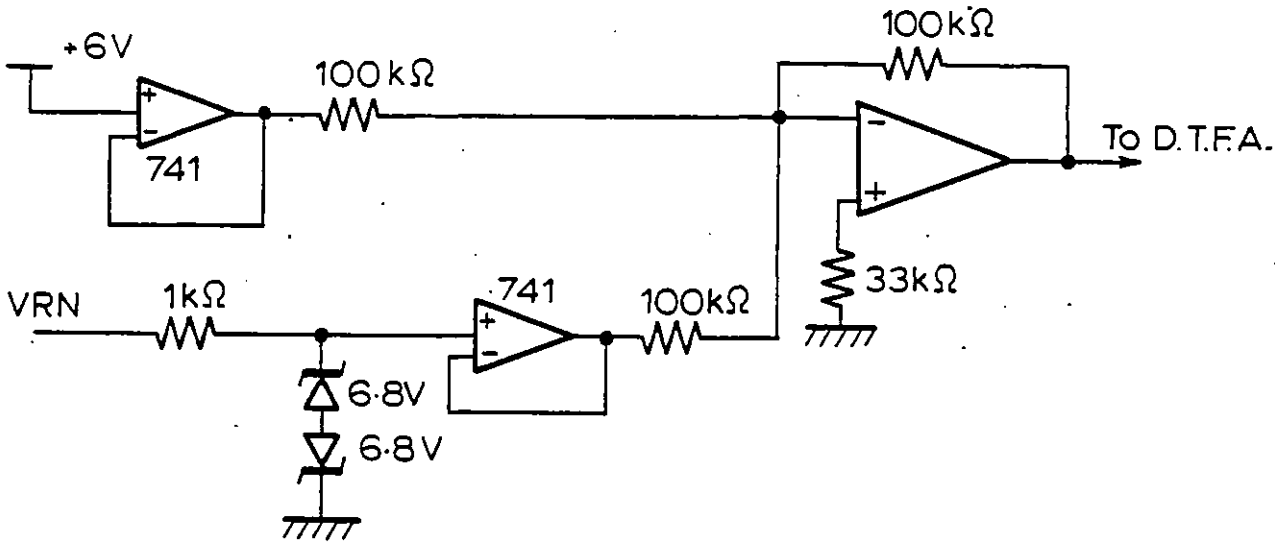

Fig 6.3: Circuit to lock D.T.F.A.

circuitry that provides both phase-shift and d.c. level is shown in fig 6.4.

As the phase shifting network provides a shift of the signal in the range of 0° to 180°, to cover the desired range of phase shift (between 0° and 360°) an inverting circuitry was built.

Path (1) shown in hatched line in fig 6.4 allows a phase shift of the output of the function generator between 0° and 180°, whereas path (2) allows a phase shift between 180° and 360°.

The bootstrap minimises the loading effects on the d.t.f.a.

The input to the correlator is the d.c. current waveform which is measured with a Hall effect device circuit which itself introduces a phase shift in the d.c. current harmonics. For the frequencies of interest, i.e. 50, 100 and 150 Hz, this phase-shift is respectively -5.7°, -11.4° and -16.8°.

To use fully the resolution of the correlator of the d.t.f.a. it was necessary to filter out the constant component of d.c. current. A fourth order Chebyshev band-pass filter was used for this purpose. The circuit diagram is shown in fig 6.5. Fig 6.6 shows the comparison between the theoretical amplitude response and the test results for this filter. Table 6.3 shows the gain and phase-shift for the frequencies of interest, obtained from tests.

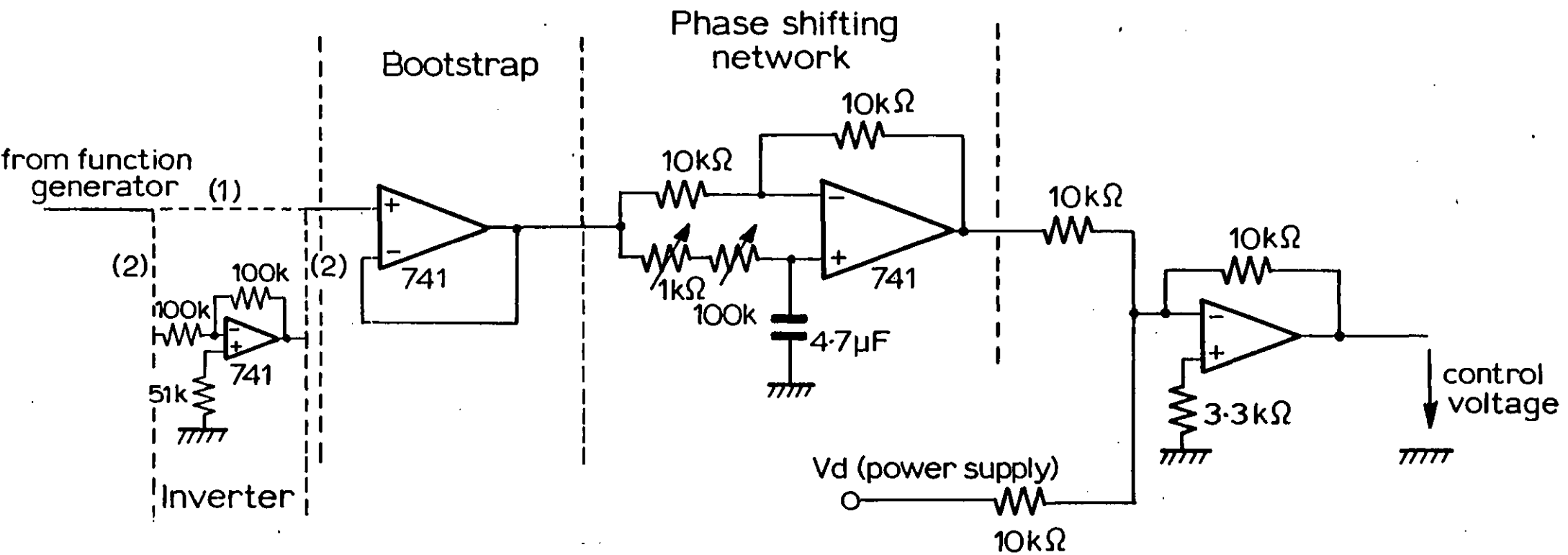

Fig 6.4: Hardware circuitry for control voltage

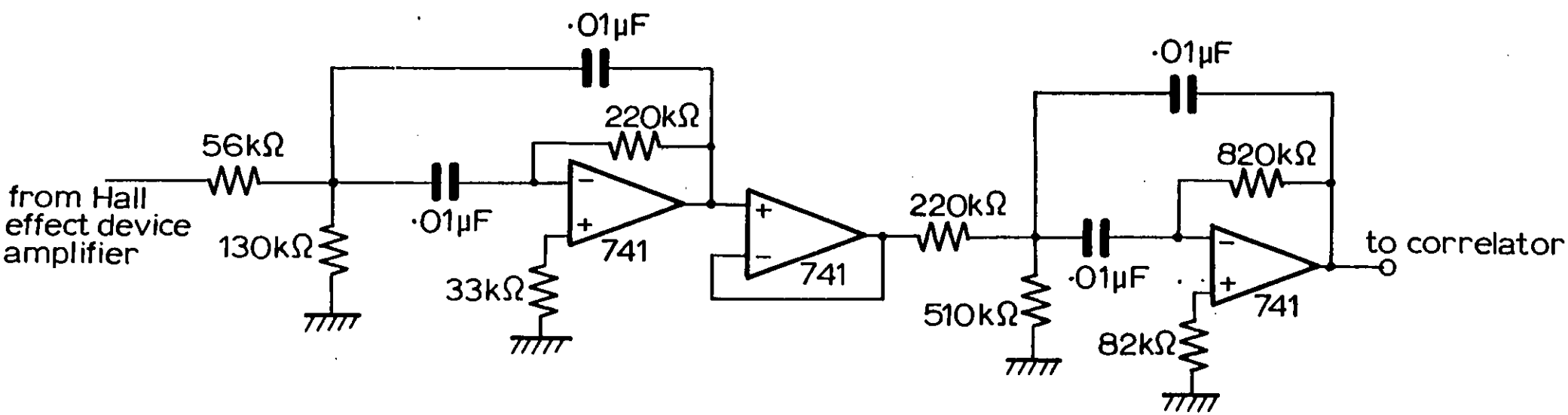

Fig 6.5: Circuit diagram of 4th order Chebyshev bandpass filter

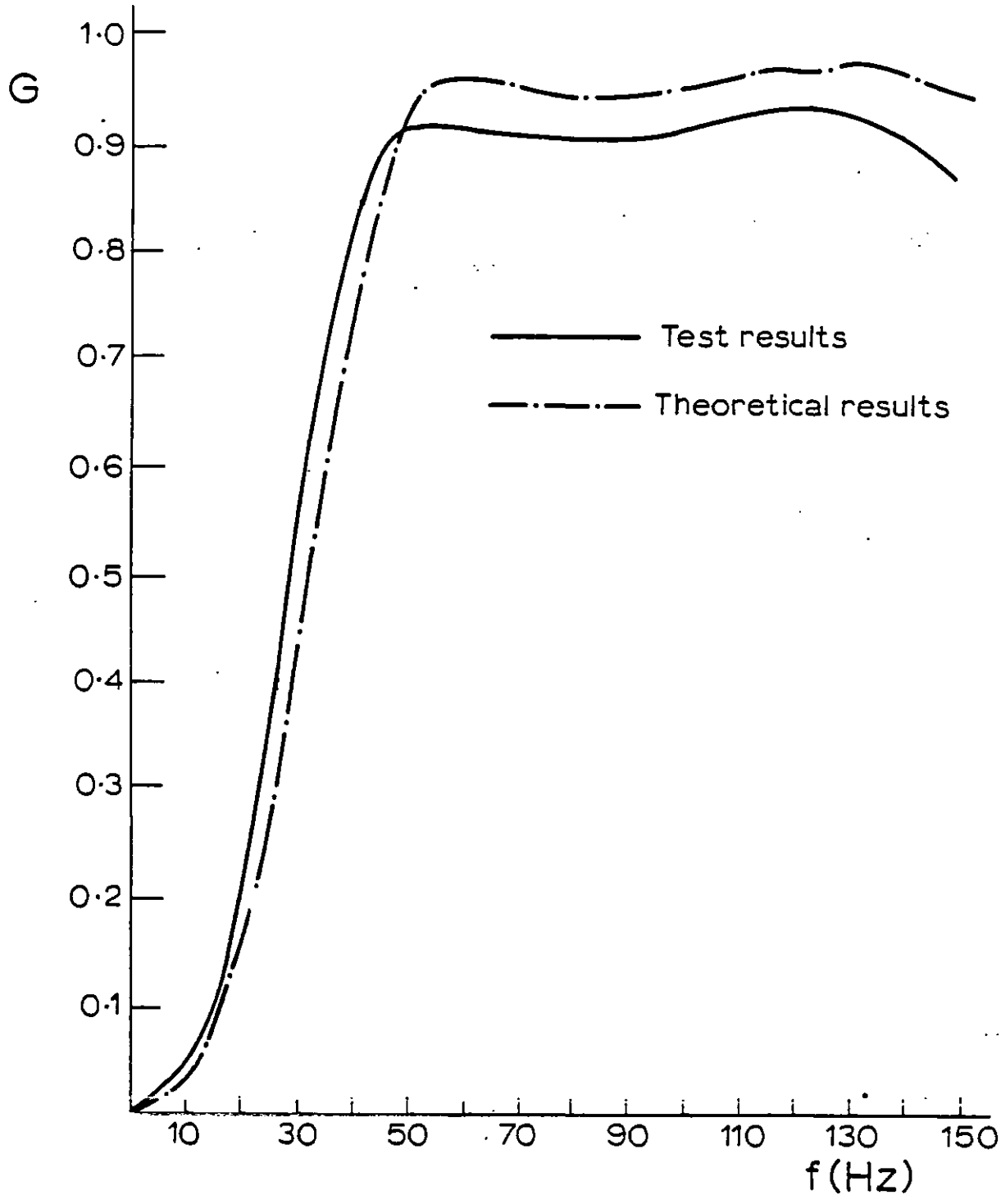

Fig 6.6: Comparison between theoretical and test results for a 4th order Chebyshev bandpass filter

Table 6.3: Gain and phase-shift of 4th order Chebyshev bandpass filter (test results)

f	Gain	Phase
50	.916	-134^{o}
100	.916	-198.3^{o}
150	.887	-245.3^{o}

The controller used (Chapter Two) employs a Pulse Phase Control algorithm which possesses a proportional characteristic between the control voltage and the firing angle with respect to a particular reference. The constant of proportionality, derived from the A/D converter, and the phase-locked-loop free running frequency is 20.45 el deg V^{-1}. To obtain the test describing function the output of the function generator is set to a particular frequency. A bias voltage obtained from a power supply sets the value of α^{o}, whereas the output of the function generator is set to an amplitude that corresponds to the desired value of $\Delta\alpha$.

The output of the Chebyshev filter is applied to the correlator input. The measurement performed by the correlator gives the amplitude and phase of the harmonic of d.c. current at the frequency set by the function generator. The reference for phase measurements are sine and cosine signals derived from the function generator. As the phase shifting circuitry is not built in the d.t.f.a. the measurements of the correlator are always performed in relation

to the same reference signals. To obtain the d.f. the phase-shift ψ introduced by the circuit of fig 6.4 must be taken into account. As the phase shift is varied through a potentiometer, any small error can affect the value of ψ, and comparison with the theoretical results may be difficult.

An alternative is to plot the ratio

$$\frac{I_{d_\omega}}{V_m} \; e^{j\phi_{d\omega}} \qquad (6.1)$$

and obtain the theoretical results in the same form. This means that although a phase shift is introduced in the modulating signal, the measurements are made relatively to the control voltage before the phase shifter ($\psi = 0^o$).

In the measurements obtained, a correction due to the gain and phase of the Chebyshev bandpass filter must be introduced. However no correction was introduced to compensate for the phase-shift due to the Hall effect device circuitry.

6.2.3 Data for the theoretical studies

For the off-line studies the data compiled in Tables 6.1 and 6.2 was considered. Although during measurements a 2% difference in the values of the source impedance for the three phases was found, this was not included in the off-line studies. Similarly any imbalances in the filter parameters for the three phases were not considered, as the off-line program does not allow the representation of imbalances in the source and filter impedances. The off-line program

can however incorporate commutating impedance imbalances and any such imbalances found during measurements were taken into account.

The value of α^{o} used in the theoretical studies was the mean value of α reference obtained during tests. The amplitude of the modulating signal was measured during tests and this value was used in theoretical studies.

The d.c. current constant term considered for all the theoretical studies was 2A.

During the tests it was observed that this parameter varied with the phase of the modulating signal, this variation being negligible for the 50 Hz and 100 Hz modulating signal frequencies. However for a modulating signal of 150 Hz and amplitude of 14.8^{o} (with $\alpha^{o} = 15^{o}$) the d.c. current 'constant' term varied between 1.5A and 2.5A.

The off-line program takes the d.c. current constant term as fixed, thus assuming a variation in the inverter e.m.f. This short-cut was used in order to avoid an iterative procedure for the evaluation of current in the theoretical studies.

The variation of the d.c. current 'constant' term affects mainly the value of the commutation angle and thus the amplitude and phase of d.c. current harmonics. We can conclude that the comparison between theoretical and test results should be worst for the 150 Hz case.

As pointed out in Chapter Five, for the 50 Hz and 150 Hz modulating signal frequencies, the fundamental a.c. voltage (on the a.c. busbar of the converter transformer) was

assumed fixed. Therefore the time reference for both the theoretical and test studies is obtained from phase R of the a.c. busbar of the converter transformer (Vac_1, in fig 6.1). It was also pointed out in Chapter Five that for the 100 Hz modulating signal frequency it is not valid to impose the fundamental on the a.c. system side of the converter transformer. This is because a 100 Hz on the d.c. side generates a 50 Hz on the a.c. side. The fundamental of the a.c. voltage is therefore imposed on the Thevenin equivalent generator. Thus to obtain the test results the d.t.f.a. was synchronised with phase R of the output side of the variac (Eac in fig 6.1).

6.3 Comparison between theoretical and test results

Test d.f.s were obtained for both high (infinity) and low (3 and 6) short circuit ratios. For high s.c.r. two cases were studied: a) base case where only imbalances inherent to the commutating reactance were considered; b) imbalances of 15.6% in one of the commutating reactances. For low s.c.r. only the base case was examined.

6.3.1 Infinite short circuit ratio

6.3.1.1 Base case

The theoretical and test results obtained with no imposed imbalance and/or distortion apart from that inherent in the a.c. mains are shown in figs 6.7 to 6.12.

Figs 6.7 and 6.8 are for 50 Hz m.s. and show that an increase

f = 50 Hz
α^{o} = 15.4
$\Delta\alpha$ = 8.4

"Base case"

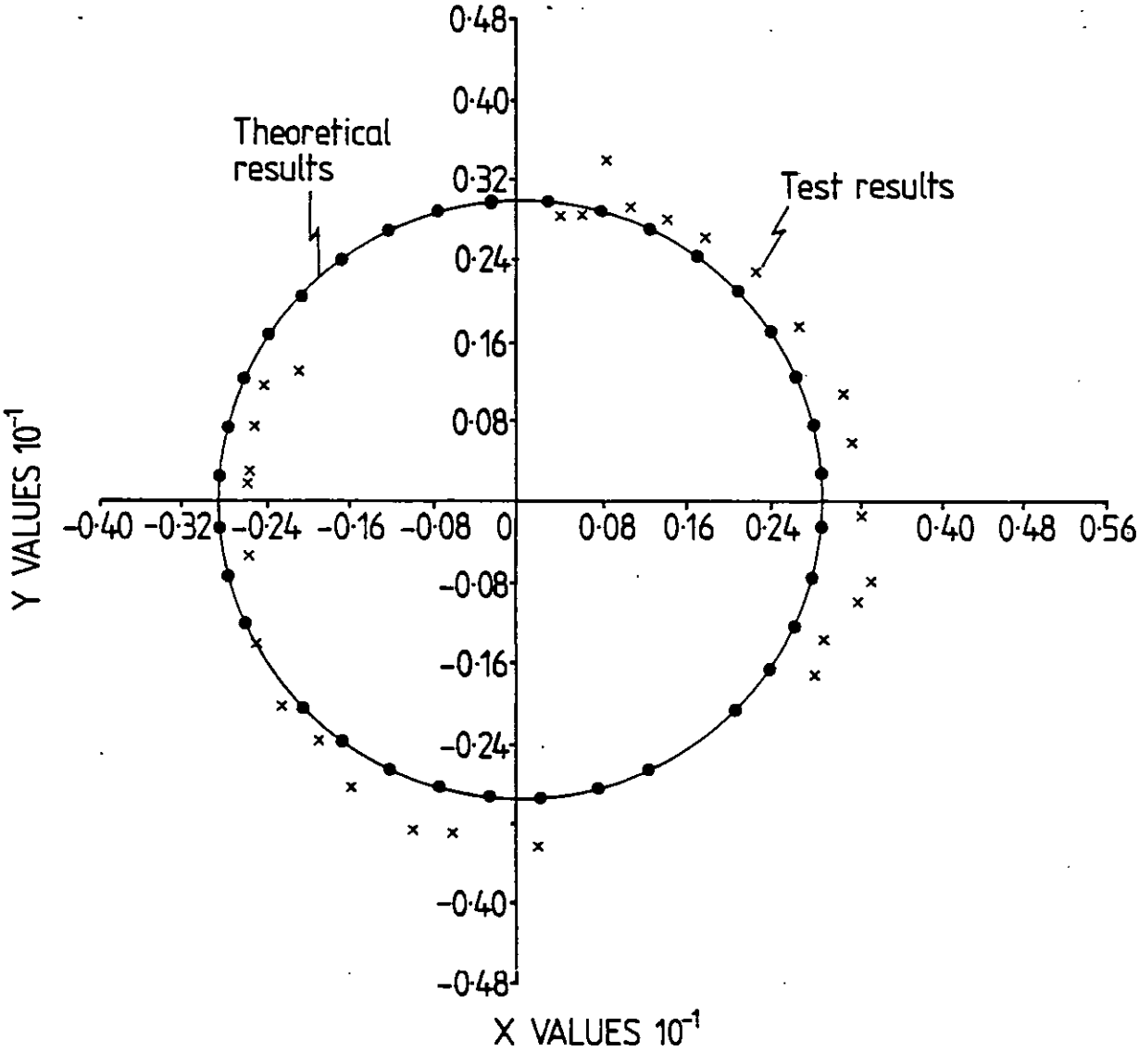

Fig 6.7: Comparison between theoretical and test results. f = 50 Hz, $\Delta\alpha$ = 8.4°. Balanced and undistorted a.c. voltages

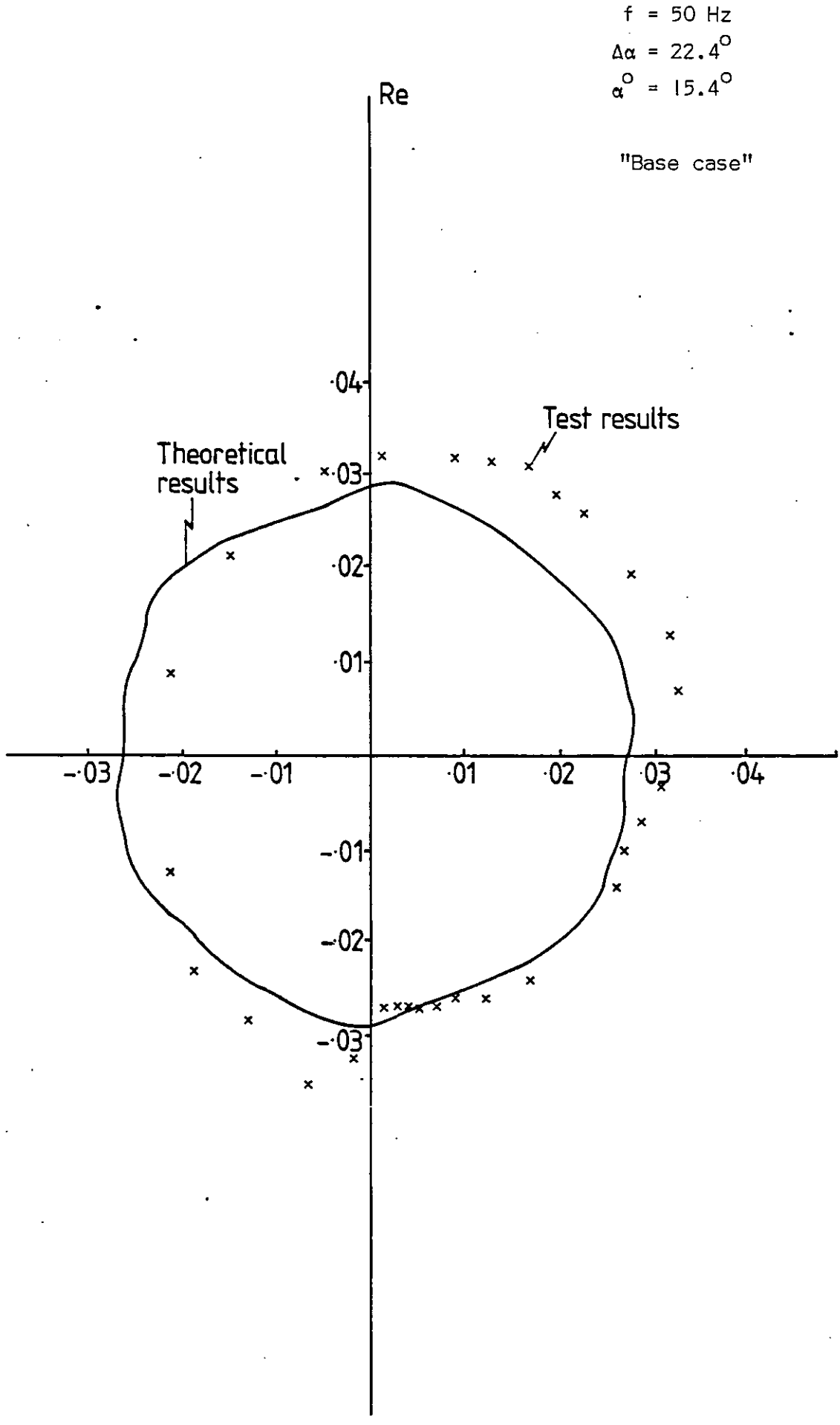

Fig 6.8: Comparison between theoretical and test results.
f = 50 Hz, Δα = 15.4°. Balanced and undistorted a.c. voltages

in the amplitude of the m.s. leads to a distortion in the theoretical and test d.f. curve.

Figs 6.9 and 6.10 refer to the 100 Hz m.s. In this case the results are sensitive to imbalance in the fundamental a.c. (assumed negligible in computed study), therefore the agreement between theoretical and test results is not as good as in the 50 Hz m.s. case. This inconsistency is illustrated in fig 6.9 where the first (1) and last (1') test points are not coincident.

Figs 6.11 and 6.12 refer to the 150 Hz m.s. case. The phase-shift between theoretical and test results is due to the d.c. current constant term experiencing a change with the phase of the m.s. This affects the commutation angle and therefore the amplitude and phase of the d.c. side harmonic of interest (150 Hz). As already mentioned (see section 6.2.3) the off-line program assumes d.c. current constant term as being fixed and allows for variations in the e.m.f. that simulates inverter behaviour.

The change of the constant term of d.c. current with the phase of the m.s. stems from the fact that for a particular phase angle all the interfiring periods are approximately identical. In this situation the d.c. current harmonic of interest is negligible, and therefore the d.f. is zero. The value of constant term of d.c. voltage attains its maximum value in this situation.

For another phase of the m.s. the 150 Hz d.c. current harmonic is maximum, and the interfiring periods of the even numbered valves are very different from those of the odd-

f = 100 Hz
"Base case"
α^{o} = 15.7°
$\Delta\alpha$ = 7.2°

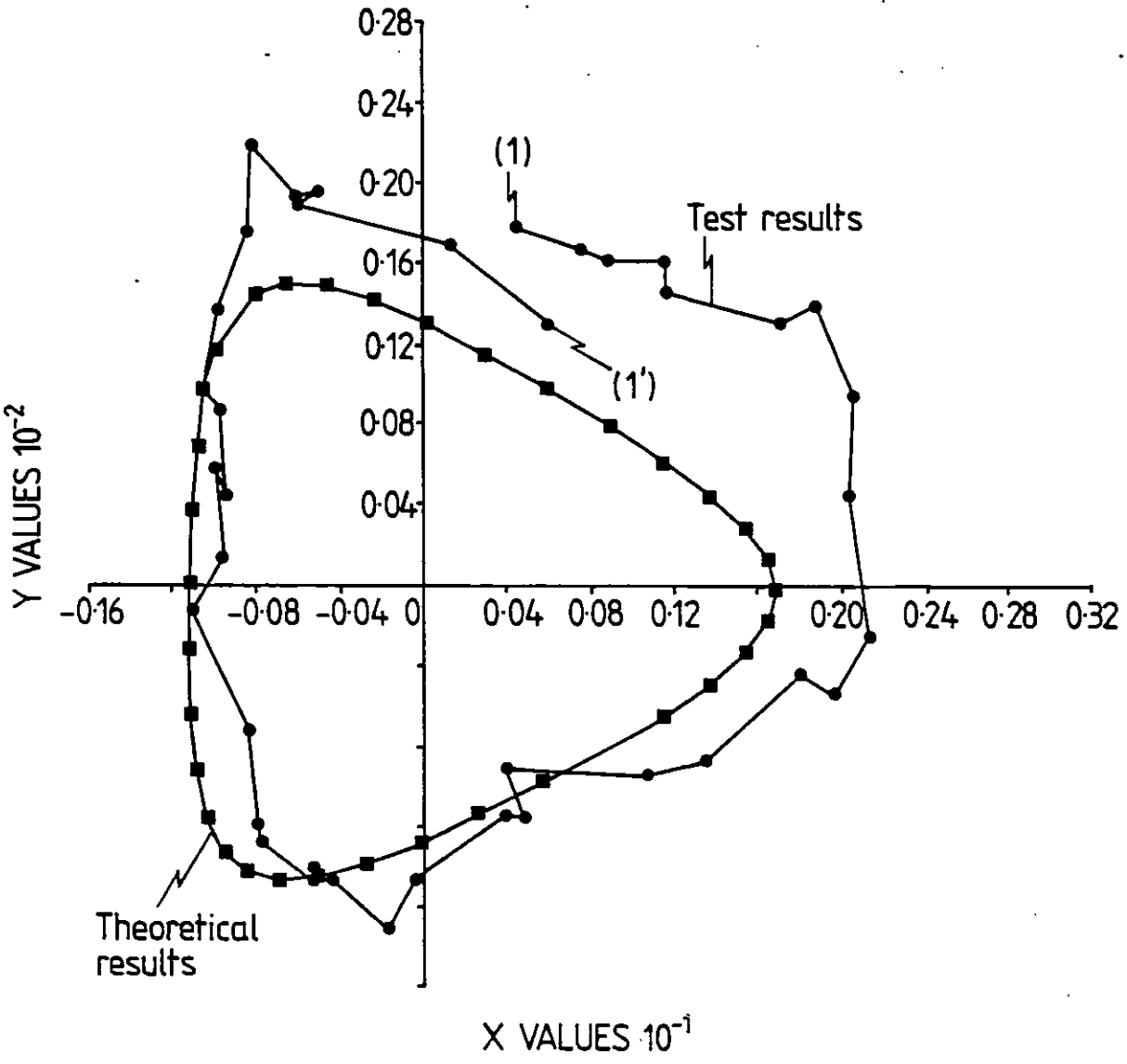

Fig 6.9: Comparison between theoretical and test results.
f = 100 Hz, $\Delta\alpha$ = 7.2°.

f = 100 Hz
"Base case"
α^{o} = 15.7°
$\Delta\alpha$ = 11.4°

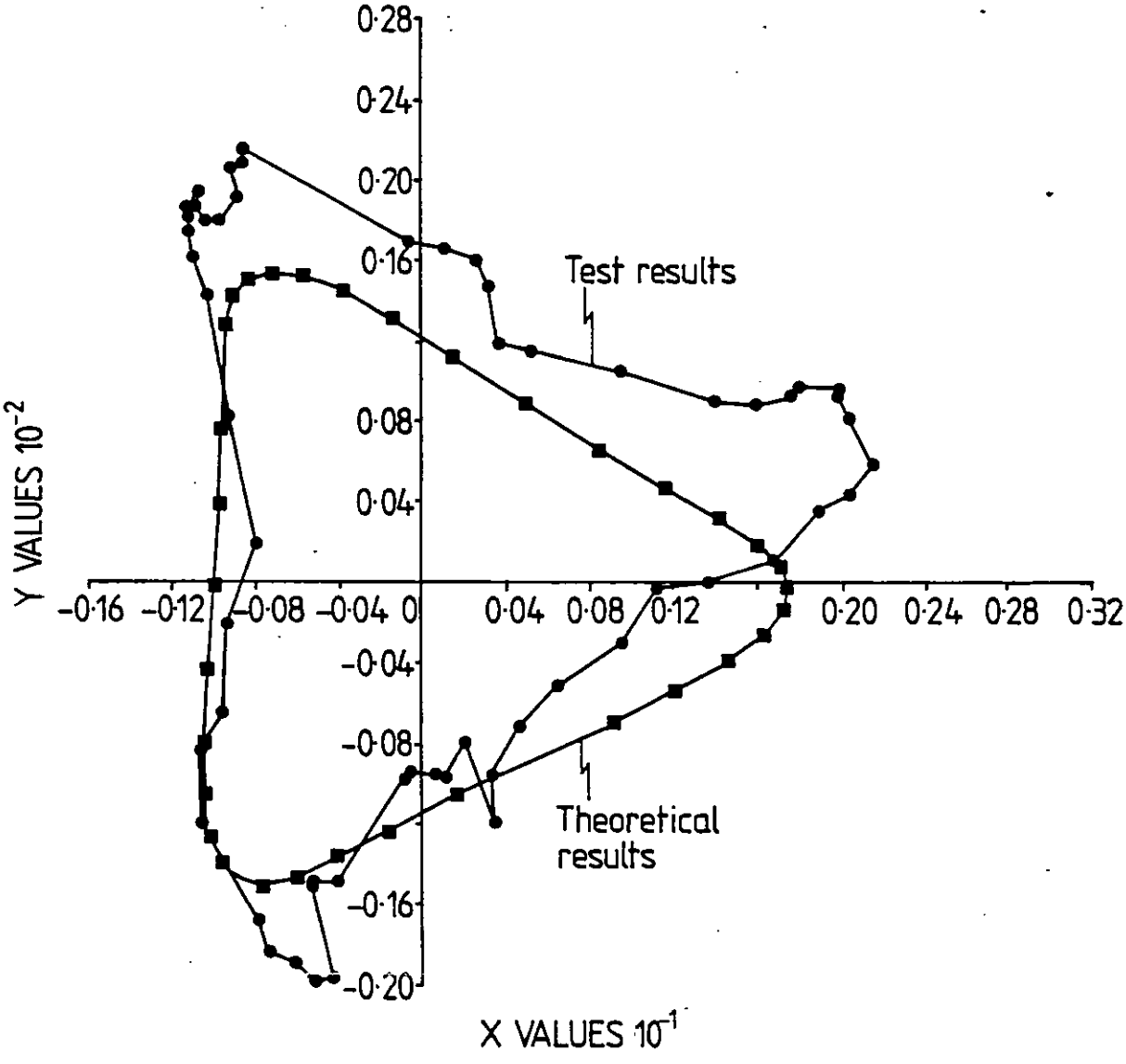

Fig 6.10: Comparison between theoretical and test results.
f = 100 Hz, $\Delta\alpha$ = 11.4°.

f = 150 Hz
α^{o} = 15.2°
$\Delta\alpha$ = 6.4°
"Base case"

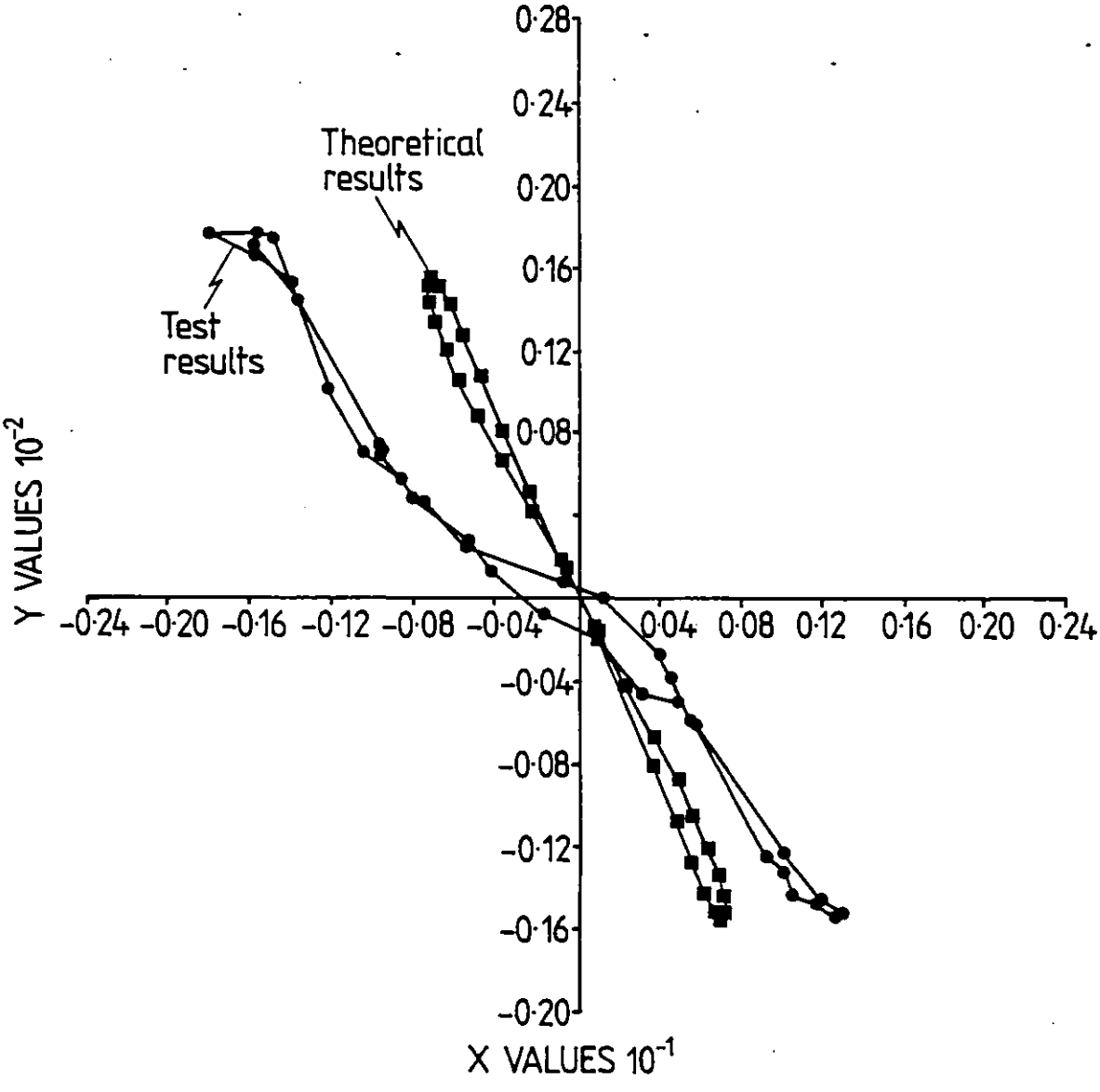

Fig 6.11: Comparison between theoretical and test results.
f = 150 Hz, $\Delta\alpha$ = 6.4°.

f = 150 Hz
α^{o} = 15.2°
$\Delta\alpha$ = 14.8°

"Base case"

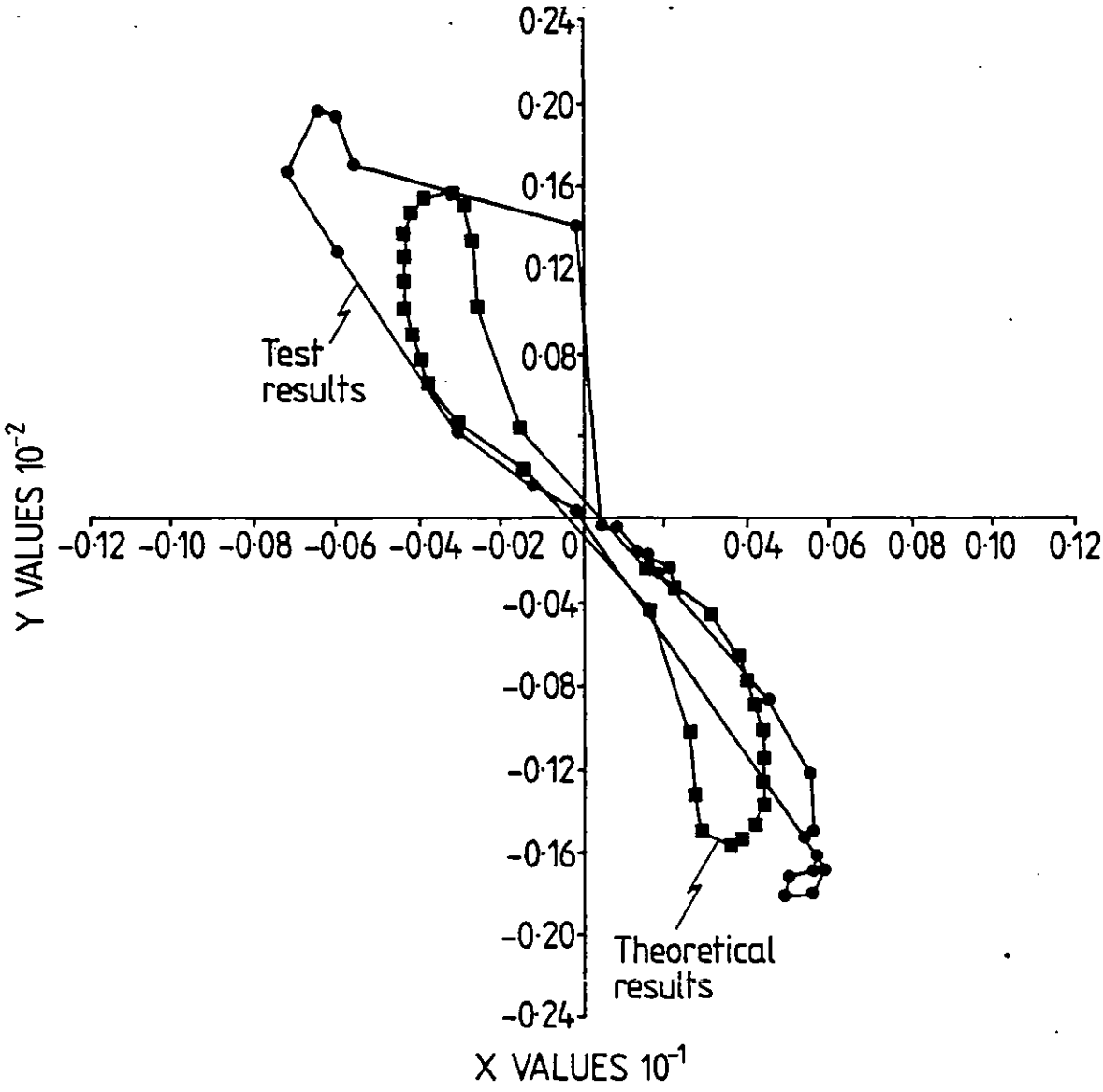

Fig 6.12: Comparison between theoretical and test results.
f = 150 Hz, $\Delta\alpha$ = 14.8°.

numbered valves. Therefore the d.c. voltage constant term and as a consequence the current diminish.

As mentioned earlier, the variation of d.c. current constant term with the phase of the m.s. is more pronounced for the 150 Hz case.

6.3.1.2 Unbalanced transformer reactances

A comparison between theoretical and test results with unbalanced transformer reactances was also carried out. A reduction in the commutating reactance of phase R resulting in a 15.6% imbalance was implemented.

Figs 6.13 and 6.14 refer to a 50 Hz m.s. In fig 6.13 two test results carried out on different days are shown. The effect of commutating reactance imbalance in the 50 Hz d.f. is negligible and this agrees with the theoretical prediction.

Fig 6.15 shows the influence of an a.c. fundamental voltage imbalance on the d.f. plot for a 100 Hz m.s.

Figs 6.16, 6.17 and 6.18 show the comparisons between theoretical and test results for a 100 Hz m.s.

Figs 6.16 and 6.17 correspond to the same amplitude of the m.s. but were obtained on different days. Unlike the 50 Hz m.s. case, differences in the two plots are noticeable. This is due to the fact that the 100 Hz frequency m.s. is greatly affected by any imbalance in the fundamental a.c. voltage. The phase shift between the theoretical and test results may be caused by imbalances not taken into account in the theoretical calculations.

Figs 6.19 and 6.20 refer to the 150 Hz frequency m.s. The results are similar to the ones obtained for the unbalanced case. Again the theoretical prediction that

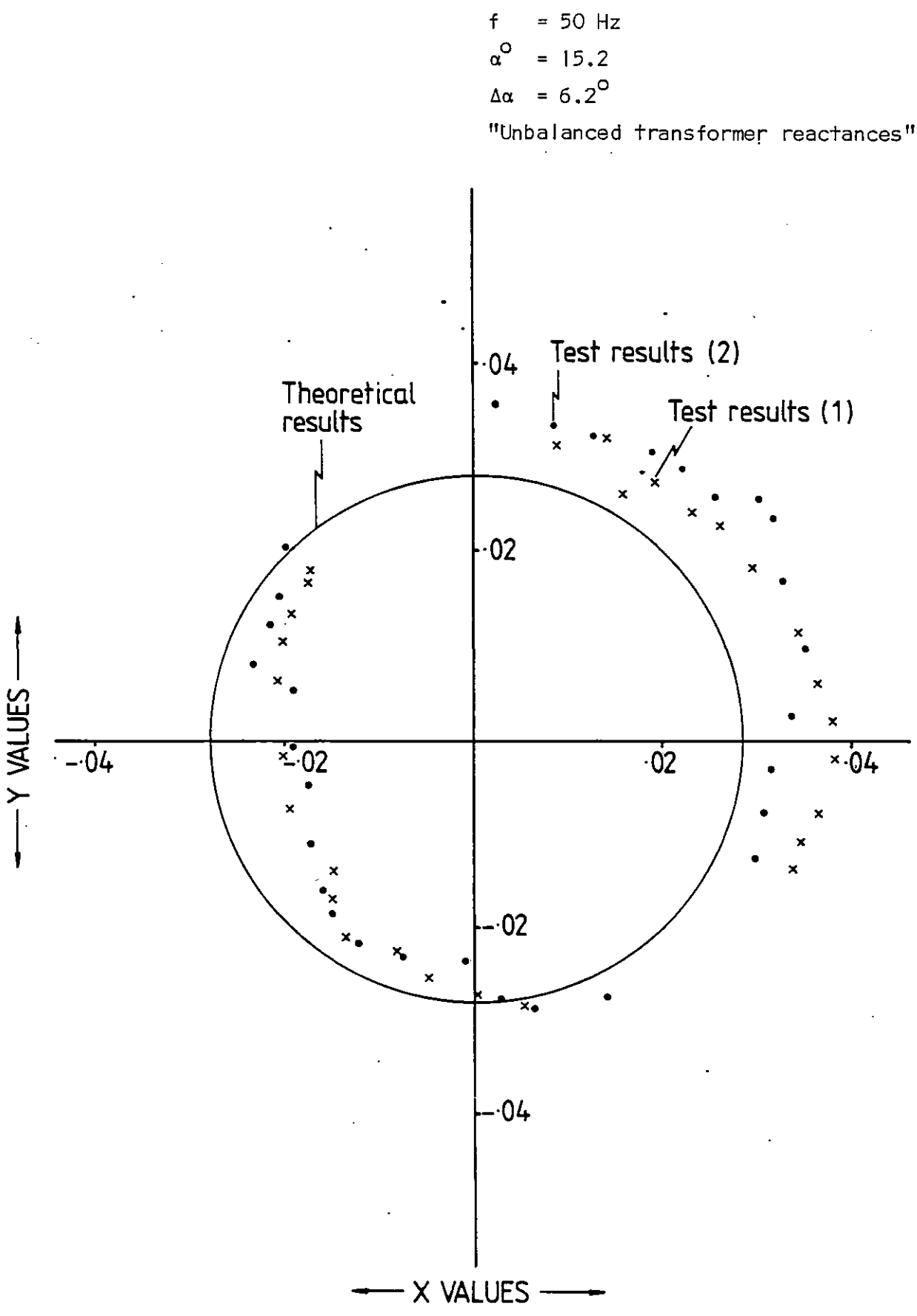

Fig 6.13: Comparison between theoretical and test results. f = 50 Hz, α° = 15.2, $\Delta\alpha$ = 6.2°. Unbalanced transformer reactances

f = 50 Hz

α^{o} = 15.2

$\Delta\alpha$ = 14.6

"Unbalanced transformer reactances"

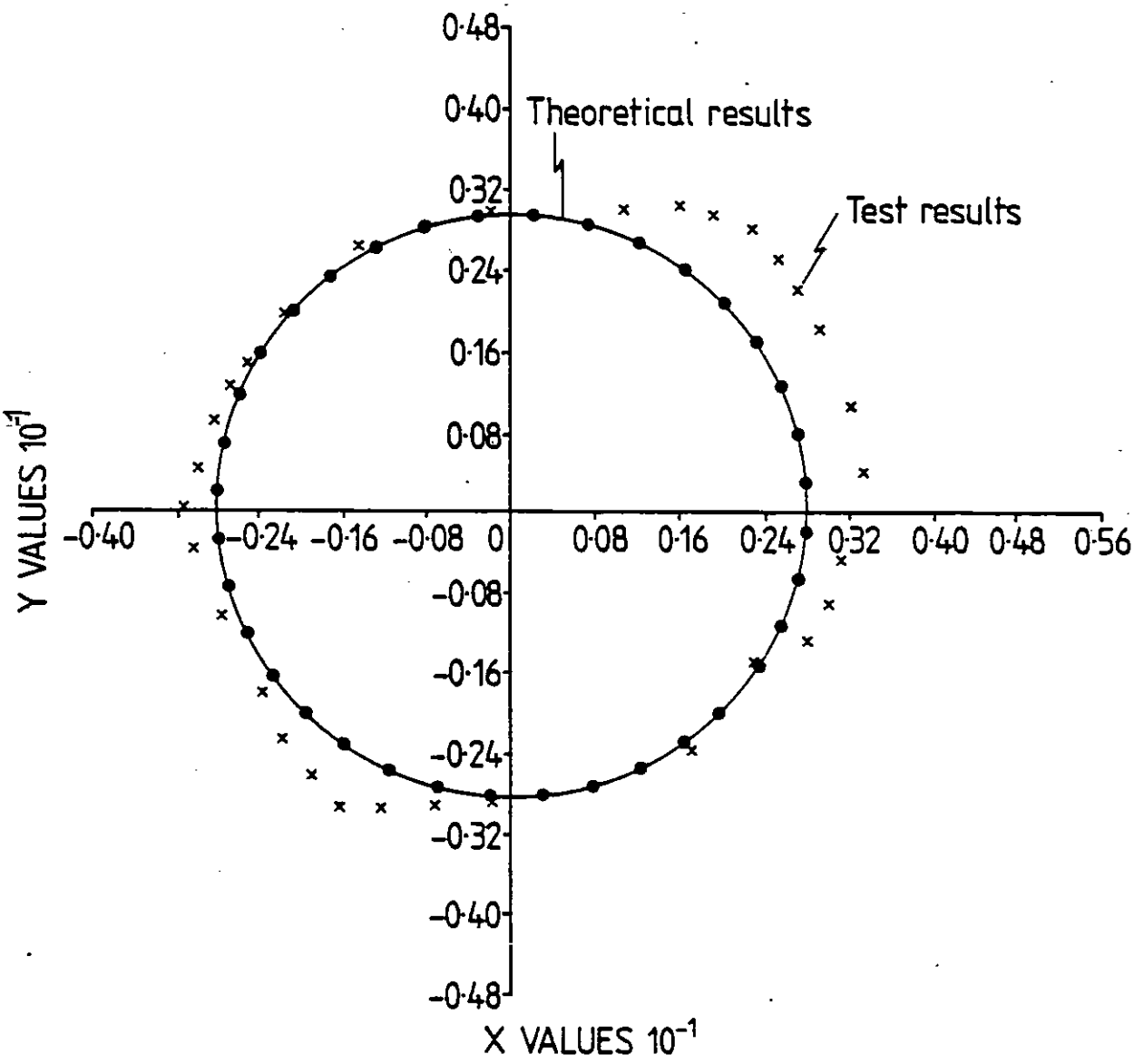

Fig 6.14: Comparison between theoretical and test results. f = 50 Hz, α^{o} = 15.2, $\Delta\alpha$ = 14.6. Unbalanced transformer reactances

f = 100 Hz
α^{o} = 15.2^{o}
$\Delta\alpha$ = 11.4^{o}
"Theoretical studies"

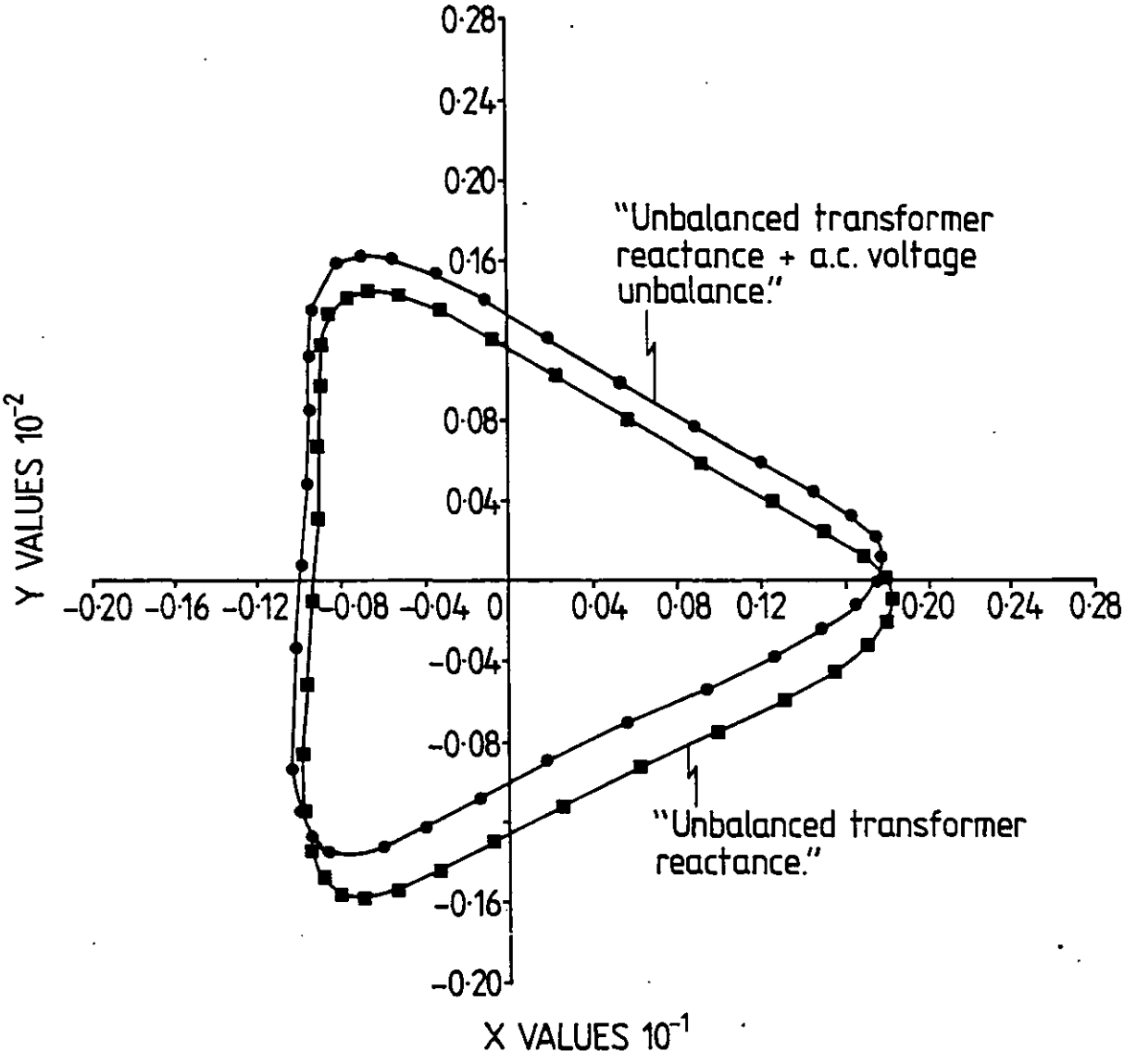

Fig 6.15: Influence of a further imbalance in the d.f. locus. 2% a.c. voltage imbalance

f = 100 Hz
α^{o} = 15.2^{o}
$\Delta\alpha$ = 6.4^{o}
"Unbalanced transformer reactances"

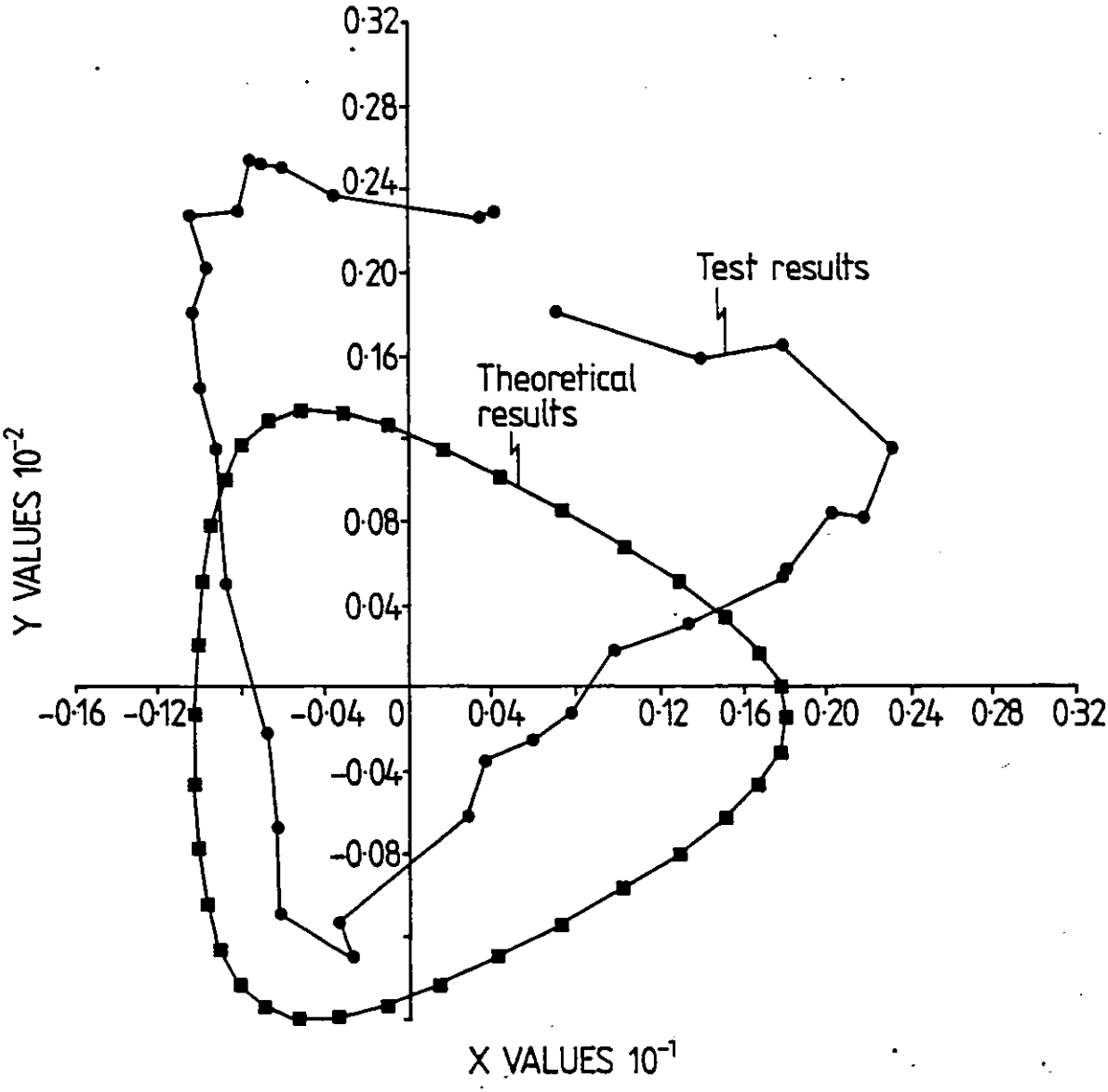

Fig 6.16: Comparison between theoretical and test results. f = 100 Hz, α^{o} = 15.2, $\Delta\alpha$ = 6.4. Unbalanced transformer reactances

f = 100 Hz
α^{o} = 15.2^{o}
$\Delta\alpha$ = 6.4^{o}

"Unbalanced transformer reactances"

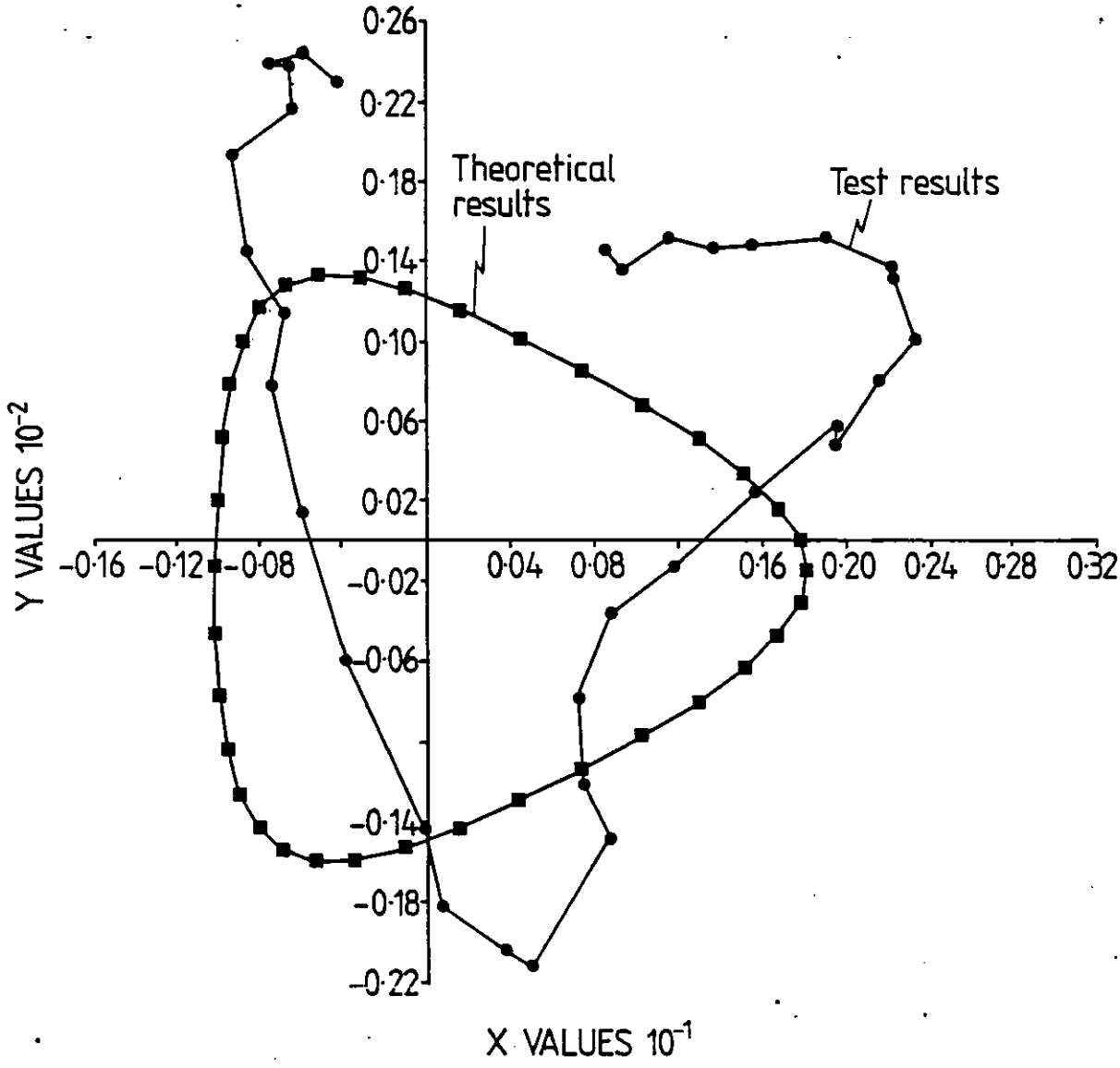

Fig 6.17: Comparison between theoretical and test results. f = 100 Hz, α^{o} = 15.2^{o}, $\Delta\alpha$ = 6.4^{o}. Unbalanced transformer reactances

f = 100 Hz
α^{o} = 15.2
$\Delta\alpha$ = 11.4

"Unbalanced transformer reactances"

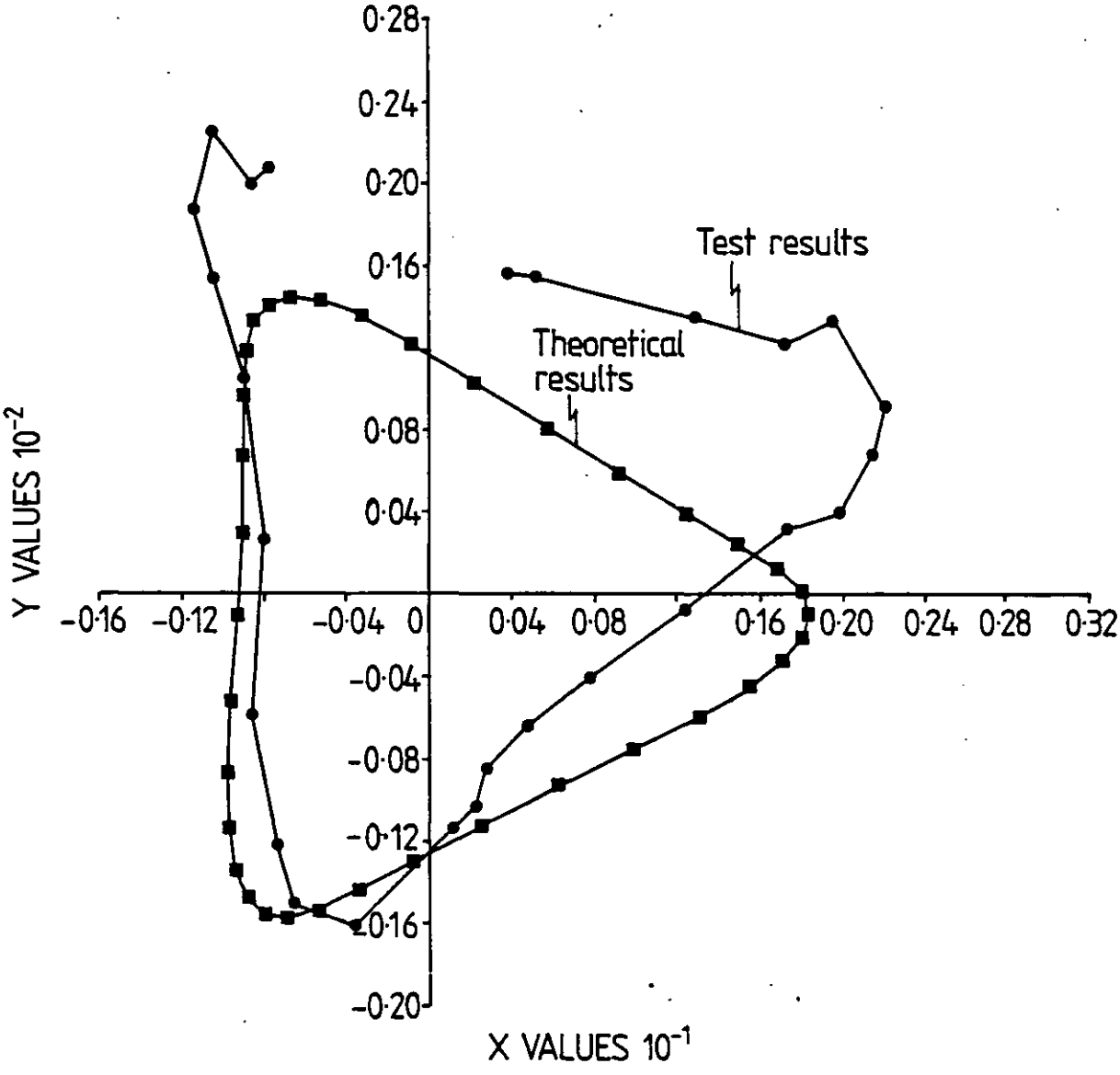

Fig 6.18: Comparison between theoretical and test results. f = 100 Hz, α^{o} = 15.2, $\Delta\alpha$ = 11.4. Unbalanced transformer reactances

f = 150 Hz

α^{o} = 15.2

$\Delta\alpha$ = 6.4

"Unbalanced transformer reactances"

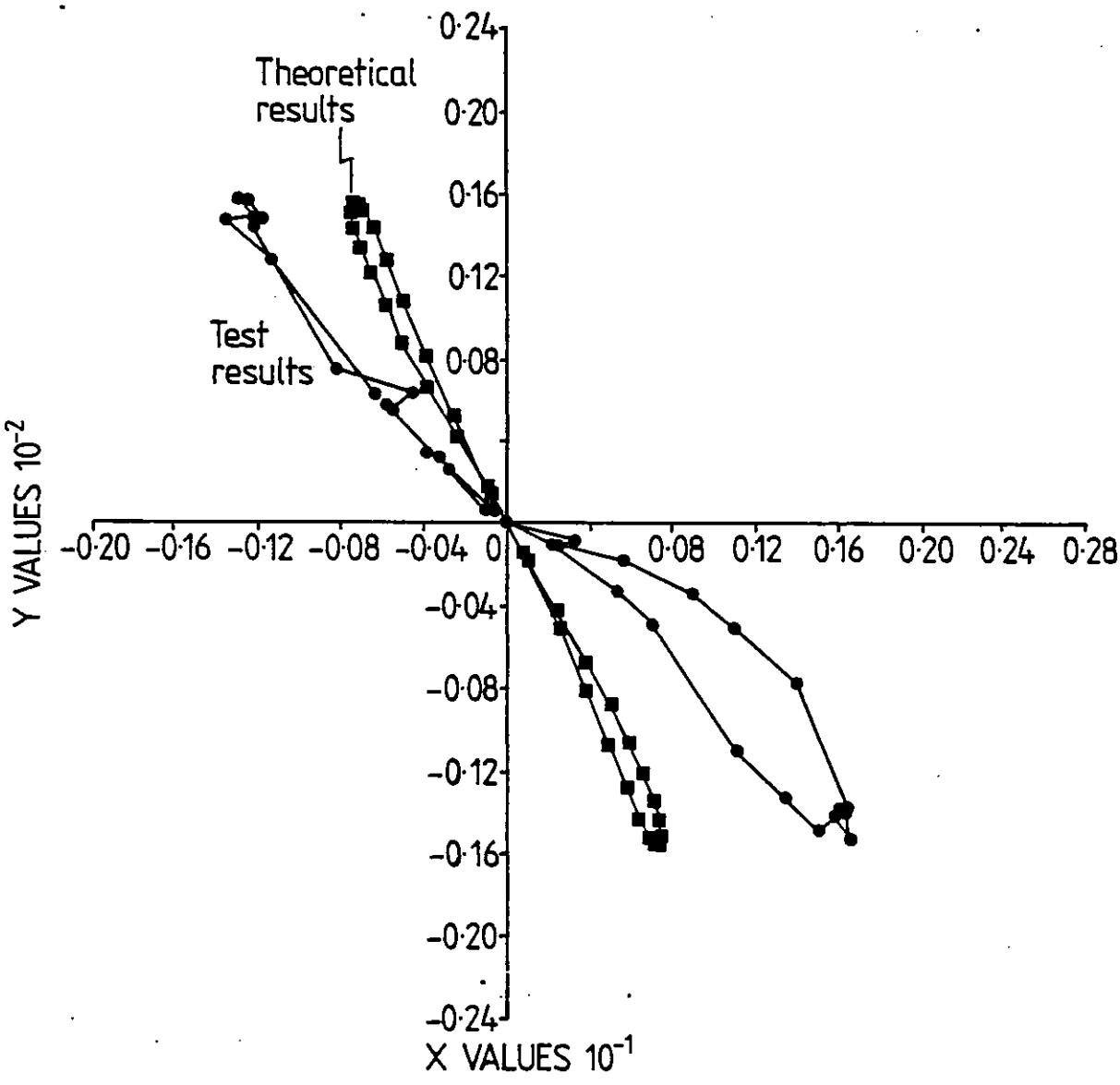

Fig 6.19: Comparison between theoretical and test results.
f = 150 Hz, α^{o} = 15.2°, $\Delta\alpha$ = 6.4°

f = 150 Hz
α^{o} = 15.2^{o}
$\Delta\alpha$ = 12.6^{o}

"Unbalanced transformer reactances"

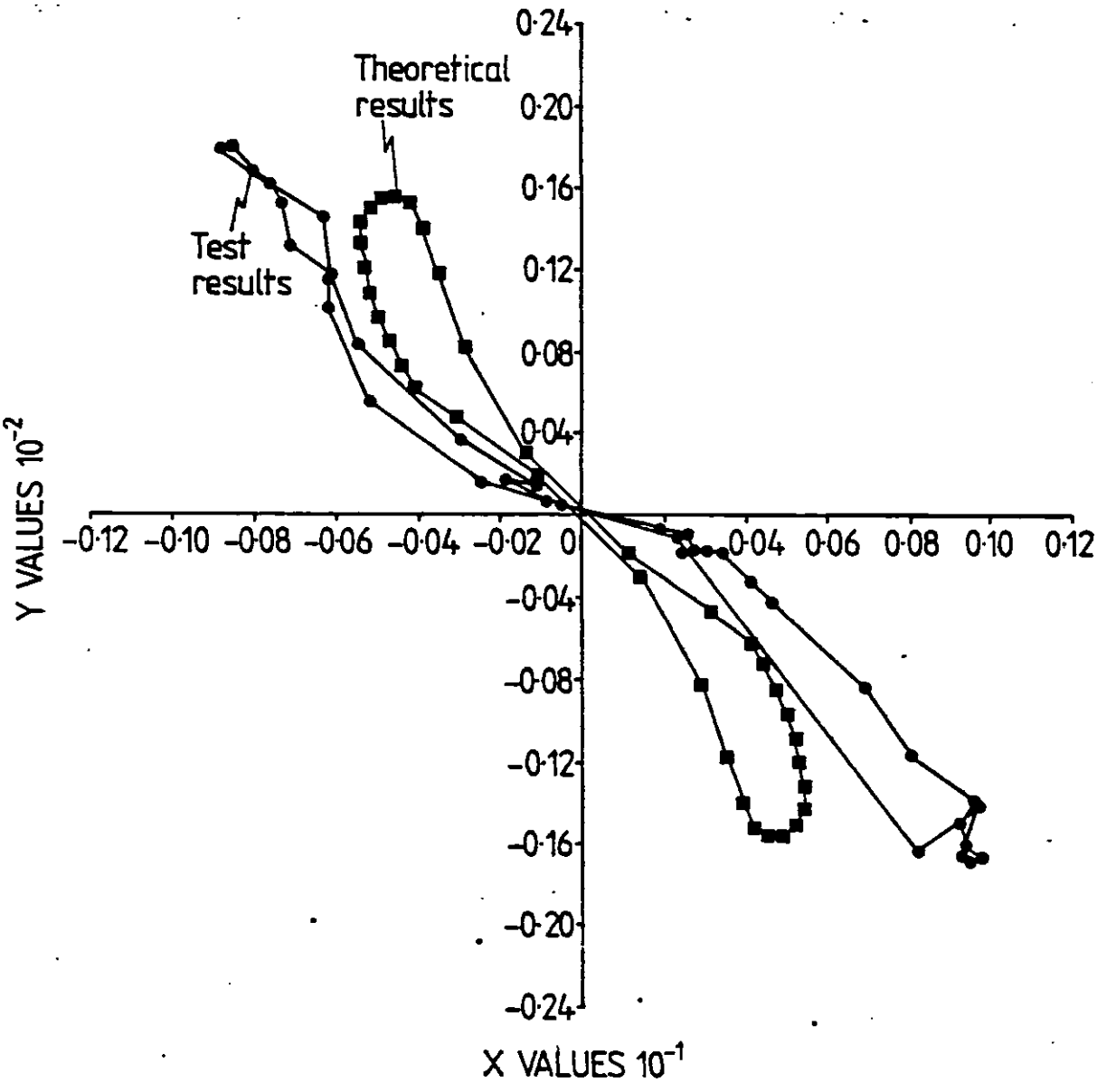

Fig 6.20: Comparison between theoretical and test results. f = 150 Hz, α^{o} = 15.2, $\Delta\alpha$ = 12.6^{o}. Unbalanced transformer reactances

imbalances either in the commutating reactances or in the a.c. fundamental voltage do not affect the d.f. for a 150 Hz frequency m.s. has been confirmed.

6.3.2 Finite short circuit ratio

Tests were conducted to obtain d.f.'s for low s.c.r.'s. No imbalances and/or distortions apart from those inherent to the commutating reactances were considered in the theoretical studies. Figs 6.21 and 6.22 refer to a 50 Hz m.s. frequency. As in the infinite s.c.r. case the theoretical and test d.f.'s are in good agreement but there are discrepancies in the size of the locus.

Figs 6.23 and 6.24 were determined for a 150 Hz m.s. The theoretical and test results show the same trends as for infinite s.c.r. Again the phase-shift between theoretical and test results is due to the d.c. current 'constant' term change with phase of the m.s.

For both 50 Hz and 150 Hz frequency modulating signals the theoretical and test results are in reasonable agreement. However, this is not the case for the 100 Hz m.s. In this case any imbalance in the source impedance or in the fundamental a.c. voltage affects decisively the d.f. plot. Such imbalances had therefore to be considered when obtaining the theoretical results. To assess the sensitivity of the d.f. plot to imbalance in the fundamental term of the a.c. voltage some theoretical studies were carried out.

In fig 6.25 the effect of a change in phase of the fundamental of the a.c. voltage is shown. The d.f. plot

Fig 6.21: Comparison between theoretical and test results.
f = 50 Hz, α^{o} = 15.2^{o}, $\Delta\alpha$ = 8.4^{o}. s.c.r. = 3

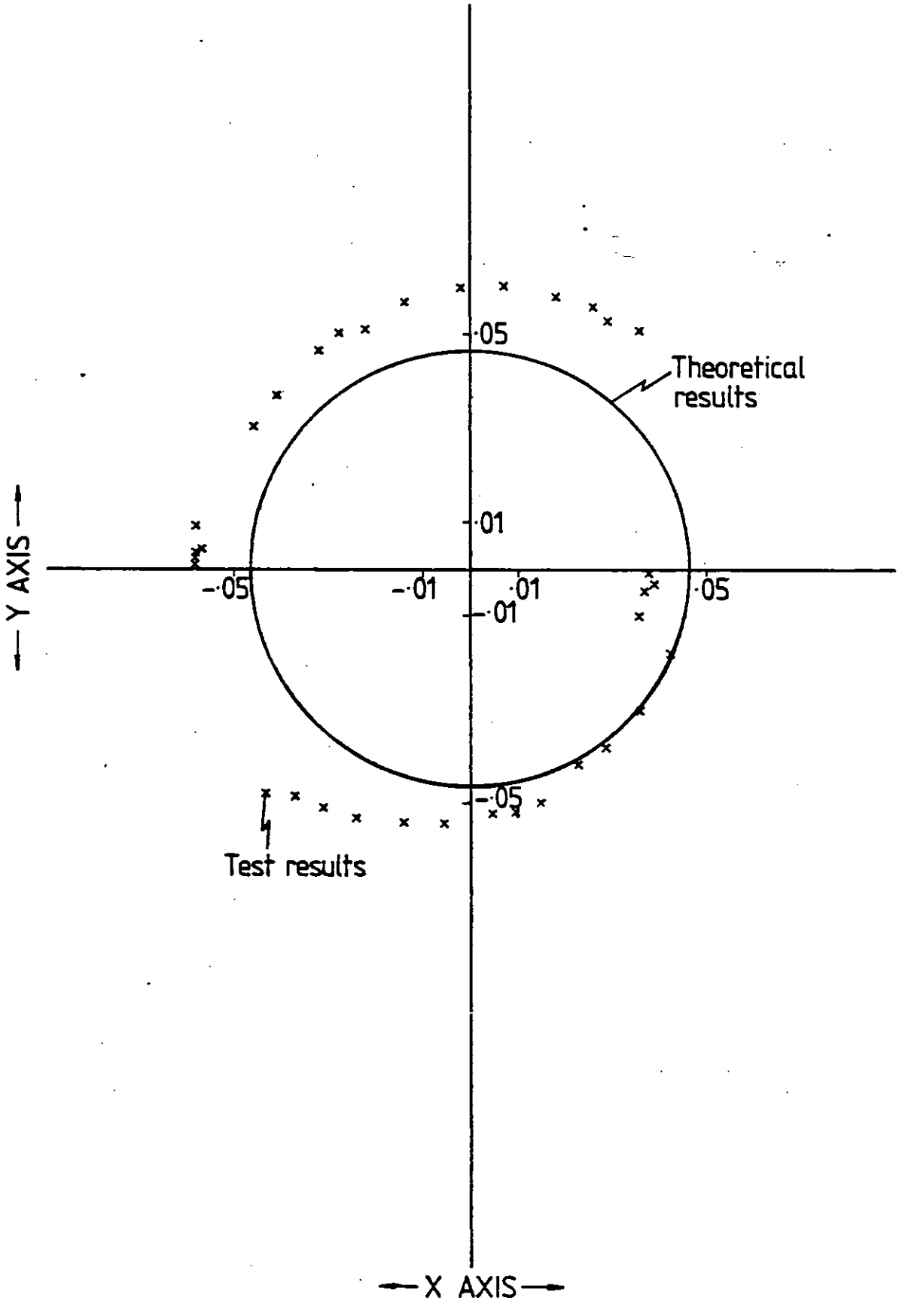

Fig 6.22: Comparison between theoretical and test results.
f = 50 Hz, α^{o} = 15.2°, $\Delta\alpha$ = 14.8°. s.c.r. = 3

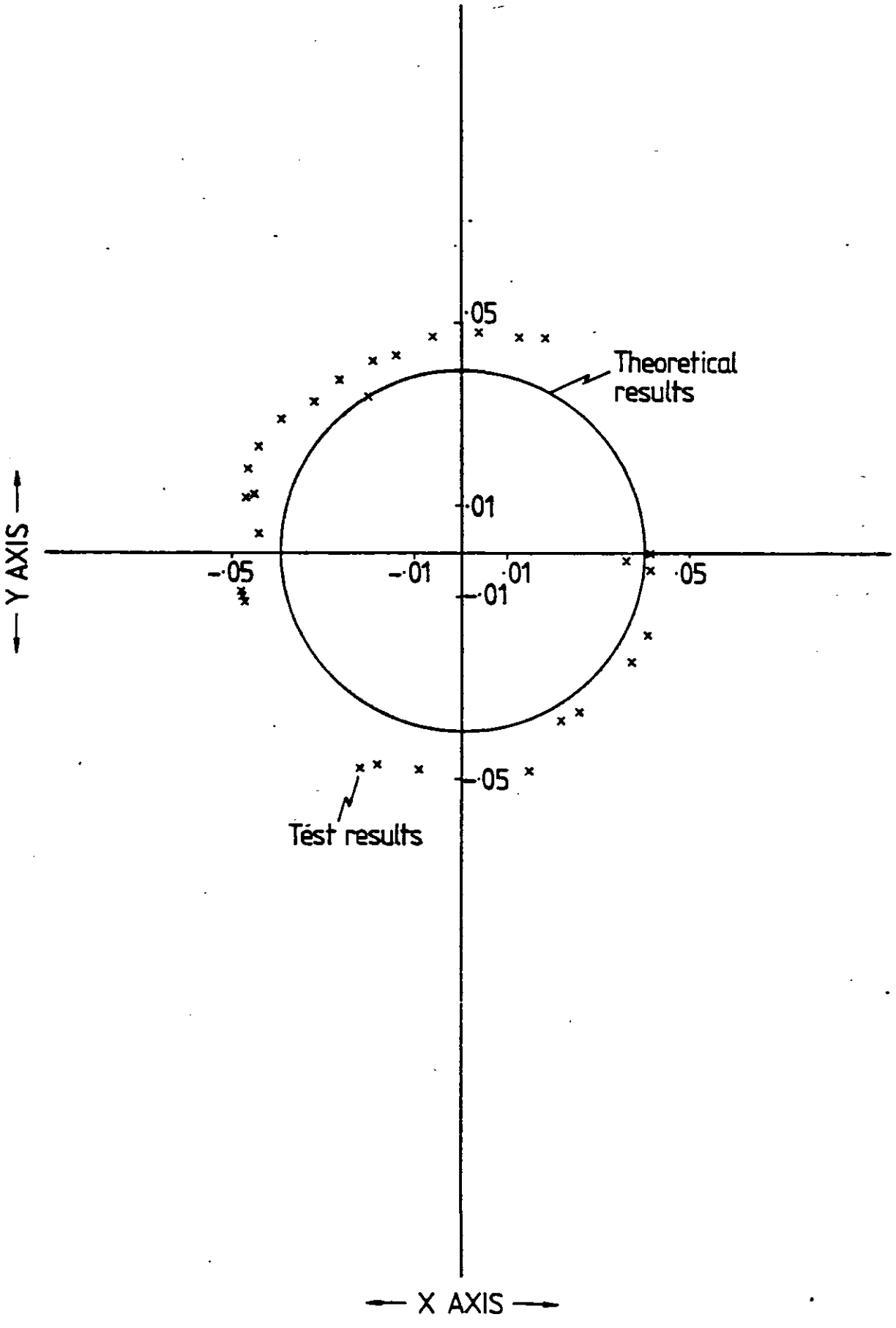

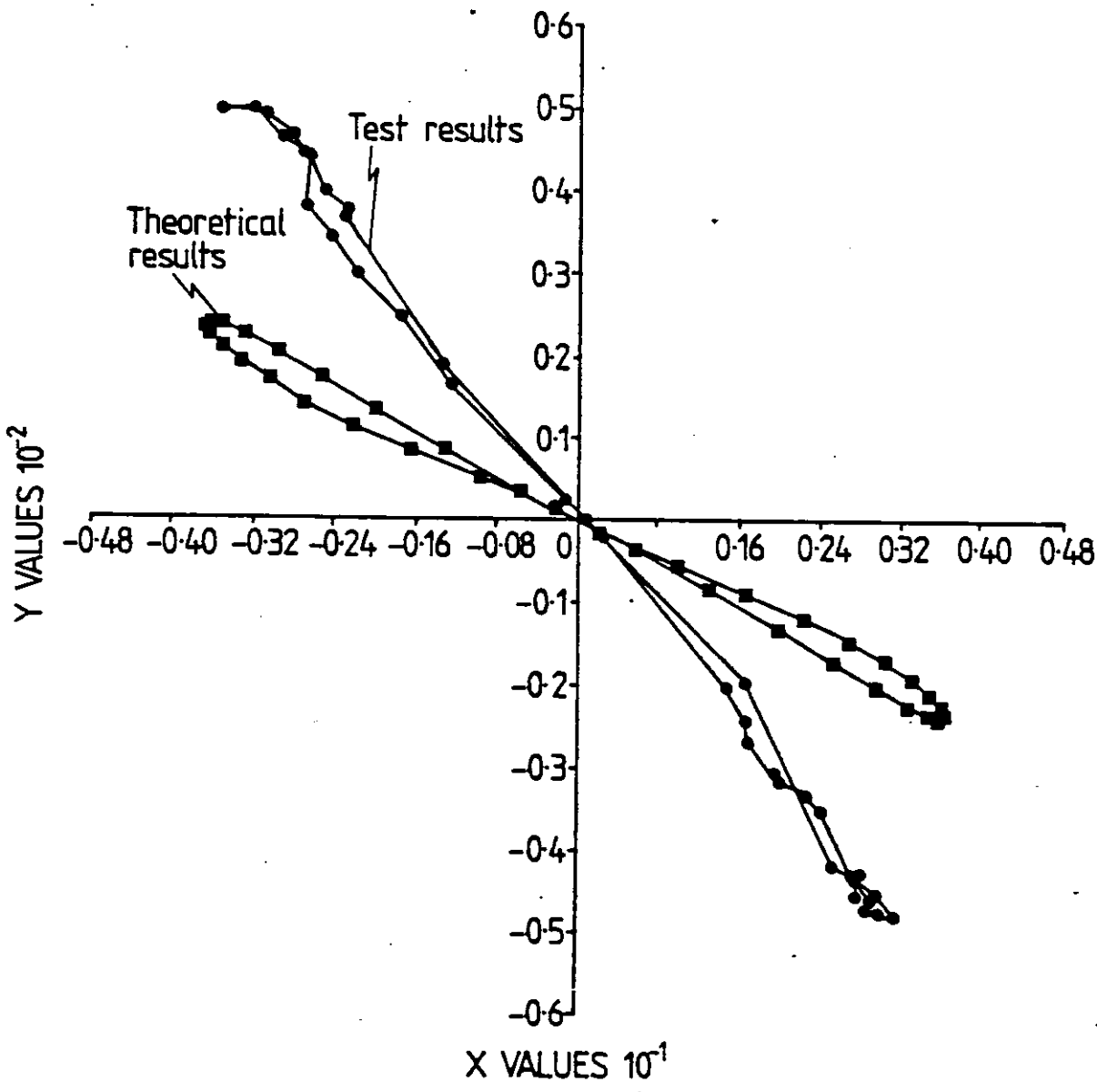

Fig 6.23: Comparison between theoretical and test results.
f = 150 Hz, α^{o} = 15.7°, $\Delta\alpha$ = 6.4°. s.c.r. = 3

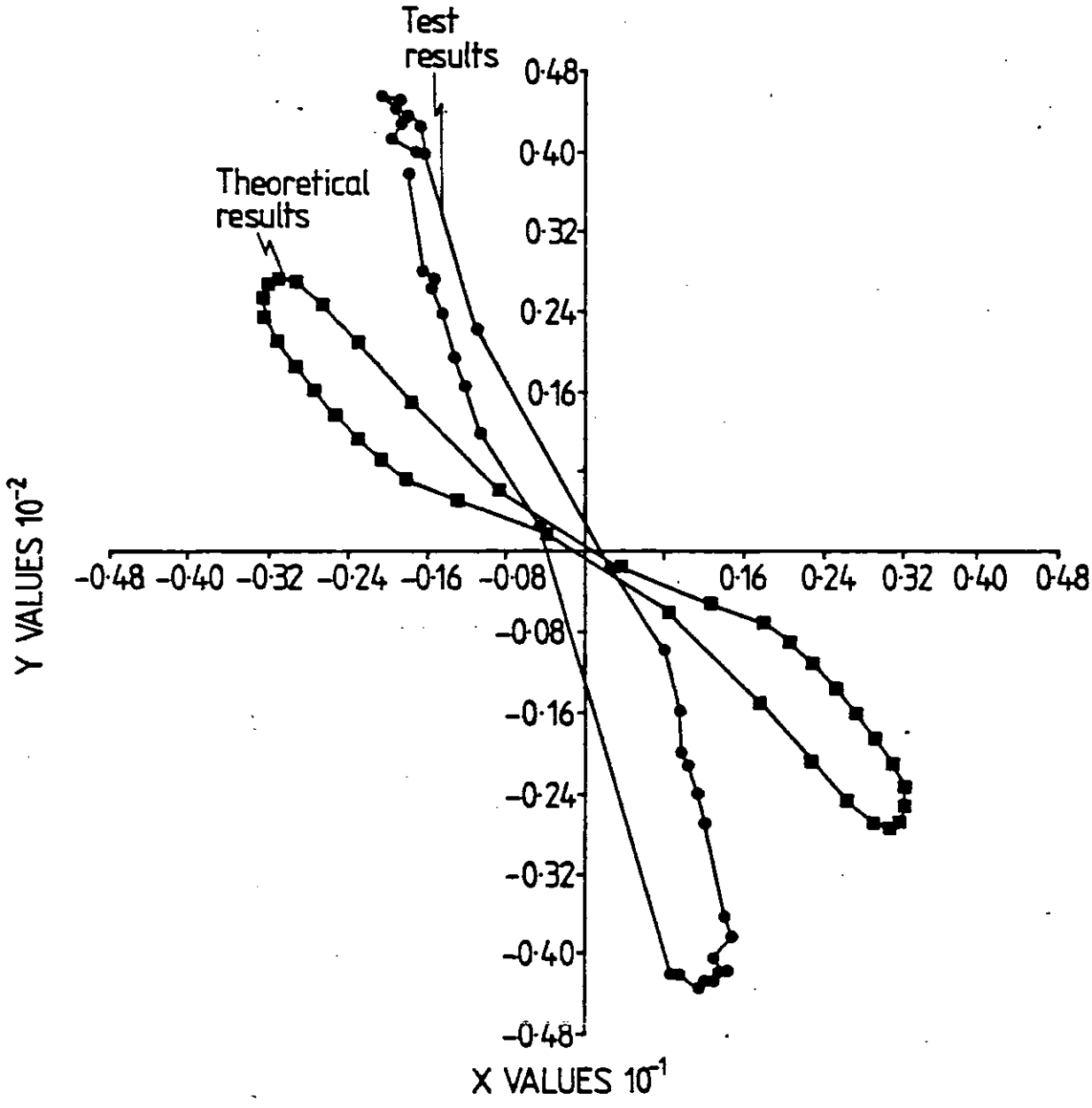

Fig 6.24: Comparison between theoretical and test results.
f = 150 Hz, α^{o} = 15.7°, $\Delta\alpha$ = 12.8°. s.c.r. = 3

shifts to the left and upward.

In fig 6.26 the effect of a change in phase and amplitude of the fundamental of the a.c. voltage is shown. Comparison of curve 2, fig 6.25 with curve 2 of fig 6.26 shows that changing the imbalance from one a.c. phase to another shifts the d.f. plot upwards. In both cases the negative sequence of the fundamental of the a.c. voltage is identical.

Fig 6.27 and fig 6.28 compare the theoretical and test results for a s.c.r. of 6 and 3 respectively. In both cases the test d.f. is larger than the theoretical curve. However the theoretical results do correctly predict the shift in the d.f. with varying short-circuit ratio.

6.4 Experimental confirmation of limit-cycle prediction

In order to assess the ability of the off-line computer program to predict limit cycle oscillations, a set of tests was carried out with both high and low short circuit ratios.

The a.c. voltage and the control voltage harmonic distortion was monitored using a spectrum analyser, these measurements used later as input data for the off-line computer program.

The linear part of the control loop incorporating controlled converters comprises two blocks in fig 6.29, namely the error processing unit (e.p.u.) and the Hall effect device plus amplifier. The block N.L. stands for non-linearity and comprises the d.c. converter system plus d.c. line.

Denoting by $G_1(j\omega)$ the transfer function of the error processing unit and by $H(j\omega)$ the transfer function of the

1 $U_R = 117\ e^{j0}$; $U_y = 123\ e^{j234.9}$; $U_B = 117\ e^{j118.4}$

2 $U_R = 117\ e^{j0}$; $U_y = 123\ e^{j240}$; $U_B = 117\ e^{j120}$

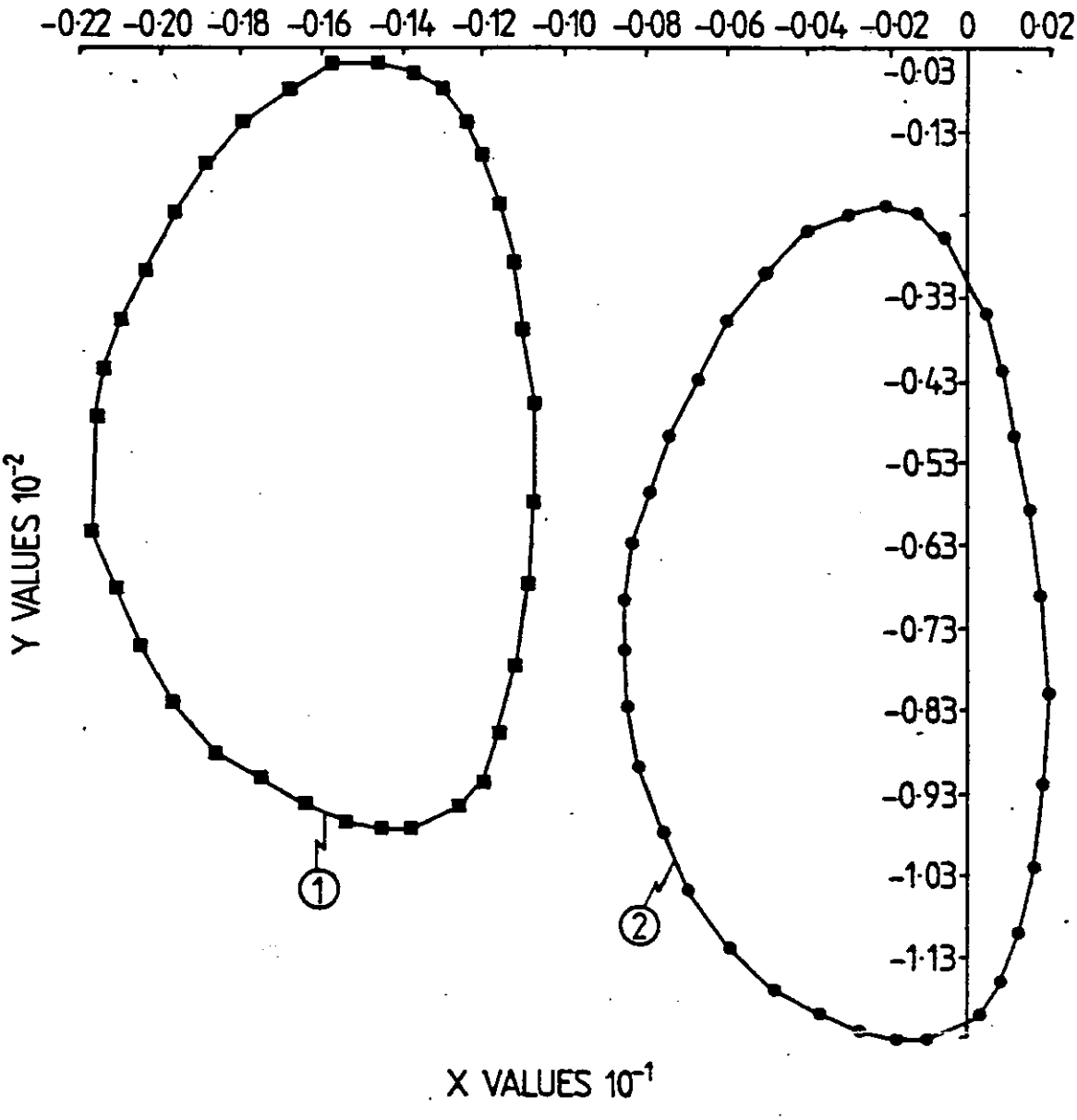

Fig 6.25: Effect of change in phase of the fundamental of the a.c. voltage in the D.F. plot for a 100 Hz m.s.

1 $U_R = 117\ e^{jo}$; $U_y = 123\ e^{j234.9}$; $U_B = 117\ e^{j118.4}$

2 $U_R = 123\ e^{jo}$; $U_y = 117\ e^{j240}$; $U_B = 123\ e^{j120}$

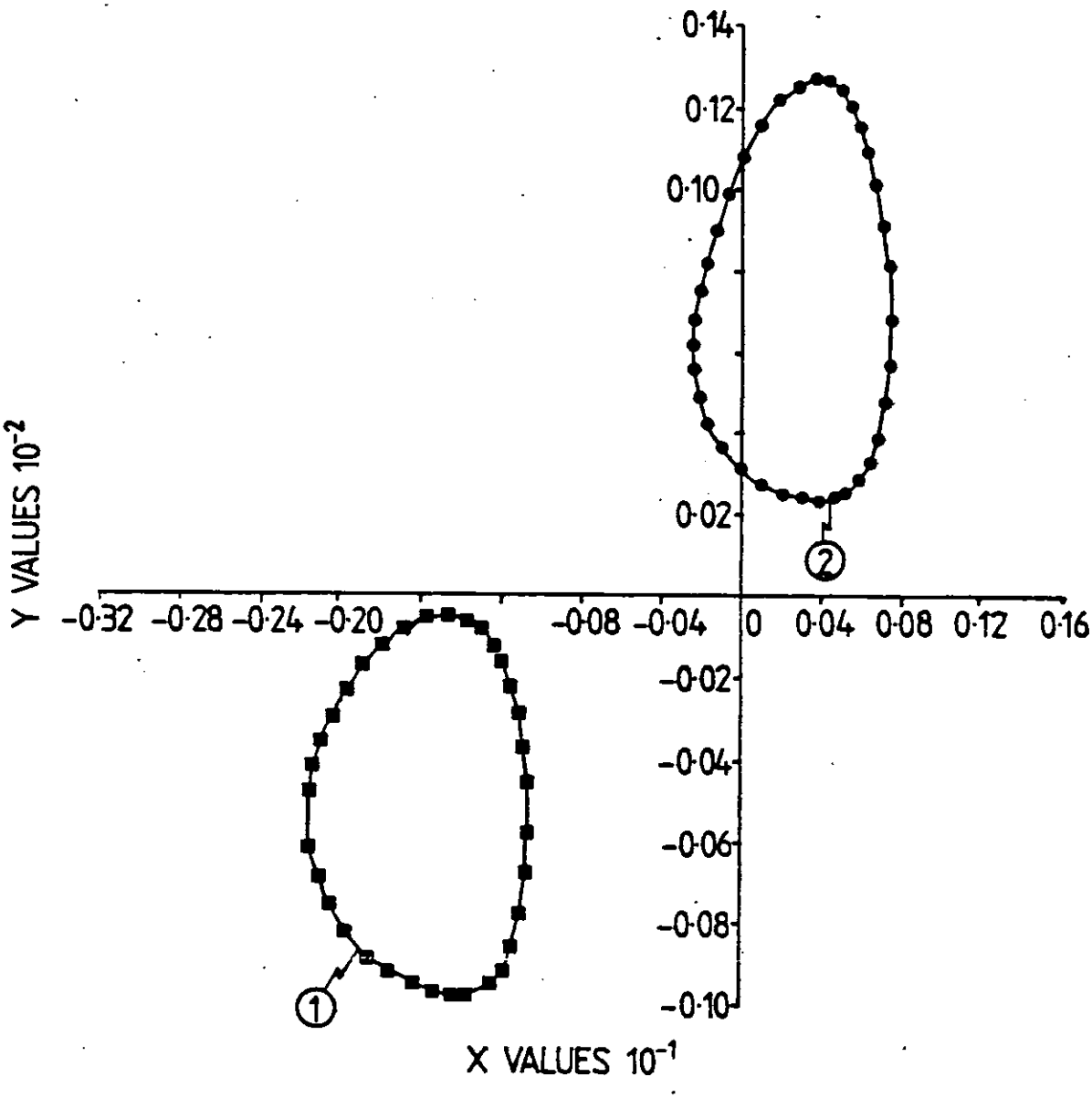

Fig 6.26: Effect of a change in phase and amplitude of the fundamental of the a.c. voltage in the d.f. plot for a 100 Hz m.s.

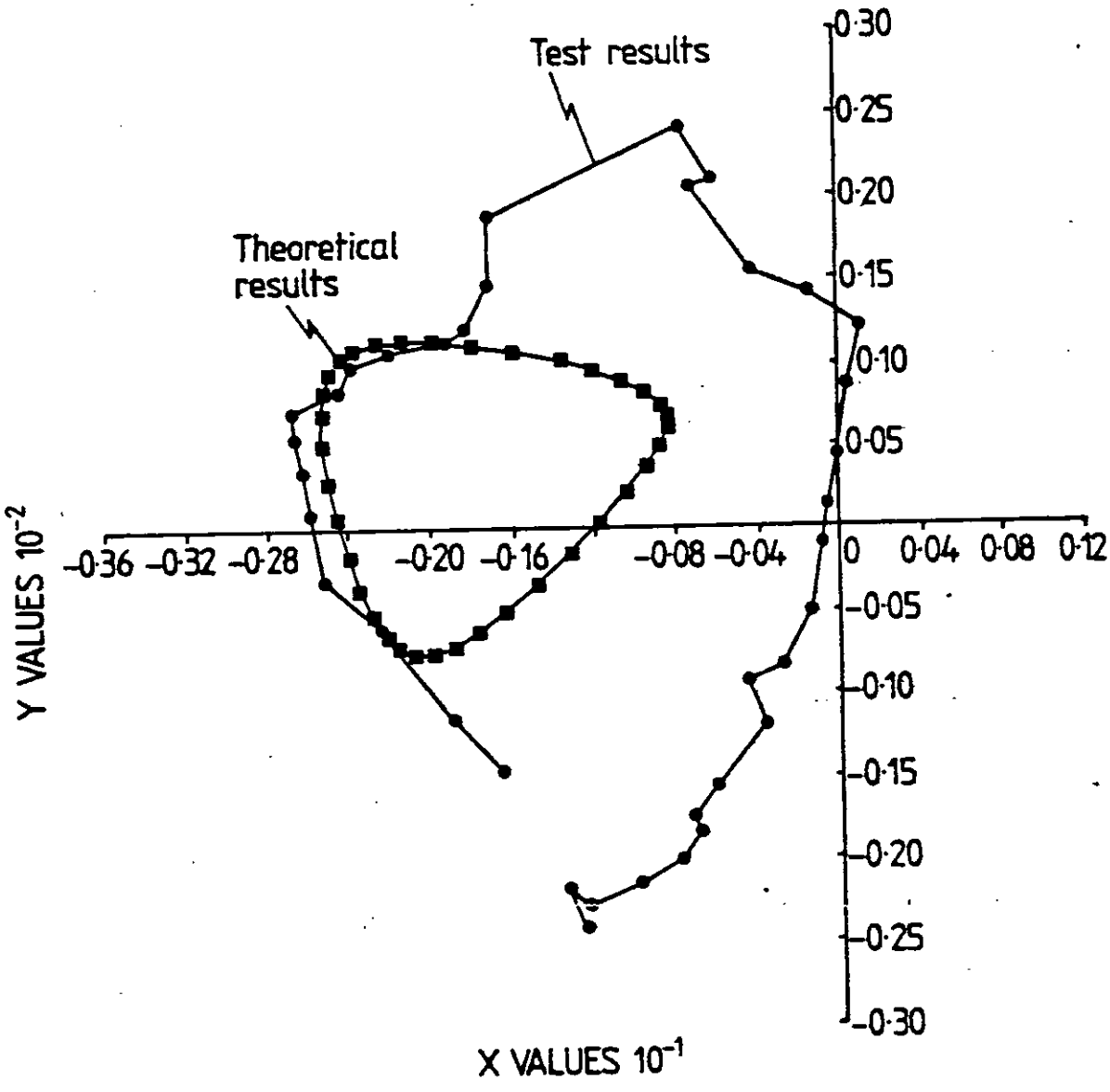

Fig 6.27: Comparison between theoretical and test results.
f = 100 Hz, α^{o} = 15.2, $\Delta\alpha$ = 8.8^{o}, s.c.r. = 6. Base case.

Fig 6.28: Comparison between theoretical and test results.
f = 100 Hz, α^{o} = 15.2, $\Delta\alpha$ = 8.8^{o}. s.c.r. = 3

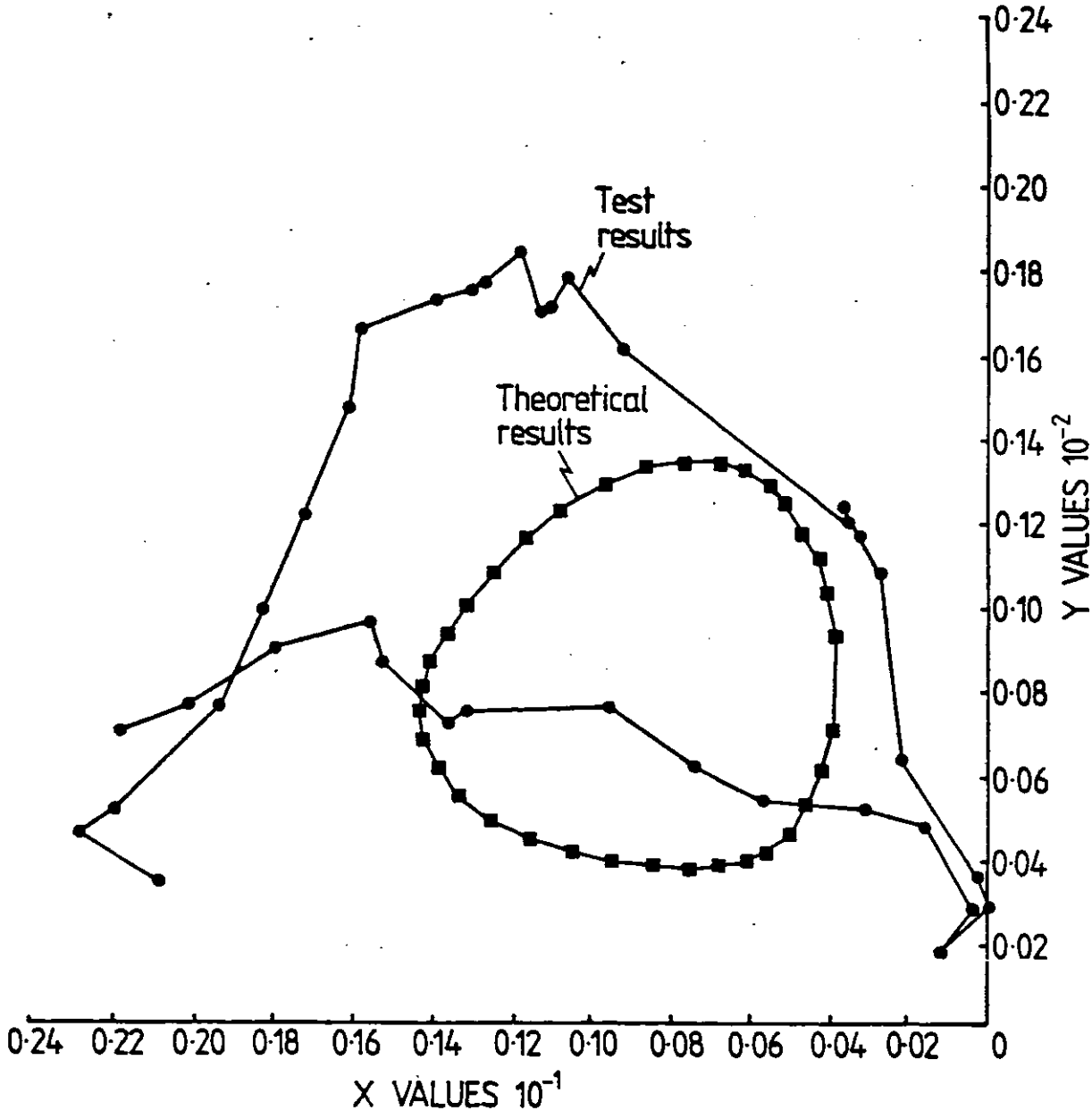

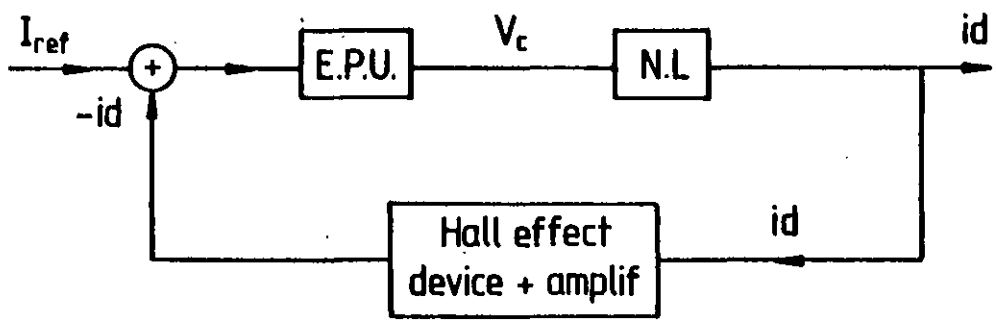

Fig 6.29: Control loop incorporating controlled converters

Hall effect device plus amplifier, the linear part of the control loop can be gathered in a single transfer function $G(j\omega)$ where:

$$|G(j\omega)| = |G_1(j\omega)H(j\omega)| \qquad (6.4(a))$$

$$\theta(\omega) = \angle G(j\omega) = \angle G_1(j\omega) + \angle H(j\omega) \qquad (6.4(b))$$

The open-loop transfer function of the linear part of the control loop is of the form

$$G(j\omega) = \frac{-K}{1+j\omega T} \qquad (6.5)$$

As the gain of the Hall effect device is unity and its time constant is very small, the gain K and time constant T in (6.5) are mainly determined by the error processing unit. For a particular time constant T, the gain K was varied up to the value where a limit cycle oscillation would occur. The value of K was then read and compared with the theoretical prediction.

As the off-line program developed can only predict oscillations synchronised with the a.c. system voltage, a set of tests for two s.c.r. conditions (infinity and 3), balanced and unbalanced conditions (an imbalance of 25% in the amplitude of phase R voltage) and for four time constants (1, 10, 100 and 1000 ms) was carried out.

Table 6.4 summarises the results obtained. Only oscillations synchronised with the a.c. system voltage are shown in this Table. Oscillations not synchronised with the a.c. system voltage were also found but they were disregarded as they cannot be predicted by the theoretical model developed.

Table 6.4: Frequency of oscillations synchronised with the a.c. system frequency

T [ms]	S.C.R: ∞ Balanced a.c. voltages	S.C.R: ∞ Unbalanced a.c. voltages	S.C.R. = 3 Balanced a.c. voltages	S.C.R. = 3 Unbalanced a.c. voltages
1	150 Hz 100 Hz	50 Hz	50 Hz	-
10	50 Hz	50 Hz 100 Hz	-	50 Hz
100	-	50 Hz	-	-
1000	-	-	-	-

Furthermore only oscillations with a considerable amplitude were registered. The amplitude of these oscillations were measured in terms of a variation of α reference and varied between 2 el deg and 10 el deg.

The following conclusions can be drawn from the results obtained.

a. Oscillations synchronised with the a.c. system voltage appear predominantly for high s.c.r. and low time constants (1, 10 ms).

b. In all the cases where oscillations synchronised with the a.c. system voltage were detected, the value of the gain is much smaller than that necessary to initiate oscillations unsynchronised with the a.c. system voltage.

c. For a low s.c.r. the gain necessary to sustain an

oscillation of detectable amplitude is much smaller than for high s.c.r.

d. The gain K for which oscillations occur decreases with decreasing time constant T.

The results of Table 6.4 indicate the area of interest, i.e. T = 10 and 100 ms for both high and low s.c.r.

6.4.1 Time constant 10 ms

Fig 6.30 shows the Nichols chart obtained from the theoretical results for the prediction of limit cycles at a frequency of 50 Hz and a s.c.r. of infinity.

The plots are shown for several values of amplitude of the modulating signal. At the time of the tests the level of both the fundamental and harmonics on the a.c. side of the converter transformer were measured and used as input data for the theoretical studies. A similar procedure was followed for all the tests performed.

The straight line $G(j100\pi)$ in fig 6.30 is the locus of the 50 Hz frequency point of $G(j\omega)$ for different values of gain K.

According to the theoretical predictions an oscillation of 5^{o} in amplitude would occur for a gain K of 37.2. Increasing the gain K would increase the amplitude of the oscillation up to a value of 2^{o}. A further increase in the gain would result in a change of phase, the amplitude of this oscillation remaining the same. Finally further increments in the value of K would lead to an oscillation of smaller amplitude.

Fig 6.30: Nichols chart. f = 50 Hz, s.c.r. = ∞ , T = 10 m.s., α^{o} = 26.4^{o}

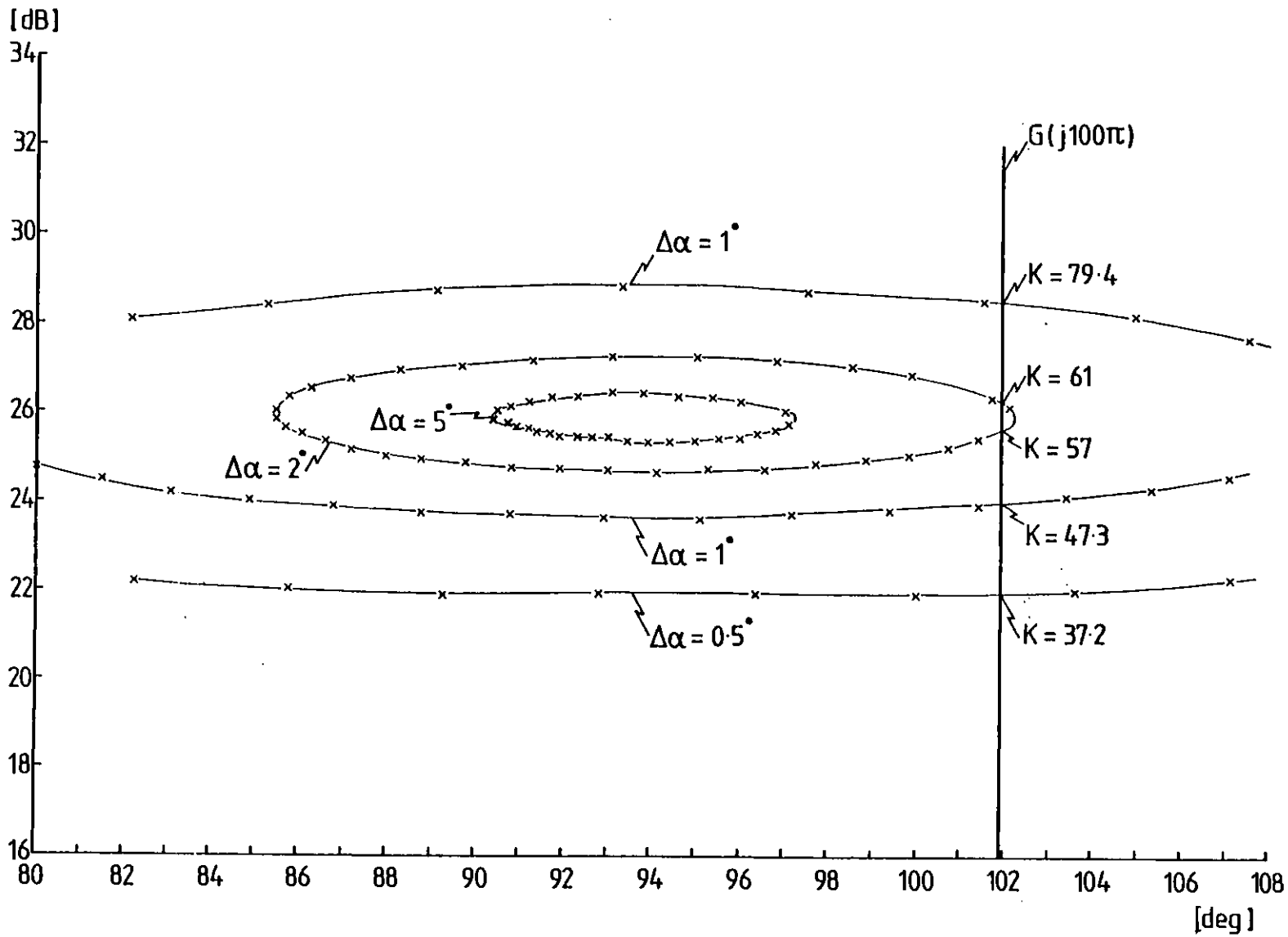

Table 6.5 details all the results obtained for a time constant of 10 ms. For the case under study an oscillation with amplitude equal to .4° exists for a gain equal to 10. A gain of 50 produces an oscillation of 5° amplitude. A further increase in gain produces a change of phase and finally the amplitude of the oscillation reduces to 4°.

Although the theoretical results explained qualitatively the behaviour of the oscillations with increasing gain K, a considerable difference was found between the calculated and measured values of the gain.

Fig 6.31 shows the Nichols chart of the theoretical results obtained to predict limit cycles at a frequency of 50 Hz, amplitude of the modulating-signal of .24° and a s.c.r. equal to 3. The straight line in this figure is the locus of the 50 Hz point of $G(j\omega)$ for different gains K.

The results shown in Table 6.5 show that in this case good agreement between the theoretical and test results was obtained.

Increasing further the gain K of the error processing unit would initiate oscillations not synchronised with the a.c. system frequency.

Figs 6.32 and 6.33 show the Nichols chart for the theoretical results and frequencies of the modulating signal equal to 100 and 50 Hz respectively and s.c.r. equal to infinity. The a.c. voltages were unbalanced.

In fig 6.32 the theoretical results predict an oscillation of .4°, frequency 100 Hz for a gain K of 11.3. Test results shown in Table 6.5 confirm this prediction.

Table 6.5: Comparison between theoretical and test results. Time constant T = 10 ms

Frequency of oscillation (Hz)	Infinity short circuit ratio				Short circuit ratio 3			
	Test results		Theoretical results		Test results		Theoretical results	
	Gain K	Amplitude of oscillations	Gain K	Amplitude of oscillations	Gain K	Amplitude of oscillations	Gain K	Amplitude of oscillations
50	10	$.4^{o}$	37.2	$.5^{o}$	20	$.24^{o}$	23.2	$.24^{o}$
	50	5^{o}	57	2^{o}	-	-	-	-
100	10	$.4^{o}$	11.3	$.4^{o}$	-	-	-	-
50 and 100	70	5^{o}(50 Hz) 3^{o}(100 Hz)	84.6	5^{o}(50 Hz) 3^{o}(100 Hz)				

Fig 6.31: Nichols chart. f = 50 Hz, s.c.r. = 3, T = 10 ms, α^{o} = 26.10^{o}, $\Delta\alpha$ = .24^{o}

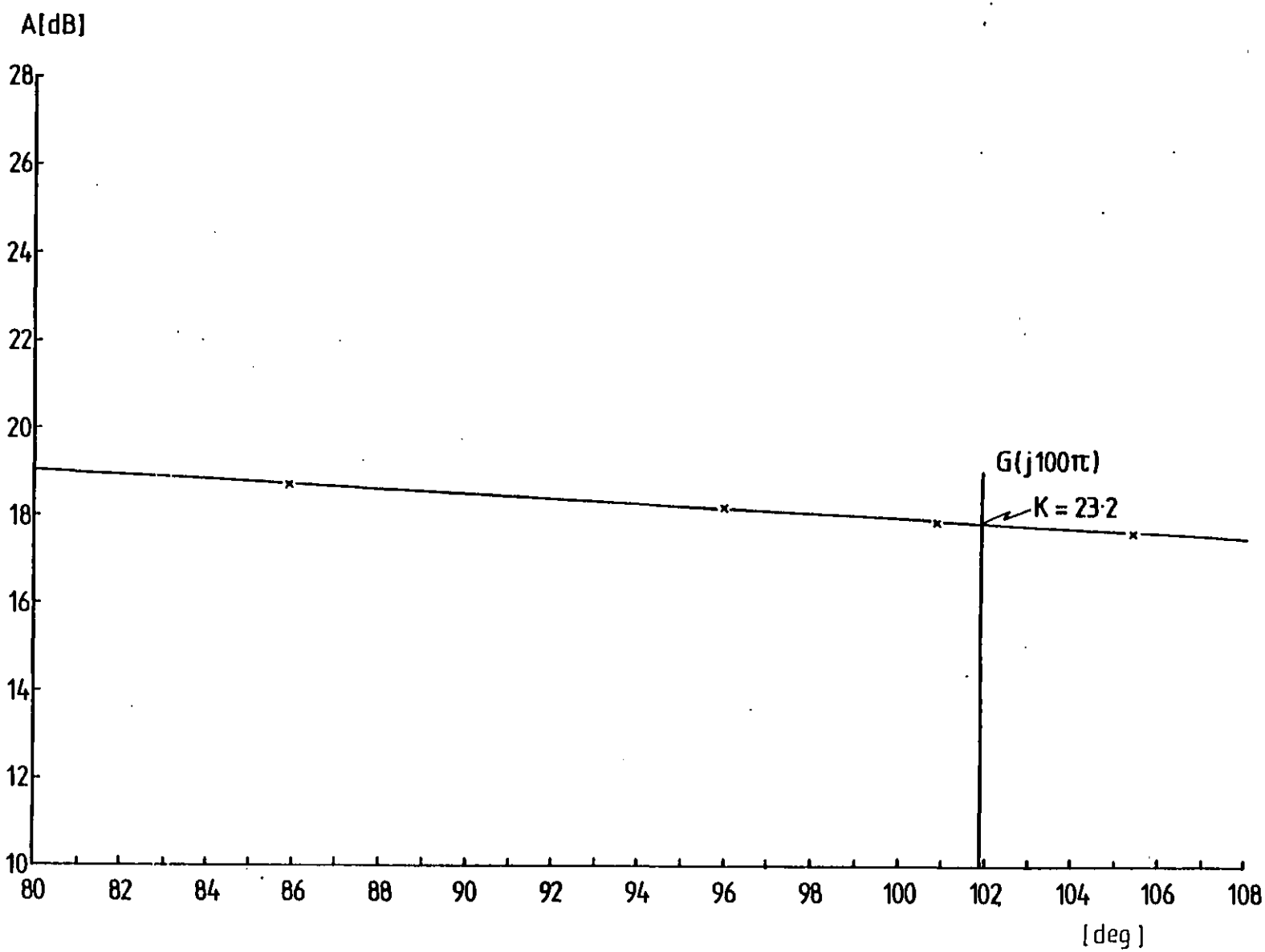

Fig 6.32: Nichols chart. f = 100 Hz, s.c.r. =∞ , T = 10 ms, α^{o} = 13.5^{o}, $\Delta\alpha$ = 0.4^{o}

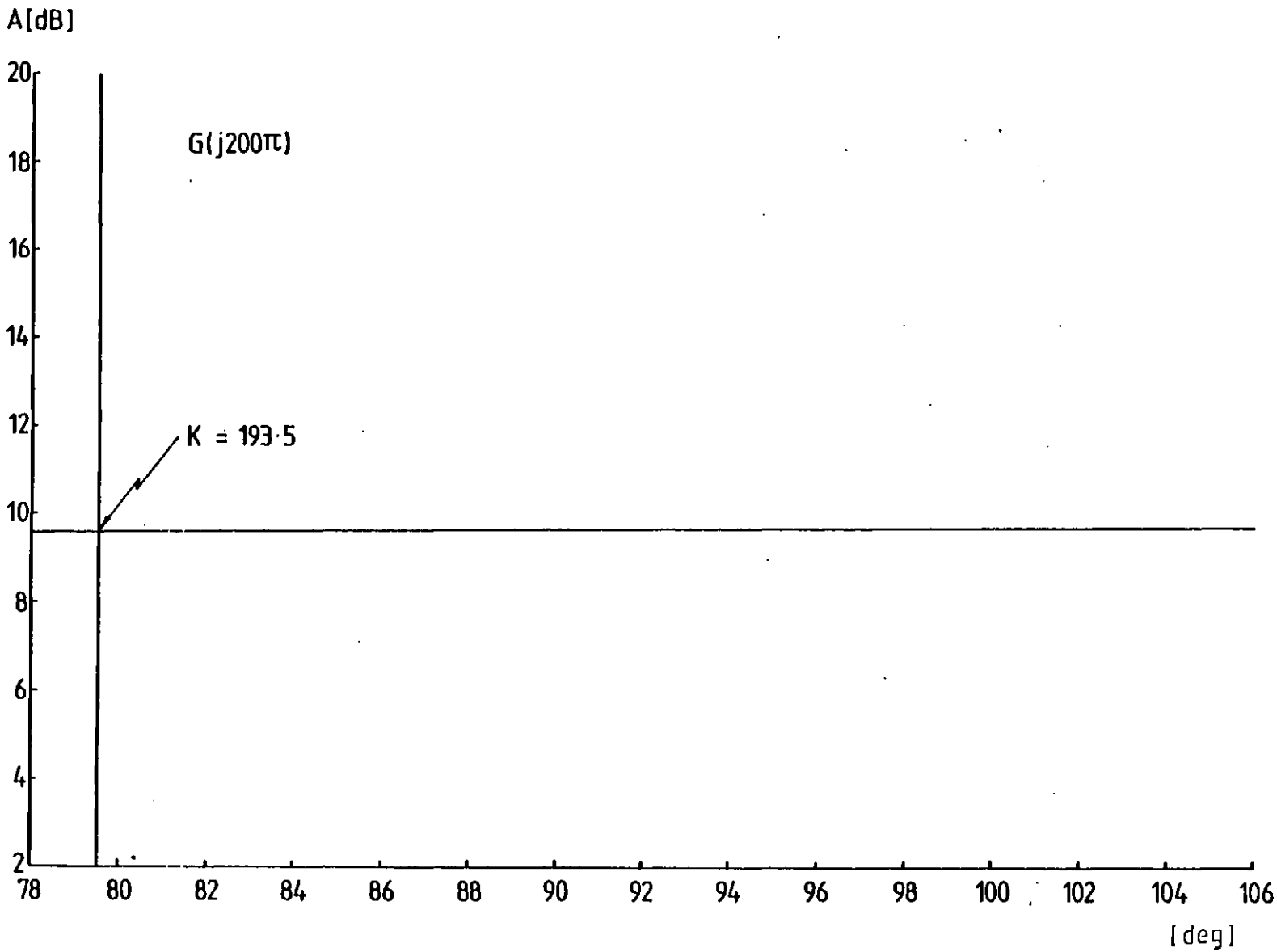

Fig 6.33: Nichol's chart. f = 50 Hz, s.c.r. = ∞ , T = 10 ms, α^{o} = 14.5^{o}

(a) Dual input D.F. around ψ = 310^{o}. Frequency of bias signal 100 Hz, amplitude 3^{o}

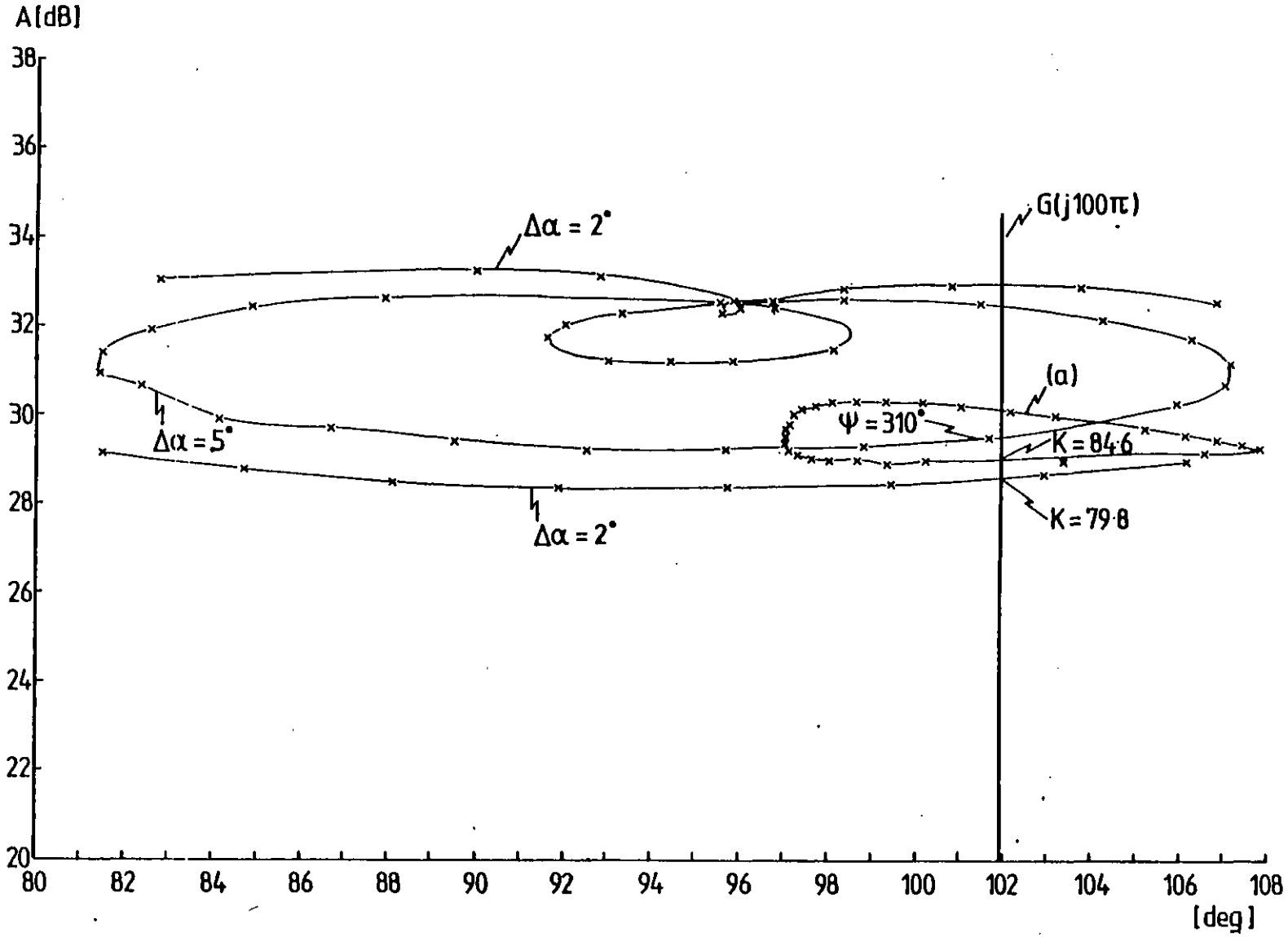

Tests showed that increasing the gain K leads to a situation where an oscillation with both 50 Hz and 100 Hz would exist. The measured amplitude of the 50 Hz component of control voltage was 5^{o} whereas the amplitude of the 100 Hz component of control voltage was 3^{o}. Table 6.5 details the gain K for which this situation occurred.

The evaluation of the dual input describing function is needed to analyse this case. The single input d.f. was first plotted for an amplitude of the m.s. equal to 2^{o} and 5^{o}. For an amplitude of the m.s. equal to 5^{o} and a phase of 310^{o} (which corresponds to the lowest value of gain margin) the d.i.d.f. was evaluated. The plot is shown in fig 6.33 (curve (a)).

As can be seen from the results shown in Table 6.5, again good agreement between theoretical and test results was found.

6.4.2 Time constant 100 ms

Fig 6.34 shows the Nichols chart of the theoretical results for a frequency equal to 50 Hz, s.c.r. infinity, amplitude of the modulating signal equal to 5^{o}.

From the theoretical results the gain for which an oscillation of 50 Hz and amplitude 5^{o} is present, should be 932.5. However the test results showed that an oscillation of amplitude 5^{o} and frequency 50 Hz existed for a gain of the error processing unit equal to 380.

Fig 6.35 shows the Nichols chart of the theoretical results for f = 100 Hz, s.c.r. $=\infty$ and $\Delta\alpha = 0.5^{o}$.

The theoretical results predict an oscillation of 100 Hz, amplitude 0.5^{o} for a gain equal to 193.5. Test results

Fig 6.34: Nichols chart. f = 50 Hz, s.c.r. =∞ , T = 100 ms, α^{o} = 14.8, $\Delta\alpha = 5^{o}$

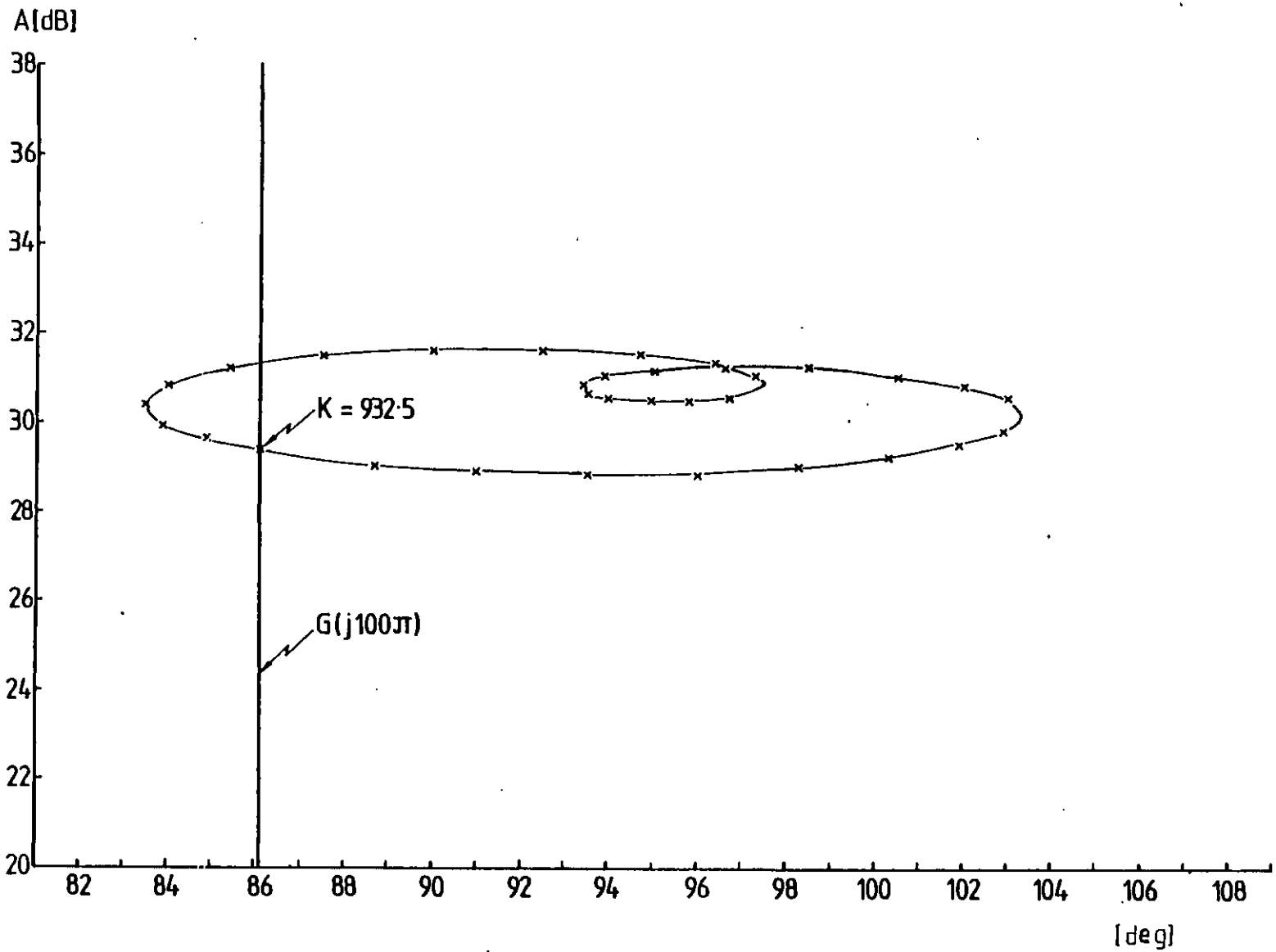

Fig 6.35: Nichols chart. f = 100 Hz, s.c.r. = ∞ , T = 100 ms, α^{o} = 22.8^{o}, $\Delta\alpha$ = 0.5^{o}

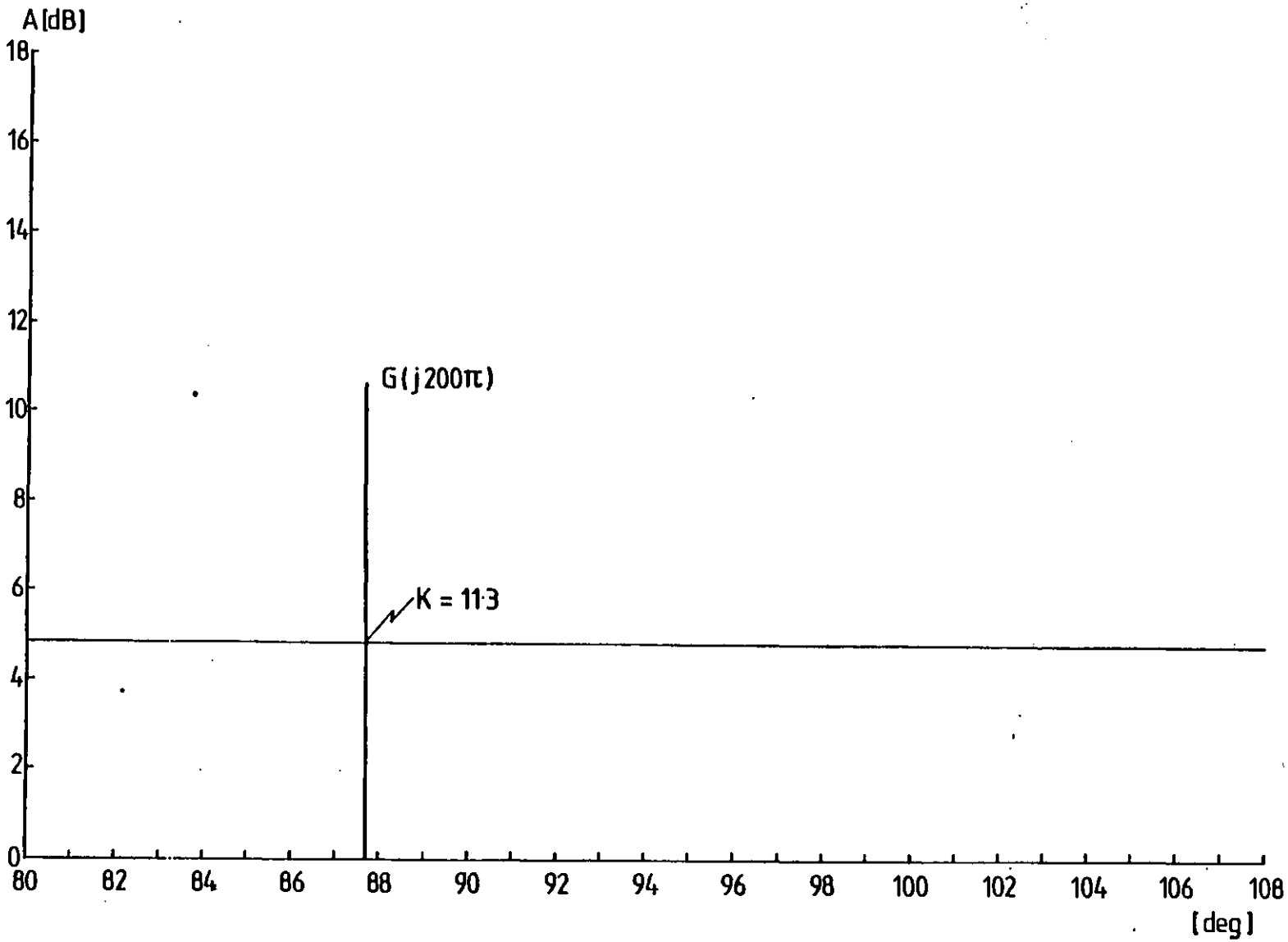

showed that this oscillation would exist for a gain K of the error processing unit equal to 150. For low short circuit ratio no oscillations synchronised with the a.c. mains were observed.

6.4.3 Firing angle irregularities

A common feature of the tests for both the 10 and 100 ms time constants was the dominance of the 50 Hz oscillation even when the fundamental of the a.c. voltage was unbalanced.

It is thought that a contributing factor towards this behaviour is the irregularity in the firing of the converter thyristor valves.

Under open-loop, the firing instant pulses produced by the digital controller are to all intents and purposes 60 el. deg. apart. These pulses are routed to the valves through a set of pulse transformers.

Tests showed that a delay exists between the instants the pulse is produced by the digital controller and the instant it is applied to the valve.

Theoretical studies were carried out in order to assess the influence of a common delay in all the firings in the d.f.

The results are shown in fig 6.36 where the Nichols chart is plotted for a 50 Hz m.s.

The plot indicates that a delay in the firing instants shifts the $-1/N(V_c, \omega, \psi)$ plot by a value which is almost identical to the delay considered. The amplitude of the $-1/N(V_c, \omega, \psi)$ also decreases.

Fig 6.36: Nichols chart. f = 50 Hz, α^{o} = 26.4, s.c.r. = ∞ , $\Delta\alpha$ = 5^{o}.

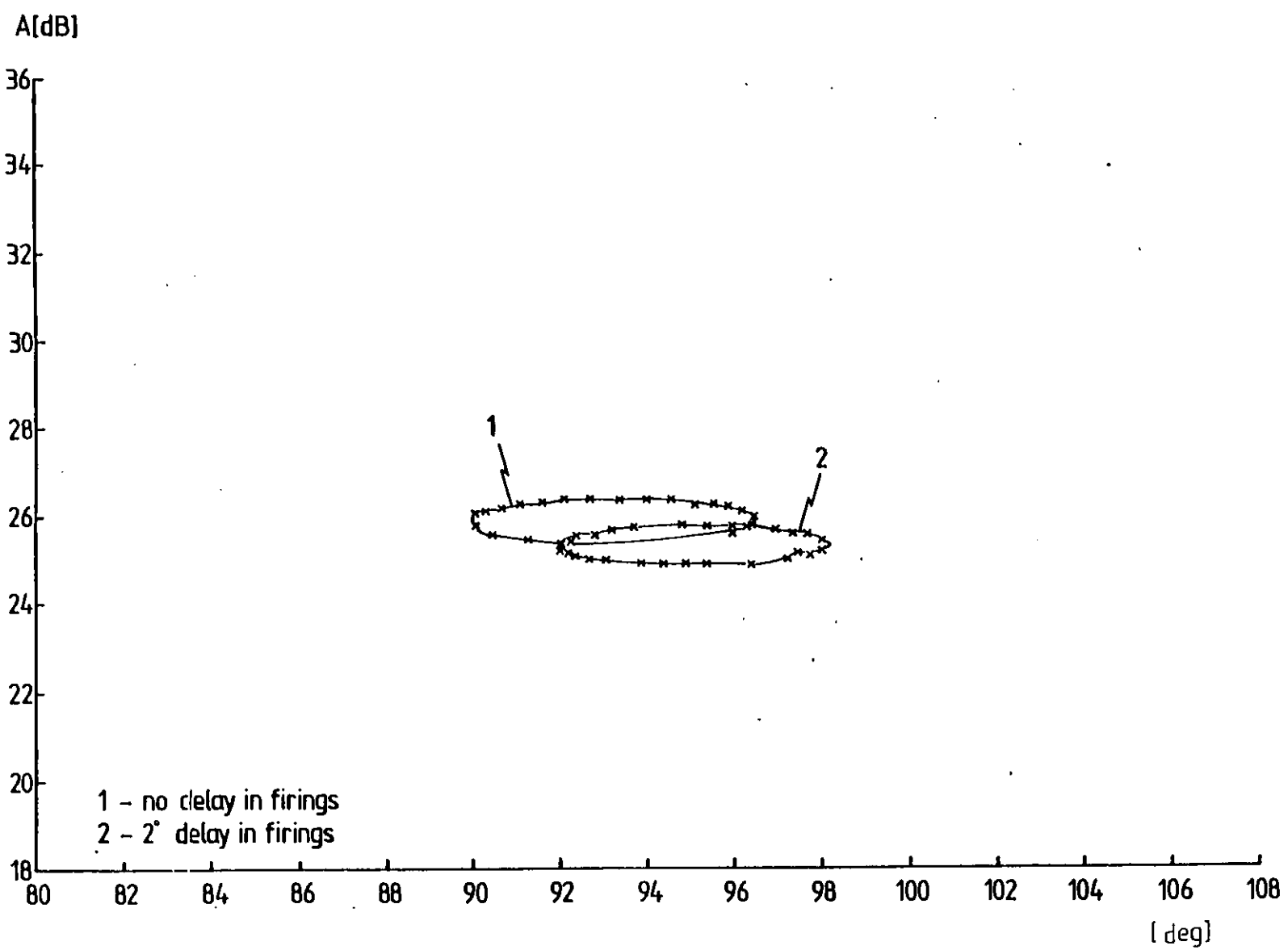

If the delay is not identical for all the valves, and this is likely due to hardware component precision, a pattern of firings is established which does not repeat itself over a 'mains' cycle. This is the cause of the 50 Hz oscillation.

6.5 Conclusions

In this chapter a comparison between the theoretical results obtained from the off-line computer program, and test results obtained from the h.v.d.c. simulator was carried out.

The experimental determination of the d.f. confirmed the theoretical predictions in nearly all the cases, agreement being better for high s.c.r.s. This is thought to be due to imbalances in the parameters of the test equipment not taken into account in the theoretical studies.

This conclusion is reinforced from the results of the 100Hz m.s.case in which the correlation between theory and tests is the poorest. However this is also the case for which the d.f. is most sensitive to a.c. system imbalances. Although some imbalances were measured at the beginning of tests and used subsequently as input data in the theoretical predictions, there was no guarantee that these imbalances remained the same during the course of the tests.

The experimental confirmation of limit cycle oscillations at a frequency synchronised with the a.c. system voltage was also carried out. Some limit cycles of 50 and 100 Hz observed experimentally were confirmed through a Nichols plot

of both the inverse d.f. and the error processing unit transfer function.

The agreement between theoretical and experimental values of the e.p.u. gain is in most cases satisfactory.

The limit cycle oscillations are in general of relatively small amplitude and result from a.c. system imperfections magnified by the closed-loop control of the d.c. current. They occur for values of the e.p.u. gain less than that necessary to initiate oscillations with a frequency not synchronised with the a.c. system voltage.

Actually the mechanism that generates oscillations synchronised with the a.c. system voltage is different from the one that generates non-synchronised oscillations. Whereas non-synchronised oscillations are mainly excited due to the closed-loop control of the d.c. current, synchronised oscillations are excited due to a.c. system imbalances and/or distortions.

These synchronised oscillations may exist even under open-loop situations, the closed-loop control simply magnifying them through modulation of the control voltage.

Chapter Seven

HARMONIC MINIMISATION CONTROLLER

7.1 Introduction

The theoretical and experimental results obtained in Chapters Five and Six suggest that oscillations synchronised with the a.c. system voltage are mainly generated by imbalances and/or harmonic distortion in the a.c. busbar of the converter transformer.

The results obtained also show that modulating the firing instants with a signal of a particular frequency generates a d.c. current harmonic of the same frequency. This current, in turn, imposes on the a.c. side voltage harmonics, which, if present independently, would have resulted in a d.c. current harmonic of the modulating signal frequency.

These two major conclusions led to a proposal of a new controller, whose primary objective is to minimise the modulation of the control voltage due to uncharacteristic d.c. current harmonics.

The type of control systems that are in use today supress the modulation of the control voltage due to d.c. current harmonics by imposing a large time constant in the error processing unit, i.e. by giving it a low-pass filter characteristic. The smaller the passband of the error processing unit the more effective the filtering effect of the error processing unit. Results obtained in Chapter Six showed that for a time constant T of the error processing unit equal to 1s, no oscillations synchronised with the a.c. system voltage were obtained.

Increasing the time constant T has, however, the drawback of slower dynamic response of the controller.

By minimising the modulation of the control voltage, the controller proposed enables the use of smaller time constants in the error processing unit.

The basic philosophy of the new controller is presented in section 7.2. Section 7.3 shows some experimental results obtained using the principle developed in section 7.2. These results were obtained using a spectrum analyser and the waveform generator of a digital transfer function analyser. Also in this section the basic design of the new controller is outlined.

Finally in section 7.4 some conclusions are drawn.

7.2 Basic philosophy of the harmonic minimisation controller

Oscillations synchronised with the a.c. system voltage are mainly due to imbalances and/or distortions in the a.c. busbar voltage of the converter transformer.

These imbalances and/or distortions generate, due to the modulation process of the converter, a set of d.c. current harmonics. Under open-loop conditions and with equidistant firing the source of non-characteristic d.c. current harmonics is the variation in commutation periods.

When the current-control loop is closed the d.c. current harmonics modulate the control voltage, thus giving rise to non-equidistant firing of the valves. This irregular firing is a secondary source of d.c. current harmonics which is likely to lead to harmonic magnification.

The basic objective of the harmonic minimisation controller (h.m.c.) now proposed is to use an auxiliary signal to demodulate the modulated control voltage.

Figure 7.1 shows the block diagram of the current-control loop of a d.c. converter system using the proposed h.m.c.

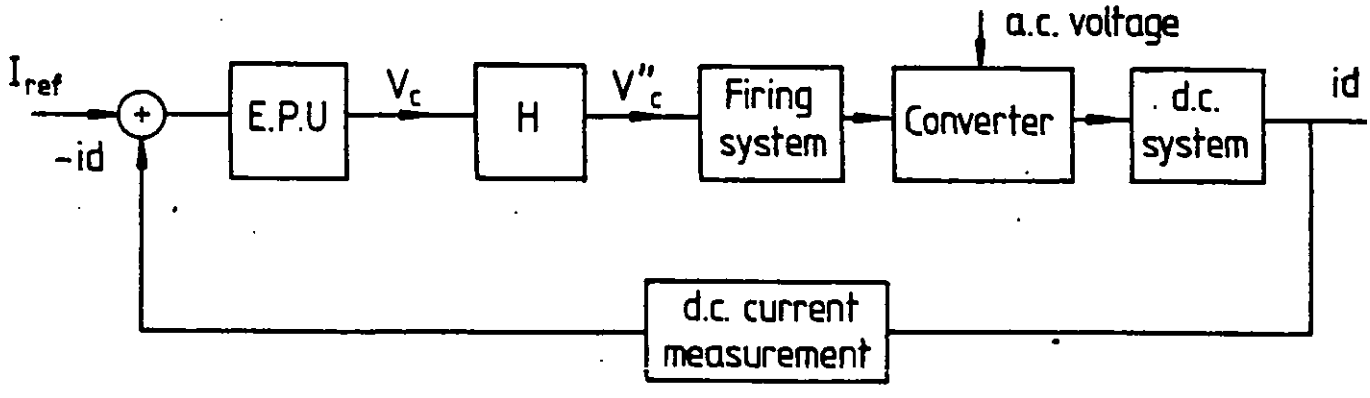

Fig 7.1: Block diagram of the current control loop using the Harmonic Minimisation Controller

Here the output signal from the error processing unit (V_c) is modified according to a particular law into V''_c which in turn is applied to the firing system. Block H in fig 7.1 performs this modifying function.

Two approaches are possible here:

a. In the first approach, the demodulation of V_c is the objective. V''_c modulates the firing instants in such a way that the d.c. current non-characteristic harmonics are minimised.

b. In the second approach, the demodulation of V''_c is the objective, i.e. in this approach the pulses applied to the thyristors are truly equidistant. The residual d.c. current non-characteristic harmonics are larger than in case (a).

Thus, in the first approach the modulation due to imbalances, distortion in the a.c. voltage and non-equidistance firing is collectively compensated, whereas in the second approach only the modulation due to the non equidistant firing is compensated.

7.3 Experimental results

The two approaches detailed above were tested using the set-up described in Chapters Two and Six.

A spectrum analyser was used to analyse the control-voltage frequency spectrum. The waveform generator of the digital transfer function analyser was used to produce a signal with a particular amplitude and frequency. The phase shifting network described in Chapter Six was used to adjust the phase of the output signal of the d.t.f.a.

To produce V''_c a summing junction was implemented. The inputs to the summing junction are the output of the error processing unit V_c, and the signal derived from the d.t.f.a. as shown in fig 7.2.

In the hatched box the phase shifting circuit described in section 6.2.2 is shown. Also the d.t.f.a. is locked with the a.c. system voltage through the circuit outlined in 6.2.2

Experiments were performed for high and low s.c.r.s.

The frequency spectrum of both V_c and V''_c obtained with the spectrum analyser was used to determine the frequency and amplitude of the signal to be provided by the waveform generator of the d.t.f.a. First, with a small amplitude of this signal, its phase was adjusted so that V_c (V''_c) diminished its amplitude. Next the amplitude was incremented to minimise the modulation in V_c (V''_c).

With the present experimental set-up it is only possible to act on one particular frequency of the spectrum of $V_c(V''_c)$.

A summary of the results obtained is shown in Table 7.1.

Tests were also performed with a s.c.r. equal to 3. Oscillations synchronised with the a.c. system voltage were detected for very small values of the gain ($\simeq$ 10) of the error processing unit. The amplitude of this oscillation was so small that correction would have been counter productive.

In the table the amplitudes of V_c are an image of the amplitudes of the uncharacteristic harmonics in the d.c. current. In all cases shown, the modulation of V_c by the auxiliary signal derived from the d.t.f.a. did not initiate other types of oscillation. Actually the frequency spectrum of V_c for all

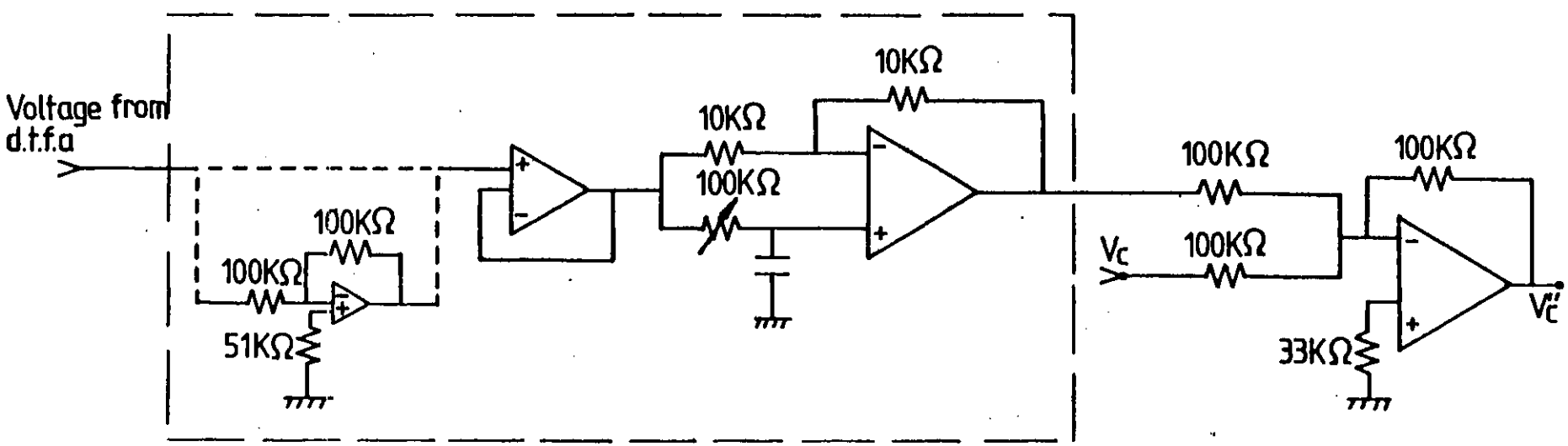

Fig 7.2 Hardware design to obtain V''_c

Table 7.1: Summary of results obtained with the H.M.C.

Short circuit ratio	Id [A]	Current controller		Harmonic Minimisation Controller			Control policy
		Frequency of oscillation	Amplitude [V]	Amplitude of auxillary signal[V]	Amplitude of V_c [V]	Amplitude of V''_c [V]	
∞	2.2	50 Hz	80×10^{-3}	64×10^{-3}	50×10^{-3}	20×10^{-3}	Control of V''_c
∞	2	50 Hz	80×10^{-3}	85.3×10^{-3}	20×10^{-3}	80×10^{-3}	Control of V_c
6	1.8	50 Hz	40×10^{-3}	40×10^{-3}	20×10^{-3}	30×10^{-3}	Control of V_c
6	1.8	50 Hz	40×10^{-3}	25×10^{-3}	30×10^{-3}	20×10^{-3}	Control of V''_c
∞	2	100 Hz	30×10^{-3}	23.5×10^{-3}	10×10^{-3}	30×10^{-3}	Control of V_c

frequencies but the one which was being controlled remained the same.

In order to assess whether the same results would apply to the control of other frequencies, an imbalance in the fundamental term of a.c. voltage was introduced. This caused a 100 Hz oscillation in the control voltage. The results are detailed in Table 7.1.

In all the tests performed the phase shift between the auxiliary signal injected and the signal modulating the control voltage V_c was found to be 180^o.

The results obtained suggest that the control of V_c is not only more effective in reducing the d.c. current non-characteristic harmonics, but is also easier to implement. It is also apparent that the amplitude of the auxiliary signal is approximately equal to the amplitude of the oscillation in V_c before the demodulation.

To derive a simple law for the control of V''_c is however more difficult, as in this case the objective is that the voltage fed into the firing system will be demodulated. Thus the amplitude of the auxiliary signal depends on the non-characteristic harmonic content contributed by the control voltage.

Figs 7.3, 7.4 and 7.5 show oscillograms of the direct voltage V_d before and after the implementation of the new control policy for infinity s.c.r. and frequency of oscillation of 50 Hz. The gain of the error processing unit is 50. The oscillograms of V_c and V''_c (with and without the auxiliary signal) are shown.

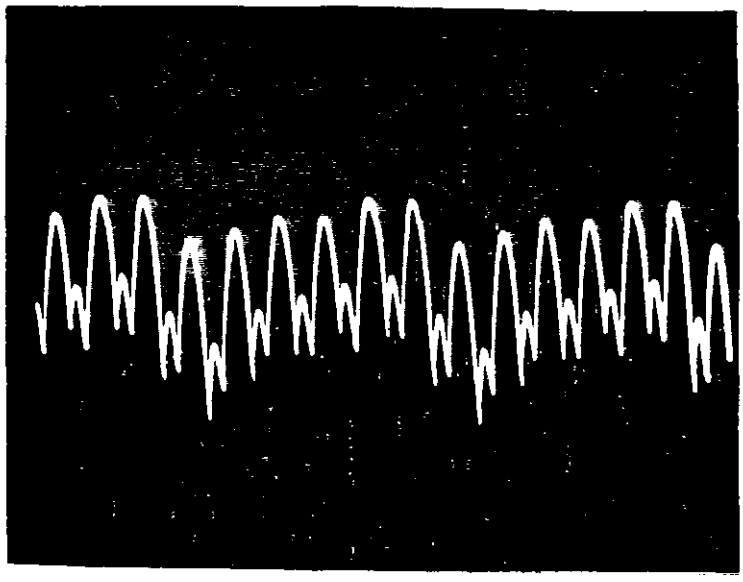

a)

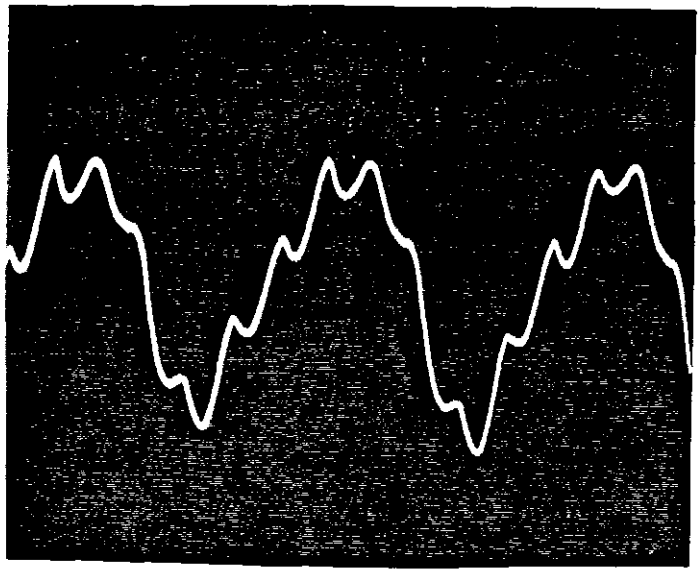

b)

Fig 7.3 Current controller
s.c.r. = α k = 50
a) V_d
b) V_c

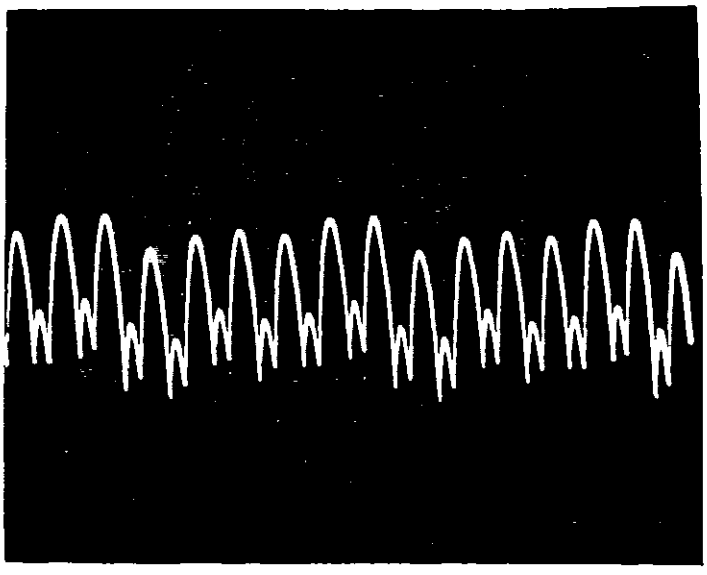

a)

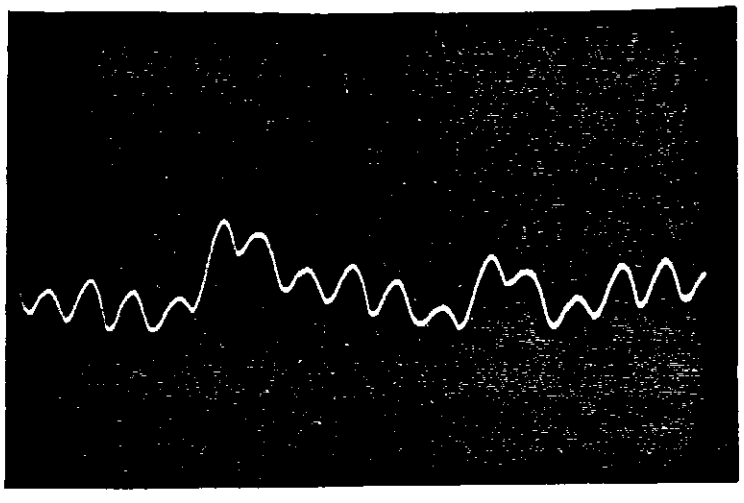

b)

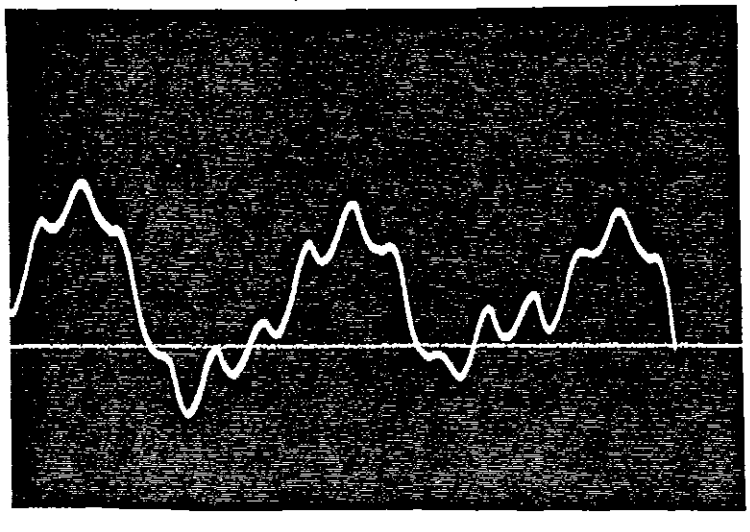

c)

Fig 7.4 Harmonic minimisation controller Control of V''_c
s.c.r. = ∞ k = 50
a) V_d b) V''_c c) V_c

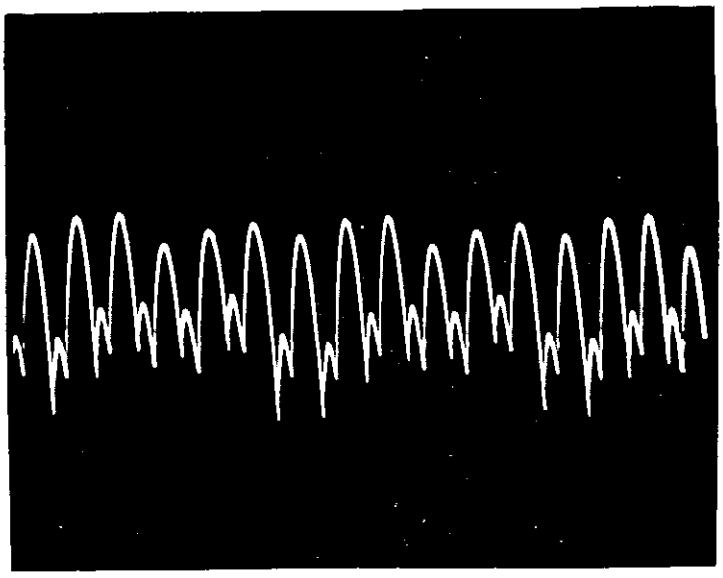

a)

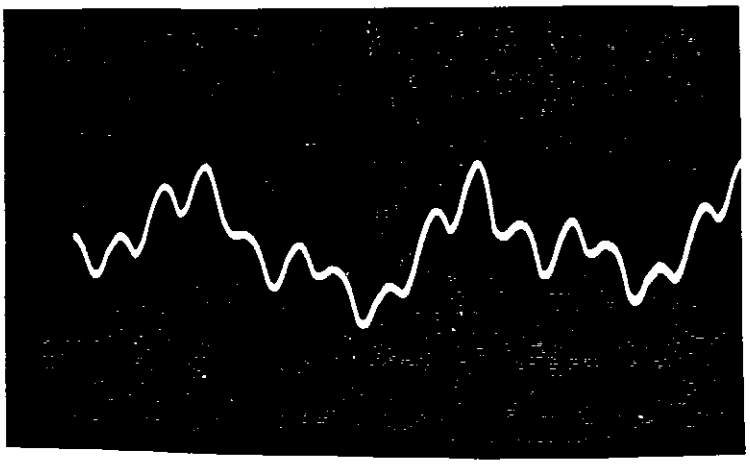

b)

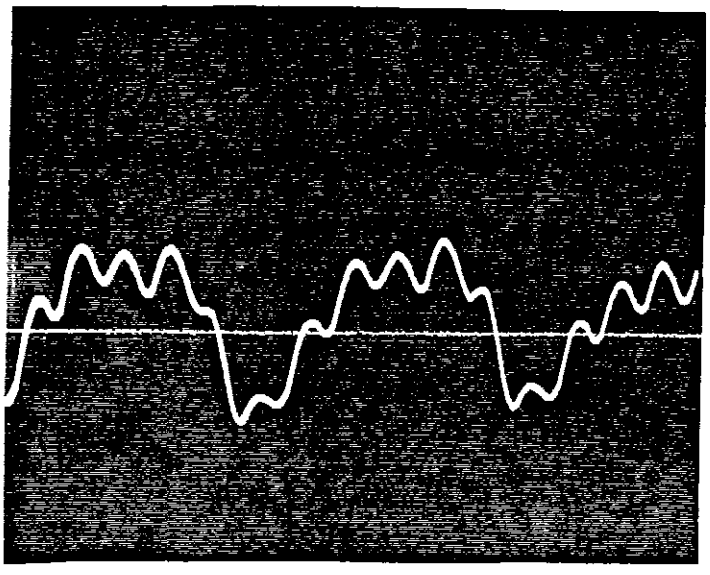

c)

Fig 7.5 Harmonic minimisation controller Control of V_c
s.c.r. $=\infty$ $k = 50$
a) V_d b) V_c c) V''_c

As already pointed out, these results were obtained with the auxiliary signal derived externally to the control-loop. To fully assess the behaviour of the new controller tests with the new auxiliary loop closed needed to be performed.

A possible way of implementing the Harmonic Minimisation Controller would be to use a microcomputer which performs the Discrete Fourier Transform (DFT) of the control voltage, thus obtaining its frequency spectrum.

The components that possess negligible amplitudes may be simply disregarded and a new spectrum built with the frequencies which are dominant. Subsequently the spectrum should be shifted by 180^{o}. From this new frequency spectrum the inverse Discrete Fourier Transform can be performed and the auxiliary signal obtained.

This signal can then be applied either in analogue form to the input of the firing system (a digital to analogue converter is thus needed) or in digital form as a correction to the software algorithm described in section 2.3.1.2.

As the control voltage is sampled 17 times in 60^{o} (see Chapter Two), these samples can be fed as data to the Discrete Fourier Transform processor.

The action of the new controller must be very slow so that its influence on the dynamic behaviour of the current-control loop is negligible. As the lowest frequency to be detected is 50 Hz a time delay of 20 ms is inherent in the correction.

7.4 Conclusions

This chapter described a new controller whose main objective is to suppress the magnification of non-characteristic harmonics due to the feedback action of the current control-loop of converter systems.

Two control policies are described. Experimental results for both control policies were obtained, using an external source to impose an auxiliary signal to demodulate the modulated control voltage.

Under these conditions the behaviour of the new controller was satisfactory. Oscillograms that compare the relevant signal with and without the new control policy were shown.

Based on the results obtained, a way of implementing the new controller was described.

Although one of the control policies is easier to implement and leads to a negligible amplitude of the harmonic supressed it does not follow that this control policy is the best. Its behaviour under closed-loop conditions must be fully assessed and the consequences of the firing instant modulation investigated.

A digital controller seems most appropriate for the incorporation of such control policies as only alterations in software are needed, the hardware remaining virtually the same.

Chapter Eight

CONCLUSIONS

8.1 Conclusions

A new model for the converter and its associated controls, suitable for the study of oscillations synchronised with the a.c. system voltage, was proposed.

The model developed takes into account the modulation and demodulation processes characterising converter behaviour, and the resulting generation of harmonics. As this detailed converter model is not amenable to an analytical approach a computer program was developed capable of analysing the mechanism of harmonic generation by the converter in the presence of imperfections in a.c. voltage, converter transformer and firing system. The program performs a detailed steady-state calculation of a complete h.v.d.c. link, yielding all the a.c. and d.c. side voltage and current harmonics up to the 30th.

The program allows the simulation of the Individual Phase Control (IPC), the Pulse Frequency Control (PFC) and Pulse Phase Control (PPC) systems, and the representation of both rectification and inversion with either infinite or finite a.c. systems.

The main burden of the computer program is the harmonic calculation of the Euler-Fourier coefficients of the d.c. voltage and a.c. currents. In order to save computing time, these coefficients are calculated analytically.

With finite a.c. system short circuit ratio, a Gauss iterative method is used to adjust the a.c. bus voltage. This algorithm requires a considerable number of iterations, specially in the presence of a.c. and/or d.c. system resonances.

Acceleration factors were implemented in order to speed up the convergence, however in some cases convergence was not achieved. This situation occurred whenever the a.c. system anti-resonant frequency and the d.c. system resonant frequency were "linked" through the modulation process inherent in the converter.

The most important findings concerning the steady-state solution of a bi-terminal h.v.d.c. system were:

a. A second harmonic distortion with positive sequence on the a.c. voltage gives rise to a component at the fundamental frequency on the d.c. voltage, and to all even harmonics on the a.c. side.

b. A second harmonic distortion with negative sequence on the a.c. voltage gives rise to all triplen harmonics on the d.c. side and to all even harmonics excluding triplens on the a.c. side.

c. An imbalance in a.c. voltage or in commutating impedance yields all even harmonics on the d.c. side and all triplen harmonics on the a.c. side.

The new model for the converter was used to compute the describing function for d.c. transmission systems. This is defined as the complex ratio of the output d.c. current at a particular frequency to the input control voltage at the same frequency.

With balanced and undistorted a.c. voltage, the d.f. expands with increasing amplitude of the input signal for 50 and 100 Hz. However, for the 150 Hz input signal this feature seems to depend on the type of system studied and on the short circuit ratio.

Imbalance and distortion of the a.c. voltage yields a significant expansion of the d.f. in those cases where the a.c. currents generated by the converter with a modulated input signal contain the same harmonic which is imposed on the a.c. busbar voltage. As a result, the d.f. for 50 Hz is expanded by a second harmonic distortion with positive sequence; for 100 Hz is expanded by voltage or transformer reactance imbalance; and for 150 Hz by a second harmonic distortion with negative sequence.

The experimental determination of the d.f. for the h.v.d.c. simulator showed good agreement with the predicted results in nearly all cases examined. Some limit cycles of 50 and 100 Hz observed experimentally were confirmed through a Nichols chart where both the inverse d.f. and the error processing unit transfer function were plotted.

The agreement between theoretical and experimental values of the error processing unit gain is in most cases satisfactory.

The limit cycles (harmonic instabilities) are in general of relatively small amplitude, and result from a.c. system imperfections magnified by the closed-loop control of the d.c. current. Oscillations synchronised with the a.c. system may indeed be present even under open-loop conditions depending on the a.c. bus voltage imperfections. The harmonics of d.c. current generated by these imperfections is fed back into the firing control system and depending on the bandwidth of the error processing unit, modulate the firing instant of the valves, thus magnifying the relevant harmonic of d.c. current.

We can conclude that the mechanism that gives rise to oscillations synchronised with the a.c. system voltage is quite different from the one responsible for the generation of oscillations at lower frequencies. As a consequence, the values of the error processing unit gain necessary to initiate oscillations synchronised with the a.c. system voltage are much smaller than the ones necessary to initiate lower frequency oscillations.

A new controller whose main function is to minimise the d.c. current non-characteristic harmonics, and thus prevent the occurrence of harmonic instability has been proposed. Tests performed with the new controller showed that oscillations synchronised with the a.c. system voltage can be eliminated. Two alternative control policies were proposed. One minimises the modulation in the control voltage fed into the firing system. The other minimises the d.c. current harmonic. Oscillograms illustrating both control policies were presented.

The describing function method, although expensive in computer time, has proved to be a powerful tool in the study of harmonic instability in h.v.d.c. systems. The results obtained led to the suggestion of a new controller which promises the prevention of harmonic instability.

8.2 Original contributions

The following are believed by the author to be original contributions:

1. Implementation of a digital control system based upon a commercially available microcomputer system (TM 990/101M).
2. A mathematical model for the evaluation of the commutation angle when the influence of d.c. current harmonics is taken into account.
3. A mathematical model for the firing control systems used in d.c. converters, i.e. individual phase control, pulse frequency control and pulse phase control.
4. A mathematical model for the inverter which takes into account the constant extinction angle mode of control.
5. The use of the non-linear model of the converter to evaluate the describing function for h.v.d.c. systems and to predict the existence of limit cycle oscillations synchronised with the a.c. system voltage.
6. A method of minimising uncharacteristic harmonics using a Fast Fourier Transform chip. This could form the basis of a new controller.

8.3 Suggestions for further work

The non-linear model of the converter developed is useful for the evaluation of the harmonics injected in the a.c. and d.c. systems and of the describing function for h.v.d.c. systems. However it possesses some limitations concerning the modelling of the a.c. system and the converter transformer:

1. When obtaining experimental results for the 100 Hz input signal it was found that imbalances in the a.c. system impedance and/or imbalances in the filter bank impedances did affect the describing function locus considerably.
2. Core saturation of the converter transformer can also contribute to harmonic instability (20). Thus the influence of the harmonic pattern generated by the transformer in the d.f. locus and shape must be determined.

It is therefore suggested that the features described above be introduced in the model and their influence on the d.f. fully assessed.

The model developed should be expanded to deal with 12-pulse operation. Nowadays h.v.d.c. links operate in a 12-pulse mode, as this minimises the number of a.c. side filters used and therefore makes h.v.d.c. systems economically more attractive. This expansion would allow a study of the type and arrangement of the a.c. side filters.

The interaction between the a.c. side harmonics and d.c. side harmonics has already been compared by some authors (1, 16, 17) to a modulation process. The direct voltage of a

converter can be seen as the result of the modulation of a carrier function by the input alternating voltage, whereas the a.c. current can be seen as the result of the modulation of a carrier function by the input d.c. current.

On the other hand, due to the d.c. current feedback, a modulation process of the firing instants occurs.

The carrier would then be modulated both by the a.c. voltage (d.c. current) and by the harmonics in control voltage due to the d.c. current feedback. Whilst the former modulation process is similar to an amplitude modulation (thus a linear modulation process), the modulation performed by the control voltage is similar to a pulse duration modulation which is a non-linear modulation process.

The new model now proposed can give a better insight into the kind of modulation performed by a converter. The development of analytical expressions that relate a.c. side harmonics and d.c. side harmonics would allow the evaluation of the harmonic pattern both on the d.c. side and a.c. side without having to perform a Fourier analysis of the waveforms. This would lead to appreciable savings in computing time, and make the analysis of an h.v.d.c. system more flexible.

The principle of a new controller has been proposed and simulated with the use of a spectrum analyser and a waveform generator.

Actual implementation on the new controller is strongly recommended as the test results obtained indicate that it may prevent the occurrence of harmonic instability.

In the set-up used to simulate the new controller, it was only possible to generate single frequency signals. As the control voltage is generally modulated by the d.c. current harmonics, the consideration of signals that possess more than one frequency is also desirable.

The two control policies suggested should be tested and their behaviour assessed. Also a stability study of the new controller for oscillations unsynchronised and synchronised with the a.c. system voltage should be performed in order to fully establish its behaviour.

REFERENCES

1 J P Sucena-Paiva, 'A steady-state stability study of converters and high voltage d.c. transmission systems'. Ph.D thesis, University of London, 1972

2 J D Ainsworth, 'The phase-locked oscillator - A new control method for controlled static converters'. IEEE Trans, Vol PAS-87, 1968, pp 859-865

3 F Busemann, 'H.v.d.c. transmission: hunting of rectifiers with marked compounding'. E R A Report No B/T104, 1951

4 F Busemann, 'The theory of the control problem of h.v.d.c. transmission with rectifiers and inverters in bridge circuit'. E R A Report No Z/T74, 1948

5 N A Bjaresten, 'The static converter as a high-speed power amplifier'. Direct Current, Vol 8, 1963, pp 154-165

6 F Fallside and A R Farmer, 'Ripple instability on closed-loop control systems with thyristor amplifiers'. Proc IEE, Vol 114, 1967, pp 139-152

7 F Fallside, C J Goodman and R D Jackson, 'Stability of first-order sampling and thyristor systems'. Electronic Letters, Vol 50, 1969, pp 566-567

8 P A Hazell and J O Flower, 'Stability properties of certain thyristor bridge control systems. Part 1 - The thyristor bridge as a discrete control system. Part 2 - The interrelationship of discrete- and continuous-design methods'. Proc IEE, Vol 117, 1970, pp 1405-1420

9 A M Reider, 'Analysis of the stability of the control systems of the Kashira-Moscow direct current transmission line'. Direct Current, Vol 3, 1957, pp 227-240; also USSR Direct Current Research, Pergamon Press, 1964, pp 137-161

10 P A Hazell, 'Sample Data Theory for Thyristor Bridge Systems'. D.Phil. Thesis, University of Sussex, 1972

11 E A Parrish and E S McVey, 'A theoretical model for single-phase silicon-controlled rectifier systems', IEEE Trans Aut Control, Vol AC-12, 1967, pp 577-579

12 J P Sucena-Paiva, R Hernandez and L L Freris, 'Stability study of controlled rectifiers using a new discrete model'. Proc IEE, Vol 119, No 9, pp 1285-1293, September 1972

13 J P Sucena-Paiva and L L Freris, 'Stability of rectifiers with voltage-controlled oscillator firing systems'. Proc IEE, Vol 120, No 6, pp 667-673, June 1973

14 R Hernandez Millan, J P Sucena-Paiva and L L Freris, 'Modelling of controlled rectifiers in feedback systems'. IEEE Transactions, Vol PAS-93, pp 167-175, January/February 1974

15 J P Sucena-Paiva and L L Freris, 'Stability of a d.c. transmission link between strong a.c. systems'. Proc IEE, Vol 120, No 10, pp 1233-1242, October 1973

16 E V Persson, 'Calculation of transfer functions in grid-controlled converter systems'. Proc IEE, Vol 117, 1970, pp 989-997

17 J P Sucena-Paiva and L L Freris, 'Stability of a d.c. transmission link between weak a.c. systems'. Proc IEE, Vol 121, No 6, pp 508-515, June 1974

18 T Sakurai, J Ohara, J Ueda, A Mase, T Horiuchi and J Arai, 'A study of a certain a.c. oscillation of h.v.d.c. system'. Paper A79 100-9, IEEE Power Engineering Society Winter Meeting, New York, February 1979

19 J C de Oliveira, 'Multiple converter harmonic calculations with non-ideal conditions'. Ph.D thesis, University of Manchester Institute of Science and Technology, 1978

20 J D Ainsworth, 'Core saturation instability in the Kingsnorth h.v.d.c. link'. CIGRE Study Committee No 14, Winnipeg, Canada, June 20-24, 1977

21 E Rumpf and S Ranade, 'Comparison of suitable control systems for h.v.d.c. stations connected to weak a.c. systems. Part 1 - New control systems. Part 2 - Operational behaviour of the h.v.d.c. transmission'. IEEE Transactions, Vol PAS-91, 1972, pp 549-564

22 J Arrillaga and G Galanos, 'Direct digital control of h.v.d.c. converters'. IEEE Transactions, Vol PAS-89, 1970, pp 2056-2065

23 J Reeve and J A Sevcemco, 'An automatic control scheme for h.v.d.c. transmission using digital techniques. Part 1 - Principles of operation. Part 2 - Circuit considerations and performance'. IEEE Winter Power Meeting, 1972, Papers No T72 178-7 and T72 179-5

24 A Gelb and W E Vander Velde, 'Multiple-input Describing Functions and Nonlinear System Design'. McGraw-Hill, 1968

25 A Ekstrom and G Liss, 'A refined h.v.d.c. control system'. IEEE Transactions, Vol PAS-89, 1970, pp 723-732

26 J D Ainsworth, 'Harmonic instability between controlled static converters and a.c. networks'. Proc IEE, Vol 114, 1967, pp 949-957

27 F Fallside and R D Jackson, 'Direct digital control of thyristor amplifiers'. Proc IEE, Vol 116, 1969, pp 873-878

28 N L Shore and L L Freris, 'Minicomputer on-line control of d.c. link converters'. Proc IEE, Vol 125, 1978, pp 215-220

29 J Reeve and W J Giesbrecht, 'Evaluation of a microcomputer for h.v.d.c. converter control'. IEEE PES Summer Meeting, Paper A 78 550-6, 1978

30 S K Tso and P T Ho, 'Dedicated microprocessor scheme for thyristor phase control of multiphase converters'. Proc IEE, Pt B Vol 128, 1981, pp 101-108

31 Pei-Chong Tang, Shui-Shong Lu and Yung-Chun Wu, 'Microprocessor base design of a firing circuit for three-phase full wave thyristor dual converter'. IEEE Transactions, Vol IE-29, 1982, pp 67-73

32 J P Sucena-Paiva, C M Alegria and L L Freris, 'On-line microcomputer control of converter systems'. 7th PSCC Lausanne 1981, pp 454-461

33 C M Alegria, 'Microprocessor control of converters for direct current transmission'. Ph.D thesis, London 1980

34 J Reeve and W Giesbrecht, 'Microprocessor control for h.v.d.c. converters'. IEE Conference Publication 205, London 1981, pp 186-193

35 Texas Instruments '9900 Family system design'. 1st edition - Texas instruments inc, 1978

36 Analog devices 'RTI-1240/1241 User's reference manual' - Analog devices inc

37 J C West, J L Douce and R K Livesley, 'The dual input describing function and its use in the analysis of non-linear feedback systems'. Proc IEE 103-B - 1956, pp 463-473

38 D P Atherton, 'Non-linear control engineering'. Van Nostrand Reinhold, 1975

39 Solartron 'Digital transfer function analyser JM 1600' Operational Manual. Solartron Electronic Group Ltd

40 Tektronix '5L4N Spectrum Analyser' Instruction Manual. Tektronix Inc, Jan 1975

41 J P Bowles, 'The model h.v.d.c. transmission system at Imperial College'. Power System Report No 44 - Imperial College, Jan 1963

42 R Yacamini and J C de Oliveira, 'Instability in h.v.d.c. schemes at low order integer harmonics'. Proc IEE, Vol 127 Pt C No 3, May 1980, pp 179-188

43 R Yacamini and W J Smith, 'Negative sequence of converters'. Proc IEE, Vol 128 Pt B No 3, May 1981, pp 161-166

44 R Jotten et al, 'Control in h.v.d.c. systems. The state of the art. Part 1 - Two terminal systems'. Paper 14-10, CIGRE - 1978

45 A Lacoste et al 'A.c. harmonic filter and reactive compensation for h.v.d.c. - a general survey'. Electra No 63, March 1979, pp 65-102

46 R W Blasco, 'V - Mos chip joins microprocessor to handle signals in real time'. Electronics/August 30 1979, pp 131-138

47 R Jotten, 'Possibilities and limits of the control in improving the recovery after a disturbance due to an a.c. or d.c. system fault'. CIGRE SC 4, Item 12.1, Rio de Janeiro, Aug 1981

48 S M Shinners, 'Modern control system theory and application'. 2nd edition. Addison-Wesley Publishing Company, 1978

49 J M D Ferreira de Jesus, L L Freris and J P Sucena-Paiva, 'Large signal harmonic stability of converters in h.v.d.c. systems'. IEE Conference Publication No 205, London 1981, pp 129-132

50 A Antoniou, 'Digital filters: analysis and design'. McGraw-Hill, 1979

51 G Daryanany, 'Principles of active network synthesis and design'. John Wiley and Sons, 1976

52 D J Comer, 'Modern electronic circuit design'. Addison-Wesley Publishing Company, 1976

53 E W Kimbark, 'Direct current transmission - Volume 1'. Wiley Interscience, 1971

54 E Uhlmann, 'Power transmission by direct current'. Springer-Verlag, 1975

Appendix A

DATA ACQUISITION INTERFACE, HARDWARE DESIGNS

A.1 Voltage zero crossing detection

The main functions of this circuit are

1 To generate logic signals that provide information regarding the valve voltage states (i.e. whether a particular commutating voltage is positive or negative);

2 Generation of the v.z.c. interrupt signals;

3 Initiation of the firing angle measurements by reseting a counter to zero;

4 To terminate an extinction angle measurement by loading the value of a counter into a latch.

Fig A.1 shows the block diagram of this circuit.

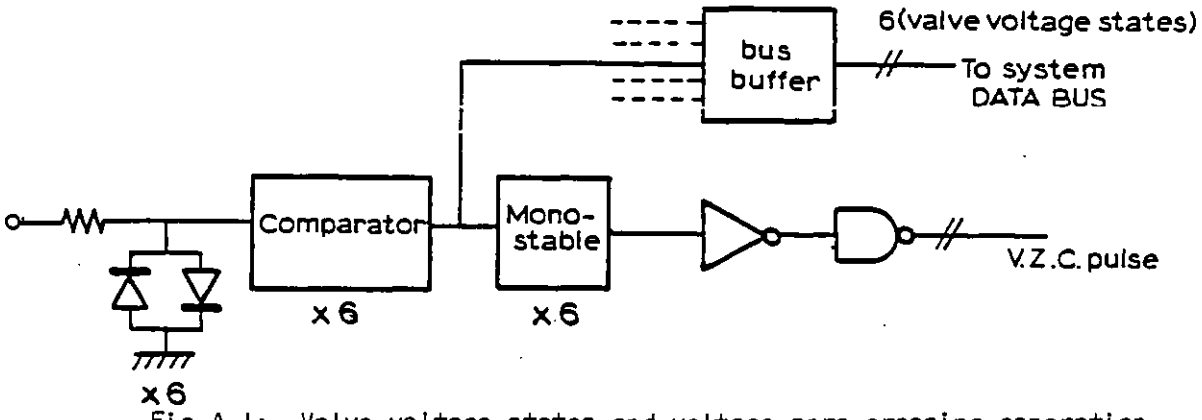

Fig A.1: Valve voltage states and voltage zero-crossing generation

A.2 Firing angle and voltage zero crossing interval measurement

The main function of this circuit is to measure the firing angle. A counter is reset every time a voltage zero crossing occurs. Thus this set-up cannot measure directly values of α greater than 60°. Firing angles greater than 60° are obtained by adding to the value of α the values of the last voltage zero crossing (if $60^{\circ} < \alpha < 120^{\circ}$) or adding the value of the last two zero crossings ($120^{\circ} < \alpha < 180^{\circ}$).

The counter used for measuring α is also used to measure the v.z.c. interval.

A register loads the value of the counter whenever a fire occurs and another register loads the value of the voltage zero crossing interval whenever a voltage zero crossing occurs.

Figure A.2 shows the block diagram.

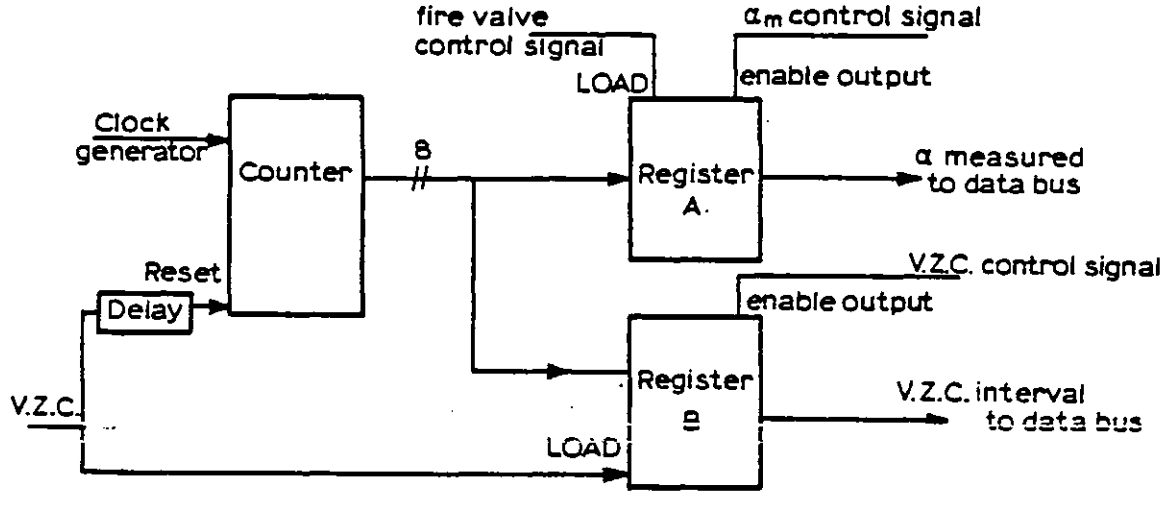

Fig A.2: Firing angle and voltage zero crossing interval measurement

A delay in the signal that resets the counter was introduced in order that the value of the voltage zero crossing interval could be stored in register B.

A.3 Current zero crossing measurement circuitry

To measure the extinction angle the knowledge of the end of valve conduction is necessary. Figure A.3 shows the block diagram of this circuit.

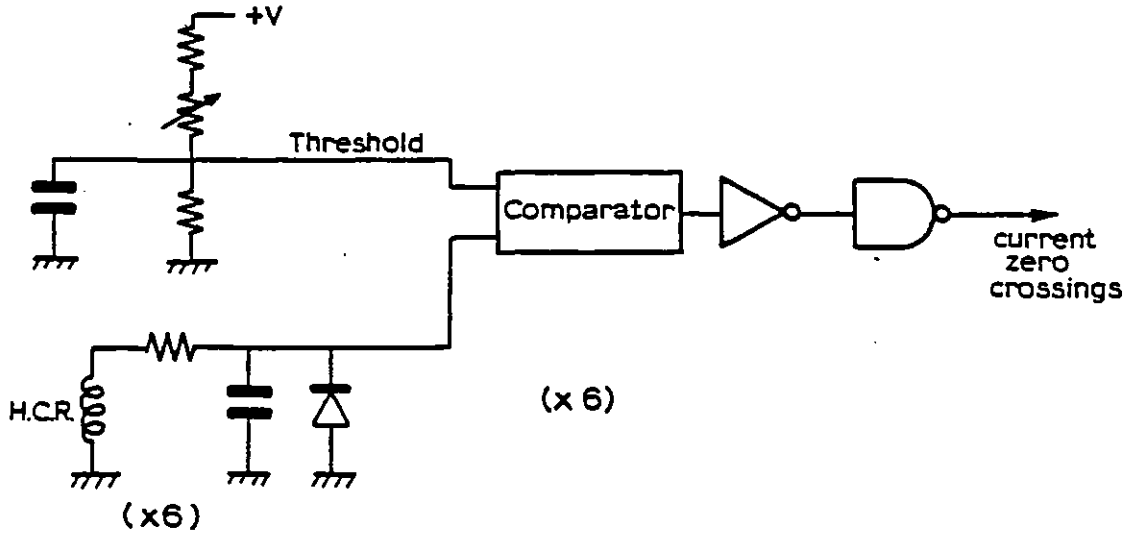

Fig A.3: Current zero crossing measurement

The detection of the valve current end of conduction is obtained through saturating toroids of H.C.R. which is a material with a narrow rectangular hysteresis loop. When the valve current falls below 10 mA the magnetisation level of the H.C.R. toroidal transformers changes, this change in

flux being detected on the signal winding of the transformer. A voltage differential comparator possessing a small positive threshold voltage amplifies this signal in order that it can be within T.T.L. voltage levels range.

The current zero crossing pulses are then processed in a way which is similar to the voltage zero crossing detection circuitry (see A.1).

A.4 Extinction angle measurement

The extinction angle is measured between the end of valve current conduction and the voltage zero crossing of the valve's commutating voltage.

The counter in figure A.4 is reset every time a current zero crossing occurs. The value in this counter is loaded into a register whenever a voltage zero crossing occurs. The extinction angle (γ) control signal enables the output of the register and the measured value of γ can then be stored into the microcomputer's memory.

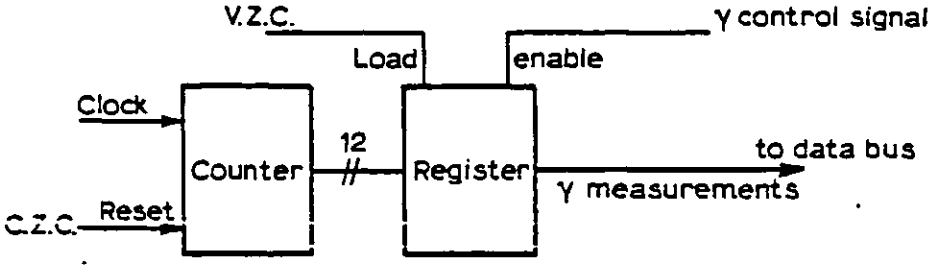

Fig A.4: Extinction angle measurement

A.5 Interfiring period measurement

This circuit is detailed in section 2.3.1.1.

A.6 Ring output latch

The software of the microcomputer based-controller sets the valve to be fired through a word of six digits which is stored into a latch. Only one of these digits is at low voltage, corresponding to the valve to be fired. Figure A.5 details the circuitry. A set of pulse transformers then apply the output signal to the gate of the appropriate thyristor.

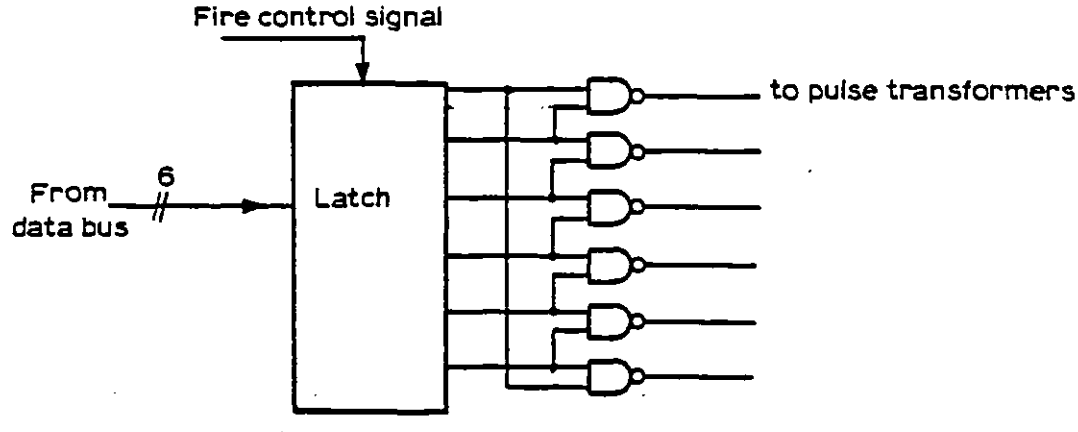

Fig A.5: Ring output latch

A.7 Phase locked-loop (PLL)

To provide the clock pulses to all measurement circuitry a phase locked-loop synchronised with the mains is used.

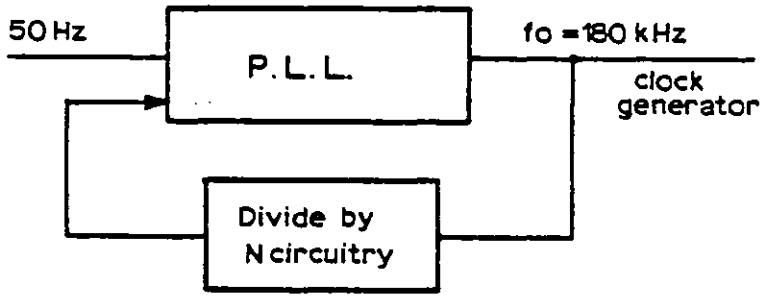

Fig A.6: Phase locked-loop

The free running frequency of the v.c.o. of the PLL is adjusted to be 180KHz (which corresponds to a 0.1^{o} definition). This signal goes through a divide by N circuitry (in the present case 3600) and the frequency of the output signal compared with the mains frequency. Any difference corresponds to a variation in the input voltage of the v.c.o. and thus an adjustment of its frequency.

A.8 Organisation of data transfer

In order that the microcomputer system may recognise the Data Acquisition Interface (DAI) as a block of words in memory, a circuitry to generate the appropriate control signals was designed. This circuitry is shown in figure A.7.

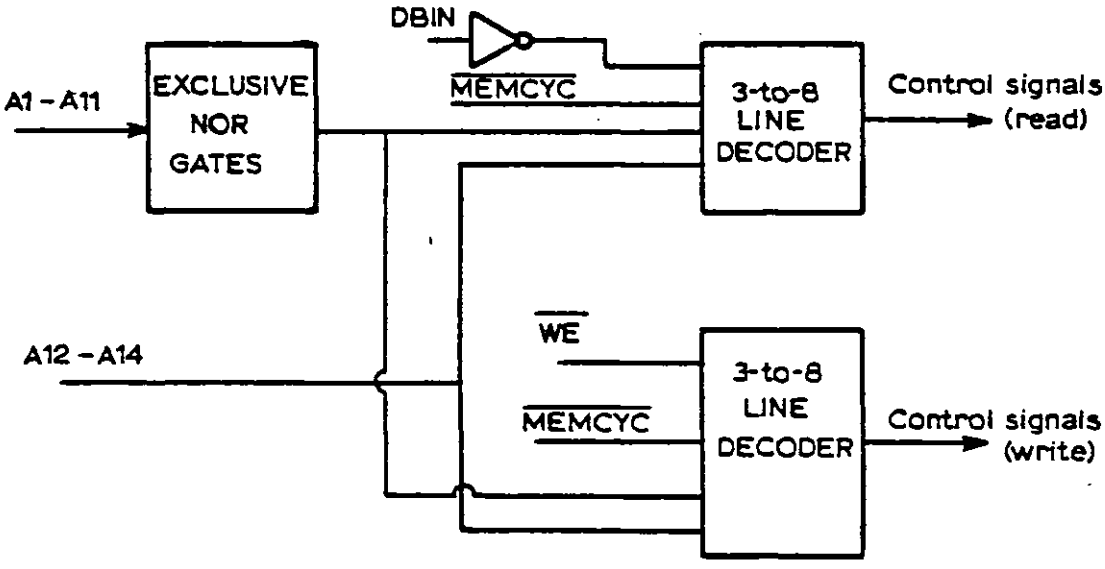

Fig A.7: Control signals generation

The 12 most significant bits of the microcomputer's address bus are processed in order to attribute to the DAI a space in memory between adress DFF0 and DFFC. Adress lines A12, A13 and A14 are processed by a 3-to-8 line decoder in order

to generate the appropriate control signal. Table A.1 shows the relationship between the adress and the control signal that enables the output of a particular register.

Hex Adress	Control signal	
DFF0	α - measurement	
DFF2	γ - measurement	Read
DFF4	v.z.c. interval	Control
DFF6	IFP (real)	Signals
DFF8	Valve voltage states	
DFFA	IFP (computed)	Write control
DFFC	Fire valve	Signals

Table A.1: control signals

Signals DBIN (Data bus input), MEMCYC (memory cycle) and WE (write enable) from the microcomputer are used to enable the appropriate decoder (Read or Write control signals).

A.9 Interrupt module

As stated in section 2.3.1.2, three levels of interrupt exist. The interrupt associated with the end-of-conversion of the A/D converter is internally generated in the RTI 1241-R.

Both the interrupt associated with the firing of a valve (which has the highest priority) and with the v.z.c. interval (which has the lowest priority) are processed in a similar way.

A dual D-type positive edge triggered flip flop with preset and clear changes the output state whenever the interrupt signal is generated, and is reset whenever the interrupt is to be cleared.

For the interrupt that generates the firing pulses, the flip-flop is set when the signal B > A of figure 2.4(a) goes high and reset when the valve actually fires.

For the lowest priority interrupt, the flip-flop is set when the v.z.c. signal goes active, and reset when the v.z.c. interval is stored into the microcomputer's memory.

Appendix B

CALCULATION OF THE COMMUTATION CURRENT

The commutation current in an incoming valve 'i' can be calculated by integration of differential equation (3.54) with the initial condition $i_i = 0$. The application of Laplace transforms yields

$$(sL_{io} + R_{io})I_i(s) = \sum_{h=1}^{P}\left[\frac{h\omega_o S_h}{s^2+(h\omega_o)^2} + \frac{sC_h}{s^2+(h\omega_o)^2}\right] + R_o\frac{I_d}{s}$$

$$+\sum_{\ell=1}^{n_d}\frac{\ell\omega_o A_\ell}{s^2+(\ell\omega_o)^2} + \frac{sB_\ell}{s^2+(\ell\omega_o)^2} \qquad (B.1)$$

Defining

$$x_h = h\omega_o\frac{S_h}{C_h} \qquad (B.2)$$

$$y_\ell = \ell\omega_o\frac{A_\ell}{B_\ell} \qquad (B.3)$$

$$T_{io} = \frac{L_{io}}{R_{io}} \qquad (B.4)$$

and substituting into equation (B.1) one obtains

$$I_i(s) = \sum_{h=1}^{P} \left[\frac{C_h}{L_{io}} \frac{s+x_h}{(s+1/T_{io})(s^2+(h\omega_o)^2)} \right] + \frac{R_o}{L_{io}} \frac{I_d}{s(s+1/T_{io})}$$

$$+ \sum_{\ell=1}^{n_d} \left[\frac{B_\ell}{L_{io}} \frac{s+y_\ell}{(s+1/T_{io})(s^2+(\ell\omega_o)^2)} \right] \qquad (B.5)$$

To obtain $i_i(t)$ the inverse Laplace transform must be calculated, yielding:

$$i_i(t) = \sum_{h=1}^{P} \frac{C_h}{L_{io}} \left[\frac{x_h - 1/T_{io}}{1/T_{io}^2+(h\omega_o)^2} e^{-t/T_{io}} \right.$$

$$\left. + \frac{1}{h\omega_o} \sqrt{\frac{y_h^2+(h\omega_o)^2}{1/T_{io}^2+(h\omega_o)^2}} \sin(h\omega_o t + \phi_{1h}) \right]$$

$$+ \frac{R_o}{R_{io}} I_d(1-e^{-t/T_{io}}) + \sum_{\ell=1}^{n_d} \frac{B_\ell}{L_{io}} \left[\frac{y_\ell - 1/T_{io}}{1/T_{io}^2+(\ell\omega_o)^2} e^{-t/T_{io}} \right.$$

$$\left. + \frac{1}{\ell\omega_o} \sqrt{\frac{y_\ell^2+(\ell\omega_o)^2}{1/T_{io}^2+(\ell\omega_o)^2}} \sin(\ell\omega_o t + \phi_{2\ell}) \right] \qquad (B.6)$$

where

$$\phi_{1h} = \tan^{-1} \left[\frac{(1/T_{io}-x_h)h\omega_o}{(h\omega_o)^2+x_h/T_{io}} \right] \qquad (B.7)$$

$$\phi_{2\ell} = \tan^{-1} \left[\frac{(1/T_{io}-y_\ell)\ell\omega_o}{(\ell\omega_o)^2+y_\ell/T_{io}} \right] \qquad (B.8)$$

The following constants are now defined

$$Z_h = \frac{1}{(h\omega_o)^2 + 1/T_{io}^2} \tag{B.9}$$

$$Z_\ell = \frac{1}{(\ell\omega_o)^2 + 1/T_{io}^2} \tag{B.10}$$

$$S_{1h} = \frac{C_h}{h\omega_o L_{io}} \sqrt{Z_h \left[x_h^2 + (h\omega_o)^2\right]} \tag{B.11}$$

$$S_{2\ell} = \frac{B}{\ell\omega_o L_{io}} \sqrt{Z_\ell \left[y_\ell^2 + (\ell\omega_o)^2\right]} \tag{B.12}$$

$$x_{1h} = \frac{G_h}{L_{io}} \left(x_h - \frac{1}{T_{io}}\right) Z_h \tag{B.13}$$

$$x_{2\ell} = \frac{B_\ell}{L_{io}} \left(y_\ell - \frac{1}{T_{io}}\right) Z_\ell \tag{B.14}$$

$$y_1 = \frac{R_o}{R_{io}} I_d \tag{B.15}$$

Substitution of equations (B.9) to (B.15) into equation (B.6) yields

$$i_1(t) = \sum_{h=1}^{P} \left[x_{1h} e^{-t/T_{io}} + S_{1h} \sin(h\omega_o t + \phi_{1h})\right] + y_1(1 - e^{-t/T_{io}}) + \sum_{\ell=1}^{n_d} \left[x_{2\ell} e^{-t/T_{io}} + S_{2\ell} \sin(\ell\omega_o t + \phi_{2\ell})\right] \tag{B.16}$$

Appendix C

CALCULATION OF THE EULER COEFFICIENTS

In this Appendix the Euler coefficients of the Fourier series expansion of certain types of periodic functions which appear in the mathematical description of the inverter d.c. voltage and a.c. current are calculated.

As is well known, a periodic function $f(t)$ with period $2T$ can be expanded in Fourier series as

$$f(t) = \frac{A_o}{2} + \sum_{n=1}^{\infty} A_n \cos n\omega_o t + \sum_{n=1}^{\infty} B_n \sin n\omega_o t \qquad (C.1)$$

where $\omega_o = \pi/T$ and A_n and B_n, the Euler coefficients, are given by

$$A_n = \frac{\omega_o}{T} \int_0^{2T} f(t) \cos n\omega_o t \, dt \qquad n = 0, 1, \ldots, \qquad (C.2)$$

$$B_n = \frac{\omega_o}{T} \int_0^{2T} f(t) \sin n\omega_o t \, dt \qquad n = 1, 2, \ldots, \qquad (C.3)$$

C.1 Assume that function $f(t)$ is

$$f(t) = A \cos k\omega_o t \tag{C.4}$$

The Euler coefficients are given by:

i) $n = 0$

$$A_n = \frac{\omega_o}{T}\int_0^{2\pi} A \cos k\omega_o t \, dt$$

$$= \frac{A}{kT}\left[\sin k\omega_o t\right]_0^{2T} \tag{C.5}$$

B_n is not defined in this case.

ii) $n \neq k$

$$A_n = \frac{\omega_o}{T}\int_0^{2T} A \cos k\omega_o t \cos n\omega_o t \, dt$$

$$= \frac{A\omega_o}{T}\left[\frac{\sin(k\omega_o+n\omega_o)t}{2(k\omega_o+n\omega_o)} + \frac{\sin(k\omega_o-n\omega_o)t}{2(k\omega_o-n\omega_o)}\right]_0^{2T} \tag{C.6}$$

$$B_n = \frac{\omega_o}{T}\int_0^{2T} A \cos k\omega_o t \sin n\omega_o t \, dt$$

$$= \frac{A\omega_o}{T}\left[-\frac{\cos(k\omega_o+n\omega_o)t}{2(k\omega_o+n\omega_o)} + \frac{\cos(k\omega_o-n\omega_o)t}{2(k\omega_o-n\omega_o)}\right]_0^{2T} \tag{C.7}$$

iii) $n = k$

$$A_n = \frac{\omega_o}{T}\int_0^{2T} A \cos^2 n\omega_o t \, dt$$

$$= \frac{A\omega_o}{T}\left[\frac{t}{2} + \frac{\sin 2n\omega_o t}{4n\omega_o}\right]_0^{2T} \tag{C.8}$$

$$B_n = \frac{\omega_o}{T}\int_0^{2T} A \cos n\omega_o t \sin n\omega_o t \, dt$$

$$= \frac{A\omega_o}{T}\left[-\frac{\cos 2n\omega_o t}{4n\omega_o}\right]_0^{2T} \qquad (C.9)$$

C.2 Assume that function f(t) is

$$f(t) = A \sin k\omega_o t \qquad (C.10)$$

The Euler coefficients are given by:

i) $n = 0$

$$A_o = \frac{\omega_o}{T}\int_0^{2\pi} A \sin k\omega_o t \, dt$$

$$= \frac{A}{kT}\left[-\cos k\omega_o t\right]_0^{2T} \qquad (C.11)$$

ii) $n \neq k$

$$A_n = \frac{\omega_o}{T}\int_0^{2T} A \sin k\omega_o t \cos n\omega_o t \, dt$$

$$= \frac{A\omega_o}{T}\left[-\frac{\cos(k\omega_o+n\omega_o)t}{2(k\omega_o+n\omega_o)} - \frac{\cos(k\omega_o-n\omega_o)t}{2(k\omega_o-n\omega_o)}\right]_0^{2T} \qquad (C.12)$$

$$B_n = \frac{\omega_o}{T}\int_0^{2T} A \sin k\omega_o t \sin n\omega_o t \, dt$$

$$= \frac{A\omega_o}{T}\left[-\frac{\sin(k\omega_o+n\omega_o)t}{2(k\omega_o+n\omega_o)} + \frac{\sin(k\omega_o-n\omega_o)t}{2(k\omega_o-n\omega_o)}\right]_0^{2T} \qquad (C.13)$$

iii) $n = k$

$$A_n = \frac{\omega_o}{T}\int_0^{2T} A \sin n\omega_o t \cos n\omega_o t \, dt$$

$$= \frac{A\omega_o}{T}\left[-\frac{\cos 2n\omega_o t}{4n\omega_o}\right]_0^{2T} \qquad (C.14)$$

$$B_n = \frac{\omega_o}{T}\int_0^{2T} A \sin^2 n\omega_o t \, dt$$

$$= \frac{A\omega_o}{T}\left[\frac{t}{2} - \frac{\sin 2n\omega_o t}{4n\omega_o}\right]_0^{2T} \qquad (C.15)$$

C.3 Assume finally that function $f(t)$ is

$$f(t) = A\, e^{-(t-t_x)/T_i} \qquad (C.16)$$

The Euler coefficients are given by:

i) $n = 0$

$$A_o = \frac{\omega_o}{T}\int_0^{2T} A\, e^{-(t-t_x)/T_i} \, dt$$

$$= \frac{A\omega_o}{T}\left[-T_i\, e^{-(t-t_x)/T_i}\right]_0^{2T} \qquad (C.17)$$

ii) $n \neq 0$

$$A_n = \frac{\omega_o}{T}\int_0^{2T} A\, e^{-(t-t_x)/T_i} \cos n\omega_o t \, dt$$

$$= \frac{A\omega_o}{T}\left[\frac{e^{-(t-t_x)/T_i}}{(n\omega_o)^2+1/T_i^2}\left(n\omega_o \sin n\omega_o t - \frac{1}{T_i}\cos n\omega_o t\right)\right]_0^{2T}$$

(C.18)

$$B_n = \frac{\omega_o}{T}\int_0^{2T} A\, e^{-(t-t_x)/T_i} \sin n\omega_o t\, dt$$

$$= \frac{A\omega_o}{T}\left[\frac{e^{-(t-t_x)/T_i}}{(n\omega_o)^2+1/T_i^2}\left(-\frac{1}{T_i}\sin n\omega_o t - n\omega_o \cos n\omega_o t\right)\right]_0^{2T}$$

(C.19)

Appendix D

EVALUATION OF THE D.C. VOLTAGE EULER COEFFICIENTS

By using equations (C.5) to (C.19) of Appendix C, the following results are obtained.

A - Integral (4.55)

A.1 - $n = 0$

$$\int_{t_a}^{t_b} V_{ik}\, dt = \left[\sum_{h=1}^{P} \left(- \frac{S_h}{h\omega_o} \cos h\omega_o t \right) + \sum_{h=1}^{P} \left(\frac{C_h}{h\omega_o} \sin h\omega_o t \right) \right]_{t_a}^{t_b} \qquad (D.1)$$

A.2 - $n \neq 0$

$$\int_{t_a}^{t_b} V_{ik} \cos n\omega_o t\, dt = \sum_{h=1}^{n-1} CO_h + CO + \sum_{h=n+1}^{P} CO_h \qquad (D.2)$$

where

$$CO_h = \left[-S_h \left(\frac{\cos(h\omega_o + n\omega_o)t}{2(h\omega_o + n\omega_o)} + \frac{\cos(h\omega_o - n\omega_o)t}{2(h\omega_o - n\omega_o)} \right) + C_h \left(\frac{\sin(h\omega_o + n\omega_o)t}{2(h\omega_o + n\omega_o)} + \frac{\sin(h\omega_o - n\omega_o)t}{2(h\omega_o - n\omega_o)} \right) \right]_{t_a}^{t_b} \quad (D.3)$$

and

$$CO = \left[S_n \left(- \frac{\cos 2n\omega_o t}{4n\omega_o} \right) + C_n \left(\frac{t}{2} + \frac{\sin 2n\omega_o t}{4n\omega_o} \right) \right]_{t_a}^{t_b} \quad (D.4)$$

B - Integral (4.56)

$$\int_{t_a}^{t_b} V_{ik} \sin n\omega_o t \, dt = \sum_{h=1}^{n-1} SI_h + SI + \sum_{h=n+1}^{P} SI_h \quad (D.5)$$

where

$$SI_h = \left[S_h \left(- \frac{\sin(h\omega_o + n\omega_o)t}{2(h\omega_o + n\omega_o)} + \frac{\sin(h\omega_o - n\omega_o)t}{2(h\omega_o - n\omega_o)} \right) + C_h \left(- \frac{\cos(h\omega_o + n\omega_o)t}{2(h\omega_o + n\omega_o)} + \frac{\cos(h\omega_o - n\omega_o)t}{2(h\omega_o - n\omega_o)} \right) \right]_{t_a}^{t_b} \quad (D.6)$$

and

$$SI = \left[S_n \left(\frac{t}{2} - \frac{\sin 2n\omega_o t}{4n\omega_o} \right) - C_n \frac{\cos 2n\omega_o t}{4n\omega_o} \right]_{t_a}^{t_b} \quad (D.7)$$

C - Integral (4.57)

C.1 - $n = 0$

$$\int_{t_a}^{t_b} V_{ic}\, dt = -WT'_{io}\left[e^{-(t-t_x)/T'_{io}}\right]_{t_a}^{t_b} + \left[\sum_{h=1}^{P} \frac{M_{ih}}{h\omega_o} \sin h\,\omega_o t\right]_{t_a}^{t_b} - \left[\sum_{h=1}^{P} \frac{N_{ih}}{h\omega_o} \cos h\,\omega_o t\right]_{t_a}^{t_b} + \left[\sum_{\ell=1}^{n_d} \frac{M_{2\ell}}{\ell\omega_o} \sin \ell\omega_o t\right]_{t_a}^{t_b} - \left[\sum_{\ell=1}^{n_d} \frac{N_{2\ell}}{\ell\omega_o} \cos \ell\omega_o t\right]_{t_a}^{t_b} + \left[K_i t\right]_{t_a}^{t_b} \qquad (D.8)$$

C.2 - $n \neq 0$

$$\int_{t_a}^{t_b} V_{ic} \cos n\,\omega_o t\, dt = CO1 + \sum_{h=1}^{n-1} CO2_h + CO_2 + \sum_{h=n+1}^{P} CO2_h + \sum_{\ell=1}^{n-1} CO3_\ell + CO3 + \sum_{\ell=n+1}^{n_d} CO3_\ell + CO4 \qquad (D.9)$$

where

$$CO1 = \left[\frac{W}{(n\omega_o)^2 + 1/T'^2_{io}}\, e^{-(t-t_x)/T'_{io}}\left(n\omega_o \sin n\omega_o t - \frac{1}{T'_{io}} \cos n\omega_o t\right)\right]_{t_a}^{t_b} \qquad (D.10)$$

$$CO2_h = \left[M_{1h} \left(\frac{\sin(h\omega_o + n\omega_o)t}{2(h\omega_o + n\omega_o)} + \frac{\sin(h\omega_o - n\omega_o)t}{2(h\omega_o - n\omega_o)} \right) - N_{1h} \left(\frac{\cos(h\omega_o + n\omega_o)t}{2(h\omega_o + n\omega_o)} + \frac{\cos(h\omega_o - n\omega_o)t}{2(h\omega_o - n\omega_o)} \right) \right]_{t_a}^{t_b} \quad (D.11)$$

$$CO2 = \left[M_{1n} \left(\frac{t}{2} + \frac{\sin 2n\omega_o t}{4n\omega_o} \right) - N_{1n} \frac{\cos 2n\omega_o t}{4n\omega_o} \right]_{t_a}^{t_b} \quad (D.12)$$

$$CO3_\ell = \left[M_{2\ell} \left(\frac{\sin(\ell\omega_o + n\omega_o)t}{2(\ell\omega_o + n\omega_o)} + \frac{\sin(\ell\omega_o - n\omega_o)t}{2(\ell\omega_o - n\omega_o)} \right) - N_{2\ell} \left(\frac{\cos(\ell\omega_o + n\omega_o)t}{2(\ell\omega_o + n\omega_o)} + \frac{\cos(\ell\omega_o - n\omega_o)t}{2(\ell\omega_o - n\omega_o)} \right) \right]_{t_a}^{t_b} \quad (D.13)$$

$$CO3 = \left[M_{2n} \left(\frac{t}{2} + \frac{\sin 2n\omega_o t}{4n\omega_o t} \right) - N_{2n} \frac{\cos 2n\omega_o t}{4n\omega_o t} \right]_{t_a}^{t_b} \quad (D.14)$$

$$CO4 = \frac{K_i}{n\omega_o} \left[\sin n\omega_o t \right]_{t_a}^{t_b} \quad (D.15)$$

D - Integral (4.58)

$$\int_{t_a}^{t_b} V_{ic} \sin n\omega_o t \, dt = SI1 + \sum_{h=1}^{n-1} SI2_h + SI2 + \sum_{h=n+1}^{P} SI2_h$$

$$+ \sum_{\ell=1}^{n-1} SI3_{\ell} + SI3 + \sum_{\ell=n+1}^{n_d} SI3_{\ell} + SI_4 \qquad (D.16)$$

where

$$SI1 = \left[\frac{W}{(n\omega_o)^2 + 1/T'^2_{io}} e^{-(t-t_x)/T'_{io}} + \left(-\frac{1}{T'_{io}} \sin n\omega_o t - n\omega_o \cos n\omega_o t \right) \right]_{t_a}^{t_b} \qquad (D.17)$$

$$SI2_h = \left[-M_{Ih} \left(\frac{\cos(h\omega_o + n\omega_o)t}{2(h\omega_o + n\omega_o)} - \frac{\cos(h\omega_o - n\omega_o)t}{2(h\omega_o + n\omega_o)} \right) + N_{Ih} \left(\frac{\sin(h\omega_o + n\omega_o)t}{2(h\omega_o + n\omega_o)} - \frac{\sin(h\omega_o - n\omega_o)t}{2(h\omega_o + n\omega_o)} \right) \right]_{t_a}^{t_b} \qquad (D.18)$$

$$SI2 = \left[-M_{In} \frac{\cos 2n\omega_o t}{4n\omega_o} + N_{In} \left(\frac{t}{2} - \frac{\sin 2n\omega_o t}{4n\omega_o} \right) \right]_{t_a}^{t_b} \qquad (D.19)$$

$$SI3_{\ell} = \left[-M_{2\ell} \left(\frac{\cos(\ell\omega_o + n\omega_o)t}{2(\ell\omega_o + n\omega_o)} - \frac{\cos(\ell\omega_o - n\omega_o)t}{2(\ell\omega_o - n\omega_o)} \right) + N_{2\ell} \left(\frac{\sin(\ell\omega_o + n\omega_o)t}{2(\ell\omega_o + n\omega_o)} - \frac{\sin(\ell\omega_o - n\omega_o)t}{2(\ell\omega_o - n\omega_o)} \right) \right]_{t_a}^{t_b} \qquad (D.20)$$

$$SI3 = \left[-M_{2n} \frac{\cos 2n\omega_o t}{4n\omega_o} + N_{2n} \left(\frac{t}{2} - \frac{\sin 2n\omega_o t}{4n\omega_o} \right) \right]_{t_a}^{t_b} \qquad (D.21)$$

$$SI4 = \frac{K_i}{n\omega_o}\left[-\cos n\,\omega_o t\right]_{t_a}^{t_b} \qquad (D.22)$$

E - Integral (4.69)

E.1 - n = 0

$$\int_{t_a}^{t_b} V_{kd}\,dt = \left[R_k I_d t\right]_{t_a}^{t_b} + \left[\sum_{\ell=1}^{n_d}\left(-\frac{R_k F_\ell - \omega_o L_k G_\ell}{\ell\omega_o}\right)\cos \ell\omega_o t + \frac{R_k G_\ell + \ell\omega_o L_k F_\ell}{\ell\omega_o}\sin \ell\omega_o t\right]_{t_a}^{t_b} \qquad (D.23)$$

E.2 - n ≠ 0

$$\int_{t_a}^{t_b} V_{kd}\cos n\,\omega_o t\,dt = COI + \sum_{\ell=1}^{n-1} CO2_\ell + CO2 + \sum_{\ell=n+1}^{n_d} CO2_\ell \qquad (D.24)$$

where

$$COI = \frac{R_k I_d}{n\,\omega_o}\left[\sin n\,\omega_o t\right]_{t_a}^{t_b} \qquad (D.25)$$

$$CO2_\ell = \left[(R_k F_\ell - \ell\omega_o L_k G_\ell)\left(\frac{\sin(\ell\omega_o + n\omega_o)t}{2(\ell\omega_o + n\omega_o)} + \frac{\sin(\ell\omega_o - n\omega_o)t}{2(\ell\omega_o - n\omega_o)}\right)\right.$$

$$\left. - (R_k G_\ell + \ell\omega_o L_k F_\ell)\left(\frac{\cos(\ell\omega_o + n\omega_o)t}{2(\ell\omega_o + n\omega_o)} + \frac{\cos(\ell\omega_o - n\omega_o)t}{2(\ell\omega_o - n\omega_o)}\right)\right]_{t_a}^{t_b} \qquad (D.26)$$

$$CO2 = \left[(R_k G_\ell + n\omega_o L_k F_\ell)\left(\frac{t}{2} + \frac{\sin 2n\omega_o t}{4n\omega_o}\right) - (R_k F_\ell - n\omega_o L_k G_\ell)\frac{\cos 2n\omega_o t}{4n\omega_o}\right]_{t_a}^{t_b} \quad (D.27)$$

F - Integral (4.40)

$$\int_{t_a}^{t_b} V_{kd} \sin n\omega_o t\, dt = SI1 + \sum_{\ell=1}^{n-1} SI2_\ell + SI2 + \sum_{\ell=n+1}^{n_d} SI2_\ell \quad (D.28)$$

where

$$SI1 = \frac{R_k I_d}{n\omega_o}\left[-\cos n\omega_o t\right]_{t_a}^{t_b} \quad (D.29)$$

$$SI2_\ell = \left[(R_k F_\ell - \ell\omega_o L_k G_\ell)\left(\frac{\sin \ell\omega_o - n\omega_o)t}{2(\ell\omega_o - n\omega_o)} - \frac{\sin(\ell\omega_o + n\omega_o)t}{2(\ell\omega_o - n\omega_o)}\right) + (R_k G_\ell + \omega_o L_k F_\ell)\left(\frac{\cos(\ell\omega_o - n\omega_o)t}{2(\ell\omega_o - n\omega_o)} + \frac{\cos(\ell\omega_o + n\omega_o)t}{2(\ell\omega_o - n\omega_o)}\right)\right]_{t_a}^{t_b} \quad (D.30)$$

$$SI2 = \left[(R_k F_\ell - n\omega_o L_k G_\ell)\left(\frac{t}{2} - \frac{\sin 2n\omega_o t}{4n\omega_o}\right) - (R_k G_\ell - n\omega_o L_k F_\ell)\frac{\cos 2n\omega_o t}{4n\omega_o}\right]_{t_a}^{t_b} \quad (D.31)$$

Appendix E

EVALUATION OF A.C. CURRENT EULER COEFFICIENTS

A - Integral (4.73)

A.1 - n = 0

$$\int_{t_a}^{t_b} i_i \, dt = \sum_{h=1}^{P} \left[-T_{io} X_{ih} \, e^{-(t-t_x)/T_{io}} - \frac{S_{1h}}{h\omega_o} \cos(h\omega_o t + \phi_{1h} - h\theta_x) \right]_{t_a}^{t_b}$$

$$+ Y_1 \left[t + T_{io} \, e^{-(t-t_x)/T_{io}} \right]_{t_a}^{t_b} + \sum_{\ell=1}^{n_d} \left[-T_{io} X_{2h} \, e^{-(t-t_x)/T_{io}} \right.$$

$$\left. - \frac{S_{2h}}{\ell\omega_o} \cos(\ell\omega_o t + \phi_{2\ell} - \ell\theta_x) \right]_{t_a}^{t_b} \qquad \text{(E.1)}$$

A.2 - n ≠ 0

$$\int_{t_a}^{t_b} i_i \cos n\omega_o t = \sum_{h=1}^{n-1} COI_h + COI + \sum_{h=n+1}^{P} COI_h$$

$$+ \sum_{\ell=1}^{n-1} CO2_\ell + CO2 + \sum_{\ell=n+1}^{n_d} CO2_\ell + CO3 \qquad (E.2)$$

where

$$CO1_h = \left[\frac{X_{1h}\, e^{-(t-t_x)/T_{io}}}{(n\omega_o)^2 + 1/T_{io}^2} \left(n\omega_o \sin n\omega_o t - \frac{1}{T_{io}} \cos n\omega_o t \right) \right]_{t_a}^{t_b}$$

$$+ S_{1h} \cos(\phi_{1h} - h\theta_x) \left[- \frac{\cos(h\omega_o + n\omega_o)t}{2(h\omega_o + n\omega_o)} - \frac{\cos(h\omega_o - n\omega_o)t}{2(h\omega_o - n\omega_o)} \right]_{t_a}^{t_b}$$

$$+ S_{1h} \sin(\phi_{1h} - h\theta_x) \left[\frac{\sin(h\omega_o + n\omega_o)t}{2(h\omega_o + n\omega_o)} + \frac{\sin(h\omega_o - n\omega_o)t}{2(h\omega_o - n\omega_o)} \right]_{t_a}^{t_b}$$

(E.3)

$$CO1 = \left[\frac{X_{1h}\, e^{-(t-t_x)/T_{io}}}{(h\omega_o)^2 + 1/T_{io}^2} \left(h\omega_o \sin h\omega_o t - \frac{1}{T_{io}} \cos h\omega_o t \right) \right]_{t_a}^{t_b}$$

$$+ S_{1h} \left[- \frac{\cos(\phi_{1h} - h\theta_x)}{4h\omega_o} \cos 2h\omega_o t + \frac{t}{2} \sin(\phi_{1h} - h\theta_x) \right.$$

$$\left. + \frac{\sin(\phi_{1h} - h\theta_x)}{4h\omega_o} \sin 2h\omega_o t \right]_{t_a}^{t_b} \qquad (E.4)$$

$$CO3 = Y_1 \left[\frac{\sin n\omega_o t}{n\omega_o} \right]_{t_a}^{t_b} - Y_1 \left[\frac{e^{-(t-t_x)/T_{io}}}{(n\omega_o)^2 + 1/T_{io}^2} \left(n\omega_o \sin n\omega_o t - \right. \right.$$

$$\left. \left. \frac{1}{T_{io}} \cos n\omega_o t \right) \right]_{t_a}^{t_b} \qquad (E.5)$$

$$CO_{2\ell} = \left[\frac{X_{2\ell}\, e^{-(t-t_x)/T_{io}}}{(\ell\omega_o)^2 + 1/T_{io}^2} \left(n\omega_o \sin n\omega_o t - \frac{1}{T_{io}} \cos n\omega_o t \right) \right]_{t_a}^{t_b}$$

$$+ S_{2\ell} \cos(\phi_{2\ell} - \ell\theta_x) \left[- \frac{\cos(\ell\omega_o + n\omega_o)t}{2(\ell\omega_o + n\omega_o)} - \frac{\cos(\ell\omega_o - n\omega_o)t}{2(\ell\omega_o - n\omega_o)} \right]_{t_a}^{t_b}$$

$$+ S_{2\ell} \sin(\phi_{2\ell} - \ell\theta_x) \left[\frac{\sin(\ell\omega_o + n\omega_o)t}{2(\ell\omega_o + n\omega_o)} + \frac{\sin(\ell\omega_o - n\omega_o)t}{2(\ell\omega_o - n\omega_o)} \right]_{t_a}^{t_b}$$

(E.6)

$$CO2 = \left[\frac{X_{2\ell}\, e^{-(t-t_x)/T_{io}}}{(\ell\omega_o)^2 + 1/T_{io}^2} \left(\ell\omega_o \sin \ell\omega_o t - \frac{1}{T_{io}} \cos \ell\omega_o t \right) \right]_{t_a}^{t_b}$$

$$+ S_{2\ell} \left[- \frac{\cos(\phi_{2\ell} - \ell\theta_x)}{4\ell\omega_o} \cos 2\ell\omega_o t + \frac{t}{2} \sin(\phi_{2\ell} - \ell\theta_x) \right.$$

$$\left. + \frac{\sin(\phi_{2\ell} - \ell\theta_x)}{4\ell\omega_o} \sin 2\ell\omega_o t \right]_{t_a}^{t_b} \qquad \text{(E.7)}$$

B - Integral (4.74)

$$\int_{t_a}^{t_b} i_i(t) \sin n\omega_o t = \sum_{h=1}^{n-1} SII_h + SII + \sum_{h=n+1}^{P} SII_h$$

$$+ \sum_{\ell=1}^{n-1} SI2_\ell + SI2 + \sum_{\ell=n+1}^{n_d} SI2_\ell + SI3 \qquad \text{(E.8)}$$

where

$$SII_h = \left[\frac{X_{Ih}\, e^{-(t-t_x)/T_{io}}}{(n\omega_o)^2 + 1/T_{io}^2} \left(-n\omega_o \cos n\omega_o t - \frac{1}{T_{io}} \sin n\omega_o t\right) \right]_{t_a}^{t_b}$$

$$+ S_{Ih} \cos(\phi_{Ih} - h\theta_x) \left[- \frac{\sin(h\omega_o + n\omega_o)t}{2(h\omega_o + n\omega_o)} + \frac{\sin(h\omega_o - n\omega_o)t}{2(h\omega_o - n\omega_o)} \right]_{t_a}^{t_b}$$

$$+ S_{Ih} \sin(\phi_{Ih} - h\theta_x) \left[- \frac{\cos(h\omega_o + n\omega_o)t}{2(h\omega_o + n\omega_o)} + \frac{\cos(h\omega_o - n\omega_o)t}{2(h\omega_o - n\omega_o)} \right]_{t_a}^{t_b}$$

(E.9)

$$SII = \left[\frac{X_{Ih}\, e^{-(t-t_x)/T_{io}}}{(h\omega_o)^2 + 1/T_{io}^2} \left(-h\omega_o \cos h\omega_o t - \frac{1}{T_{io}} \sin h\omega_o t\right) \right]_{t_a}^{t_b}$$

$$+ S_{Ih} \left[- \frac{\sin(\phi_{Ih} - h\theta_x)}{4h\omega_o} \cos 2h\omega_o t + \frac{t}{2} \cos(\phi_{Ih} - h\theta_x) - \right.$$

$$\left. - \frac{\cos(\phi_{Ih} - h\theta_x)}{4h\omega_o} \sin 2h\omega_o t \right]_{t_a}^{t_b}$$

(E.10)

$$SI2_\ell = \left[\frac{X_{2\ell}\, e^{-(t-t_x)/T_{io}}}{(n\omega_o)^2 + 1/T_{io}^2} \left(-n\omega_o \cos n\omega_o t - \frac{1}{T_{io}} \sin n\omega_o t\right) \right]_{t_a}^{t_b}$$

$$+ S_{2\ell} \cos(\phi_{2\ell} - \ell\theta_x) \left[- \frac{\sin(\ell\omega_o + n\omega_o)t}{2(\ell\omega_o + n\omega_o)} + \frac{\sin(\ell\omega_o - n\omega_o)t}{2(\ell\omega_o - n\omega_o)} \right]_{t_a}^{t_b}$$

$$+ S_{2\ell} \cos(\phi_{2\ell} - \ell\theta_x) \left[- \frac{\cos(\ell\omega_o + n\omega_o)t}{2(\ell\omega_o + n\omega_o)} + \frac{\cos(\ell\omega_o - n\omega_o)t}{2(\ell\omega_o - n\omega_o)} \right]_{t_a}^{t_b}$$

(E.11)

$$SI2 = \left[\frac{X_{2\ell}\, e^{-(t-t_x)/T_{io}}}{(\ell\omega_o)^2 + 1/T_{io}^2} \left(-\ell\omega_o \cos \ell\omega_o t - \frac{1}{T_{io}} \sin \ell\omega_o t\right) \right]_{t_a}^{t_b}$$

$$+ S_{2\ell} \left[- \frac{\sin(\phi_{2\ell} - \ell\theta_x)}{4\,\ell\omega_o} \cos 2\,\ell\omega_o t + \frac{t}{2} \cos(\phi_{2\ell} - \ell\theta_x) \right.$$

$$\left. - \frac{\cos(\phi_{2\ell} - \ell\theta_x)}{4\,\ell\omega_o} \sin 2\,\ell\omega_o t \right]_{t_a}^{t_b} \qquad \text{(E.12)}$$

$$SI3 = - \frac{Y_l}{n\omega_o} \left[\cos n\omega_o t\right]_{t_a}^{t_b} + \frac{Y_l}{(n\omega_o)^2 + 1/T_{io}^2} \left[e^{-(t-t_x)/T_{io}} \right.$$

$$\left. (n\omega_o \cos n\omega_o t - \frac{1}{T_{io}} \sin n\omega_o t) \right]_{t_a}^{t_b} \qquad \text{(E.13)}$$

C - Integral (4.75)

C.1 - $n = 0$

$$\int_{t_a}^{t_b} i_i(t)\, dt = \left[I_d\, t \right]_{t_a}^{t_b} + \sum_{\ell=1}^{n_d} \left[- \frac{L_\ell}{\ell\omega_o} \cos \ell\omega_o t \right]_{t_a}^{t_b}$$

$$+ \sum_{\ell=1}^{n_d} \left[\frac{M_\ell}{\ell\omega_o} \sin \ell\omega_o t \right]_{t_a}^{t_b} \qquad \text{(E.14)}$$

C.2 - $n \neq 0$

$$\int_{t_a}^{t_b} i_d(t) \cos n\omega_o t \, dt = CCI + \sum_{\ell=1}^{n-1} CC_\ell + CC + \sum_{\ell=n+1}^{n_d} CC_\ell$$

(E.15)

where

$$CCI = \frac{I_d}{n\omega_o}\left[\sin n\omega_o t\right]_{t_a}^{t_b} \qquad (E.16)$$

$$CC_\ell = L_\ell\left[-\frac{\cos(\ell\omega_o + n\omega_o)t}{2(\ell\omega_o + n\omega_o)} - \frac{\cos(\ell\omega_o - n\omega_o)t}{2(\ell\omega_o - n\omega_o)}\right]_{t_a}^{t_b}$$

$$+ M_\ell\left[\frac{\sin(\ell\omega_o + n\omega_o)t}{2(\ell\omega_o + n\omega_o)} + \frac{\sin(\ell\omega_o - n\omega_o)t}{2(\ell\omega_o - n\omega_o)}\right]_{t_a}^{t_b} \qquad (E.17)$$

$$CC = L_\ell - \left[\frac{\cos 2\ell\omega_o t}{4\ell\omega_o}\right]_{t_a}^{t_b} + M_\ell\left[\frac{t}{2} + \frac{\sin 2\ell\omega_o t}{4\ell\omega_o}\right]_{t_a}^{t_b} \qquad (E.18)$$

D - Integral (4.76)

$$\int_{t_a}^{t_b} i_d(t) \sin n\omega_o t = SSI + \sum_{\ell=1}^{n-1} SS_\ell + SS + \sum_{\ell=n+1}^{n_d} SS_\ell \qquad (E.19)$$

where

$$SSI = -\frac{I_d}{n\omega_o}\left[\cos n\omega_o t\right]_{t_a}^{t_b} \qquad (E.20)$$

$$SS_{\ell} = L_{\ell}\left[-\frac{\sin(\ell\omega_o + n\omega_o)t}{2(\ell\omega_o + n\omega_o)} + \frac{\sin(\ell\omega_o - n\omega_o)t}{2(\ell\omega_o - n\omega_o)}\right]_{t_a}^{t_b}$$

$$+ M_{\ell}\left[\frac{\cos(\ell\omega_o + n\omega_o)t}{2(\ell\omega_o + n\omega_o)} + \frac{\cos(\ell\omega_o - n\omega_o)t}{2(\ell\omega_o - n\omega_o)}\right]_{t_a}^{t_b} \qquad (E.21)$$

$$SS = L_{\ell}\left[\frac{t}{2} - \frac{\cos 2\ell\omega_o t}{4\ell\omega_o}\right]_{t_a}^{t_b} + M_{\ell}\left[-\frac{\cos 2\ell\omega_o t}{4\ell\omega_o}\right]_{t_a}^{t_b} \qquad (E.22)$$

Appendix F

TABLES OF RESULTS CORRESPONDING TO FINITE S.C.R. ON BOTH RECTIFIER AND INVERTER SIDES

TERMINAL NUMBER 1

D.C. CURRENT CONSTANT TERM 2.00000

D.C. CURRENT HARMONICS

ORDER	MAGNITUDE (KA)	PHASE (DEG)
6	.019660	155.31
12	.003748	-10.09
18	.002791	256.48
24	.000917	103.90
30	.000643	-13.40

TERMINAL NUMBER 2

D.C. CURRENT CONSTANT TERM 2.00000

D.C. CURRENT HARMONICS

ORDER	MAGNITUDE (KA)	PHASE (DEG)
6	.019343	249.55
12	.003567	305.67
18	.003009	274.34
24	.001009	246.20
30	.000618	301.03

TERMINAL NUMBER: 1

A.C. VOLTAGE HARMONICS-BUSBAR SIDE

ORDER	PHASE R MAGNITUDE (KV)	PHASE R PHASE (DG)	PHASE Y MAGNITUDE (KV)	PHASE Y PHASE (DG)	PHASE B MAGNITUDE (KV)	PHASE B PHASE (DG)
1	230.940000	0	230.940000	-120.00	230.940000	120.00
5	.277275	216.67	.277275	-23.33	.277275	96.67
7	.314944	219.63	.314944	99.63	.314944	-20.37
11	.048469	235.28	.048469	-4.72	.048469	115.28
13	.059037	140.54	.059037	20.54	.059037	260.54
17	.592724	208.22	.592724	-31.78	.592724	88.22
19	.223609	97.82	.223609	-22.07	.223610	217.93
23	.169083	135.14	.169083	255.14	.169083	15.14
25	.154173	85.36	.154172	-34.64	.154172	205.36
29	.113024	166.44	.113024	-73.56	.113023	46.44

TERMINAL NUMBER: 2

A.C. VOLTAGE HARMONICS-BUSBAR SIDE

ORDER	PHASE R MAGNITUDE (KV)	PHASE R PHASE (DG)	PHASE Y MAGNITUDE (KV)	PHASE Y PHASE (DG)	PHASE B MAGNITUDE (KV)	PHASE B PHASE (DG)
1	230.940000	2.00	230.940000	-118.00	230.940000	122.00
5	.255070	-33.73	.255070	86.27	.255070	206.27
7	.289159	-30.75	.289159	89.25	.289159	-150.75
11	.044378	-3.28	.044378	96.72	.044378	216.72
13	.052669	2.03	.052669	242.03	.052669	122.03
17	.530187	24.09	.530187	144.09	.530186	264.09
19	.199325	109.97	.199325	-130.03	.199325	229.97
23	.150566	150.43	.150566	270.43	.150566	-89.57
25	.141855	103.05	.141856	-136.95	.141856	-16.95
29	.103171	163.86	.103171	-76.14	.103171	43.86

Table F.1 Base Case s.c.r. = 12

TERMINAL NUMBER 1

D.C. CURRENT CONSTANT TERM 2.00000

D.C. CURRENT HARMONICS

ORDER	MAGNITUDE (KA)	PHASE (DEG)
6	.019676	105.38
12	.003741	-10.03
18	.002799	237.08
24	.000920	154.26
30	.000642	-13.04

TERMINAL NUMBER 2

D.C. CURRENT CONSTANT TERM 2.00000

D.C. CURRENT HARMONICS

ORDER	MAGNITUDE (KA)	PHASE (DEG)
6	.019355	249.83
12	.003566	306.93
18	.002996	274.75
24	.001006	243.24
30	.000616	300.98

TERMINAL NUMBER: 1

A.C. VOLTAGE HARMONICS-BUSBAR SIDE

ORDER	PHASE R MAGNITUDE (KV)	PHASE R PHASE (DG)	PHASE Y MAGNITUDE (KV)	PHASE Y PHASE (DG)	PHASE B MAGNITUDE (KV)	PHASE B PHASE (DG)
1	230.940000	0	230.940000	-120.00	230.940000	120.00
5	.276829	215.99	.276829	-24.01	.276829	95.99
7	.316202	218.93	.316202	98.93	.316202	-21.07
11	.046477	234.98	.046477	-5.02	.046477	114.98
13	.057866	140.15	.057866	20.15	.057866	260.15
17	.566047	200.10	.566046	-39.90	.566048	80.10
19	.215055	94.88	.215054	-25.12	.215055	214.88
23	.157037	133.35	.157038	253.35	.157037	13.35
25	.153329	83.71	.153328	-36.29	.153329	203.71
29	.113345	164.92	.113345	-75.08	.113344	44.92

TERMINAL NUMBER: 2

A.C. VOLTAGE HARMONICS-BUSBAR SIDE

ORDER	PHASE R MAGNITUDE (KV)	PHASE R PHASE (DG)	PHASE Y MAGNITUDE (KV)	PHASE Y PHASE (DG)	PHASE B MAGNITUDE (KV)	PHASE B PHASE (DG)
1	230.940000	2.00	230.940000	-118.00	230.940000	122.00
5	.254675	-34.26	.254671	85.74	.254671	205.74
7	.292167	80.64	.292167	-39.36	.292167	200.64
11	.044393	-23.43	.044393	96.57	.044394	336.57
13	.052568	2.45	.052568	242.45	.052569	122.45
17	.477393	15.94	.477393	135.94	.477394	255.94
19	.177904	103.84	.177903	-16.16	.177904	223.84
23	.158215	115.03	.158215	235.03	.158214	-4.97
25	.140774	71.55	.140774	-48.45	.140773	-168.45
29	.105264	102.92	.105264	-77.08	.105264	42.92

Table F.2 Base case s.c.r. = 3

TERMINAL NUMBER: 1 TYPE 1
DATA A.C. BUSBAR VOLTAGES

ORDER	PHASE R MAGNITUDE (KV)	PHASE R PHASE (DG)	PHASEY MAGNITUDE (KV)	PHASEY PHASE (DG)	PHASEB MAGNITUDE (KV)	PHASEB PHASE (DG)
1	230.940000	0	228.640000	-118.00	230.940000	120.00

CONTROL ANGLE (DG) = 15.00
SHORT CIRCUIT RATIO = 3.00

TERMINAL NUMBER: 2 TYPE 2
DATA A.C. BUSBAR VOLTAGES

ORDER	PHASE R MAGNITUDE (KV)	PHASE R PHASE (DG)	PHASEY MAGNITUDE (KV)	PHASEY PHASE (DG)	PHASEB MAGNITUDE (KV)	PHASEB PHASE (DG)
1	230.940000	2.00	230.940000	-118.00	230.940000	122.00

CONTROL ANGLE (DG) = 18.00
SHORT CIRCUIT RATIO = 3.00

TERMINAL NUMBER 1

D.C. CURRENT CONSTANT TERM 2.00000

D.C. CURRENT HARMONICS

ORDER	MAGNITUDE (KA)	PHASE (DEG)
2	.008710	116.08
4	.001083	48.61
6	.019591	165.10
8	.000333	53.90
10	.000200	-55.68
12	.003746	-10.68
14	.000137	-72.51
16	.000161	147.03
18	.002778	256.49
20	.000127	158.83
22	.000118	45.34
24	.000900	163.21
30	.000642	-14.76

TERMINAL NUMBER 2

D.C. CURRENT CONSTANT TERM 2.00000

D.C. CURRENT HARMONICS

ORDER	MAGNITUDE (KA)	PHASE (DEG)
2	.001381	8.16
6	.019253	249.72
12	.003584	-53.33
18	.002988	-85.89
24	.000989	242.71
30	.000625	-59.59

Table F.3

Unbalanced fundamental voltage (rectifier side) s.c.r. = 3

TERMINAL NUMBER: 1

A.C. VOLTAGE HARMONICS-BUSBAR SIDE

ORDER	PHASE R MAGNITUDE (KV)	PHASE R PHASE (DG)	PHASE Y MAGNITUDE (KV)	PHASE Y PHASE (DG)	PHASE B MAGNITUDE (KV)	PHASE B PHASE (DG)
1	230.940000	0	228.640000	-118.00	230.940000	120.00
3	.012055	232.13	.368429	211.87	.379833	32.51
5	.277982	218.42	.278827	-20.28	.272916	99.22
7	.314586	222.18	.314020	104.36	.324571	-16.64
9	.042669	209.27	.081878	206.02	.124502	27.13
11	.048331	239.57	.049825	2.93	.046584	122.87
13	.055375	145.88	.056587	31.22	.060448	267.58
15	.036592	7.11	.074844	-.82	.111105	181.78
17	.574274	203.55	.607793	-25.89	.495255	92.35
19	.213857	98.13	.190865	-9.76	.238928	228.64
21	.008803	231.82	.022263	230.57	.031100	50.89
23	.173960	144.10	.172243	-88.90	.154470	27.03
25	.150625	95.30	.144803	-18.07	.162326	220.33
27	.006351	219.32	.014103	226.82	.020435	44.48
29	.112167	177.62	.120823	-64.33	.102346	66.01

TERMINAL NUMBER: 2

A.C. VOLTAGE HARMONICS-BUSBAR SIDE

ORDER	PHASE R MAGNITUDE (KV)	PHASE R PHASE (DG)	PHASE Y MAGNITUDE (KV)	PHASE Y PHASE (DG)	PHASE B MAGNITUDE (KV)	PHASE B PHASE (DG)
1	230.940000	2.00	230.940000	-118.00	230.940000	122.00
5	.253486	-34.10	.253368	85.89	.253453	205.87
7	.290384	80.47	.290667	-39.50	.290667	200.44
11	.044017	-22.94	.043992	97.11	.043971	217.05
13	.051941	3.12	.052012	243.04	.051914	123.01
17	.472875	17.81	.474904	137.86	.473567	258.05
19	.180156	105.54	.179058	-14.35	.179899	225.90
23	.155895	114.70	.155524	234.61	.155912	-5.46
25	.143929	193.56	.144266	73.67	.144337	-46.50
29	.107856	163.82	.107656	-76.05	.107539	43.80

Table F.3 (cont)

TERMINAL NUMBER: 1 TYPE 1
DATA A.C. BUSBAR VOLTAGES

ORDER	PHASE R MAGNITUDE (KV)	PHASE R PHASE (DG)	PHASEY MAGNITUDE (KV)	PHASEY PHASE (DG)	PHASEB MAGNITUDE (KV)	PHASEB PHASE (DG)
1	230.940000	0	230.940000	-120.00	230.940000	120.00

CONTROL ANGLE (DG) = 15.00
SHORT CIRCUIT RATIO = 3.00

TERMINAL NUMBER: 2 TYPE 2
DATA A.C. BUSBAR VOLTAGES

ORDER	PHASE R MAGNITUDE (KV)	PHASE R PHASE (DG)	PHASEY MAGNITUDE (KV)	PHASEY PHASE (DG)	PHASEB MAGNITUDE (KV)	PHASEB PHASE (DG)
1	230.940000	2.00	228.540000	-116.00	230.940000	122.00

CONTROL ANGLE (DG) = 18.00
SHORT CIRCUIT RATIO = 3.00

TERMINAL NUMBER 1

D.C. CURRENT CONSTANT TERM 2.00000

D.C. CURRENT HARMONICS

ORDER	MAGNITUDE (KA)	PHASE (DEG)
2	.001269	-3.69
6	.019659	155.45
12	.003744	-10.03
18	.002794	257.09
24	.000920	154.30
30	.000642	-13.06

TERMINAL NUMBER 2

D.C. CURRENT CONSTANT TERM 2.00000

D.C. CURRENT HARMONICS

ORDER	MAGNITUDE (KA)	PHASE (DEG)
2	.008003	243.96
4	.000943	-76.45
6	.019877	249.22
8	.000311	186.78
10	.000185	135.31
12	.003420	-52.91
14	.000119	67.68
16	.000135	34.12
18	.003052	-85.46
20	.000109	-59.57
22	.000102	-24.65
24	.001107	248.16
30	.000552	-51.11

Table F.4

Unbalanced fundamental voltage (inverter side) s.c.r. = 3

TERMINAL NUMBER: 1

A.C. VOLTAGE HARMONICS-BUSBAR SIDE

ORDER	PHASE R MAGNITUDE (KV)	PHASE R PHASE (DG)	PHASE Y MAGNITUDE (KV)	PHASE Y PHASE (DG)	PHASE B MAGNITUDE (KV)	PHASE B PHASE (DG
1	230.940000	0	230.940000	-120.00	230.940000	120.00
5	.276852	216.01	.276758	-24.01	.276871	95.99
7	.318013	218.92	.318265	98.96	.318305	-21.10
11	.048501	234.94	.048455	-5.05	.048471	114.90
13	.057822	140.16	.057921	20.16	.057853	260.09
17	.567189	200.12	.565241	-39.82	.565822	79.98
19	.214402	94.93	.215530	-25.06	.215193	214.72
23	.167220	133.41	.166795	253.37	.167102	13.27
25	.153082	83.72	.153500	-36.23	.153402	203.61
29	.113524	164.93	.113231	-75.01	.113311	44.82

TERMINAL NUMBER: 2

A.C. VOLTAGE HARMONICS-BUSBAR SIDE

ORDER	PHASE R MAGNITUDE (KV)	PHASE R PHASE (DG)	PHASE Y MAGNITUDE (KV)	PHASE Y PHASE (DG)	PHASE B MAGNITUDE (KV)	PHASE B PHASE (DG)
1	230.940000	2.00	228.640000	-126.00	230.940000	122.00
3	.274249	24.92	.282931	-6.94	.282980	233.05
5	.255280	-28.45	.257788	90.45	.256710	211.49
7	.302109	37.77	.296622	-33.03	.293460	207.01
9	.097255	-11.93	.021275	165.91	.075954	357.93
11	.045467	-9.89	.045025	106.75	.047505	227.29
13	.056892	14.04	.052688	255.40	.056030	133.42
15	.089990	118.64	.018730	-53.58	.071479	-63.45
17	.570797	30.01	.474502	151.80	.519197	270.05
19	.150118	113.62	.184077	1.75	.149276	229.14
21	.024909	-33.03	.003785	149.60	.021129	146.50
23	.143633	136.89	.160855	257.38	.151993	22.74
25	.143585	221.02	.140270	95.44	.139835	-20.47
27	.015493	-66.59	.002823	99.64	.012756	-40.43
29	.106873	147.83	.110063	-46.91	.120931	75.22

Table F.4 (cont)

TERMINAL NUMBER: 1 TYPE 1
DATA A.C. BUSBAR VOLTAGES

ORDER	PHASE R MAGNITUDE (KV)	PHASE R PHASE (DG)	PHASEY MAGNITUDE (KV)	PHASEY PHASE (DG)	PHASEB MAGNITUDE (KV)	PHASEB PHASE (DG
1	230.940000	0	228.640000	-118.00	230.940000	120.00

CONTROL ANGLE (DG) = 15.00
SHORT CIRCUIT RATIO = 3.00

TERMINAL NUMBER: 2 TYPE 2
DATA A.C. BUSBAR VOLTAGES

ORDER	PHASE R MAGNITUDE (KV)	PHASE R PHASE (DG)	PHASEY MAGNITUDE (KV)	PHASEY PHASE (DG)	PHASEB MAGNITUDE (KV)	PHASEB PHASE (DG
1	230.940000	2.00	228.640000	-116.00	230.940000	122.00

CONTROL ANGLE (DG) = 18.00
SHORT CIRCUIT RATIO = 3.00

TERMINAL NUMBER 1

D.C. CURRENT CONSTANT TERM 2.00000

D.C. CURRENT HARMONICS

ORDER	MAGNITUDE (KA)	PHASE (DEG)
2	.008097	108.06
4	.001080	49.94
6	.019574	165.17
8	.000332	54.32
10	.000200	-55.87
12	.003749	-10.69
14	.000138	-71.97
16	.000163	146.80
18	.002779	256.50
20	.000128	159.41
22	.000118	44.92
24	.000901	163.23
30	.000642	-14.78

TERMINAL NUMBER 2

D.C. CURRENT CONSTANT TERM 2.00000

D.C. CURRENT HARMONICS

ORDER	MAGNITUDE (KA)	PHASE (DEG)
2	.007331	253.50
4	.000946	-80.68
6	.019774	249.21
8	.000310	186.15
10	.000186	184.55
12	.003439	-52.90
14	.000119	65.97
16	.000135	33.64
18	.003024	-83.78
20	.000109	-61.15
22	.000106	-65.35
24	.001090	243.08
30	.000561	-60.86

Table F.5

Unbalanced fundamental a.c. voltage (rectifier and inverter side)
s.c.r. = 3

TERMINAL NUMBER: 1

A.C. VOLTAGE HARMONICS-BUSBAR SIDE

ORDER	PHASE R MAGNITUDE (KV)	PHASE R PHASE (DG)	PHASE Y MAGNITUDE (KV)	PHASE Y PHASE (DG)	PHASE B MAGNITUDE (KV)	PHASE B PHASE (DG)
1	230.940000	0	228.640000	-118.00	230.940000	120.00
3	.038315	239.16	.363605	207.94	.396867	30.81
5	.277974	218.43	.278785	-20.29	.272962	99.22
7	.314406	222.17	.314056	104.39	.324712	-16.67
9	.044158	210.27	.081281	205.14	.125418	26.91
11	.048342	239.57	.049814	2.94	.046579	122.85
13	.055334	145.89	.056620	31.24	.060454	267.54
15	.037854	6.82	.073951	-.98	.111716	181.62
17	.574994	203.55	.607441	-25.83	.494813	92.27
19	.213392	98.13	.191171	-9.67	.239047	228.54
21	.009326	231.31	.021857	230.44	.031205	50.72
23	.174074	144.13	.172104	-88.88	.154485	26.97
25	.150430	95.30	.144918	-18.02	.162397	220.27
27	.006641	219.50	.013911	226.60	.020518	44.33
29	.112315	177.60	.120794	-54.28	.102294	65.96

TERMINAL NUMBER: 2

A.C. VOLTAGE HARMONICS-BUSBAR SIDE

ORDER	PHASE R MAGNITUDE (KV)	PHASE R PHASE (DG)	PHASE Y MAGNITUDE (KV)	PHASE Y PHASE (DG)	PHASE B MAGNITUDE (KV)	PHASE B PHASE (DG)
1	230.940000	2.00	228.640000	-116.00	230.940000	122.00
3	.251652	21.36	.032075	36.65	.282706	203.07
5	.254089	-28.32	.256506	90.61	.259513	211.62
7	.300373	87.98	.292121	-32.77	.292967	209.00
9	.095513	-12.48	.020740	165.93	.074784	167.95
11	.045102	-9.50	.044631	107.18	.047095	228.35
13	.056257	14.55	.052151	255.92	.055439	138.88
15	.088052	118.63	.017881	-53.64	.070375	-63.33
17	.561176	31.36	.467444	153.00	.508147	262.91
19	.150015	116.13	.183897	3.70	.187826	231.29
21	.024218	-33.30	.003422	149.28	.020799	146.29
23	.144022	137.95	.160951	258.29	.152396	23.65
25	.143474	221.89	.140042	96.45	.129980	-19.49
27	.015177	-66.92	.002677	97.94	.012612	116.26
29	.106058	198.95	.108788	-48.79	.119751	76.17

Table F.5 (cont)

TERMINAL NUMBER: 1 TYPE 1
DATA A.C. BUSBAR VOLTAGES

ORDER	PHASE R MAGNITUDE (KV)	PHASE R PHASE (DG)	PHASEY MAGNITUDE (KV)	PHASEY PHASE (DG)	PHASEB MAGNITUDE (KV)	PHASEB PHASE (DG)
1	230.940000	0	230.940000	-120.00	230.940000	120.00
2	2.300000	0	2.300000	120.00	2.300000	240.00

CONTROL ANGLE (DG) = 15.00

SHORT CIRCUIT RATIO = 3.00

TERMINAL NUMBER: 2 TYPE 2
DATA A.C. BUSBAR VOLTAGES

ORDER	PHASE R MAGNITUDE (KV)	PHASE R PHASE (DG)	PHASEY MAGNITUDE (KV)	PHASEY PHASE (DG)	PHASEB MAGNITUDE (KV)	PHASEB PHASE (DG)
1	230.940000	2.00	230.940000	-118.00	230.940000	122.00

CONTROL ANGLE (DG) = 18.00

SHORT CIRCUIT RATIO = 3.00

TERMINAL NUMBER 1

D.C. CURRENT CONSTANT TERM 2.00000

D.C. CURRENT HARMONICS

ORDER	MAGNITUDE (KA)	PHASE (DEG)
3	.006035	-66.08
6	.019673	165.39
9	.000430	218.11
12	.003736	-10.08
15	.000178	43.54
18	.002788	257.07
21	.000162	-73.70
24	.000915	164.44
30	.000637	-13.29

TERMINAL NUMBER 2

D.C. CURRENT CONSTANT TERM 2.00000

D.C. CURRENT HARMONICS

ORDER	MAGNITUDE (KA)	PHASE (DEG)
3	.000391	-50.37
6	.019355	249.72
12	.003566	-53.30
18	.002996	-85.58
24	.001006	242.79
30	.000616	-59.59

Table F.6

2nd harmonic distortion (neg seq, 1%). Rectifier side

s.c.r. = 3

TERMINAL NUMBER: 1

A.C. VOLTAGE HARMONICS-BUSBAR SIDE

ORDER	PHASE R MAGNITUDE (KV)	PHASE R PHASE (DG)	PHASE Y MAGNITUDE (KV)	PHASE Y PHASE (DG)	PHASE B MAGNITUDE (KV)	PHASE B PHASE (DG)
1	230.940000	0	230.940000	-120.00	230.940000	120.00
2	3.289407	10.94	3.289416	130.94	3.289413	250.94
4	.091439	-1.46	.091439	238.54	.091440	118.54
5	.276792	215.98	.276792	-24.02	.276792	95.98
7	.318112	218.92	.318112	98.92	.318112	-21.08
8	.299932	60.11	.299937	180.11	.299934	-59.89
10	.036959	-2.24	.036959	237.76	.036959	117.76
11	.048440	234.93	.048440	-5.07	.048440	114.93
13	.057797	140.16	.057797	20.16	.057797	260.16
14	.028955	227.70	.028955	-12.30	.028954	107.70
16	.120535	107.37	.120537	-12.63	.120534	227.37
17	.563572	200.15	.563570	-39.85	.563573	80.15
19	.213814	94.80	.213814	-25.20	.213815	214.80
20	.019551	84.78	.019550	204.78	.019551	-35.22
22	.012397	9.92	.012397	249.92	.012398	129.92
23	.166438	133.23	.166439	253.23	.166438	13.23
25	.152720	83.63	.152720	-36.37	.152719	203.63
26	.011113	56.26	.011114	176.26	.011113	-63.73
28	.011626	-2.66	.011626	237.34	.011626	117.35
29	.112733	164.96	.112733	-75.04	.112732	44.96

TERMINAL NUMBER: 2

A.C. VOLTAGE HARMONICS-BUSBAR SIDE

ORDER	PHASE R MAGNITUDE (KV)	PHASE R PHASE (DG)	PHASE Y MAGNITUDE (KV)	PHASE Y PHASE (DG)	PHASE B MAGNITUDE (KV)	PHASE B PHASE (DG)
1	230.940000	2.00	230.940000	-118.00	230.940000	122.00
5	.254678	-34.26	.254678	85.74	.254678	205.74
7	.292173	80.25	.292173	-39.75	.292173	200.25
11	.044401	-23.34	.044401	96.66	.044401	216.66
13	.052561	2.48	.052561	242.48	.052561	122.48
17	.478949	16.00	.478949	136.00	.478947	256.00
19	.177758	103.89	.177758	-16.11	.177757	223.89
23	.158250	115.04	.158250	235.04	.158250	-4.96
25	.140761	191.91	.140761	71.91	.140761	-48.09
29	.108261	162.93	.108261	-77.07	.108261	42.93

Table F.6 (cont)

TERMINAL NUMBER: 1 TYPE 1
DATA A.C. BUSBAR VOLTAGES

ORDER	PHASE R MAGNITUDE (KV)	PHASE R PHASE (DG)	PHASEY MAGNITUDE (KV)	PHASEY PHASE (DG)	PHASEB MAGNITUDE (KV)	PHASEB PHASE (DG)
1	230.940000	0	230.940000	-120.00	230.940000	120.00
2	2.300000	0	2.300000	240.00	2.300000	120.00

CONTROL ANGLE (DG) = 15.00

SHORT CIRCUIT RATIO = 3.00

TERMINAL NUMBER: 2 TYPE 2
DATA A.C. BUSBAR VOLTAGES

ORDER	PHASE R MAGNITUDE (KV)	PHASE R PHASE (DG)	PHASEY MAGNITUDE (KV)	PHASEY PHASE (DG)	PHASEB MAGNITUDE (KV)	PHASEB PHASE (DG)
1	230.940000	2.00	230.940000	-118.00	230.940000	122.00

CONTROL ANGLE (DG) = 18.00

SHORT CIRCUIT RATIO = 3.00

TERMINAL NUMBER 1.

D.C. CURRENT CONSTANT TERM 2.00000

D.C. CURRENT HARMONICS

ORDER	MAGNITUDE (KA)	PHASE (DEG)
1	.004373	250.74
5	.000428	244.76
6	.019820	165.45
7	.000416	207.71
11	.000155	117.92
12	.003735	-9.97
13	.000078	126.85
17	.000104	-20.11
18	.002787	257.08
19	.000102	-40.64
23	.000082	246.61
24	.000916	164.49
25	.000082	216.71
29	.000051	122.77
30	.000638	-13.19

TERMINAL NUMBER 2

D.C. CURRENT CONSTANT TERM 2.00000

D.C. CURRENT HARMONICS

ORDER	MAGNITUDE (KA)	PHASE (DEG)
1	.018050	19.71
5	.000166	-45.03
6	.021305	251.91
7	.000161	167.78
11	.000050	219.11
12	.002225	-60.52
13	.000055	87.78
17	.000034	102.73
18	.002659	-70.68
19	.000033	-43.25
23	.000031	6.50
24	.001473	254.65
25	.000032	219.43
29	.000023	-86.92
30	.000396	252.72

Table F.7

2nd harmonic distortion (pos seq, 1%), rectifier side

s.c.r. = 3

TERMINAL NUMBER: I

A.C. VOLTAGE HARMONICS-BUSBAR SIDE

ORDER	PHASE R MAGNITUDE (KV)	PHASE R PHASE (DG)	PHASE Y MAGNITUDE (KV)	PHASE Y PHASE (DG)	PHASE B MAGNITUDE (KV)	PHASE B PHASE (DG)
1	230.940000	0	230.940000	-120.00	230.940000	120.00
2	2.072601	12.99	2.072541	252.99	2.072552	132.99
4	.076887	-75.75	.076880	44.25	.076877	164.25
5	.276858	215.97	.276876	-24.02	.276829	95.98
6	.194541	197.32	.023524	247.50	.210384	22.25
7	.318000	218.93	.318090	98.93	.318053	-21.09
8	.197979	117.20	.198019	-2.79	.198019	237.20
10	.021410	-67.05	.021413	52.97	.021405	172.97
11	.048431	234.89	.048463	-5.09	.048439	114.93
12	.227037	251.44	.026350	-34.66	.235791	77.59
13	.057783	140.16	.057832	20.12	.057773	260.10
14	.020375	-79.24	.020388	160.74	.020377	40.72
16	.068201	35.11	.068268	155.15	.068188	-84.82
17	.562664	199.85	.564816	-40.10	.563355	80.07
18	.054649	236.83	.006956	-10.29	.052378	63.85
19	.213864	94.52	.214932	-25.54	.214206	214.24
20	.016671	144.16	.016698	24.10	.016665	264.05
22	.009240	-64.22	.009259	55.91	.009232	175.95
23	.169410	131.90	.169825	252.05	.169225	12.09
24	.014582	209.58	.001113	19.27	.013484	30.42
25	.149938	84.89	.150491	-35.15	.150142	204.69
26	.007742	124.56	.007767	4.48	.007746	244.36
28	.007811	-67.30	.007832	52.86	.007803	172.91
29	.110274	164.34	.110820	-75.61	.110462	44.61
30	.013956	207.52	.000598	-10.79	.013490	29.09

TERMINAL NUMBER: 2

A.C. VOLTAGE HARMONICS-BUSBAR SIDE

ORDER	PHASE R MAGNITUDE (KV)	PHASE R PHASE (DG)	PHASE Y MAGNITUDE (KV)	PHASE Y PHASE (DG)	PHASE B MAGNITUDE (KV)	PHASE B PHASE (DG)
1	230.940000	2.00	230.940000	-118.00	230.940000	122.00
2	.857892	62.64	.857894	-57.36	.857858	182.64
4	.026538	124.87	.026533	244.87	.026536	4.86
5	.260637	-39.49	.260647	80.51	.260643	200.52
6	.023139	-3.49	.064808	103.24	.062237	262.28
7	.307465	72.94	.307473	-47.06	.307485	192.94
8	.051674	62.76	.051657	-57.25	.051660	182.77
10	.003218	128.33	.003219	248.38	.003216	8.36
11	.053357	-36.62	.053360	83.37	.053364	203.38
12	.014699	28.66	.037945	153.07	.032024	-49.18
13	.068547	-14.55	.068561	225.45	.068555	105.44
14	.002865	223.23	.002853	103.31	.002867	-16.71
17	.893561	-33.61	.893205	86.37	.893676	206.38
18	.002908	-.12	.005397	155.02	.003069	-48.51
19	.261817	24.05	.261863	264.00	.261630	144.01
23	.099750	69.85	.099816	189.92	.099677	-50.08
24	.000382	-51.82	.000129	-75.74	.000512	121.87
25	.104325	154.55	.104267	34.61	.104392	-85.39
30	.122164	127.26	.122275	247.24	.122268	7.30

Table F.7 (cont)

TERMINAL NUMBER: 1 TYPE 1
DATA A.C. BUSBAR VOLTAGES

ORDER	PHASE R MAGNITUDE (KV)	PHASE R PHASE (DG)	PHASEY MAGNITUDE (KV)	PHASEY PHASE (DG)	PHASEB MAGNITUDE (KV)	PHASEB PHASE (DG)
1	230.940000	0	230.940000	-120.00	230.940000	120.00

CONTROL ANGLE (DG) = 15.00

SHORT CIRCUIT RATIO = 3.00

TERMINAL NUMBER: 2 TYPE 2
DATA A.C. BUSBAR VOLTAGES

ORDER	PHASE R MAGNITUDE (KV)	PHASE R PHASE (DG)	PHASEY MAGNITUDE (KV)	PHASEY PHASE (DG)	PHASEB MAGNITUDE (KV)	PHASEB PHASE (DG)
1	230.940000	2.00	230.940000	-118.00	230.940000	122.00
2	2.300000	2.00	2.300000	-118.00	2.300000	122.00

CONTROL ANGLE (DG) = 18.00

SHORT CIRCUIT RATIO = 3.00

TERMINAL NUMBER 1

D.C. CURRENT CONSTANT TERM 2.00000

D.C. CURRENT HARMONICS

ORDER	MAGNITUDE (KA)	PHASE (DEG)
1	.016661	17.78
5	.000193	-52.33
6	.019822	165.47
7	.000186	155.19
11	.000062	180.57
12	.004739	-9.94
13	.000055	46.45
17	.000050	52.28
18	.002790	257.07
19	.000048	261.89
23	.000038	-55.32
24	.000919	164.36
25	.000039	154.74
29	.000025	180.50
30	.000642	-13.04

TERMINAL NUMBER 2

D.C. CURRENT CONSTANT TERM 2.00000

D.C. CURRENT HARMONICS

ORDER	MAGNITUDE (KA)	PHASE (DEG)
1	.003320	143.16
5	.000388	3.75
6	.021744	251.70
7	.000363	111.99
11	.000130	-89.38
12	.002127	-62.24
13	.000093	60.70
17	.000063	141.30
18	.002645	-69.38
19	.000063	267.44
23	.000066	61.54
24	.001527	256.55
25	.000067	174.80
29	.000049	-26.02
30	.000436	247.70

Table F.8

2nd harmonic distortion, (pos seq, 1%)

s.c.r. = 3

TERMINAL NUMBER: 1

A.C. VOLTAGE HARMONICS-BUSBAR SIDE

ORDER	PHASE R MAGNITUDE (KV)	PHASE R PHASE (DG)	PHASE Y MAGNITUDE (KV)	PHASE Y PHASE (DG)	PHASE B MAGNITUDE (KV)	PHASE B PHASE (DG)
1	230.940000	0	230.940000	-120.00	230.940000	120.00
2	.872373	-44.48	.872369	195.52	.872363	75.52
4	.027747	-82.20	.027747	37.80	.027747	157.81
5	.276894	215.99	.276900	-24.01	.276897	95.99
6	.025603	31.67	.069573	147.57	.062756	-54.05
7	.318138	218.94	.318141	98.94	.318149	-21.06
8	.053348	-.09	.053346	239.91	.053349	119.91
10	.003616	-37.07	.003617	82.94	.003616	202.96
11	.048482	234.92	.048485	-5.09	.048486	114.92
12	.015123	97.73	.043424	236.60	.033548	39.33
13	.057866	140.12	.057873	20.12	.057872	260.11
14	.003136	202.28	.003137	82.30	.003138	-37.74
17	.566250	199.89	.566365	-40.13	.566531	79.89
18	.001950	96.76	.005786	262.73	.003924	75.75
19	.215692	94.47	.215780	-25.50	.215827	214.47
23	.170178	132.15	.170245	252.14	.170248	12.16
25	.150857	84.90	.150902	-35.08	.150925	204.89

TERMINAL NUMBER: 2

A.C. VOLTAGE HARMONICS-BUSBAR SIDE

ORDER	PHASE R MAGNITUDE (KV)	PHASE R PHASE (DG)	PHASE Y MAGNITUDE (KV)	PHASE Y PHASE (DG)	PHASE B MAGNITUDE (KV)	PHASE B PHASE (DG)
1	230.940000	2.00	230.940000	-118.00	230.940000	122.00
2	2.146913	10.75	2.146987	250.75	2.146806	130.75
4	.054379	254.76	.054396	14.79	.054365	134.79
5	.262288	-37.76	.262305	82.23	.262347	202.24
6	.137564	-6.74	.151378	168.82	.017777	-47.98
7	.309874	75.35	.309784	-44.64	.309895	195.37
8	.143090	87.47	.142983	-32.53	.143042	207.51
10	.016854	235.79	.016870	-4.21	.016864	115.84
11	.054396	-32.93	.054368	87.04	.054410	207.03
12	.172708	20.91	.198009	195.78	.030224	-15.11
13	.070330	-10.33	.070343	229.73	.070405	109.69
14	.016982	224.11	.016969	104.18	.016992	-15.82
16	.066043	-42.49	.066138	77.42	.066186	197.54
17	.949577	-29.33	.946931	90.73	.947418	210.56
18	.047734	-10.27	.057100	163.40	.010994	-45.34
19	.282129	27.11	.283512	267.11	.282828	146.87
20	.016897	72.63	.016895	-47.18	.016944	192.73
22	.008128	214.97	.008149	-25.31	.008173	94.96
23	.092492	73.07	.093277	193.09	.092863	-46.50
24	.009795	-47.16	.012775	127.60	.003150	-69.02
25	.088462	161.00	.097778	40.88	.097939	-78.71

Table F.8 (cont)